The Dissertation Committee for Michelle Elizabeth Dose Certifies that this is the approved version of the following dissertation:

Fundamental Gas Transport in Thermally Cross-linked Diaminophenylindane (DAPI) Containing Polyimides

Committee:

Benny D. Freeman, Supervisor

Donald R. Paul, Co-Supervisor

Isaac C. Sanchez

Nathaniel Lynd

Judy Riffle

Fundamental Gas Transport in Thermally Cross-linked Diaminophenylindane (DAPI) Containing Polyimides

by

Michelle Elizabeth Dose

Dissertation

Presented to the Faculty of the Graduate School of

The University of Texas at Austin

in Partial Fulfillment

of the Requirements

for the Degree of

Doctor of Philosophy

The University of Texas at Austin

December 2018

Dedication

To my family and mentors

Acknowledgements

First and foremost, I would like to thank my family and friends. Without your support and guidance, I would not be the person I am today.

Second, I am very thankful for my graduate advisors, Dr. Benny D. Freeman and Dr. Donald R. Paul. Your mentorship and continuous support has helped me grow both as a polymer scientist and leader. Your patience and editing of my dyslexic writing was greatly appreciated. In addition to my advisors, I would also like to thank the rest of my committee members: Dr. Isaac Sanchez, Dr. Nathaniel Lynd, and Dr. Judy Riffle. I have been extremely fortunate to receive advice and guidance from some of the best minds in polymer science and engineering.

Dr. Michele Galizia and Dr. Kris Gleason also provided a significant amount of support to me throughout my time at the University of Texas at Austin, including day-to-day advisement, trouble shooting experimental design, building new pieces of automated equipment that limited my midnight trips to the lab, and, of course, endless scientific discussions.

Additionally, I would like to thank my mentors and advisors from Georgia Tech who helped me make the decision to pursue my Ph.D. Dr. Ryan P. Lively, Dr. William J. Koros, Dr. Ronald R. Chance, and Dr. Benjamin McCool each helped me develop my research skills, build my confidence, and gave me opportunities for which I will always be grateful.

I also would like to thank my fellow labmates and graduate students for the stimulating discussions, venting sessions, and fun we have had over the years. Trips to

Adelbert's, Posse East, and C. Hunts were invaluable to maintaining my sanity throughout graduate school.

Finally, I cannot forget to mention my loving dog, Miss Diva. Your never failing love and endless tail wags helped me through the toughest times of grad school.

Fundamental Gas Transport in Thermally Cross-linked Diaminophenylindane (DAPI) Containing Polyimides

Michelle Elizabeth Dose, Ph.D.

The University of Texas at Austin, 2018

Supervisor: Benny D. Freeman

Co-Supervisor: Donald R. Paul

The trust of this work is to critically examine the chemical and morphological structure of thermally cross-linked polyimides and to identify the effect cross-linking has on fundamental gas transport and plasticization resistance of these materials. To accomplish this goal, a polyimide containing diaminophenylindane (DAPI), hexafluoroisopropylindene (6FDA), and diaminobenzoic acid (DABA), referred to as 6FDA-DAPI/DABA, was synthesized and characterized. The thermal cross-linking process was found to occur by thermal decarboxylation of the carboxylic acid groups contained in DABA. Additionally, upon cross-linking, gas permeability was found to increase with increased cross-linking due to an apparent increase in polymer chain spacing. While thermal cross-linking showed improved plasticization resistance to pure CO_2, C_2H_4, and C_2H_6, mixed gas permeation experiments revealed linear 6FDA-DAPI/DABA was more resistant to plasticization than its cross-linked analog. By studying sorption induced dilation, we concluded that linear 6FDA-DAPI/DABA more readily excluded C_2H_6 from the free volume elements, compared to cross-linked 6FDA-DAPI/DABA, correlating well with the minimal plasticization effects observed in the mixed gas experiments. Additionally, the dilation and sorption data were used to estimate the accessible free

volume in the polymer-penetrant mixture. While correlating the diffusion coefficients of CO_2, C_2H_4, and C_2H_6 with the penetrant weight fraction showed anomalous behavior, the relative increase in diffusion coefficients with accessible fractional free volume accurately reflected the plasticization behavior observed in mixed gas permeation experiments. Additionally, this dissertation investigated the fundamental transport of gases in thermally rearranged (TR) polymers and polymers of intrinsic microporosity (PIM) to gain an understanding of why these materials tend to perform at or beyond the Robeson Upper Bound for select gas pairs.

Table of Contents

List of Tables

List of Figures

Chapter 1: Introduction

1.1. Background and Motivation

In recent years, the drive to achieve more efficient and environmentally friendly separations has resulted in the rapid development of membrane processes. Advances in polymer science and membrane fabrication have allowed membranes to become a competitive alternative to many conventional gas separation technologies, with still further room for improvement in these areas and other potential applications yet to be explored. One significant challenge to the membrane community is the separation of olefins from paraffins, largely due to the condensability and strongly sorbing nature of these gases in polymers as well as the small size and condensability difference between, for example, ethylene and ethane [1, 2]. Olefin/paraffin separations are among the most energy intensive separations practiced today, requiring cryogenic distillation columns that can reach upwards of 300 ft tall, 35 ft in diameter, and contain nearly 200 trays [3]. The overarching goal of this fundamental study is to systematically investigate the transport of highly condensable species, like ethylene, propylene, and other paraffin analogs, in polymer membranes and determine the impact crosslinking has on such systems.

Increasing gas permeability of a polymer can improve the efficiency of the separation, reducing the area of the membrane needed to achieve a specified flux or membrane productivity. Similarly, a higher selectivity for a gas pair can increase the purity of the desired product. However, a tradeoff exists for polymer based membranes, where an increase in permeability is often accompanied by a loss in selectivity. This tradeoff is referred to as the Robeson Upper Bound and was first empirically described by Robeson in 1991, revisited in 2008, and fundamentally described by theory by Freeman in 1999 [4-6]. Over the years, several polymers have been found that meet or exceed this upper bound

for several gas pairs, including O_2/N_2 and CO_2/CH_4 gas pairs. This work will take a close look at the fundamental transport properties of the so called "upper bound materials", to better understand what physical properties allow a material to perform at or beyond the upper bound.

Gas permeation in polymeric films can be described by the solution-diffusion model, in which a penetrant is sorbed into the dense film from a high activity upstream, diffuses through the film driven by a chemical gradient, and then desorbed on the lower activity downstream. In this model, the permeability, *P*, can be expressed as the product of diffusivity, *D*, and solubility, *S*, of the molecule in the polymer.

For most gases, a slight decrease in permeability with an increase in applied pressure is observed in glassy polymers commonly used for gas separations due to so-called dual mode effects (cf., Figure 1.1). However, if plasticization occurs, an increase in permeability and decrease in selectivity with increasing pressure are often observed, for both pure and mixed gas experiments. Plasticization refers to the swelling of a polymer in the presence of highly soluble penetrant molecules, which increases the spacing between polymer chains, thereby causing an increase in gas diffusivity for all components in the gas mixture. This phenomenon is often accompanied by a loss in permeability selectivity due to the diffusion coefficient of the larger penetrant molecule increasing more than that of the smaller penetrant molecule (cf., Figure 1.1) [7]. For this reason, resistance to plasticization is important for polymer membranes used in applications where the membranes are exposed to high concentrations of plasticizing agents, like CO_2 and C_{2+} hydrocarbons.

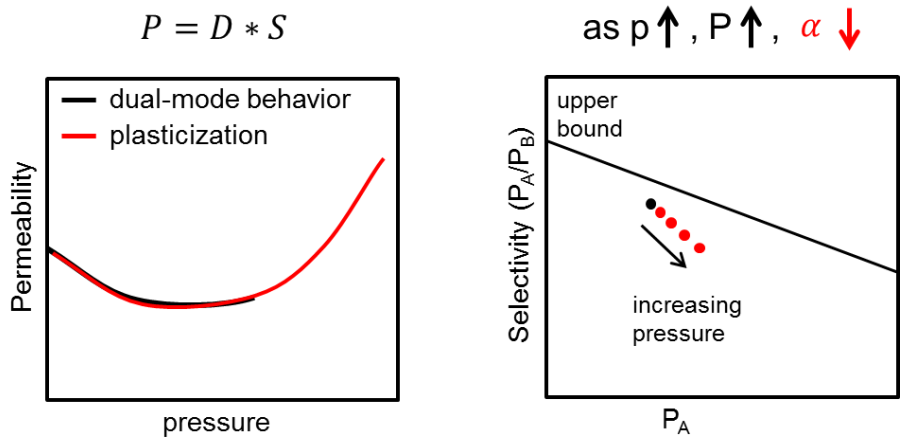

Figure 1.1. In plasticization, highly soluble/condensable penetrant molecules induce swelling of the polymer matrix, which results in a significant decrease in diffusion selectivity, and thus a decrease in permeability selectivity with increasing pressure.

Several techniques have been employed to aid in suppressing the plasticization effect, including increasing the rigidity of the polymer matrix by adding rigid moieties to the polymer backbone or physically blending a more flexible polymer with a more rigid polymer, and employing chemical cross-linking induced through thermal treatment, exposure to UV light, or by chemical means [8-11]. For gas mixtures containing CO_2 and CH_4, where CO_2 is a plasticizing gas, chemical and thermal cross-linking are capable of preventing plasticization in many polymer systems. This work aims to extend these studies and investigate whether thermal cross-linking can help reduce the effects of plasticization from ethane and ethylene.

1.2. Dissertation Outline

The materials and experimental methods for the results in this dissertation are provided in Chapter 2. This chapter includes the polymer synthesis procedures,

characterization methods, and experimental procedures used to analyze the materials discussed in this dissertation.

Chapter 3 focuses on developing an understanding of why thermally rearranged (TR) polymers and polymers of intrinsic microporosity (PIM) perform at or above the Robeson upper bounds for O_2/N_2 and CO_2/CH_4 separations. By comparing the transport properties of several TR polymers and PIM materials to the properties of non-upper bound materials, it was determined that the unique separation performance of these materials is due to a combination of high gas diffusivity and high gas diffusivity selectivity combined with very high gas solubility. This chapter is based on the study published in collaboration with Dr. Lloyd Robeson in the Journal of Polymer Science [12]. Additional supporting information for this chapter is included in Appendix A.

Chapter 4, Chapter 5, and Chapter 6 investigate the structure and fundamental gas transport in thermally cross-linked polyimides that contain diaminophenylindane (DAPI). The favorable transport properties of Matrimid®, a commercially available polyimide comprised of DAPI and 3,3',4,4'-benzophenone tetracarboxylic dianhydride (BTDA), are often associated with the bulky, isomeric structure of DAPI [13, 14]. This dissertation further explores the structure-property relationships of DAPI by incorporating the isomeric monomer into a polyimide with hexafluoroisopropylidene diphthalic anhydride (6FDA) and diaminobenzoic acid (DABA). In this dissertation, this polymer is referred to as 6FDA-DAPI/DABA. Including DABA in the polymer structure provides reactive acid sites for thermal cross-linking to occur [10, 14-19].

Chapter 4 focuses on the synthesis and structure characterization of the thermally cross-linked polyimides. The cross-linking mechanism and resulting cross-linked structure were investigated using thermal gravimetric analysis combined with mass spectroscopy, solid-state nuclear magnetic resonance (SS-NMR) spectroscopy, and wide angle x-ray

scattering (WAXS). Additionally, a basic study of the pure gas permeability of H_2, N_2, CH_4, O_2, CO_2, C_2H_4, and C_2H_6 in the thermally cross-linked polyimides is presented. These results revealed that permeability of all gases increase with increased cross-linking due to an increase in polymer chain d-spacing that is induced by thermal cross-linking. This chapter is based on the study submitted to Polymer [20], and additional supporting information is included in Appendix B.

Chapter 5 extends the work from Chapter 4, focusing on the pure gas sorption of N_2, CH_4, CO_2, C_2H_4, and C_2H_6 in thermal cross-linking 6FDA-DAPI/DABA and the plasticization resistance to high pressure pure CO_2, C_2H_4, and C_2H_6. To better understand how the polymer structure and thermal cross-linking effected the plasticization resistance of 6FDA-DAPI/DABA, a mixed gas permeation study was conducted using a gas feed mixture of 50:50 (mol:mol) of C_2H_4 and C_2H_6. While no significant plasticization from pure C_2H_4 and C_2H_6 was measured in cross-linked 6FDA-DAPI/DABA, mixed gas permeation measurements showed the linear polymer was more resistant to plasticization than the linear polymer. This chapter is based on the study in preparation for submission to the Journal of Membrane Science [21], and additional supporting information for this work is included in Appendix C.

Chapter 6 further investigates the fundamental transport of CO_2, C_2H_4, and C_2H_6 in thermally cross-linked 6FDA-DAPI/DABA. The volumetric dilation of the polymers from CO_2, C_2H_4, and C_2H_6. By combining the volumetric dilation data with the gas sorption data presented in Chapter 5, we were able to determine the partial molar volume of the penetrants dissolved in the polymer. Additionally, the trends in diffusion coefficients of CO_2, C_2H_4, and C_2H_6 were investigated. The results from these studied revealed that the smaller inter-chain spacing of linear 6FDA-DAPI/DABA more readily excluded C_2H_6 from the free volume elements, thus reducing the about of plasticization, and correlating

with the mixed gas permeation results that were presented in Chapter 5. This chapter is based on the study being prepared for submission to the Journal of Polymer Science Part B: Polymer Physics [22], and additional supporting information for this work is included in Appendix D. The conclusions from Chapter 3 – Chapter 6 are summarized and presented with recommendations for future work in Chapter 7.

Appendix E focuses on investigating the effect processing history has on TR polymers and their precursors. This was performed by preparing TR polymer films using three different solvents and four different casting procedures. While no significant difference in fractional free volume was measured, CO_2 and CH_4 permeability varied by 40% between the films cast using different solvents and procedures. However, it was found that the different transport properties correlated qualitatively with the residual solvent remaining in the polymer when a solid film was formed during casting.

Appendix F briefly discusses use of UV cross-linked poly(arylene ether ketone)s (PAEKs) for C_2H_4/C_2H_6 separation. It However, due to non-homogeneous UV exposure and cross-linking, it was difficult to isolate how UV cross-linked affects the plasticization resistance of PAEKs. Additionally, the PAEKs studied exhibited both low permeability and low C_2H_4/C_2H_6 selectivity, making them unfavorable polymers for olefin/paraffin separations.

1.3. REFERENCES

[1] R.L. Burns, W.J. Koros, Defining the Challenges for C_3H_6/C_3H_8 Separation Using Polymeric Membranes, Journal of Membrane Science, 211 (2003) 299-309.

[2] K. Tanaka, A. Taguchi, J. Hao, H. Kita, K. Okamoto, Permeation and Separation Properties of Polyimide Membranes to Olefins and Paraffins, Journal of Membrane Science, 121 (1996) 197-207.

[3] B.R. Eldridge, Olefin/Paraffin Separation Technology: A Review Industrial & Engineering Chemistry Research, 32 (1993) 2208-2212.

[4] L.M. Robeson, Correlation of Separation Factor Versus Permeability for Polymeric Membranes, Journal of Membrane Science, 62 (1991) 165-185.

[5] L.M. Robeson, The Upper Bound Revisited, Journal of Membrane Science, 320 (2008) 390-400.

[6] B.D. Freeman, Basis of Permeability/Selectivity Tradeoff Relations in Polymeric Gas Separation Membranes, Macromolecules, 32 (1999) 375-380.

[7] J.H. Petropoulos, Mechanisms and Theories for Sorption and Diffusion of Gases in Polymers, in: Polymeric Gas Separation Membranes, CRC Press, Inc, Boca Raton, FL, 1994.

[8] A. Bos, I.G.M. Pu, M. Wessling, S. H, Suppression of CO_2 Plasticization by Semiinterpenetrating Polymer Network Formation, Journal of Polymer Science Part B: Polymer Physics, 36 (1997) 1547-1556.

[9] A. Bos, I. Pünt, H. Strathmann, M. Wessling, Suppression of Gas Separation Membrane Plasticization by Homogeneous Polymer Blending, AIChE Journal, 47 (2001) 1088-1093.

[10] C. Staudt-Bickel, W. J. Koros, Improvement of CO_2/CH_4 Separation Characteristics of Polyimides by Chemical Crosslinking, Journal of Membrane Science, 155 (1999) 145-154.

[11] C. Zhou, The Accelerated CO_2 Plasticization of Ultra-Thin Polyimide Films and the Effect of Surface Chemical Cross-linking on Plasticization and Physical Aging, Journal of Membrane Science, 225 (2003) 125-134.

[12] L.M. Robeson, M.E. Dose, B.D. Freeman, D.R. Paul, Analysis of the Transport Properties of Thermally Rearranged (TR) Polymers and Polymers of Intrinsic Microporosity (PIM) Relative to Upper Bound Performance, Journal of Membrane Science, 525 (2017) 18-24.

[13] I.V. Farr, Synthesis and Characterization of Novel Polyimide Gas Separation Membrane Material Systems, Virginia Polytechnic Institute and State University 1999.

[14] I.V. Farr, D. Kratzner, T.E. Glass, D. Dunson, Q. Ji, J.E. McGrath, The Synthesis and Characterization of Polyimide Homopolymers Based on 5(6)-Amino-1-(4-Aminophenyl)1,3,3-Trimethylindane, Journal of Polymer Science Part A: Polymer Chemistry, 38 (2000) 2840-2854.

[15] N.L. Le, Y. Wang, T.-S. Chung, Synthesis, Cross-linking Modifications of 6FDA-NDA/DABA Polyimide Membranes for Ethanol Dehydration via Pervaporation, Journal of Membrane Science, 415-416 (2012) 109-121.

[16] A.M. Kratochvil, W.J. Koros, Decarboxylation-Induced Cross-Linking of a Polyimide for Enhanced CO_2 Plasticization Resistance, Macromolecules, 41 (2008) 7920-7927.

[17] C. Zhang, P. Li, B. Cao, Decarboxylation Crosslinking of Polyimides with High CO_2/CH_4 Separation Performance and Plasticization Resistance, Journal of Membrane Science, 528 (2017) 206-216.

[18] W. Qiu, C.-C. Chen, L. Xu, L. Cui, D.R. Paul, W.J. Koros, Sub-Tg Cross-Linking of a Polyimide Membrane for Enhanced CO_2 Plasticization Resistance for Natural Gas Separation, Macromolecules, 44 (2011) 6046-6056.

[19] N. Du, M.M. Dal-Cin, G.P. Robertson, M.D. Guiver, Decarboxylation-Induced Cross-Linking of Polymers of Intrinsic Microporosity (PIMs) for Membrane Gas Separation, Macromolecules, 45 (2012) 5134-5139.

[20] M.E. Dose, M. Chwatko, I. Hubacek, N.A. Lynd, D.R. Paul, B.D. Freeman, Thermally Cross-linked Diaminophenylindane (DAPI) Containing Polyimides for Membrane Based Gas Separations, Polymer, Submitted (2018).

[21] M.E. Dose, I. Hubacek, D.R. Paul, B.D. Freeman, CO_2, C_2H_4, and C_2H_6 Sorption and Mixed Gas Permeability of Thermally Cross-linked Diaminophenylindane (DAPI) Containing Polyimides, Journal of Membrane Science, Submitted (2018).

[22] M.E. Dose, J.D. Moon, I. Hubacek, D.R. Paul, B.D. Freeman, Fundamental Gas Transport and Dilation of Studies in Thermally Cross-linked Diaminophenylindane (DAPI) Containing Polyimides, Journal of Polymer Science Part B: Polymer Physics, In Preparation (2018).

Chapter 2: Materials and Experimental Methods

This chapter describes the materials and experimental methods used throughout this dissertation. This materials section describes the synthesis, casting, and treatments of all the polymers used in this work and the experimental section describes the characterization techniques, permeability experiments, gas sorption experiments, and high pressure gas dilation measurements. [1]

[1] This chapter has been adapted with permission from sections of (1) M.E. Dose, M. Chwatko, I. Hubacek, N.A. Lynd, D.R. Paul, B.D. Freeman, Thermally Cross-linked Diaminophenylindane (DAPI) Containing Polyimides for Membrane Based Gas Separations, Polymer, Submitted (2018). (2) M.E. Dose, I. Hubacek, D.R. Paul, B.D. Freeman, CO_2, C_2H_4, and C_2H_6 Sorption and Mixed Gas Permeability of Thermally Cross-linked Diaminophenylindane (DAPI) Containing Polyimides, Journal of Membrane Science, In Preparation (2018). (3) M.E. Dose, J.D. Moon, I. Hubacek, D.R. Paul, B.D. Freeman, Fundamental Gas Transport and Dilation Studies in Thermally Cross-linked Diaminophenylindane (DAPI) Containing Polyimides, Journal of Polymer Science Part B: Polymer Physics, In Preparation (2018). For each of these publications, I was the primary author, developed the experimental design, conducted the experiments, and preformed most of the analysis. The co-authors from these papers contributed to the analysis and helped run supporting experiments.

2.1. MATERIALS

2.1.1. Polymer Synthesis

2.1.1.1. Reactants

Ethanol, triethylamine (TEA), n-methyl-2-pyrrolidone (NMP), o-dichlorobenzene (o-DCB), and acetic anhydride were used as-received from Sigma Aldrich. Methanol, ≥ 99.8% ACS grade, was used as-received from BDH Chemicals. Hexafluoroisopropylidene diphthalic anhydride (6FDA) was purchased from Alfa Aesar and dried at 200°C for 6 h under partial vacuum, then held at 150°C under full vacuum overnight to cyclize any residual diacid moieties. Diaminophenylindane (DAPI) was provided by Dottikon Exclusive Synthesis (Dottikon, Switzerland) and dried at 60°C under full vacuum overnight. Diaminobenzoic acid (DABA) was purchased from Sigma Aldrich and dried at 150°C under full vacuum overnight.

2.1.1.2. Synthesis of 6FDA-DAPI

6FDA-DAPI was synthesized via an ester-acid route presented in Figure 2.1 [4, 5]. A three-neck flask fitted with a Dean-Stark trap, a condenser, a mechanical stirrer, and a nitrogen inlet was used as the reaction vessel. 6FDA (10.0 mmol, 4.4424 g), excess ethanol (1200 mmol, 70 mL), and excess TEA (40 mmol, 5.3 mL) were reacted under reflux conditions for 1 h to form the ester-acid of the dianhydride. Excess ethanol and TEA were distilled, leaving a viscous ester-acid solution in the reaction vessel. The diamine, DAPI (10.2 mmol, 2.7170 g), was added in slight molar excess to account for slight impurities in the monomer. NMP (50 mL) and *o*-DCB (10 mL) were added to achieve 10 wt% solids, and the Dean-Stark trap was filled with the azeotroping solvent, *o*-DCB. To synthesize the polyimide, the solution was held at 180°C for 24 h, forming a viscous solution. After cooling, the solution was precipitated into methanol while stirring, vacuum filtered, soaked

in fresh methanol overnight to remove any residual solvent, and then vacuum filtered again. The resulting powder was dried at 180°C under vacuum for 24 h.

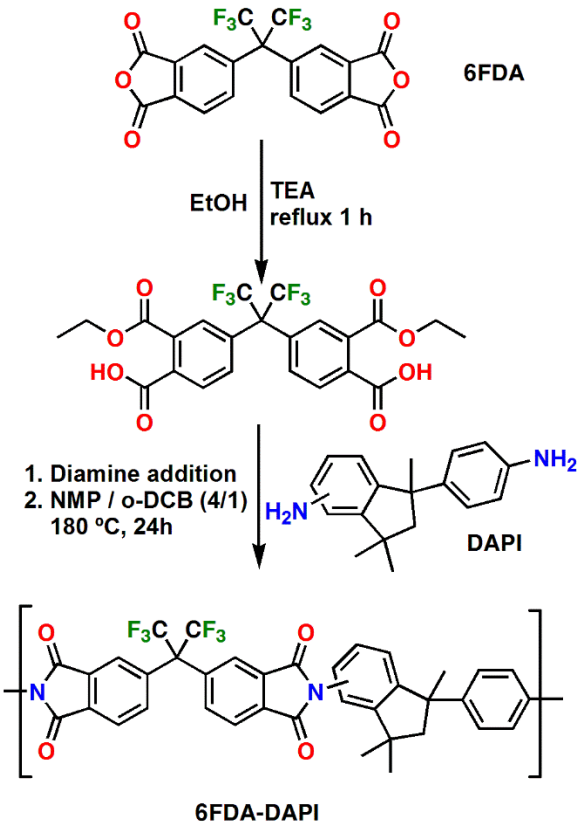

Figure 2.1. 6FDA-DAPI ester acid synthetic route.

2.1.1.3. Synthesis of 6FDA-DAPI/DABA

A polyimide was synthesized from 6FDA, DAPI, and DABA in a 0.5/0.33/0.17 molar ratio, referred to as 6FDA-DAPI/DABA, was synthesized via a chemical imidization route (Figure 2.2). Chemical imidization was used to minimize temperatures needed to form the polyimide and prevent potential reaction of the carboxylic acid moiety on DABA in solution. DAPI (6.66 mmol, 1.7758 g), DABA (3.33 mmol, 0.5072 g), and NMP (16 mL) were added to a three-neck flask fitted with a Dean-Stark trap, a condenser, a

mechanical stirrer, and a nitrogen inlet. After the diamines completely dissolved, the reaction flask was placed in an ice bath. Then, 6FDA (10.00 mmol, 4.4424 g) was slowly added over 2 h, and additional NMP (10 mL) was added to bring the solution to 20 wt% solids. Over 24 h, the reaction mixture rose back to room temperature, and the polyamic acid formed. To cyclize the polyamic acid, acetic anhydride (60 mmol, 5.7 mL) and TEA (60 mmol, 8.4 mL) were added along with additional NMP to bring the solution to 10 wt% solids. The solution was heated to 60°C for 24 h, cooled to room temperature, and precipitated in stirred methanol. After soaking in fresh methanol overnight, the resulting polymer powder was vacuum filtered and dried at 180°C under vacuum for 24 h. Based on previous studies and no apparent phase separation in cast films, 6FDA-DAPI/DABA is believed to be a random co-polymer [1-6].

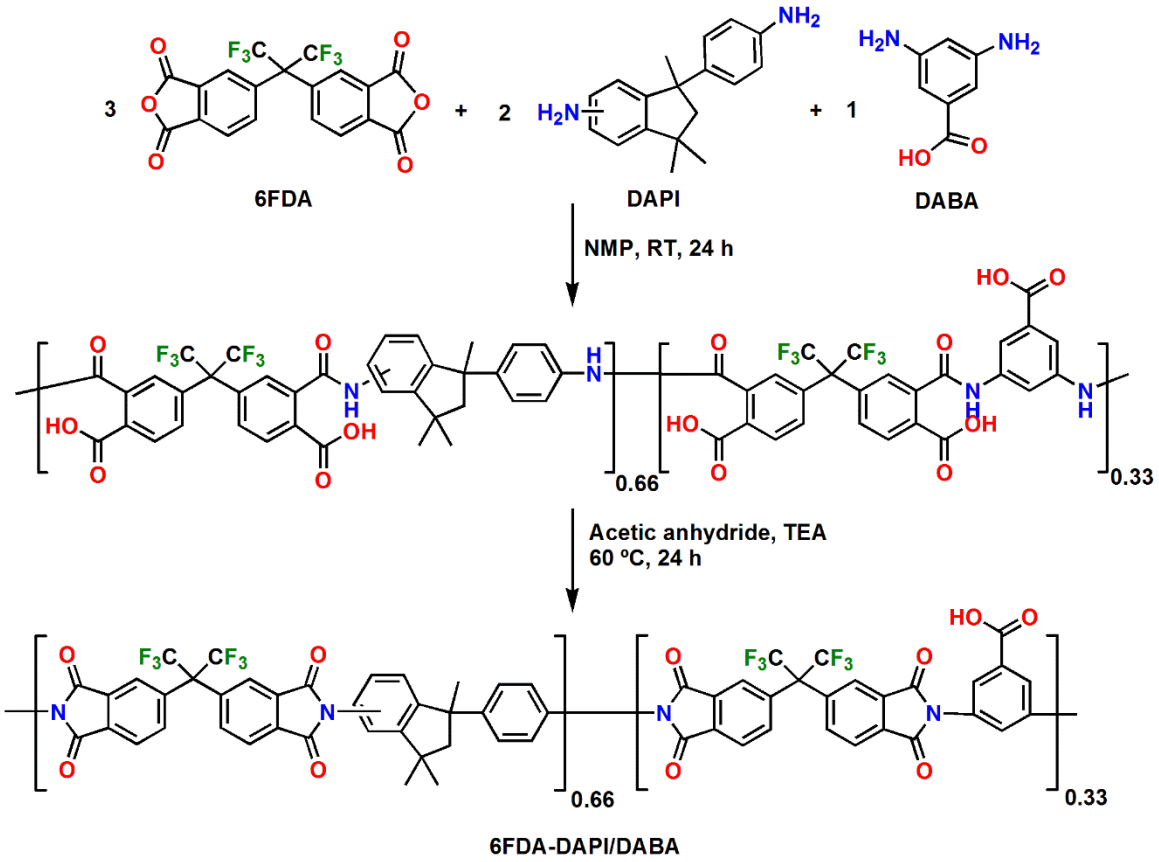

Figure 2.2. 6FDA-DAPI/DABA chemical imidization synthetic route

2.1.2. Film Casting

Dense polymer films 15 – 25 µm thick were formed by dissolving the polyimides in tetrahydrofuran (THF, Sigma Aldrich, anhydrous) to prepare a 2 wt% solution. Particulates were removed by filtering the solution through a 1.2 µm Titan3^{TM} GMF syringe filter, and the solution was cast onto a glass plate inside a THF saturated glove bag to slow solvent evaporation. After solvent evaporation, the dense polymer film was removed from the glass plate, and residual solvent was removed by heating the sample to 220°C under full vacuum for 24 h. Solvent removal was confirmed using thermogravimetric analysis, and no mass loss was observed prior to that associated with thermal decarboxylation.

2.1.3. Thermal Cross-linking

Polyimide films were cross-linked by thermal decarboxylation, which is reported to proceed according to the mechanism shown in Figure 2.3 [14, 15, 17]. To cross-link a film, it was heated in a tube furnace under a flow of N2 (~90 cm3/min) at a rate of 40°C/min to 15°C above the glass transition temperature of the cross-linked film, held for 10 – 40 min, and then rapidly quenched by quickly removing the sample from the furnace and cooling to room temperature. To prevent curling, samples were placed between two ceramic plates in the tube furnace. As the DABA-containing polyimide underwent cross-linking, its mass decreased. To quantify the conversion to the cross-linked structure, the degree of cross-linking was defined according to Eq. 2.1.

$$\% XL = \frac{Actual\ Mass\ Loss}{Theoretical\ Mass\ Loss} x\ 100 \qquad \text{Eq. 2.1}$$

The "Actual Mass Loss" is the mass loss observed by weighing the sample before and after the thermal treatment described above, and the "Theoretical Mass Loss" is the mass loss expected if the reaction shown in Figure 2.3 were to proceed to completion. Gel fractions were determined using a Soxhlet extractor (Wilmad-LabGlass, P/N LG-6900-100) with THF as the solvent. Samples were refluxed in THF for 24 h, or until the sample was fully dissolved. After drying at 220°C for 24 h, the gel fraction was calculated by dividing the final dry mass after solvent exposure by the initial sample mass.

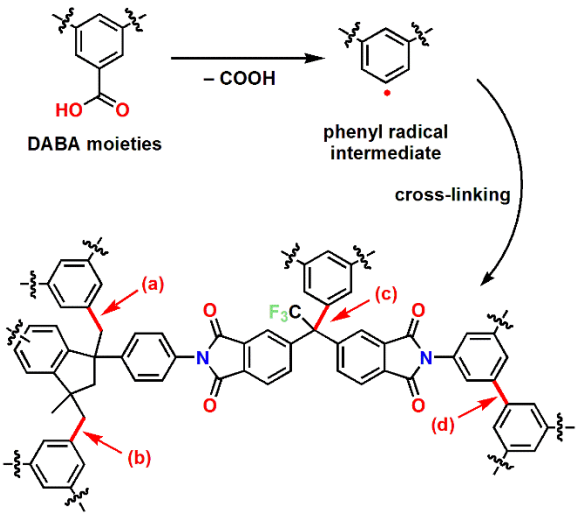

Figure 2.3 Potential cross-linking mechanisms for DABA moieties through thermal decarboxylation for 6FDA-DAPI/DABA [3, 5, 7].

2.1.4. Fugacity of Non-Ideal Gases and Gas Mixtures

The fugacity coefficients for pure gases were calculated using the NIST Reference Fluid Thermodynamic and Transport Properties Database (REFPROP). The fugacity was calculated using Eq. 2.2 and Eq. 2.3, where Figure 2.4 details the compressibility factors, Z_i, for N_2, CH_4, C_2H_4, and C_2H_6 calculated using the REFPROP equation of state.

$$\ln(\phi_i) = \int_0^p (Z_i - 1)\frac{dp}{p} \qquad \text{Eq. 2.2}$$

$$f_i = \phi_i p_i \qquad \text{Eq. 2.3}$$

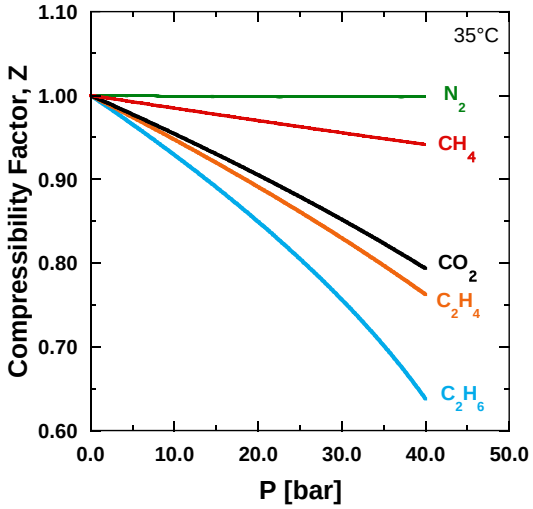

Figure 2.4. Compressibility factors, Z_i, vs pressure for N_2 [green], CH_4 [red], CO_2 [black], C_2H_4 [orange], and C_2H_6 [light blue], determined using the REFPROP equation of state at 35°C [8].

Similar to pure gas fugacity, the REFPROP equation of state from Aspen was used to determine the fugacity of a 50:50 molar mixture of C_2H_4 and C_2H_6, given a system pressure. The pure and mixed gas fugacity for C_2H_4 and C_2H_6 are compared in Figure 2.5.

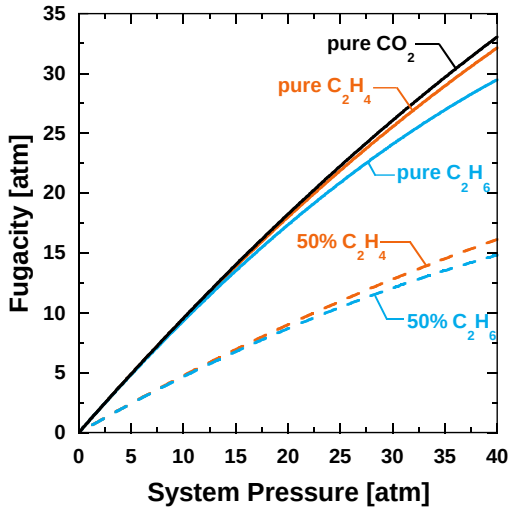

Figure 2.5. Pure (solid) and mixed (dashed) gas fugacity for C_2H_4 (orange), C_2H_6 (blue), and CO_2 (black) verses system pressure at 35°C, determined using the REFPROP equation of state from Aspen.

2.1.5. Pure Gas Permeability and Selectivity Measurements

Permeability and selectivity are intrinsic properties used to characterize separation performance of polymeric membranes. Permeability is a measure of the membrane productivity, where permeability of species i, P_i, through a dense film is defined as the molar flux, J_i, though the membrane normalized by the partial pressure difference across the film, Δp_i, and the film thickness, ℓ, as shown in Eq. 2.4.

$$P_i = \frac{J_i \ell}{\Delta p_i} \qquad \text{Eq. 2.4}$$

For non-ideal gases under high pressure, it is more appropriate to describe the driving force for permeation using a fugacity difference, Δf_i, rather than a partial pressure difference. The units of Barrer were used to describe permeability, where 1 Barrer = 10^{-10} $cm^3(STP) \cdot cm / (s \cdot cm^2 \cdot cmHg)$. Ideal selectivity between two gases, *i* and *j*, is used to describe the

separation efficiency of a polymer and is defined as the ratio of their pure gas permeabilities, as described in Eq. 2.5.

$$\alpha_{i/j} = \frac{P_i}{P_j} \qquad \text{Eq. 2.5}$$

Gas transport following dual-mode behavior, typical of glassy polymers, predicts a decrease in permeability at low partial pressure driving force and approaches a constant value at higher pressures [9]. However, highly condensable and strongly sorbing gases, like CO_2, C_2H_4, and C_2H_6, can interact strongly with the polymer and induce plasticization, or swelling of the polymer matrix, at high pressures.

Pure gas permeabilities of H_2, CH_4, N_2, O_2, CO_2, C_2H_4, and C_2H_6 were measured at 35°C over a pressure range of 3 – 45 atm using a constant volume, variable pressure method [10]. The permeability of each gas was determined using Eq. 2.6,

$$P_i = \frac{V\ell}{fRTA}\left[\left(\frac{dp}{dt}\right)_{SS} - \left(\frac{dp}{dt}\right)_{leak}\right] \qquad \text{Eq. 2.6}$$

where V is the downstream volume, ℓ is the sample thickness, f is the fugacity of the gas feed calculated from the REFPROP equation of state [8], T is the absolute temperature, A is the sample area, $(dp/dt)_{SS}$ is the steady state pressure rise in the downstream volume, and $(dp/dt)_{leak}$ is the system leak rate [10].For this work, each pure gas was tested at the same pressure points and each pressure point was held for 6 times the time lag while the downstream was kept under near vacuum (<10 Torr) for the entire test [10]. The gases were tested in the previously mentioned order and a new sample was used after exposure to CO_2, C_2H_4, and C_2H_6. To check reproducibility, H_2 was measured on each new sample to ensure transport properties were consistent among samples of the same material.

The upstream pressure was monitored using a 1000 psig STJE pressure transducer (Honeywell Sensotec, Columbus, OH USA), and the downstream pressure was monitored

using a capacitance manometer (Baratron 626A, MKS Instruments, Andover, MA USA). Membranes were masked using a brass disk and sealed with epoxy (Devcon, No. 145250, Danvers, MA USA) to provide a well-defined area [10]. All measurements were made at 35°C with UHP grade gases (Airgas, Radnor, PA USA) and each pressure point was held for 6 times the time lag to ensure steady state was achieved [10].

2.1.6. Mixed Gas Permeability and Selectivity Measurements

Mixed gas permeabilities were measured on the apparatus illustrated in Figure 2.6, and was operated in a similar manor as described by O'Brian et al. [11], for a mixture of 50:50 C_2H_4 and C_2H_6 (Airgas, Radnor, PA USA). Each pressure point was held for six times the time lag determined from pure C_2H_6 permeation experiments, collecting the permeate only after steady state was achieved. The permeate concentrations were measured five times for each data point and were determined using an Agilent 7890A (Santa Clara, CA USA) equipped with a Gow-Mac (Bethlehem, PA USA) thermal conductivity detector (TCD) and an Agilent Porapak Q packed column (5 ft, 0.318 in ID).

Figure 2.6 details the schematic of the mixed gas permeation instrument used for the mixed gas permeation measurements in this work. The pressure of the upstream feed gas was regulated at the cylinder and monitored using a 1000 psig pressure transducer, P1 (STJE, Honeywell Sensotec, Columbus, OH, USA). The flow rate was manually controlled using a regulating needle valve located after the permeation cell and monitored using a bubble flow meter. The total membrane flux was measured using a constant volume variable pressure method and the temperature of the permeation cell and the system downstream were held at 35°C using a water bath. The downstream pressure, P2, was

monitored using a 10 Torr capacitance manometer (Baratron 626A, MKS Instruments, Andover, MA USA). A cross-over valve was used to allow the feed gas to either bypass (position 2) or pass through the permeation cell (position 1).

Upstream gas flow rates were chosen to be high enough to prevent concentration polarization at the upstream face of the film. At least two upstream flowrates were tested to ensure there was no dependence of the gas permeation rates on the gas feed flowrate. For the mixed gas permeation measurements in this work, the stage cut (ratio of the upstream flow rate to the permeation rate) was less than 0.1%. To start a mixed gas measurement, the membrane was first degassed for a minimum of 18 h by pulling vacuum on the upstream and downstream faces of the sample, leaving V1, V2, V4, V11, and V12 closed, placing the crossover valve such that permeation cell is open to vacuum, and the remaining valves were open. Depending on the expected flux through the sample, the auxiliary volumes were left open/closed as needed. The system leak rate was measured by closing valves V1, V2, V3, V4, V5, V6, and V9 for at least 1 h, measuring the rate of the upstream and downstream pressure rise. To start a permeation measurement, the cross-over valve was set to bypass, valves V2, V3, V5, V6, and V9 were closed, and V1 and V10 were opened. The feed pressure was then set at the cylinder and V2 was opened, using the regulating valve to set the feed flowrate. After setting the feed pressure and flowrate, the cross-over valve was switched to expose the upstream face of the sample to the test gas, starting the permeability experiment. The upstream and downstream pressures were recorded using LABVIEW. To ensure steady state was achieved, the pressure steps were held for 6θ, where θ is the time lag determined for pure C_2H_6 permeation. After 1.5θ, the

downstream was evacuated by opening V6 for 5 min to ensure all non-steady state permeate was removed from the downstream. Then V6 was closed and steady state permeate was collected in the downstream for the remaining 4.5θ. After the permeation measurement was complete, the permeate was then transferred to the evacuated GC sample charging volume by closing V7 and V8 and opening V9. The GC sample charging volume pressure, P3, was monitored using a 10 Torr capacitation manometer. Once pressure equilibrated between the downstream and the GC charging volume, V9 was closed and V8 was opened to feed a portion of the sample gas to the evacuated TCD sample loop, and the concentration was measured using the GC. A total of 5 GC measurements were made on each permeate sample.

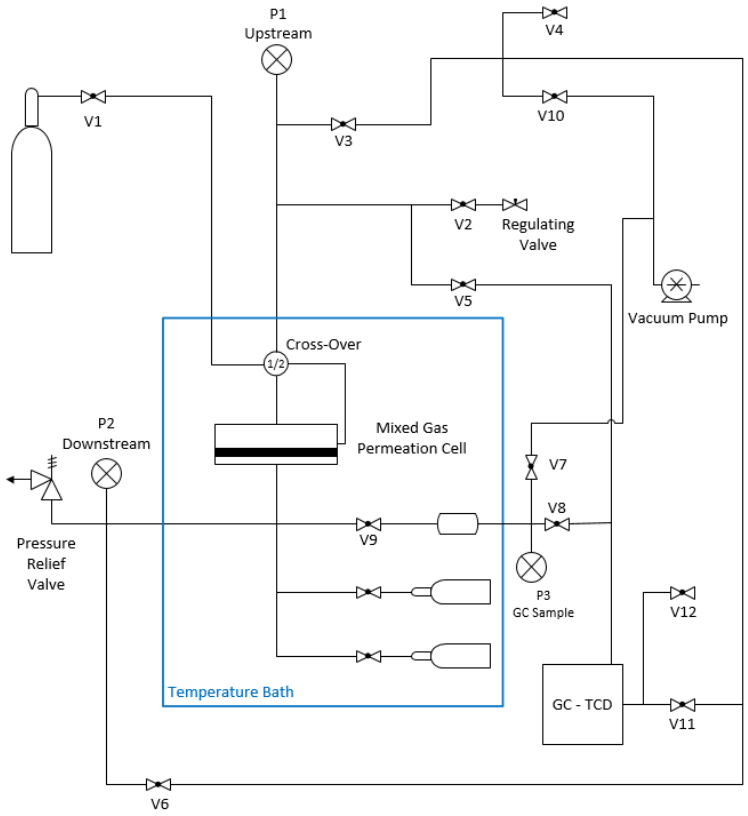

Figure 2.6. Mixed Gas Permeation Schematic

Mixed gas permeability of gas i, P_i, was calculated using the following equation:

$$P_i = \frac{V\ell y_i}{f_i RTA}\left[\left(\frac{\partial p}{\partial t}\right)_{ss} - \left(\frac{\partial p}{\partial t}\right)_{leak}\right] \qquad \text{Eq. 2.7}$$

where V is the downstream volume of the system, ℓ is the sample thickens, y_i is permeate molar fraction of species i, f_i is the upstream fugacity of species i, R is the universal gas constant, T is the system temperature (35°C), A is the sample area, and $(\partial p/\partial t)_{ss}$ and $(\partial p/\partial t)_{leak}$ are the rates of pressure rise in the downstream volume during steady state and leak tests, respectively. To account for non-idealities in mixed gas, the REFPROP equation of state was used to calculate the ethane and ethylene fugacity for a 50:50 C_2H_4:C_2H_6 mixture, as shown in Figure 2.5.

Mixed gas selectivity, $\alpha^*_{i/j}$, was calculated using the following equation:

$$\alpha^*_{i/j} = \frac{y_i/y_j}{x_i/x_j} \quad \text{Eq. 2.8}$$

where y_i and y_j are the downstream mol fractions and x_i and x_j are the upstream mol fractions of species i and j, respectively. For 50:50 feed mixtures, as used in this work, Eq. 2.8 reduces to the ideal gas selectivity expression, Eq. 2.5.

2.1.7. Pure Gas Sorption Measurements

The pure gas solubility of N_2, CH_4, CO_2, C_2H_4, and C_2H_6 were determined at 35°C using a dual-volume pressure decay apparatus [10]. A minimum of 0.3 g of polymer was placed in the sample cell and the entire system was degassed for at least 18 h. After isolating the sample cell from the charging cell, the charging cell was filled with the target gas. Then the target gas was introduced to the sample cell by briefly opening and closing the valve between the charging and sample volumes. The pressure in the charging and sample cells were monitored using two 500 psig STJE pressure transducers (Honeywell Sensotec, Columbus, OH USA). After equilibrium was reached, more gas was introduced to the charging cell and the experiment was repeated in a stepwise manor until a maximum pressure of about 30 atm was reached. The difference between the initial and final pressures in the charging and sample cells were used to perform a mole balance and determine the gas concentration in the polymer phase at equilibrium [10]. After the sorption isotherm was collected, the system was evacuated in preparation for the next gas. To avoid effects of conditioning from potentially plasticizing gases, fresh samples were installed after exposure to CO_2, C_2H_4, or C_2H_6. CH_4 sorption was measured on the new sample to ensure continuity between samples. To account for non-ideal gas behavior, the equilibrium pressures were corrected using the NIST Reference Fluid Thermodynamic and Transport Properties Database (REFPROP) equation of state (cf., Figure 2.4).

The sorption data were fit to the dual-mode sorption model using a weighted least squares non-linear fit with Wolfram Mathematica software (WolframAlpha, Champaign, IL USA):

$$C = k_D f + \frac{C'_H b f}{1 + bf} \quad \text{Eq. 2.9}$$

Where C is the concentration of penetrant per volume of polymer, f is the fugacity, k_D is the Henry's law solubility constant, C'_H is the Langmuir capacity constant, and b is the affinity constant [9]. The parameters k_D and b were not constrained to trends with critical temperature as the quality of fit to the data were significantly reduced. The apparent solubility coefficient, S, for a penetrant is defined as the penetrant concentration, C, divided by the pressure, or fugacity, as shown in Eq. 2.10 [9].

$$S = \frac{C}{f} \quad \text{Eq. 2.10}$$

Permeability, P_i, in dense films is the product of the penetrant solubility coefficient, S_i, and diffusion coefficient, D_i [12]:

$$P_i = S_i \cdot D_i \quad \text{Eq. 2.11}$$

The ideal permeability selectivity, $\alpha_{i/j}$, between two gases, i and j, is defined as the ratio of their pure gas permeabilities, P_i/P_j [12]. When combined with Eq. 2.5, permeability selectivity can be separated in solubility selectivity, S_i/S_j, and diffusivity selectivity, D_i/D_j, as shown below:

$$\alpha_{i/j} = \frac{P_i}{P_j} = \frac{S_i}{S_j} \cdot \frac{D_i}{D_j} \quad \text{Eq. 2.12}$$

2.1.8. Polymer Dilation from High Pressure Gas

Pure gas polymer dilation at high pressures were measured using the same apparatus adopted by Raharjo et al. and Rubeiro et al. [13, 14]. A strip of polymer, about 70 mm in

length and 5 mm in width, was placed in the sample holder and guided by a wire track so that the polymer could freely dilate along the its length and prevent curling. The length of the polymer strip was monitored as a function of time using digital CCD camera with a 35 mm lens (DMK 23U274 and C3516-M(KP), The Imaging Source, Charlotte, NC USA). The smallest detectable change in length with this device is 0.02 mm. The dilation of all polymers was assumed to be isotropic and the fractional change in volume, $\Delta V_i/V_o$, was calculated using Eq. 2.13,

$$\frac{\Delta V_i}{V_o} = \left(\frac{L_i}{L_o}\right)^3 - 1 \qquad \text{Eq. 2.13}$$

where L_o is the initial length of the polymer, and L_i is the polymer length after equilibrating with the penetrant gas at the desired pressure. The swelling isotherms were determined using incremental pressure steps, similar to those used in the pure gas sorption experiments. To ensure the film was equilibrated with the gas, the sample was held at pressure and the sample length was monitored with time until no change in length was detected. Due to the dimensions of the apparatus viewing window and the smallest detectable change in sample width, changes in the width of the polymer samples fell within the uncertainty of the instrumentation. To ensure exposure history did not affect the measurements, a fresh sample was used for each test.

2.2. MATERIAL CHARACTERIZATION

2.2.1. Solution NMR Structure Characterization

The chemical structure of the linear polyimides was confirmed using solution ^{1}H NMR, ^{13}C NMR, and ^{1}H-^{1}H COSY NMR spectroscopy using an Agilent MR 400 MHz spectrometer, Varian Inova 500MHz, and Varian Mercury 400 MHz, respectively. A polymer was dissolved in tetrahydrofuran-d8 (Sigma-Aldrich, ≥ 99.5 %) to prepare a 5 wt% solution.

2.2.2. Solid State NMR Structure Characterization

Due to the insolubility of the cross-linked polymers, solid-state ^{13}C CP/TOSS (total suppression of spinning side bands) NMR measurements were performed using a Bruker AVANCE III HD 400 MHz instrument. A 4mm H/X cross-polarization magic-angle spinning (CP-MAS) probe was used for these experiments. Approximately equal mass of the linear and cross-linked co-polymer powdered samples were used so a direct comparison could be drawn between structures.

2.2.3. Size Exclusion Chromatography

Size exclusion chromatography (SEC) was collected on a custom Agilent system (Santa Clara, CA) with a 1260 Infinity isocractic pump, degasser, and thermostated column chamber held at 30ºC. The chamber contained Agilent PLgel 10 μm MIXED-B and 5 μm MIXED-C columns with a combined operating range of 200–10,000,000 g/mol relative to polystyrene standards. Tetrahydrofuran flowing at 0.5 mL/min was used as the mobile phase. Measurement of polymer concentration, molecular weight, and viscosity was provided by a suite of detectors from Wyatt Technologies (Santa Barbara, CA). Static light scattering was measured using a DAWN HELEOS II Peltier system, with differential refractive index measured with an Optilab TrEX, and differential viscosity measured using a Viscostar II. Refractive index increments (dn/dc) were measured with an Optilab TrEX refractometer.

2.2.4. Wide Angle X-ray Scattering

A Xenocs Ganesha small angle scattering instrument fitted with a moveable Dectris 300k detector was used to record wide angle x-ray scattering (WAXS) data. The instrument is fitted with a microfocus Cu k-alpha source operated at 50kV and 0.6mA. Data were corrected for incident beam strength by measuring I_o directly on the Dectris detector and

for sample thickness to give absolute scattering intensities. A manufacturer supplied utility, SAXSGUI was used to make the corrections and reduced the 2D detector data into intensity versus scattering angle data.

2.2.5. Fourier Transform Infrared Spectrometry

A Thermo Nicolet Nexus 470 E.S.P. Fourier transform infrared spectrometer (FT-IR) was used to characterize the linear and cross-linked polyimide films. FT-IR was conducted in transmission mode or absorbance mode at a spectral resolution of 4 cm^{-1}, 256 scans, were collected for each spectrum

2.2.6. Thermal Gravimetric Analysis with Mass Spectrometry

The thermal stability and mass loss associated with thermal crosslinking of the polyimides was monitored using a TA Instruments Q500 thermogravimetric analyzer coupled with a Thermostar GSD 320 mass spectrometer (TGA-MS). TGA-MS scans were conducted under nitrogen (Airgas, 99.999 %, 60 mL/min) between 40-800°C using 5°C/min heating rate.

2.2.7. Differential Scanning Calorimetry

The heat flow and glass transition temperatures (T_g) were estimated from the first, second, and third scans using a TA Instruments Q100 differential scanning calorimeter (DSC). The DSC samples were heated at 10°C/min from 25-400°C under nitrogen (Airgas, 99.999 %, 50 mL/min). T_g values are reported as the midpoint of the step change in heat capacity for each of the scans.

2.2.8. Density Measurements

Density was determined by Archimedes' principle using a density measurement kit (Mettler-Toledo GmbH, P706039, Columbus, OH) and a Mettler-Toledo Balance (ME-T

Analytical Balance, Columbus, OH). The buoyant liquid used for the measurement was *n*-heptane (Sigma, >99 %); the total *n*-heptane uptake in the samples was <1%. Eight separate measurements were made for each sample, and the propagation of error method was used to estimate the uncertainty in density values [15].

2.3. REFERENCES

[1] C. Staudt-Bickel, W. J. Koros, Improvement of CO_2/CH_4 Separation Characteristics of Polyimides by Chemical Crosslinking, Journal of Membrane Science, 155 (1999) 145-154.

[2] N.L. Le, Y. Wang, T.-S. Chung, Synthesis, Cross-linking Modifications of 6FDA-NDA/DABA Polyimide Membranes for Ethanol Dehydration via Pervaporation, Journal of Membrane Science, 415-416 (2012) 109-121.

[3] A.M. Kratochvil, W.J. Koros, Decarboxylation-Induced Cross-Linking of a Polyimide for Enhanced CO_2 Plasticization Resistance, Macromolecules, 41 (2008) 7920-7927.

[4] S.H. Han, N. Misdan, S. Kim, C.M. Doherty, A.J. Hill, Y.M. Lee, Thermally Rearranged (TR) Polybenzoxazole: Effects of Diverse Imidization Routes on Physical Properties and Gas Transport Behaviors, Macromolecules, 43 (2010) 7657-7667.

[5] N. Du, M.M. Dal-Cin, G.P. Robertson, M.D. Guiver, Decarboxylation-Induced Cross-Linking of Polymers of Intrinsic Microporosity (PIMs) for Membrane Gas Separation, Macromolecules, 45 (2012) 5134-5139.

[6] C. Zhang, P. Li, B. Cao, Decarboxylation Crosslinking of Polyimides with High CO_2/CH_4 Separation Performance and Plasticization Resistance, Journal of Membrane Science, 528 (2017) 206-216.

[7] W. Qiu, C.-C. Chen, L. Xu, L. Cui, D.R. Paul, W.J. Koros, Sub-Tg Cross-Linking of a Polyimide Membrane for Enhanced CO_2 Plasticization Resistance for Natural Gas Separation, Macromolecules, 44 (2011) 6046-6056.

[8] E.W. Lemmon, M.O. McLinden, D.G. Friend, Thermophysical Properties of Fluid Systems, in: P.J. Linstrom, W.G. Mallard (Eds.) NIST Chemistry WebBook, NIST Standard Reference Database Number 69, National Institute of Standards and Technology, Gaithersburg MD, 2018.

[9] D.R. Paul, Gas Sorption and Transport in Glassy Polymers, Reports of the Bunsen Society for Physical Chemistry, 83 (1979) 294-302.

[10] H. Lin, B.D. Freeman, Chapter 7: Permeation and Diffusion, in: Springer Handbook of Materials Measurement Methods, 2006, pp. 371-387.

[11] K.C. O'Brien, W.J. Koros, T.A. Barbari, A New Technique for the Measurement of Multicomponent Gas Transport Through Polymeric Films, Journal of Membrane Science, 29 (1986) 229-238.

[12] J.G. Wijmans, R.W. Baker, The Solution-Diffustion Model: A Review, Journal of Membrane Science, 107 (1995) 1-21.

[13] C.P.R. Jr., B.D. Freeman, Sorption, Dilation, and Partial Molar Volumes of Carbon Dioxide and Ethane in Cross-Linked Poly(ethylene oxide), Macromolecules, 41 (2008) 9458-9468.

[14] R. Raharjo, B. Freeman, E. Sanders, Pure and Mixed Gas CH_4 and n-C_4H_{10} Sorption and Dilation in Poly(dimethylsiloxane), Journal of Membrane Science, 292 (2007) 45-61.

[15] P.R. Bevington, D.K. Robinson, Error Analysis, in: Data Reduction and Error Analysis, McGraw-Hill, New York, NY, 2003, pp. 36-50.

Chapter 3: Analysis of the Transport Properties of Thermally Rearranged (TR) Polymers and Polymers of Intrinsic Microporosity (PIM) Relative to Upper Bound Performance

A critical analysis comparing the diffusion selectivity, solubility selectivity, diffusivity, and solubility coefficients of thermally rearranged (TR) polymers and polymers of intrinsic microporosity (PIM), two types of polymers which consistently perform at or beyond the polymer upper bound for certain gas pairs (O_2/N_2 and CO_2/CH_4), is reported here. Although most polymers in these two classes exhibit transport properties in the range of typical glassy polymers, several variants offer exceptional performance. The diffusivity selectivity for O_2/N_2 and CO_2/CH_4 for TR polymers and PIM lies outside the range of the glassy polymer database. The solubility coefficients for O_2 are at the upper end of the range of both TR and PIM polymers, as is also the case for CO_2 solubility coefficients for PIM polymers. The O_2/N_2 and CO_2/CH_4 solubility selectivities for both PIM and TR polymers are in the range of typical glassy polymers. Thus, unique separation values for these polymers are a manifestation of maximizing diffusivity selectivity combined with very high gas solubility. Additionally, the previously determined diffusion gas kinetic diameters, d_g, were found to correlate best with diffusion coefficients of PIM and TR polymers and serve to better analyze transport properties of upper bound materials.[2]

[2]This chapter has been adapted with permission from sections of: Lloyd M. Robeson, Michelle E. Dose, Benny D. Freeman, Donald R. Paul, Analysis of the transport properties of thermally rearranged (TR) polymers and polymers of intrinsic microporosity (PIM) relative to upper bound performance, Journal of Membrane Science, Volume 525, 1 March 2017, Pages 18-24. For this publication, I was the primary author and contributed significantly to the analysis. Lloyd M. Robeson gathered most of the literature data and preformed the initial analysis that served as the foundation for this paper. The remaining co-authors from contributed to the analysis.

3.1. INTRODUCTION

Polymer membranes were first used for gas phase separations on a commercial scale in the late 1970s by Permea, now Air Products and Chemicals Inc., with the use of their Prism® membranes systems for hydrogen recovery from ammonia plant purge streams [1-3]. As of 2016, commercial membrane systems are now employed in many applications, including separation of gas pairs such as O_2/N_2, CO_2/CH_4, H_2/N_2, H_2/CO_2, He/air, and H_2O/natural gas [1-5].

The limits of polymer membrane performance for gas separations has been defined by a relationship termed the "upper bound" [6, 7]. The upper bound is an empirical relationship from a log-log plot of ideal permselectivity (α_{ij}) versus permeability (P_i), where i represents the more permeable component of the gas pair i and j, and αij is defined as the ratio of gas pair permeability values (P_i/P_j). On these plots, an upper bound line can be drawn above which virtually no data exist, indicating there is a trade-off between permeability and selectivity. In 1999, this empirical relationship was supported by a theoretical prediction of the upper bound parameters by Freeman [6, 8]. To delve further into the fundamental properties that lead to this trade-off, the permeability, diffusivity (D), and solubility (S) values for a large database of glassy polymers were evaluated. The diffusivity selectivity (D_i/D_j) was determined to be the primary factor in establishing the slope of the upper bound, while the solubility selectivity (S_i/S_j) had only a modest contribution [9]. Additionally, the gas pair solubility selectivity decreases with increasing free volume and permeability when the diameter of the more permeable gas, *i*, is smaller than that of the less permeable gas, *j* [9]. Analysis of the diffusion data in glassy polymers yielded a set of gas diameters that were hypothesized to be more relevant for correlating gas diffusion in polymers than prior determinations. In a more recent paper, it was shown that while diffusion coefficients determine the slope of the upper bound, glassy polymers,

as opposed to rubbery polymers, tend to dominate the upper bound due to higher solubility coefficient values [10].

Two classes of polymers, in particular, exhibit upper bound properties for many gas pairs and exceed upper bound performance in some cases (e.g., O_2/N_2 and CO_2/CH_4). These groups of polymers are generally referred to as polymers of intrinsic microporosity (PIM) [11-34] and thermally rearranged (TR) polymers [35-44].

PIM were initially investigated by Budd, McKeown and coinvestigators at the University of Manchester [11-17, 21]. Their synthesis of "ladder" type polymers of intrinsic microporosity (defined as containing interchain spacing or "pores" of < 2 nm) revealed gas separation properties with high gas permeability and upper bound selectivity. The rigid polybenzodioxane backbones of these polymers result in poor molecular packing and thus exhibit high free volume. The upper bound performance of these polymers was attributed to high gas solubility, allowing increased permeability without sacrificing selectivity [15]. This view agrees with the observation that glassy polymers dominate the upper bound, relative to rubbery polymers, due to the dual mode sorption behavior of glassy polymers [10].

Thermally rearranged (TR) polybenzoxazole polymers, initially reported by Lee and coinvestigators, have also generated significant interest for gas separation membranes, specifically for CO_2 based separations [35]. Due to the low solubility of polybenzoxazoles, TR polymers are traditionally formed by the solid state thermal conversion of hydroxyl-containing polyimides to polybenzoxazoles at temperatures ranging from 300-450°C for a prescribed time [45, 46]. The exceptional CO_2/CH_4 selectivity and high permeability of the initial materials were attributed to "well-tuned" cavity formation during thermal rearrangement process. Positron annihilation lifetime spectroscopy (PALS) lent credence

to this concept by showing a narrow distribution of the free volume or pore structure after rearrangement.

A critical analysis of the diffusion selectivity, solubility selectivity, diffusion coefficients, and solubility coefficients of PIM and TR polymers, as compared with other glassy polymers, is detailed in this paper. A large database of permeability, diffusivity, and solubility data for glassy polymers for the analysis in a previous study was employed in this work [9]. While TR polymers and PIM materials perform at or beyond the upper bound for several different gas pairs, O_2/N_2 and CO_2/CH_4 were used for this analysis due to the widespread availability of permeability, solubility, and diffusivity data for O_2, N_2, CO_2 and CH_4, and the lack of necessary data for other gases.

3.2. Analysis of the transport properties of PIM and TR polymers

Permeability data reported for PIM [15, 20, 22-34] and TR polymers [36, 43, 44, 47-50] are compared for O2/N2 and CO2/CH4 separations in Figure 3.1 and Figure 3.2, respectively. For each case, the data are compared with the appropriate empirical 2008 upper bound [7]. Both PIM and TR polymers have data points above the upper bound for O_2/N_2 while predominately TR polymers exceed the upper bound for CO_2/CH_4. However, most of the data reported for PIM and TR polymers are close to but below the upper bound relationship, with the exception of a few recently developed PIM materials which significantly exceed the upper bound [27, 29, 30, 32-34]. Some of the PIM variants reported were used to establish the empirical 2008 upper bound [7] and recently, due to the excellent performance of newly developed PIM materials, Swaidan et al. have proposed a new 2015 upper bound for O_2/N_2 separation [28]. While several TR polymers exceed the 2008 upper bound, TR polymers are not solution-processable and therefore are not formally

used to determine the position of the Robeson upper bounds. To serve as reference points, PIM-1 [16] and TR-450 [43] polymers have been highlighted in many of the following figures. PIM-1 is a heavily studied polymer of intrinsic microporosity formed from the condensation of 5,5',6,6'-tetrahydroxy-3,3,3',3'-tetramethyl-1,1'-spirobisindane and tetrafluoroterephthalonitrile. The data used in the remainder of this work is for PIM-1 treated with methanol [16]. TR-450 is the polymer formed from the thermal treatment of a hydroxyl-containing polyimide based off of 2,2-bis(3-amino-4-hydroxyphenyl)-hexafluoropropane (bisAPAF) and 4,4′-hexafluoroisopropylidene diphthalic anhydride (6FDA) moieties, heated at 450°C for 1 h.

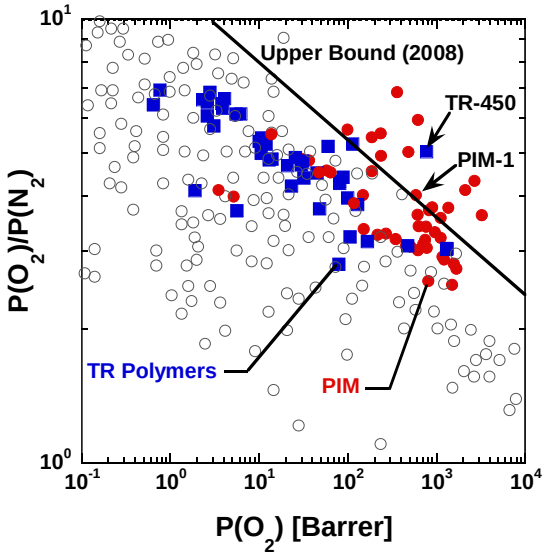

Figure 3.1. Upper bound relationship for PIM (red circles) and TR polymers (blue squares) for O_2/N_2 separation. The unfilled circles represent glassy polymers from a previously reported database [9]. The data points for TR-450 [43] and PIM-1 [16] have been highlighted with arrows.

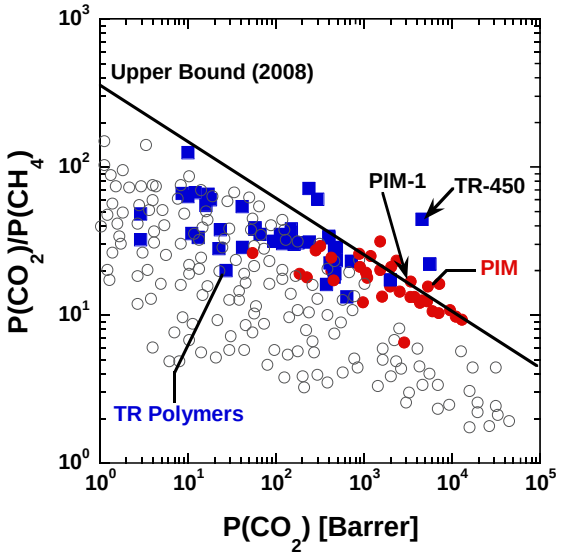

Figure 3.2. Upper bound relationship for PIM (red circles) and TR polymers (blue squares) for CO_2/CH_4 separation. The unfilled circles represent glassy polymers from a previously reported database [9]. The data points for TR-450 [43] and PIM-1 [16] have been highlighted with arrows.

In a previous paper [10], gas diffusion coefficients (D) for rubbery and glassy polymers were compared by correlating data sets using the following equation:

$$\ln D = \alpha + \beta d_g^2 \qquad \text{Eq. 3.1}$$

where α and β are fit for each polymer data set, and β serves as a measure of the size sieving ability of the polymer. The gas diameters, dg, were determined in reference 9 by analysis of diffusion in glassy polymers, which provided a prediction of the gas diameters of He, H_2, O_2, N_2, and CO_2 once the diameter of CH_4 was fixed. By plotting the diffusion coefficients for a gas of intermediate diameter (O_2, d_g = 3.23 Å) as a function of the slope, β, as defined by Eq. 3.1, considerable overlap in the data for glassy and rubbery polymers suggested only modest differences in the diffusion selectivity between the two different polymer classes [10]. This deeper analysis of diffusion coefficients contradicted previous beliefs that glassy polymers dominated the upper bound due to higher diffusivity selectivity

than rubbery polymers [9, 10]. This analysis has been extended to this study, as shown in Figure 3.3. Additional data have been added to the previous analysis [10], where diffusion values of at least 5 of the 6 mentioned gases have been reported [51-61]. Values for PIM [15, 22-33], TR polymers [36, 43, 44], and liquid crystalline polymers (LCPs) [51, 61, 62] have also been included to provide a comparison for gas diffusivity in polymers with high and very low permeabilities. Each point on the plot represents a polymer from the indicated data set. As in the previous paper, the glassy and rubbery polymer correlation lines are quite similar [10]. Thus, the diffusion selectivity of glassy and rubbery polymers are not as different as once believed, even for upper bound materials such as PIM and TR polymers. The data points for TR-450 and PIM-1, highlighted in Figure 3.3, lie above the glassy polymer correlation. Thus, both families of materials have diffusion coefficients significantly higher than other polymers of similar β value (i.e., similar size sieving ability). For this reason, PIM-1 [16] and TR-450 [43] have been selected to represent the PIM and TR polymer data sets. Liquid crystalline polymers also exhibit higher diffusion coefficients versus the correlation line at the lower end of the permeability range.

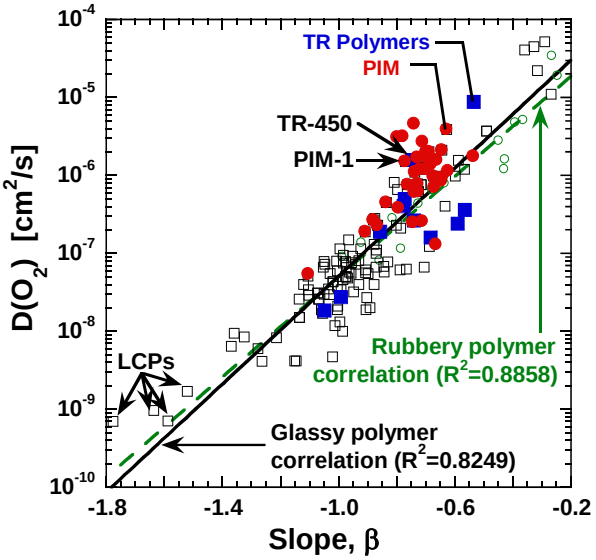

Figure 3.3. Correlation of glassy (black unfilled squares) and rubbery (green unfilled circles) polymer data for oxygen diffusion coefficients (d_g = 3.25 Å) from Eq. 3.1 [10], with PIM (red circles) and TR polymers (blue squares) highlighted to indicate agreement with previous analysis. Liquid crystalline polymers (LCPs), TR-450, and PIM-1 are indicated by arrows.

Figure 3.4 presents a comparison of diffusion coefficients for TR-450 and PIM-1 versus gas diameter. The gas diameter values utilized for this figure were those noted for Figure 3.3 and reported in reference 10. As predicted by Eq. 3.1, the diffusion coefficients follow a linear correlation with gas diameter squared, and there is no discernible difference between the trends for PIM-1 and TR-450. The parameters fitting Eq. 3.1 to PIM-1 and TR-450 diffusion coefficients are included in Table 3.1. These results agree with previous observations [9] that the dependence of gas diffusion coefficients on the square of gas diameters (i.e., β in Eq. 3.1) is similar when polymers have similar diffusion coefficients. Interestingly, the diffusion coefficient of CO_2 (d_g^2 = 11.8 Å^2) in TR-450 lies significantly above the linear correlation. This deviation may contribute to the fact that TR-450 exceeds the 2008 upper bound properties for CO_2/CH_4 separation (cf., Figure 3.2) [7].

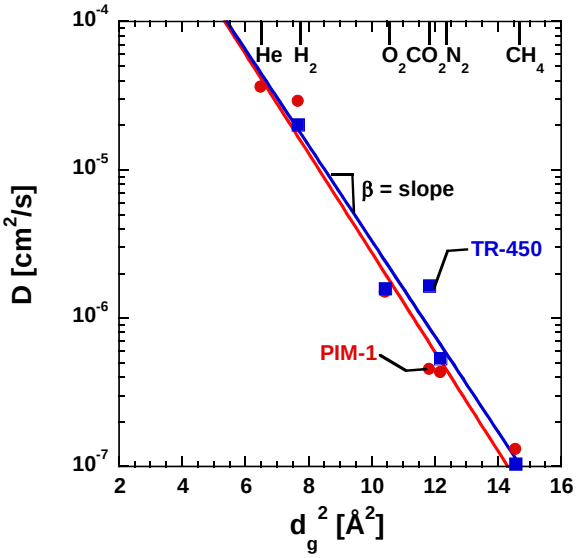

Figure 3.4. Diffusion coefficients versus gas diameter squared (d_g^2) for PIM-1 (red circles) and TR-450 (blue squares). The specific expressions of Eq. 3.1 for TR-450 [43]. The parameters for the shown linear fits to Eq. 3.1 are included in Table 3.1.

Material	**α**	**β**	**R^2**
PIM-1	-5.3 ± 0.2	-0.75 ± 0.01	0.968
TR-450	-5.2 ± 0.2	-0.74 ± 0.02	0.955

Table 3.1. Parameters for Eq. 3.1 used to correlate diffusion coefficients (cm^2/s) for PIM-1 and TR-450 versus the gas diffusion diameters, d_g ($Å^2$). The parameters and uncertainties were determined assuming a 10% uncertainty in the diffusion coefficient values and a least square fit analysis.

PIM and TR polymers are often reported to have transport properties near or above the upper bound for the O_2/N_2 and CO_2/CH_4 gas pairs. The diffusivity selectivity for PIM and TR polymers are compared to the rest of the glassy polymer database in Figure 3.5 and Figure 3.6 for O_2/N_2 and CO_2/CH_4, respectively. As expected, the glassy polymer data show a distinct upper bound relationship for both gas pairs in log-log plots of diffusivity

selectivity (D_i/D_j) versus diffusivity of the faster component (D_i). Similar to the permeability upper bound (cf., Figure 3.1), several PIM and TR polymers lie on or above the diffusivity upper bound for O_2/N_2. For CO_2/CH_4 separation, several TR polymers show equal or higher diffusivity selectivity than the glassy polymer diffusivity upper bound, while PIM have properties comparable to those of other glassy polymers. Power law fits for D_i/D_j with respect to D_i (i.e., $\log\left(\frac{D_i}{D_j}\right) = A\log(D_i) + B$) have been included for all data points in Figure 3.5 and Figure 3.6 to show the general trend of decreasing diffusion selectivity with increasing diffusivity.

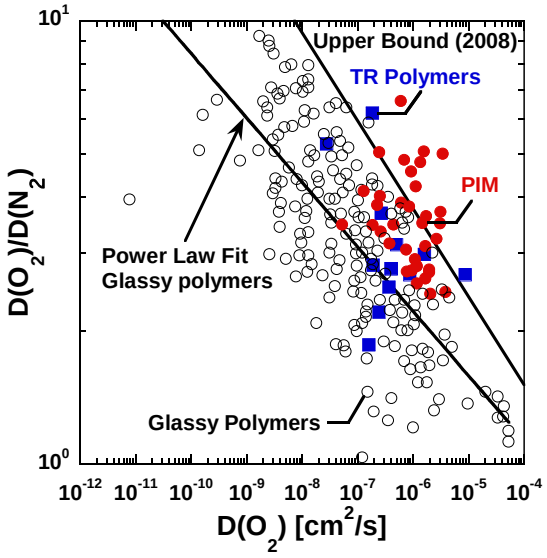

Figure 3.5. Diffusivity upper bound correlation for O_2/N_2, comparing PIM (red circles) and TR polymers (blue squares) to the glassy polymer database (unfilled circles) [9].

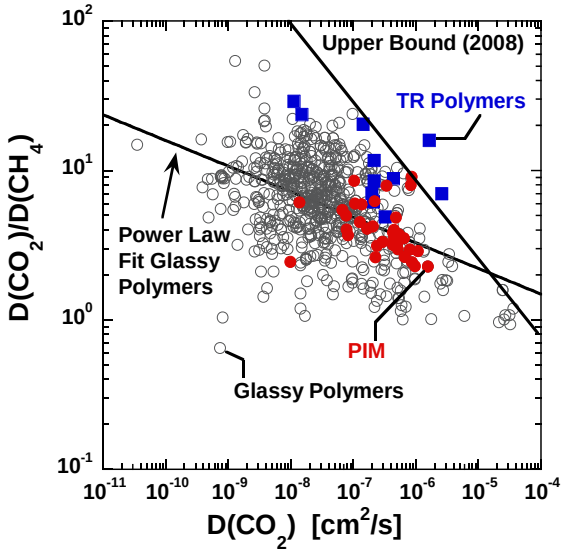

Figure 3.6. Diffusivity upper bound correlation for CO_2/CH_4, comparing PIM (red circles) and TR polymers (blue squares) to the glassy polymer database (unfilled circles) [9].

The solubility data for PIM [11-34] and TR polymers [35-44] were obtained from the references noted earlier. A plot of solubility constants versus permeability coefficients is shown for O_2 solubility (Figure 7) and CO_2 solubility (Figure 8). These data are compared with similar data for other glassy polymers from reference 9. All data shown fall within the trend noted previously [9], where the solubility coefficients generally increase with increasing permeability. However, both PIM and TR polymers show O_2 solubility values towards the higher end of the trend. Additionally, PIM materials exhibit higher CO_2 solubility coefficients relative to the spread of the data for glassy polymers, while TR polymers have values scattered within the glassy polymer data set. Compared to other glassy polymers, TR polymers and PIM have both high solubility and diffusivity coefficients. These "upper limit" transport properties contribute significantly to the upper bound behavior of these two polymer classes.

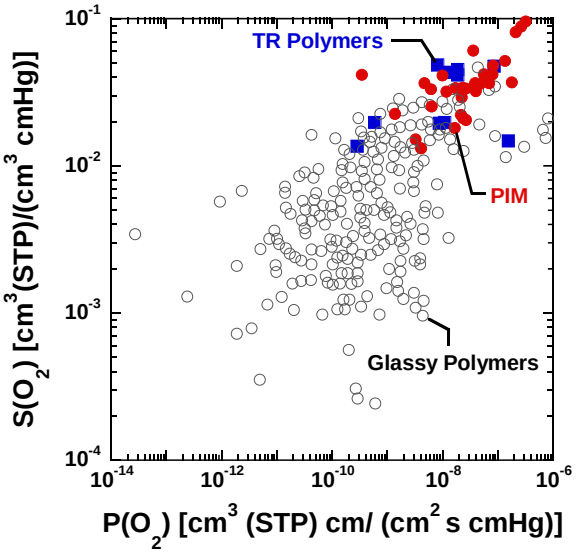

Figure 3.7. Comparison of O_2 solubility coefficient data of PIM (red circles) and TR variants (blue squares) with the glassy polymer database (unfilled circles) [9].

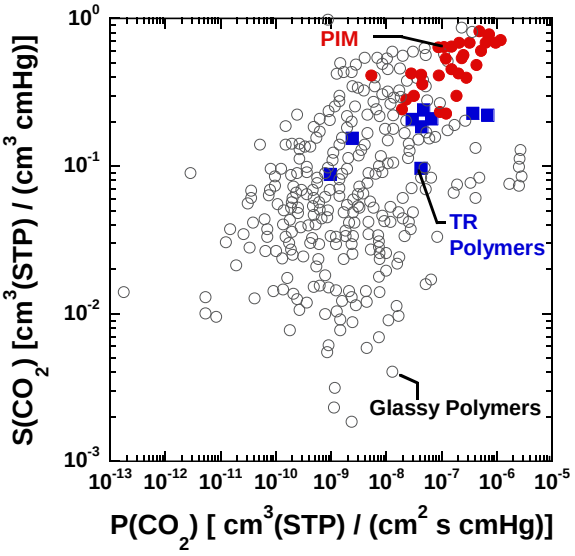

Figure 3.8. Comparison of CO_2 solubility coefficient data of PIM (red circles) and TR polymers (blue squares) with the glassy polymer database (unfilled circles) [9].

The gas pair selectivities (S_i/S_j) were calculated for PIM and TR polymers. The results are summarized in Table 3.2, where the average and range of solubility selectivity values are reported. These results indicate both PIM and TR polymers have solubility selectivities within the general range of glassy polymers. This supports the previous analysis that high solubility, rather than solubility selectivity, contributes to polymers dominating upper bound behavior.

	$S(O_2)/S(N_2)$		$S(CO_2)/S(CH_4)$	
Polymer	**Average**	**Range**	**Average**	**Range**
glassy polymers [9]	1.30	0.31 – 2.50	5.00	0.93 – 47.5
PIM [15, 22-24]	1.16	1.03 – 1.44	4.35	3.19 – 5.09
TR polymers [36, 43, 44]	1.39	1.05 – 1.83	3.02	2.50 – 4.30

Table 3.2. O_2/N_2 and CO_2/CH_4 gas pair selectivity values for glassy polymers, PIM, and TR polymers. The indicated references denote which data sets were used to obtain the average value and range shown.

3.3. CORRELATION OF PIM AND TR POLYMER DIFFUSION DATA WITH GAS DIAMETER

Correlations of gas diffusion coefficients in polymers with gas molecular dimensions (i.e., diameter squared or gas molecule volume) have been often reported in the literature. Grün, and several others since, have correlated diffusion coefficients with van der Waals molecular volume for a variety of gas permeants, ranging from He to n-hexane, in both polymers and solvents [63, 64]. However, for small molecules, this correlation tends to be weak due to the non-spherical nature of gas molecules like H_2, O_2, N_2, and CO_2. For this reason, several prominent correlations relating diffusion coefficients to the gas kinetic diameter exist. These include: the kinetic diameter determined from zeolite data (Breck diameters) [65], the Lennard-Jones gas diameter and collision diameter [66, 67], the effective diameter [59], the Dal-Cin correlation diameter from analysis of the

upper bound [68], the permeability correlation diameter [69], the Teplyakov-Meares (T-M) diameter [70], and the diffusion correlation diameter determined from glassy polymer data [9]. The Teplyakov-Meares (T-M) diameter correlation comprises a comprehensive list of gas diameters based on analysis of noble gas diffusion in a series of polymers to yield a fit to Eq. 3.1. While several of these correlations use the diameter of methane (a relatively spherical molecule) as a reference point, the T-M correlation used noble gases [70]. This choice resulted in diameters significantly lower than the other noted correlations (cf.,Table 3.3). While the absolute values of the T-M diameters are lower, the correlation ability to fit the gas diffusion data to the relative difference in the diameter squared is the key factor, not the magnitude of the gas diameter values. A comparison of the gas diameters utilized to correlate diffusion data is shown in Table 3.3.

Gas	Gas Diameter (Å)							
	Teplyakov-Meares (T-M) [70]	**Lennard-Jones [67]**	**Dal-Cin [68]**	**Lennard-Jones Collision [66]**	**Permeability [69]**	**Breck [65]**	**Effective [59]**	**Diffusion, dg [9]**
He	1.78	2.551	2.555	2.576	2.644	2.6	2.59	2.55
H_2	2.14	2.827	2.854	2.915	2.875	2.89	2.90	2.77
O_2	2.89	3.467	3.374	3.433	3.347	3.46	3.44	3.23
CO_2	3.02	3.941	3.427	3.996	3.325	3.3	3.63	3.44
N_2	3.04	3.798	3.588	3.681	3.568	3.64	3.66	3.49
CH_4	3.18	3.758	3.882	3.822	3.817	3.8	3.81	3.817

Table 3.3. Gas diameters determined by different methods reported in the literature.

The literature database for glassy [9] and rubbery polymers [10] yields the following relationship for diffusion coefficients: D(He) > D(H_2) > D(O_2) > D(CO_2) > D(N_2) > D(CH_4). The closest proximity for the gas pairs is with D(CO_2) and D(N_2), with D(CO_2) only slightly higher than D(N_2). Four of the noted gas diameter correlations show this trend with the diameter of CO_2 being only slightly smaller than N_2. These include the T-M diameter, effective diameter, Dal-Cin correlation diameter, and the diffusion correlation diameter. While the permeability [69] and Breck [65] correlations give the diameters for CO_2 and N_2 in the appropriate size order, the differences are too large to reflect the small observed difference in diffusion coefficients. A comparison of these diameters (squared) plotted against the diffusion correlation diameter (d_g) is shown in Figure 3.9 with a polynomial fit of the data. The comparison illustrated in Figure 3.9 shows convex behavior for the effective diameter and the T-M diameter relative to the diffusion correlation diameter (all squared). The Dal-Cin diameter is quite close to linearity but shows a slight deviation for CO_2.

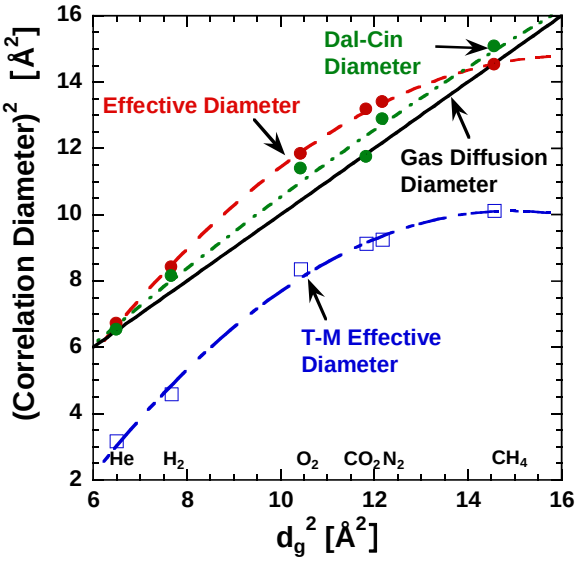

Figure 3.9. Comparison of the effective [59], Dal-Cin [68], and Teplyakov-Meares [70] diameter correlations to the gas diffusion correlation diameter squared (d_g^2) [9]. A parity line (the solid, straight line) for the gas diffusion correlation diameter has been included as a reference.

A comparison of the diffusion correlation diameter and the T-M diameter is presented in Figure 3.10 with diffusion coefficient data for PIM-1 and TR-450. A linear fit of the data as well as a quadratic fit are shown, and a statistical assessment of these fits has been performed in the Supporting Information, included in Appendix A. Good linearity, as predicted by Eq. 3.1, is observed for the diffusion correlation diameter data, whereas convex behavior is observed for the T-M diameter data. The linear behavior is also observed with several other TR polymers as shown in Figure 3.11. While the TR and PIM polymers better obey correlations with the diffusion correlation diameters, the T-M diameters often yield a better fit, as compared to dg, with typical rubbery and non-upper bound glassy polymers. The gas diffusion correlation diameter (based only on glassy polymer data) often yields modestly concave behavior for *ln(D)* versus d_g^2 plots for rubbery and non-upper bound glassy polymers. The better fit of the TR and PIM diffusivities with the diffusion correlation diameters than with diameters from other correlations appears to

be a consequence of the larger relative gas diameter difference between O_2, N_2, and CH_4 in d_g than in the other correlations.

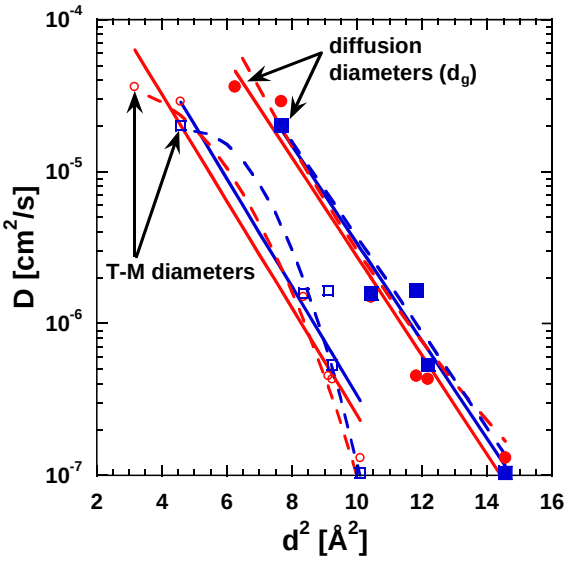

Figure 3.10. Comparison of the fit of Eq. 3.1 for PIM-1 (red circles) [16] and TR-450 (blue squares) [43] employing the T-M diameters (unfilled markers) and the diffusion correlation diameters (filled markers). A linear fit (solid line) and a quadratic fit (dashed line) are shown for each correlation. The linear and quadratic fit parameters are listed in Table A.1.

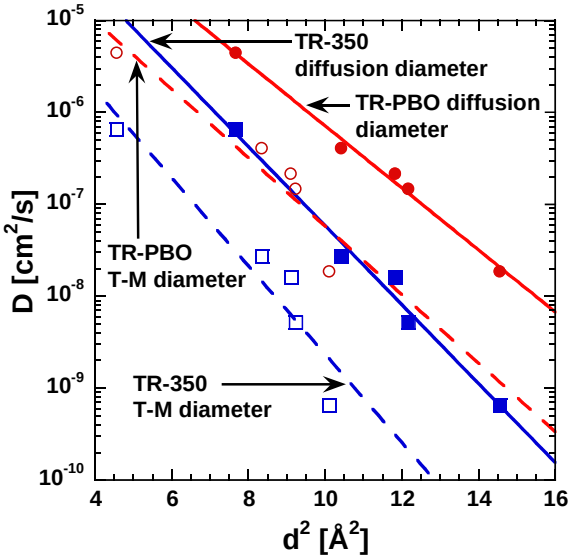

Figure 3.11. Comparison of TR-PBO (red circles) and TR-350 (blue squares) diffusion data [43] fit with Eq. 3.1 employing the T-M diameters (open markers) and the diffusion correlation diameters (filled markers). Linear correlations for each data set are included. TR-350 is a TR polymer treated at 350°C for 1 h for partial conversion to the PBO structure, and TR-PBO is a polymer treated at 450°C for 1 h to achieve 100% conversion to the PBO structure [43].

3.4. CONCLUSIONS

The transport properties of PIM and TR polymers variants have been compared with the spread of data for glassy polymers [71]. The diffusivity selectivity of common gases for specific TR and PIM variants is modestly higher than most glassy polymers. For specific gas pairs (i.e., O_2/N_2 and CO_2/CH_4), some TR and PIM variants also offer higher diffusivity selectivity than other glassy polymers when compared on a diffusivity selectivity upper bound plot (i.e., $log(D_i/D_j)$ versus D_i), although most of the variants are in the range of other glassy polymers. The natural log diffusion coefficient versus gas diameter squared correlations (i.e., Eq. 3.1) is best fit by the diffusion correlation diameters, dg, than by various other gas diameter correlations commonly employed for polymers.

The solubility coefficients of PIM variants for O_2 and CO_2 are in the higher range of the spread of glassy polymer data. TR variants show higher O_2 solubility coefficients relative to other glassy polymers but have CO_2 solubility coefficients more in the range of other glassy polymers. The O_2/N_2 and CO_2/CH_4 solubility selectivities for both PIM and TR variants are in the expected range for glassy polymers.

The basic conclusion from this analysis is that the upper bound performance (i.e., combination of high permeability and permeability selectivity) for specific PIM and TR polymers is due to a combination of higher diffusion selectivity, high diffusion coefficients, and high solubility coefficients, relative to other glassy polymers. The high solubility coefficients are a consequence of high free volume combined with high glass transition temperatures, leading to significant dual mode sorption, as noted previously [9]. Elevated solubility shifts the data to higher permeability values relative to other polymers at a given selectivity on the upper bound plots. This point has been recognized in an earlier hypothesis on PIM variants [15] and further supported by the evidence presented in this study. Thus, the excellent performance of TR and PIM variants is a consequence of maximizing diffusion selectivity, diffusion coefficients, and gas solubility. They appear to fit the solution-diffusion model and are not uniquely different in their transport mechanism than other polymers. Thus, upper bound behavior can be achieved when diffusion selectivity, diffusion coefficients, and gas solubility are simultaneously maximized.

3.5. ACKNOWLEDGEMENTS

This material is based upon work supported by the National Science Foundation Graduate Research Fellowship under Grant No. DGE-1610403. Additionally, the authors gratefully acknowledge support from the Division of Chemical Sciences, Geosciences, and Biosciences, Office of Basic Energy Sciences of the U.S. Department of Energy (DOE) through Grant DE-FG02-02ER15362.

3.6. REFERENCES

[1] J.M.S. Henis, Commercial and Practical Aspects of Gas Separation Membranes, in: D.R. Paul, Y.P. Yampol'skii (Eds.) Polymeric Gas Separation Membranes, CRC Press, Boca Raton, FL, 1994, pp. 442-468.

[2] R.W. Baker, Membrane Technology and Applications, in: Membrane Technology, John Wiley & Sons, Ltd, Chichester, UK, 2004, pp. 545.

[3] W.A. Bollinger, D.L. MacLean, R.S. Narayan, Separation Systems For Oil Refining And Production, Chemical Engineering Progress, 78 (1982) 27-32.

[4] D.F. Sanders, Z.P. Smith, R. Guo, L.M. Robeson, J.E. McGrath, D.R. Paul, B.D. Freeman, Energy-Efficient Polymeric Gas Separation Membranes For A Sustainable Future: A Review, Polymer, 54 (2013) 4729-4761.

[5] Y. Yampolskii, Polymeric Gas Separation Membranes, Macromolecules, 45 (2012) 3298-3311.

[6] L.M. Robeson, Correlation of Separation Factor Versus Permeability for Polymeric Membranes, Journal of Membrane Science, 62 (1991) 165-185.

[7] L.M. Robeson, The Upper Bound Revisited, Journal of Membrane Science, 320 (2008) 390-400.

[8] B.D. Freeman, Basis of Permeability/Selectivity Tradeoff Relations in Polymeric Gas Separation Membranes, Macromolecules, 32 (1999) 375-380.

[9] L.M. Robeson, Z.P. Smith, B.D. Freeman, D.R. Paul, Contributions of Diffusion and Solubility Selectivity to the Upper Bound Analysis for Glassy Gas Separation Membranes, Journal of Membrane Science, 453 (2014) 71-83.

[10] L.M. Robeson, Q. Liu, B.D. Freeman, D.R. Paul, Comparison of Transport Properties of Rubbery and Glassy Polymers and the Relevance to the Upper Bound Relationship, Journal of Membrane Science, 476 (2015) 421-431.

[11] N.B. McKeown, S. Hanif, K. Msayib, C.E. Tattershall, P.M. Budd, Porphyrin-based nanoporous network polymers, Chemical Communications, (2002) 2782-2783.

[12] P.M. Budd, B. Ghanem, K. Msayib, N.B. McKeown, C. Tattershall, A nanoporous network polymer derived from hexaazatrinaphthylene with potential as an adsorbent and catalyst support, Journal of Materials Chemistry, 13 (2003) 2721-2726.

[13] P.M. Budd, B.S. Ghanem, S. Makhseed, N.B. McKeown, K.J. Msayib, C.E. Tattershall, Polymers of intrinsic microporosity (PIMs): robust, solution-processable, organic nanoporous materials, Chemical Communications, (2004) 230-231.

[14] P.M. Budd, E.S. Elabas, B.S. Ghanem, S. Makhseed, N.B. McKeown, K.J. Msayib, C.E. Tattershall, D. Wang, Solution-Processed, Organophilic Membrane Derived from a Polymer of Intrinsic Microporosity, Advanced Materials, 16 (2004) 456-459.

[15] P.M. Budd, N.B. McKeown, D. Fritsch, Free volume and intrinsic microporosity in polymers, Journal of Materials Chemistry, 15 (2005) 1977-1986.

[16] P. Budd, N. McKeown, B. Ghanem, K. Msayib, D. Fritsch, L. Starannikova, N. Belov, O. Sanfirova, Y. Yampolskii, V. Shantarovich, Gas Permeation Parameters and Other Physicochemical Properties of a Polymer of Intrinsic Microporosity: Polybenzodioxane PIM-1, Journal of Membrane Science, 325 (2008) 851-860.

[17] N.B. McKeown, P.M. Budd, Exploitation of Intrinsic Microporosity in Polymer-Based Materials, Macromolecules, 43 (2010) 5163-5176.

[18] C.R. Mason, L. Maynard-Atem, N.M. Al-Harbi, P.M. Budd, P. Bernardo, F. Bazzarelli, G. Clarizia, J.C. Jansen, Polymer of Intrinsic Microporosity Incorporating Thioamide Functionality: Preparation and Gas Transport Properties, Macromolecules, 44 (2011) 6471-6479.

[19] N. Du, G.P. Robertson, J. Song, I. Pinnau, S. Thomas, M.D. Guiver, Polymers of Intrinsic Microporosity Containing Trifluoromethyl and Phenylsulfone Groups as Materials for Membrane Gas Separation, Macromolecules, 41 (2008) 9656-9662.

[20] N. Du, G.P. Robertson, I. Pinnau, M.D. Guiver, Polymers of Intrinsic Microporosity with Dinaphthyl and Thianthrene Segments, Macromolecules, 43 (2010) 8580-8587.

[21] P. Budd, K. Msayib, C. Tattershall, B. Ghanem, K. Reynolds, N. McKeown, D. Fritsch, Gas separation membranes from polymers of intrinsic microporosity, Journal of Membrane Science, 251 (2005) 263-269.

[22] D. Fritsch, G. Bengtson, M. Carta, N.B. McKeown, Synthesis and Gas Permeation Properties of Spirobischromane-Based Polymers of Intrinsic Microporosity, Macromolecular Chemistry and Physics, 212 (2011) 1137-1146.

[23] B.S. Ghanem, N.B. McKeown, P.M. Budd, D. Fritsch, Polymers of Intrinsic Microporosity Derived from Bis(phenazyl) Monomers, Macromolecules, 41 (2008) 1640-1646.

[24] M. Carta, P. Bernardo, G. Clarizia, J.C. Jansen, N.B. McKeown, Gas Permeability of Hexaphenylbenzene Based Polymers of Intrinsic Microporosity, Macromolecules, 47 (2014) 8320-8327.

[25] B.S. Ghanem, R. Swaidan, E. Litwiller, I. Pinnau, Ultra-microporous triptycene-based polyimide membranes for high-performance gas separation, Adv Mater, 26 (2014) 3688-3692.

[26] B.S. Ghanem, R. Swaidan, X. Ma, E. Litwiller, I. Pinnau, Energy-efficient hydrogen separation by AB-type ladder-polymer molecular sieves, Adv Mater, 26 (2014) 6696-6700.

[27] R. Swaidan, M. Al-Saeedi, B. Ghanem, E. Litwiller, I. Pinnau, Rational Design of Intrinsically Ultramicroporous Polyimides Containing Bridgehead-Substituted Triptycene for Highly Selective and Permeable Gas Separation Membranes, Macromolecules, 47 (2014) 5104-5114.

[28] R. Swaidan, B. Ghanem, I. Pinnau, Fine-Tuned Intrinsically Ultramicroporous Polymers Redefine the Permeability/Selectivity Upper Bounds of Membrane-Based Air and Hydrogen Separations, ACS Macro Letters, 4 (2015) 947-951.

[29] Y. Rogan, R. Malpass-Evans, M. Carta, M. Lee, J.C. Jansen, P. Bernardo, G. Clarizia, E. Tocci, K. Friess, M. Lanč, N.B. McKeown, A highly permeable polyimide with enhanced selectivity for membrane gas separations, Journal of Materials Chemistry A, 2 (2014) 4874.

[30] Y. Zhuang, J.G. Seong, Y.S. Do, H.J. Jo, Z. Cui, J. Lee, Y.M. Lee, M.D. Guiver, Intrinsically Microporous Soluble Polyimides Incorporating Tröger's Base for Membrane Gas Separation, Macromolecules, 47 (2014) 3254-3262.

[31] Z. Wang, D. Wang, J. Jin, Microporous Polyimides with Rationally Designed Chain Structure Achieving High Performance for Gas Separation, Macromolecules, 47 (2014) 7477-7483.

[32] M. Carta, M. Croad, R. Malpass-Evans, J.C. Jansen, P. Bernardo, G. Clarizia, K. Friess, M. Lanc, N.B. McKeown, Triptycene induced enhancement of membrane gas selectivity for microporous Troger's base polymers, Adv Mater, 26 (2014) 3526-3531.

[33] M. Carta, R. Malpass-Evans, M. Croad, Y. Rogan, J.C. Jansen, P. Bernardo, F. Bazzarelli, N.B. McKeown, An efficient polymer molecular sieve for membrane gas separations, Science, 339 (2013) 303-307.

[34] I. Rose, M. Carta, R. Malpass-Evans, M.-C. Ferrari, P. Bernardo, G. Clarizia, J.C. Jansen, N.B. McKeown, Highly Permeable Benzotriptycene-Based Polymer of Intrinsic Microporosity, ACS Macro Letters, 4 (2015) 912-915.

[35] H.B. Park, C.H. Jung, Y.M. Lee, A.J. Hill, S.J. Pas, S.T. Mudie, E. Van Wagner, B.D. Freeman, D.J. Cookson, Polymers with Cavities Tuned for Fast Selective Transport of Small Molecules and Ions, Science, 318 (2007) 254-258.

[36] M. Calle, Y.M. Lee, Thermally Rearranged (TR) Poly(ether−benzoxazole) Membranes for Gas Separation, Macromolecules, 44 (2011) 1156-1165.

[37] S. Li, H.J. Jo, S.H. Han, C.H. Park, S. Kim, P.M. Budd, Y.M. Lee, Mechanically robust thermally rearranged (TR) polymer membranes with spirobisindane for gas separation, Journal of Membrane Science, 434 (2013) 137-147.

[38] Y.S. Do, J.G. Seong, S. Kim, J.G. Lee, Y.M. Lee, Thermally rearranged (TR) poly(benzoxazole-co-amide) membranes for hydrogen separation derived from 3,3′-dihydroxy-4,4′-diamino-biphenyl (HAB), 4,4′-oxydianiline (ODA) and isophthaloyl chloride (IPCl), Journal of Membrane Science, 446 (2013) 294-302.

[39] Y.F. Yeong, H. Wang, K. Pallathadka Pramoda, T.-S. Chung, Thermal induced structural rearrangement of cardo-copolybenzoxazole membranes for enhanced gas transport properties, Journal of Membrane Science, 397-398 (2012) 51-65.

[40] H. Wang, T.-S. Chung, The Evolution of Physicochemical and Gas Transport Properties of Thermally Rearranged Polyhydroxyamide (Pha), Journal of Membrane Science, 385-386 (2011) 86-95.

[41] Y. Jiang, F.T. Willmore, D. Sanders, Z.P. Smith, C.P. Ribeiro, C.M. Doherty, A. Thornton, A.J. Hill, B.D. Freeman, I.C. Sanchez, Cavity Size, Sorption and Transport Characteristics of Thermally Rearranged (TR) Polymers, Polymer, 52 (2011) 2244-2254.

[42] S.H. Han, N. Misdan, S. Kim, C.M. Doherty, A.J. Hill, Y.M. Lee, Thermally Rearranged (TR) Polybenzoxazole: Effects of Diverse Imidization Routes on Physical Properties and Gas Transport Behaviors, Macromolecules, 43 (2010) 7657-7667.

[43] S. Kim, H.J. Jo, Y.M. Lee, Sorption and transport of small gas molecules in thermally rearranged (TR) polybenzoxazole membranes based on 2,2-bis(3-amino-4-hydroxyphenyl)-hexafluoropropane (bisAPAF) and 4,4′ -hexafluoroisopropylidene diphthalic anhydride (6FDA), Journal of Membrane Science, 441 (2013) 1-8.

[44] S. Kim, K.T. Woo, J.M. Lee, J.R. Quay, M. Keith Murphy, Y.M. Lee, Gas sorption, diffusion, and permeation in thermally rearranged poly(benzoxazole-co-imide) membranes, Journal of Membrane Science, 453 (2014) 556-565.

[45] I. Kardash, A.N. Pravednikov, Aromatic polyimides containing hydroxy and methyl groups, Vysokomol Soyed, 9 (1967) 873-876.

[46] G. Tullos, L. Mathias, Unexpected thermal conversion of hydroxy-containing polyimides to polybenzoxazoles, Polymer, 40 (1999) 3463-3468.

[47] C.A. Scholes, C.P. Ribeiro, S.E. Kentish, B.D. Freeman, Thermal rearranged poly(benzoxazole-co-imide) membranes for CO_2 separation, Journal of Membrane Science, 450 (2014) 72-80.

[48] W. Liu, W. Xie, Acetate-Functional Thermally Rearranged Polyimides Based on 2,2-Bis(3-amino-4-hydroxyphenyl)hexafluoropropane and Various Dianhydrides for Gas Separations, Industrial & Engineering Chemistry Research, 53 (2014) 871-879.

[49] B. Comesaña-Gándara, M. Calle, H.J. Jo, A. Hernández, J.G. de la Campa, J. de Abajo, A.E. Lozano, Y.M. Lee, Thermally rearranged polybenzoxazoles membranes with biphenyl moieties: Monomer isomeric effect, Journal of Membrane Science, 450 (2014) 369-379.

[50] R. Guo, D.F. Sanders, Z.P. Smith, B.D. Freeman, D.R. Paul, J.E. McGrath, Synthesis and Characterization of Thermally Rearranged (TR) Polymers: Effect of Glass Transition Temperature of Aromatic Poly(hydroxyimide) Precursors on TR Process and Gas Permeation Properties, Journal of Materials Chemistry A, 1 (2013) 6063-6072.

[51] J.S. Chiou, D.R. Paul, Gas transport in a thermotropic liquid-crystalline polyester, Journal of Polymer Science Part B: Polymer Physics, 25 (1987) 1699-1707.

[52] J.C.I. Lara-Estévez, C. Camacho-Zuñiga, F.A. Ruiz-Treviño, E. Bucio, P.E. Cassidy, C.J. Booth, Gas Transport Properties of Some Fluorine-Containing Polyethers, Industrial & Engineering Chemistry Research, 49 (2010) 11948-11953.

[53] C.M. Zimmerman, W.J. Koros, Polypyrrolones for membrane gas separations. I. Structural comparison of gas transport and sorption properties, Journal of Polymer Science Part B: Polymer Physics, 37 (1999) 1235-1249.

[54] K. Tanaka, M. Okano, H. Toshino, H. Kita, K.-I. Okamoto, Effect of methyl substituents on permeability and permselectivity of gases in polyimides prepared from methyl-substituted phenylenediamines, Journal of Polymer Science Part B: Polymer Physics, 30 (1992) 907-914.

[55] Y.J. Cho, H.B. Park, High Performance Polyimide with High Internal Free Volume Elements, Macromolecular Rapid Communications, 32 (2011) 579-586.

[56] K. Terada, K. Mizoguchi, T. Hirose, Gas transport in poly(vinyl methylbenzoates), Journal of Polymer Science Part B: Polymer Physics, 30 (1992) 539-548.

[57] K. Tanaka, H. Kita, K.-i. Okamoto, Permeability and permselectivity of gases in fluorinated polyimides., Sen'i Gakkaishi, 46 (1990) 541-547.

[58] M.W. Hellums, W.J. Koros, G.R. Husk, D.R. Paul, Gas transport in halogen-containing aromatic polycarbonates, Journal of Applied Polymer Science, 43 (1991) 1977-1986.

[59] J.-J. Shieh, T.-S. Chung, Gas permeability, diffusivity, and solubility of poly(4-vinylpyridine) film, Journal of Polymer Science Part B: Polymer Physics, 37 (1999) 2851-2861.

[60] N.A. Plate, S.G. Durgarjan, V.S. Khotimskii, V.V. Teplyakov, Y.P. Yampol'skii, Novel poly(silicon olefins) for gas separations, Journal of Membrane Science, 52 (1990) 289-304.

[61] D.H. Weinkauf, D.R. Paul, Gas Transport Properties of Thermotropic Liquid-Crystalline Copolyesters. I. The Effects of Orientation and Annealing, Journal of Polymer Science Part B: Polymer Physics, 30 (1992) 817-835.

[62] D.H. Weinkauf, D.R. Paul, Gas Transport Properties of Liquid Crystalline Poly(Ethylene Terephthalate-co-p-Oxybenzoate), Journal of Polymer Science Part B: Polymer Physics, 29 (1991) 329-340.

[63] F. Grün, Diffusionsmessungen an Kautschuk, Experientia, 3 (1947) 490-492.

[64] R.W. Baker, B.T. Low, Gas Separation Membrane Materials: A Perspective, Macromolecules, 47 (2014) 6999-7013.

[65] D.W. Breck, Zeolite molecular sieves: structure, chemistry, and use, Wiley, New York, 1974.

[66] R.B. Bird, W.E. Stewart, E.N. Lightfoot, Transport Phenomena, 2nd ed., John Wiley & Sons, 1961.

[67] R.C. Reid, J.M. Prausnitz, T.K. Sherwood, The Properties of Gases and Liquids, McGraw Hill Book Co.,New York, NY, 1977.

[68] M.M. Dal-Cin, A. Kumar, L. Layton, Revisiting the experimental and theoretical upper bounds of light pure gas selectivity–permeability for polymeric membranes, Journal of Membrane Science, 323 (2008) 299-308.

[69] L.M. Robeson, B.D. Freeman, D.R. Paul, B.W. Rowe, An Empirical Correlation of Gas Permeability and Permselectivity in Polymers and Its Theoretical Basis, Journal of Membrane Science, 341 (2009) 178-185.

[70] V. Teplyakov, P. Meares, Correlation aspects of the selective gas permeabilities of polymeric materials and membranes, Gas Separation & Purification, 4 (1990) 66-74.

[71] A. Alentiev, Y. Yampolskii, Correlation of Gas Permeability and Diffusivity with Selectivity: Orientations of the Clouds of the Data Points and the Effects of Temperature, Industrial & Engineering Chemistry Research, 52 (2013) 8864-8874.

Chapter 4: Thermally Cross-linked Diaminophenylindane (DAPI) Containing Polyimides for Membrane Based Gas Separations

This study aims to expand structure-property relationships of diaminophenylindane (DAPI)-containing polyimides and the influence of thermal cross-linking on gas transport properties of such materials. A polyimide synthesized from hexafluoroisopropylidene diphthalic anhydride (6FDA), DAPI, and diaminobenzoic acid (DABA) in a molar ratio of 0.5/0.33/0.17, $6FDA_{0.5}$-$DAPI_{0.33}$/$DABA_{0.17}$, was crosslinked by thermal decarboxylation. After cross-linking, pure gas permeability of $6FDA_{0.5}$-$DAPI_{0.33}$/$DABA_{0.17}$ increased with increased cross-linking time; gas permeability increased by about 30% after cross-linking at 353°C for 40 min. This increase in permeability correlated with an increase in d-spacing measured by wide angle x-ray scattering, suggesting an increase in inter-chain spacing upon cross-linking. Minimal changes in O_2/N_2 and N_2/CH_4 selectivities occurred with increased thermal cross-linking time for $6FDA_{0.5}$-$DAPI_{0.33}$/$DABA_{0.17}$. However, CO_2/CH_4 and C_2H_4/C_2H_6 pure gas selectivities increased with thermal treatment, suggesting a potential narrowing of free volume distribution.[3]

[3] This Chapter has been adapted with permission from: Michelle E. Dose, Malgorzata Chwatko, Ivo Hubacek, Nathaniel A. Lynd, Donald R. Paul, Benny D. Freeman. Thermally Cross-linked Diaminophenylindane (DAPI) Containing Polyimides for Membrane Based Gas Separations. **Submitted to Polymer 23 August 2018**. For this paper, I was the primary author, developed the experimental design, conducted the experiments, and preformed most of the analysis. The co-authors from these papers contributed to the analysis and helped run supporting experiments.

4.1. INTRODUCTION

Polyimides are widely used and studied as gas separation membrane materials [1, 2]. Those most commonly explored are solution processable, amorphous glassy polymers with rigid polymer backbones [3]. Polyimides are typically synthesized from at least one dianhydride and at least one diamine. Matrimid®, a commercially available polyimide, is comprised of two monomer units, 3,3',4,4'-**b**enzophenone **t**etracarboxylic **d**i**a**nhydride (BTDA) and isomeric 5(6)-amino-1-(4-aminophenyl)-1,3,3-trimethylindane (**d**i**a**mino**p**hyenyl**i**ndane, DAPI). Its favorable transport properties have been attributed in part to the rigid, bulky, and isomeric structure of DAPI [4, 5]. However, DAPI has not been thoroughly investigated in other polymer structures due to its previously limited commercial availability. Previoius studies incorporated DAPI with several dianhydrides, but those studies focused primarily on O_2/N_2 separations [4, 5]. This work extends structure-property studies involving DAPI by incorporating the isomeric diamine into a thermally cross-linkable polymer. Cross-linking polyimides is reported to help reduce plasticization effects in applications such as natural gas and hydrocarbon separations [6, 7].

Recently, there has been increasing interest in small scale hydrocarbon separations due to rapid growth of shale gas in the United States [8, 9]. Currently, light hydrocarbons like ethane, ethylene, propane, and propylene are separated using fractional distillation [1, 10]. High pressures and sub-ambient temperatures are needed to achieve these separations due to the small size and volatility differences between ethylene/ethane and propane/propylene (cf., Table B.1) [11, 12]. These features make olefin/paraffin separations among the most energy intensive processes in the petrochemical industry [1, 10, 13].

Previous studies have shown CO_2 plasticization resistance can be improved by cross-linking carboxylic acid containing polyimides and polymers of intrinsic microporosity (PIM) by thermal decarboxylation [14-17]. Motivated by these prior results, this study focuses on cross-linking 6FDA$_{0.5}$-DAPI$_{0.33}$/DABA$_{0.17}$, which contains a molar ratio of 0.5/0.33/0.17 of 6FDA/DAPI/DABA, via thermal decarboxylation. The –C(CF$_3$)$_2$– linkages in 6FDA often increase polymer fractional free volume, thereby improving permeability while maintaining reasonable selectivity for a given gas pair [18-20]. Additionally, there is speculation in the literature that the fluorocarbon functionality of –CF$_3$ moieties may reduce solubility of hydrocarbons due to thermodynamically unfavorable interactions with hydrocarbons [20-22]. The inclusion of isomeric DAPI may also improve backbone rigidity and free volume due to its asymmetric, bulky structure [4]. Moreover, DABA provides reactive acid sites for cross-linking and/or modification [5, 14-17, 23, 24]. A 2:1 ratio of DAPI:DABA was selected to permit this work to be compared with results from thermal cross-linking of 6FDA$_{0.5}$-DAM$_{0.33}$/DABA$_{0.17}$, where DAM is 2,3-**di**amino**m**esitylene. 6FDA$_{0.5}$-DAM$_{0.33}$/DABA$_{0.17}$ was cross-linked at 389°C, 15°C above its glass transition temperature, for 40 min and showed improved plasticization resistance to CO_2 at high pressure [15].

Here, the synthesis and characterization of thermally cross-linked 6FDA$_{0.5}$-DAPI$_{0.33}$/DABA$_{0.17}$ is investigated. Pure gas permeability coefficients of H_2, O_2, N_2, CH_4, CO_2, C_2H_4, C_2H_6 at 35°C and pressures up to 30 atm are reported for 6FDA$_{0.5}$-DAPI$_{0.5}$, linear 6FDA$_{0.5}$-DAPI$_{0.33}$/DABA$_{0.17}$, and thermally cross-linked 6FDA$_{0.5}$-DAPI$_{0.33}$/DABA$_{0.17}$. To further understand structure-property relationships of DAPI-containing polyimides and thermal cross-linking, the performance of the three polymers investigated in this work are compared to Matrimid®, 6FDA$_{0.5}$-DAM$_{0.5}$, linear 6FDA$_{0.5}$-DAM$_{0.33}$/DABA$_{0.17}$, and 6FDA$_{0.5}$-DAM$_{0.33}$/DABA$_{0.17}$ cross-linked at 389°C for 40 min. An analysis of pure gas

solubility, diffusivity, and C_2H_4/C_2H_6 mixed gas permeability is presented elsewhere [25, 26].

For the remainder of this study 6FDA$_{0.5}$-DAPI$_{0.33}$/DABA$_{0.17}$ and 6FDA$_{0.5}$-DAM$_{0.33}$/DABA$_{0.17}$ cross-linked for 40 min will be referred to as 6FDA-DAPI/DABA(40 min) and 6FDA-DAM/DABA(40 min), respectively, for brevity. 6FDA-DAPI/DABA and 6FDA-DAM/DABA were cross-linked at 15°C above their respective glass transition temperatures, unless otherwise specified. Additionally, 6FDA$_{0.5}$-DAPI$_{0.5}$ and 6FDA$_{0.5}$-DAM$_{0.5}$ will be referred to as 6FDA-DAPI and 6FDA-DAM.

4.2. Results and Discussion

4.2.1. Polymer Structure

The molecular weights and molecular weight distributions of the linear polyimides were determined by SEC and are presented in Table B.2. The molecular weights of all samples were sufficiently high to form mechanically robust free standing films. The structures and complete imidization of these polymers were confirmed by NMR and FTIR, as explained in more detail in the SI.

The cross-linking mechanism was investigated via transmission mode FT-IR [14-16]. The spectra for linear 6FDA-DAPI, linear 6FDA-DAPI/DABA, and 6FDA-DAPI/DABA(40 min), normalized to the imide ring deformation at 720 cm^{-1}, are included in Figure 4.1-a. More complete FT-IR results are presented in the SI. After cross-linking, the broad peak between 3100 – 3500 cm^{-1} associated with the carboxylic acid –OH stretch decreased nearly to the same absorbance observed for 6FDA-DAPI, indicating that disappearance of these groups is due to the thermal treatment [15, 17]. After equilibrating with ambient air, the water content of both 6FDA-DAPI/DABA and 6FDA-DAPI/DABA(40 min) films were ca. 0.25 wt%, based on TGA. The low and similar water

contents in both films suggest that the change in the broad peak between 3100 – 3500 cm^{-1} is due to a structural change between the cross-linked and linear samples, not simply differences related to water absorbed by the samples. Additionally, as shown in Figure 4.1-b, a double peak at 1720 cm^{-1} was observed for linear 6FDA-DAPI/DABA, and after cross-linking at 353°C for 40 min, only a single peak was observed. This additional peak was likely associated with the carboxylic acid group in the DABA monomer unit. The disappearance of this peak after heating is consistent with the loss of the DABA carboxylic acid groups in the cross-linked structure, which is consistent with the cross-linking mechanisms presented in Figure 2.3 and other reports for similar structures [15, 17].

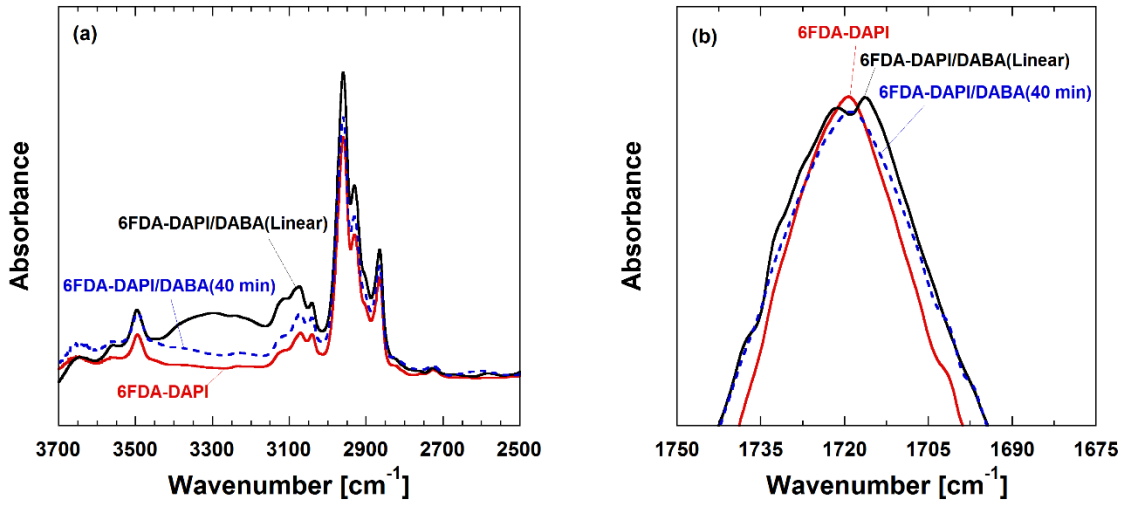

Figure 4.1. (a) High frequency range of the transmission FTIR spectra of 6FDA-DAPI [red], linear 6FDA-DAPI/DABA [black], and 6FDA-DAPI/DABA(40 min) [blue]. (b) Carbonyl stretch, showing the additional peak at 1717 cm^{-1} associated with the carboxylic acid group in DABA for linear 6FDA-DAPI/DABA.

Once the polyimide films were cast and dried, TGA-MS and DSC were used to confirm complete solvent removal and to investigate thermal properties. TGA

measurements coupled with mass spectroscopy of the evolved gases were conducted to characterize the thermal decarboxylation and decomposition of the polymers. Figure 4.2-*a* shows the mass loss and derivative mass loss of 6FDA-DAPI and linear 6FDA-DAPI/DABA. For both polymers, no significant mass loss was observed below 200°C, indicating no residual solvent remained in the cast films. Linear 6FDA-DAPI/DABA exhibited two distinct mass loss regions, a smaller loss starting at about 200°C and a larger mass loss starting at 450°C. The lower temperature mass loss is attributed to thermal decarboxylation of the DABA moieties (cf. Figure 2.3), and the higher temperature mass loss is attributed to thermal degradation of the polymer backbone. This conclusion is supported by TGA-MS of linear 6FDA-DAPI/DABA, reported in Figure 4.2-*b*, where a peak in the atomic mass intensities for CO_2 (m/z = 44) and H_2O (m/z = 18) correlated with the lower temperature mass loss region and a peak in degradation products, such as $–CF_3$ (m/z = 69), correlated with the higher temperature mass loss [27]. Furthermore, 6FDA-DAPI exhibited only one mass loss region, starting at about 450°C, which is attributed to thermal degradation of the polymer backbone. While some cross-linking mechanisms indicate the evolution of H_2O, CO_2, and CO during decarboxylation of pendent –COOH groups, CO (m/z = 28) could not be detected since its molecular mass overlapped that of the N_2 sweep gas (m/z = 28) [14-17].

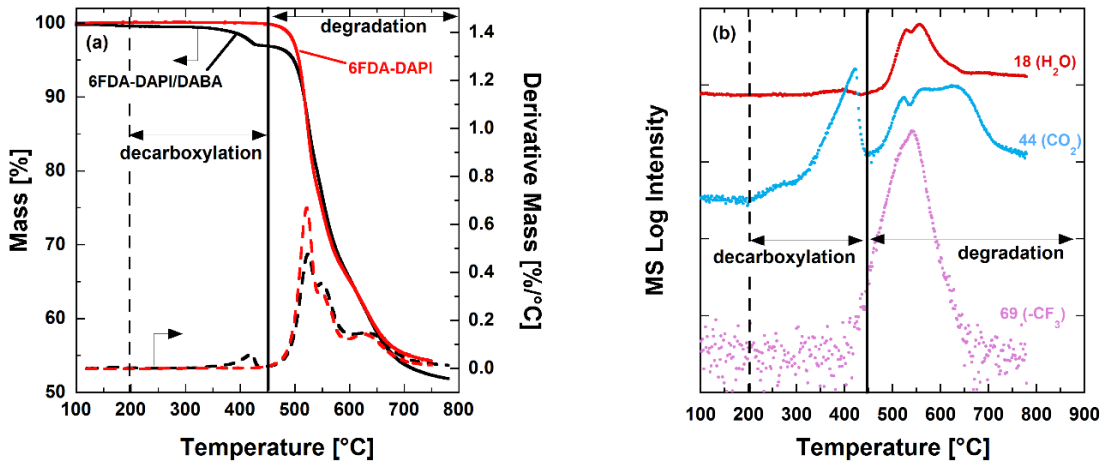

Figure 4.2. (a) TGA mass loss and derivative mass loss with temperature of 6FDA-DAPI [red] and linear 6FDA-DAPI/DABA [black] (b) The corresponding mass spec signal from the evolved gases of linear 6FDA-DAPI/DABA during TGA for H_2O (mz = 18, red), CO_2 (mz = 44, blue), and -CF_3 (mz = 69, pink).The mass spec signal for H_2O is also reported separately in Figure B.5 of the SI.

The glass transition temperature, T_g, of 6FDA-DAPI was 322°C, defined as the mid-point of the step change in heat capacity during the second DSC heating scan (cf., Figure 4.3). For linear 6FDA-DAPI/DABA, several features, including a broad endothermic band from 270 – 380°C, were observed on the first scan, and no clear glass transition temperature was observed. While the small thermal event around 240°C could be due to decarboxylation, poor contact with the sample pan, or sample processing history, the broad endothermic peak occurs in the same temperature range as the large peak in the mass spec signal for CO_2 (cf., Figure 4.2-*b*). The broad endothermic peak is ascribed to decarboxylation of the DABA moieties. On the second scan, only a glass transition was observed, at 338°C, and it increased slightly on subsequent scans, consistent with most of the DABA undergoing decarboxylation during the first heating cycle.

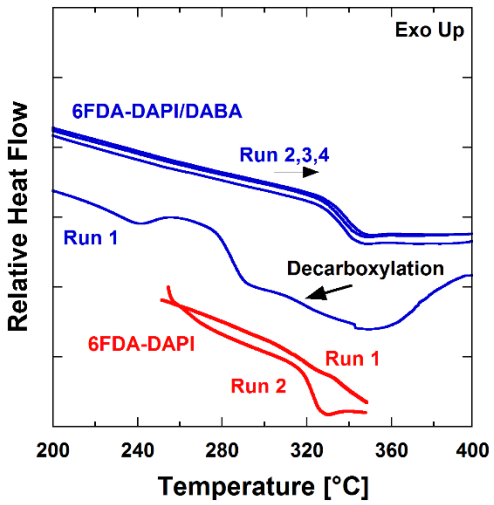

Figure 4.3. Glass transition temperatures of 6FDA-DAPI [red] and 6FDA-DAPI/DABA [blue], linear and cross-linked at 353°C for 40 min, determined by DSC.

Compared to Matrimid® (T_g = 310°C [28]), 6FDA-DAPI has a higher glass transition temperature, consistent with the –$C(CF_3)_2$– linkages contributing to a higher T_g relative to the benzophenone linkages in BTDA in Matrimid®. As observed with similar polymers, polymer chain mobility was potentially reduced slightly when DABA and cross-linking were introduced in 6FDA-DAPI/DABA [14, 15, 17]. 6FDA-DAM and cross-linked 6FDA-DAM/DABA(40 min) have T_g values of 372°C and 376°C, respectively [29]. Thus, DAPI reduces T_g relative to DAM in these polymers.

4.2.2. Polymer Cross-linking

As mentioned above, DABA decarboxylation was assessed by measuring the mass loss associated with the lower temperature mass loss region (200 – 440°C) in the TGA scan of linear 6FDA-DAPI/DABA (cf. Figure 4.2-*a*). This mass loss was 2.40 %, which is slightly greater than the expected theoretical mass loss of 2.36%, assuming 100% decarboxylation according to the mechanism in Figure 2.3. Due to the separation between

thermal decarboxylation (200 – 440°C) and thermal degradation (>450°C), 6FDA-DAPI/DABA appears to be cross-linked prior to the onset of significant thermal degradation. For this study, a cross-linking temperature of 353°C, 15°C above the measured T_g of the cross-linked polymer but below to onset of large scale degradation, was selected. While others [14, 15, 17] have demonstrated cross-linking of similar materials below T_g, we used a temperature above T_g to favor rapid and near theoretical conversion to the cross-linked structure, since rapid polymer chain motion would facilitate cross-linking.

To prepare cross-linked samples for further study, the heating protocol detailed in Figure B.1 was followed. In this protocol, samples were heated in a tube furnace under a N_2 atmosphere at a ramp rate of 40°C/min from ambient to 353°C and held for 10, 20, or 40 min at 353°C before being rapidly quenched to room temperature. The observed mass loss, theoretical conversion, gel fraction, and measured density of each thermally treated sample are recorded in Table 4.1. As cross-linking time increased from 10 to 40 min, the theoretical conversion of 6FDA-DAPI/DABA to the cross-linked structure increased from 32.2% to 103%, respectively. The 3% excess mass loss observed for the 40 min cross-linked sample may be due to water loss and/or a small amount of thermal degradation occurring during the longest thermal treatment time considered. Similarly, gel fraction increased with theoretical conversion, with the 10 min treated sample remaining fully soluble in hot THF. The 20 min and 40 min samples had gel fractions of 93.9% and 97.2 %, respectively. While the 10 min sample remained soluble, it may be partially cross-linked with a cross-link density lower than that needed to form an insoluble network [30].

Thermally treating linear 6FDA-DAPI at 353°C for 40 min resulted in a gel fraction of 30.1%, despite the absence of carboxylic acid groups for cross-linking. The fact that the linear polymer is partially insoluble may be due to the thermal treatment increasing inter-chain charge transfer complexes which have been shown to decrease solubility of aromatic

polyimides [17, 31, 32]. Thus, the increase in gel fraction with increasing thermal treatment time appears to derive from both cross-linking via the DABA units as well as other mechanisms, such as formation of charge transfer complexes.

Polymer	Thermal Treatment	Mass Loss (%)	Theor. Conv. (%)	Gel Fraction (%)	Density (g/cm^3)	FFV (route d)**	FFV (route a & b)**
6FDA-DAPI	None	--	--	0	1.296 ± 0.009	0.181 ± 0.003	
	353°C, 40 min	1.655	--	30.1	--	--	
6FDA-DAPI/DABA	None	--	--	0	1.337 ± 0.008	0.179 ± 0.002	
	353°C, 10 min	0.761	32.2	0	1.334 ± 0.008	0.180 ± 0.002	0.181 ± 0.002
	353°C, 20 min	1.37	58.3	93.3	1.333 ± 0.009	0.181 ± 0.002	0.183 ± 0.002
	353°C, 40 min	2.42	103	97.2	1.338 ± 0.009	0.177 ± 0.002	0.181 ± 0.002

** Note: FFV was calculated according to Eq. B.1 in the SI, using experimental density values and group contribution theory to predict the occupied volume, and Eq. B.2, assuming cross-linking occurs by either 100% radical combination (Route *d* in Figure 2.3) or 100% methyl hydrogen abstraction (Route *a* and *b* in Figure 2.3).

Table 4.1. Mass loss, gel fraction, density, and fractional free volume (FFV) of 6FDA-DAPI and 6FDA-DAPI/DABA cross-linked at 353°C for 0, 10, 20, 40 min.

The linear and cross-linked films were tested for solubility in chloroform ($CHCl_3$), dichoromethane (CH_2Cl_2), tetrahydrofuran (THF), toluene, N-methyl-2-pyrrolidinone (NMP), and N,N-dimethylacetamide (DMAc). As shown in Table B.3, 6FDA-DAPI was soluble in all solvents considered, and linear 6FDA-DAPI/DABA was soluble in THF, NMP, and DMAc. The 6FDA-DAPI/DABA(40 min) cross-linked sample did not dissolve in any of the solvents considered and showed no visual signs of swelling or deformation when boiled in NMP or DMAc.

4.2.3. Polymer Density, Fractional Free Volume (FFV), and Cross-linking Route

Based on previous studies, the two most likely cross-linking methods are radical combination (Route *d* in Figure 2.4) and/or methyl-hydrogen abstraction (Routes *a* and *b* in Figure 2.4). While it is possible for the radicals generated by carboxylic acid decomposition to abstract hydrogens from other locations on the polymer backbone or to react with the fluorine groups in 6FDA, these reaction pathways are structurally hindered or require higher activation energies [15-17, 33]. To better identify the potential cross-linking mechanism, and due to the insolubility of cross-linked samples, ^{13}C CP/TOSS solid-state NMR measurements were performed on the linear and the most cross-linked (353°C, 40 min) samples. The results are presented in Figure 4.4 with the labeled peaks corresponding to the carbons in the structure. After cross-linking, only a slight increase in peaks at 140 and 127 ppm, associated with aromatic carbons, was observed. Additionally, no significant change in the peak at 170 ppm, associated with the C=O groups, after cross-linking was observed, likely due to the overwhelming signal from the imide ring C=O groups, which outnumber the carboxylic acid C=O groups 12:1. The absence of changes in the peaks associated with $–CH_2-$ and $–CH_3$ (peaks between 25 – 60 ppm) likely indicates that most cross-linking occurs between two aromatic groups (Route *d* in Figure 2.3), rather than by abstraction of methyl hydrogens (Routes *a* and *b* in Figure 2.3). Cross-linking by Routes *a* and *b* may still occur, but the presence of functional groups associated with this mechanism are below the detection limit. To better investigate the cross-linking route by SS-NMR, increasing the quantity of DABA in the copolymer (i.e., using a DAPI:DABA ratio of 1:1 or 1:2, rather than 2:1) is suggested, but this study is beyond the scope of the current investigation.

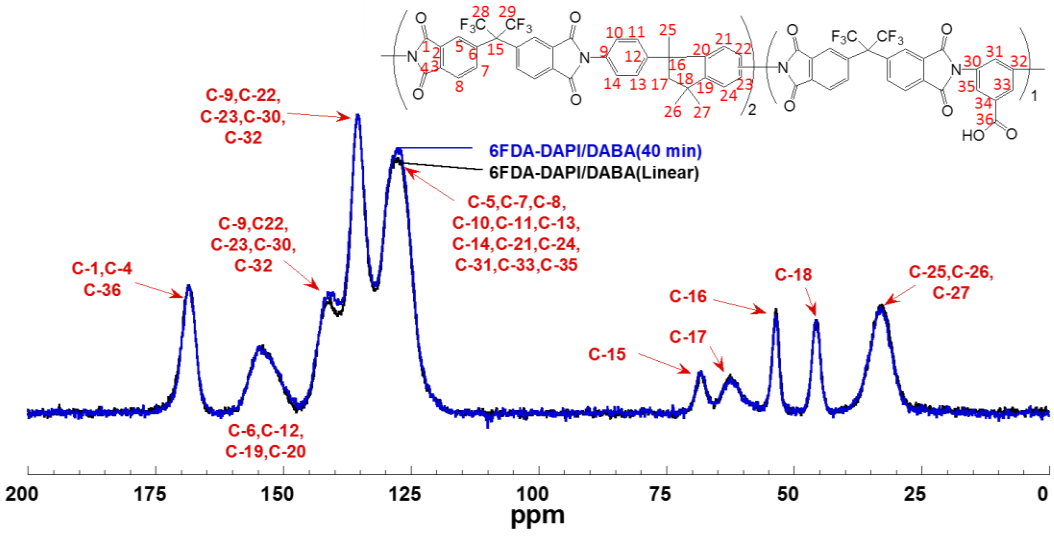

Figure 4.4. ^{13}C CP/TOSS solid state NMR of linear 6FDA-DAPI/DABA [black] and 6FDA-DAPI/DABA(40 min) [blue]. The data was collected using a 5 second relaxation delay with 2048 total scans. Labeled carbons correspond to carbons in noted structure.

To estimate the FFV of cross-linked samples, the occupied volume, V_o, was calculated using group contribution theory for Routes *a*, *b*, and *d*. Using group contribution theory, Routes *a* and *b* cannot be distinguished, so these reaction pathways have been grouped together for FFV analysis. While it is possible that both cross-linking pathways occur simultaneously, the two routes are considered separately, either solely by radical coupling or solely by methyl hydrogen abstraction, to help identify how each route contributes to the total FFV of the polymer matrix. Fractional free volume was calculated using the methods described in the SI [34], adjusting V_o for each polymer based on the fractional conversion to the cross-linked structure (cf. Eq. B.1 and Eq. B.2) and using the experimental density values from Table 4.1.

The density values for 6FDA-DAPI and 6FDA-DAPI/DABA cross-linked at 353°C for 0, 10, 20, and 40 min are recorded in Table 4.1 along with the FFV values for the two

cross-linking mechanisms. The polar –COOH groups in linear 6FDA-DAPI/DABA likely favor increased hydrogen bonding, producing a more dense polymer matrix than in 6FDA-DAPI. However, the density of 6FDA-DAPI/DABA samples heated at 353°C for 10, 20, and 40 min remained constant, with any potential differences falling within the experimental uncertainty. According to group contribution theory, there is only a minimal difference in the theoretical occupied volume for the two potential cross-linked structures (Figure B.6), which results in no discernable difference in FFV between the two potential cross-linking mechanisms (Table 4.1 and Figure B.6). The FFV values are not sensitive to the cross-linking routes, and within the experimental uncertainty of the density measurements, no discernable differences in FFV between any of the DAPI-containing polymers in this study were detected.

To further characterize these materials, WAXS was used to probe inter-and intra-polymer chain spacing within the samples. As shown in Figure 4.5-a and Figure B.7, two scattering peaks were observed for all polymers, a lower intensity scattering peak around 5°, corresponding to scattering distances of about 17Å, and a higher intensity scattering peak around 15°, corresponding to scattering distances of about 5.7Å. The scattering peak around 15°, reported in Figure 4.5-b, is in the same range as other 6FDA containing polyimides [35]. A slight increase in the maximum peak intensity and slight shift in d-spacing were observed as 6FDA-DAPI/DABA cross-linking time increased. Linear 6FDA-DAPI/DABA and 6FDA-DAPI/DABA(10 min) had a d-spacing of 5.63Å, while 6FDA-DAPI/DABA(20 min), 6FDA-DAPI/DABA(40 min), and 6FDA-DAPI had d-spacing values of 5.66Å, 5.73Å, and 5.76Å, respectively. Additionally, an increase in absolute scattering intensity was observed, following the same trend as the d-spacing shift, with 6FDA-DAPI having the highest scattering intensity, indicating an increase in structural order with increasing d-spacing. This slight increase in d-spacing qualitatively correlates

with the measured gas permeability (as shown below), suggesting there may be a slight increase in FFV with increased cross-linking time, although any change in FFV was too subtle to detect via density-based FFV calculations. This point will be discussed in detail later and additional WAXS analysis is included in the SI.

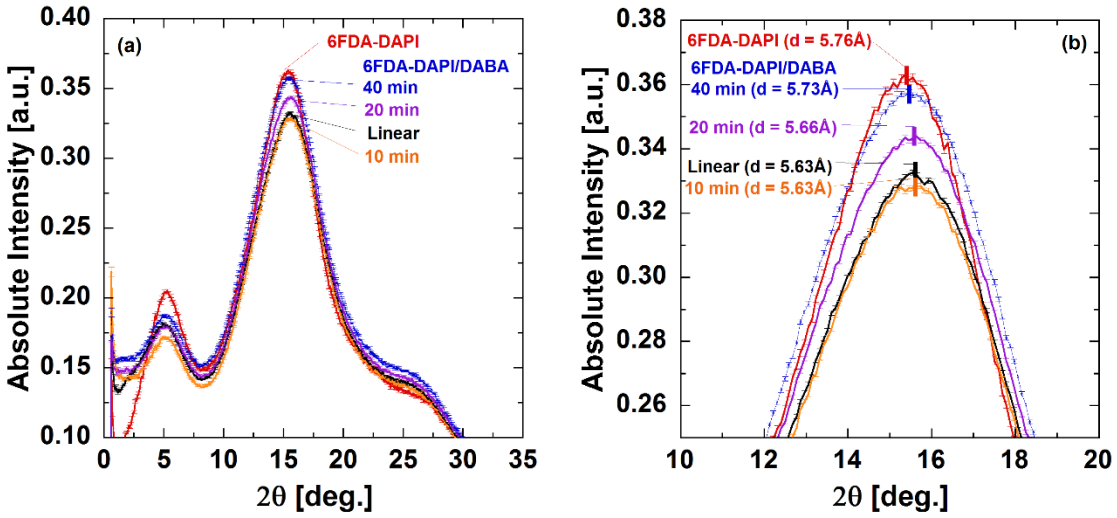

Figure 4.5. (a) The full 2θ range of wide angle x-ray scattering of 6FDA-DAPI [red], linear 6FDA-DAPI/DABA [black], and 6FDA-DAPI/DABA(10 min) [orange], 6FDA-DAPI/DABA(20 min) [purple], and 6FDA-DAPI/DABA(40 min) [blue] and (b) the large scatting peak at $10° < 2\theta < 20°$. The noted d-spacing for each sample were calculated using the 2θ at the maximum scattering intensity of the large peak.

Compared to similar polymers, FFV increases in the following order: Matrimid® (17.0% [28]) < linear 6FDA-DAPI/DABA (17.9 ± 0.02%) ≈ 6FDA-DAPI (18.1 ± 0.03%) < linear 6FDA-DAM/DABA (18.3% [29]), < 6FDA-DAM (19.0% [29]). Comparing 6FDA-DAPI to Matrimid®, the $–C(CF_3)_2–$ linkages in 6FDA contributed to a higher FFV than the benzophenone linkages in BTDA. Relative to 6FDA-DAM, FFV decreased when DABA was introduced into 6FDA-DAM/DABA, suggesting incorporating DABA into the backbone may have facilitated additional hydrogen bonding and reduced FFV. This effect

was minimal for the DAPI-containing polyimides in this work, with no detectible change in FFV when DABA was incorporated into the polymer structure. Consistent with the trends in T_g, the rigid, bulky DAM structure gave a higher FFV in 6FDA-DAM and linear 6FDA-DAM/DABA than DAPI in 6FDA-DAPI and linear 6FDA-DAPI/DABA. The changes in FFV with changes in polymer structure are reflected in pure gas permeability coefficients, as shown in Table B.6 in the SI [34].

4.2.4. Influence of Cross-linking on Pure Gas Permeability and Selectivity

As presented in Figure 4.6-a, Figure B.10, and Figure B.11, all materials show minimal pressure dependence for H_2, O_2, N_2, and CH_4 pure gas permeability coefficients. In contrast, CO_2, C_2H_4, and C_2H_6 permeabilities increase at high pressures for some samples. This behavior is typical of gas transport in glassy-polymers, where dual-mode behavior predicts a decrease in permeability at low partial pressure driving force and approaches a constant value at higher pressures [36]. However, highly condensable and strongly sorbing gases, like CO_2, C_2H_4, and C_2H_6, can interact strongly with the polymer and induce plasticization, or swelling, of the polymer matrix, at high pressures. Both linear 6FDA-DAPI/DABA and 6FDA-DAPI/DABA(40 min) showed minimal increase in C_2H_4 and C_2H_6 permeability at high pressures, suggesting potentially improved plasticization resistance compared to 6FDA-DAPI. Plasticization resistance and C_2H_4/C_2H_6 mixed gas permeability of these polymers will discussed further in a subsequent publication [25, 26].

The pure gas permeability data at 5 atm are summarized in Table B.6. The ideal selectivity at 5 atm for several relevant gas pairs were calculated using Eq. 2.4 and are summarized in Table B.7. For all polymers, gas permeabilities followed the trend shown in Figure 4.6-a, $P(C_2H_6) < P(CH_4) < P(C_2H_4) < P(N_2) < P(O_2) < P(CO_2) < P(H_2)$, where permeability increased with decreasing gas diameter (Table B.6), with CO_2 and C_2H_4 deviating slightly from this trend. This result is demonstrated in Figure 4.6-b, where pure

gas permeabilities at 5 atm for 6FDA-DAPI, linear 6FDA-DAPI/DABA, and 6FDA-DAPI/DABA(40 min) are plotted versus gas diameter squared, d_g^2. This trend is consistent with diffusion controlled gas transport, and the deviation of CO_2 and C_2H_4 is often observed due to their relatively high solubility coefficients in polymers [37].

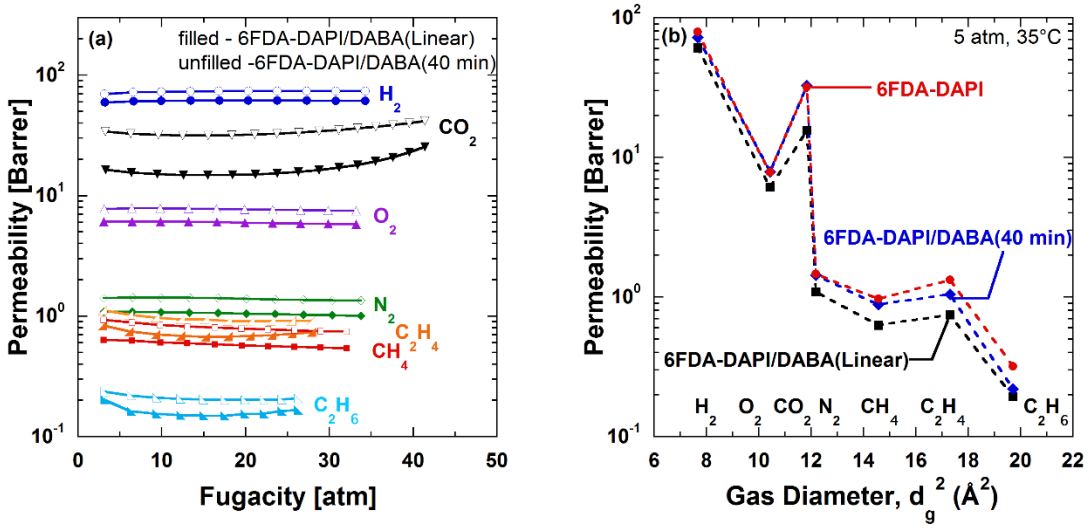

Figure 4.6. (a) Pure gas permeability of linear 6FDA-DAPI/DABA [filled markers] and 6FDA-DAPI/DABA(40 min) [unfilled markers] for H_2 [●], CO_2 [▼], O_2 [▲], N_2 [♦], C_2H_4 [◢], CH_4 [■], and C_2H_6 [◣]. (b) Pure gas permeability in 6FDA-DAPI [●], linear 6FDA-DAPI/DABA [■] and 6FDA-DAPI/DABA(40 min) [♦], at 35°C and 5 atm as a function of gas diameter squared. Gas diameter values, d_g, were taken from literature, and are recorded in Table B.1 [38]. Fugacity was used to calculate permeability of CO_2, C_2H_4, and C_2H_6 and pressure was used to calculate permeability of N_2 and CH_4.

When comparing the transport properties of 6FDA-DAPI to linear 6FDA-DAPI/DABA, introduction of the DABA moiety decreases permeability for all gases. The percent decrease in permeability was CO_2 (50.4%), C_2H_4 (46.6%), C_2H_6 (41.9%), CH_4 (37.1%), N_2 (25.9%), O_2 (22.6%), and H_2 (17.0%). Larger and more condensable gases exhibited a larger decrease in permeability than smaller, less condensable species.

Additionally, the ideal selectivity, for most of the gas pairs summarized in Table B.7, increased when DABA was incorporated into the polymer backbone structure.

After thermally treating linear 6FDA-DAPI/DABA for various times, the permeability of all gases increased with increasing conversion to the cross-linked structure (cf., Table B.6). The permeability coefficients of linear 6FDA-DAPI/DABA and 6FDA-DAPI/DABA(40 min) are plotted versus fugacity in Figure 4.6-a. As conversion increased from the linear structure to the fully crosslinked structure (353°C, 40 min), the permeability of each gas increased as follows: H_2 (18.8%) < C_2H_6 (13.3%) < O_2 (29.1%) < N_2 (31.8%) < C_2H_4 (39.3%) < CH_4 (41.4%) < CO_2 (109%). The ideal selectivity remained relatively constant as conversion increased (cf., Table B.7). An example of this trend can be observed in Figure 4.7-a, where O_2 permeability increased by 30% as cross-linking time increased from 0 min to 40 min, and O_2/N_2 ideal selectivity was generally independent of conversion. Due to the larger increase in CO_2 permeability than other gases upon cross-linking, pure gas selectivity for gas pairs including CO_2 (CO_2/CH_4, CO_2/N_2) increase with increasing conversion (cf. Table B.6), with CO_2/CH_4 selectivity increasing by 48% and CO_2/N_2 selectivity increasing by 64% as conversion increased from 0 to 103%. This large increase in CO_2 permeability coupled with increases in selectivities, may be due to increased CO_2 diffusivity, as judged based on the slight increase in d-spacing, which may reflect a slight increase in inter-chain spacing, with cross-linking.

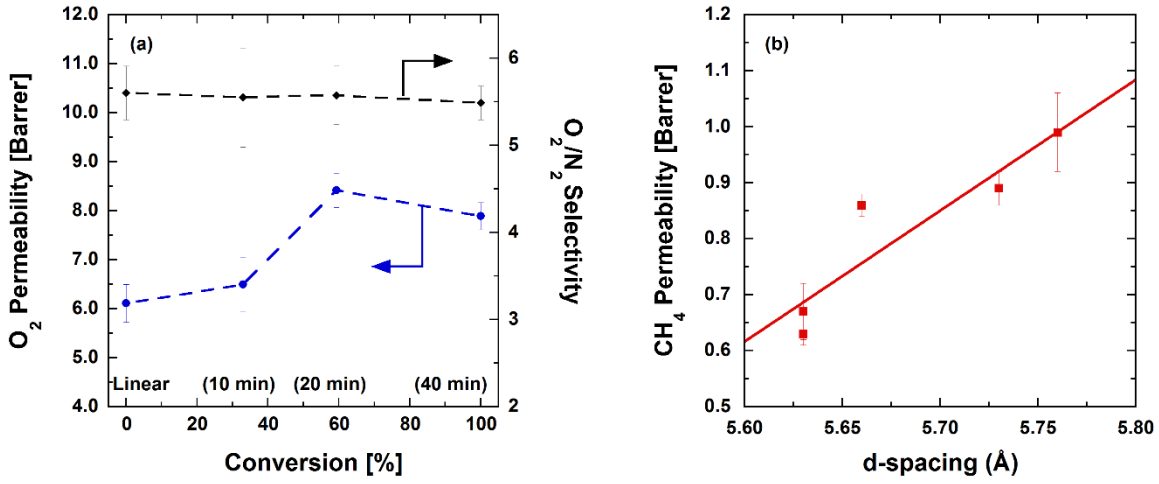

Figure 4.7. (a) O_2 permeability [●] and O_2/N_2 selectivity [♦] versus theoretical conversion of 6FDA-DAPI/DABA cross-linked at 353°C, reported at 35°C and 5 atm. (b) CH_4 permeability (■) at 5 atm and 35°C versus inter-chain d-spacing of DAPI-containing polyimides (cf., Table B.5) measured by WAXS.

This increase in pure gas permeability with increased thermal treatment time suggests a more open polymer matrix after cross-linking. In many cases, cross-linking a polymer significantly decreases its permeability due to a reduction in FFV and reduced segmental chain motion that permits slower diffusion [39, 40]. In our case, there was no observable difference in FFV upon cross-linking. However, there was a slight increase in inter-chain d-spacing, which did correlate, roughly, with permeability. An example of this correlation is shown in Figure 4.7-b for CH_4 and for other gases in Figure B.12 and Figure B.13. By cross-linking above T_g, the polymer chains may organize to a slightly higher, though undetectable, FFV, which is trapped upon cross-linking and quenching to ambient temperature. To confirm that the higher gas permeability was long-lived, 6FDA-DAPI/DABA(40 min) was held at 220°C for 24 h under vacuum, which might be expected to relax any highly non-equilibrium excess free volume [41, 42]. As shown in Figure 4.8 for CH_4, the aged, cross-linked sample had slightly higher pure gas permeabilities than the

cross-linked sample, so any changes in free volume were not short-lived. This indicates any additional free volume incorporated into the matrix during the cross-linking process is likely permanent.

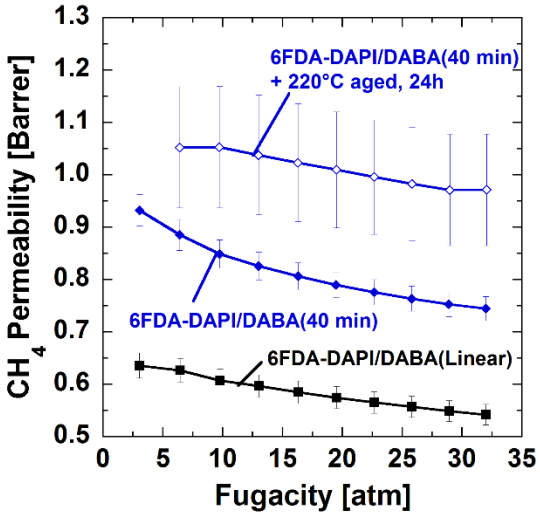

Figure 4.8. CH_4 pure gas permeability in linear 6FDA-DAPI/DABA [■], 6FDA-DAPI/DABA(40 min) [♦], and 6FDA-DAPI/DABA(40 min) aged at 220°C for 24h [◇]. Permeation results for other gases in "aged" cross-linked 6FDA-DAPI/DABA are included in Figure B.14.

4.2.5. Pure Gas Selectivity

The C_2H_4/C_2H_6 and CO_2/CH_4 pure gas selectivities are presented in Figure 4.9 on upper bound plots for 6FDA-DAPI, linear 6FDA-DAPI/DABA, and 6FDA-DAPI/DABA(40 min). As is evident in the C_2H_4/C_2H_6 upper bound plot, the permeability of C_2H_4 in linear 6FDA-DAPI/DABA is lower than that of 6FDA-DAPI and only a minimal decrease in selectivity is observed. After cross-linking 6FDA-DAPI/DABA, both pure gas permeability and selectivity increased. The increase in permeability is consistent with the cross-linked polymer having a more open structure than both linear polymers, and the increase in selectivity is likely due to increased size sieving in the cross-linked polymer matrix (cf., Figure 4.5 and Section 3.3 discussing the density and FFV analysis). These

results will be investigated further in a subsequent publication reporting mixed gas permeation properties as well as gas solubility and diffusivity data in these polymers [25, 26].

For the CO_2/CH_4 gas pair, both pure gas permeability and selectivity were lower in linear 6FDA-DAPI than in linear 6FDA-DAPI/DABA. The decrease in selectivity for this particular gas pair is due to a stronger Langmuir-type decrease in CO_2 permeability than for CH_4, resulting in an apparent decrease in selectivity (cf., Figure 4.6-a and Figure B.10). After fully cross-linking 6FDA-DAPI/DABA, both permeability and selectivity increased, resulting in similar values to those of linear 6FDA-DAPI.

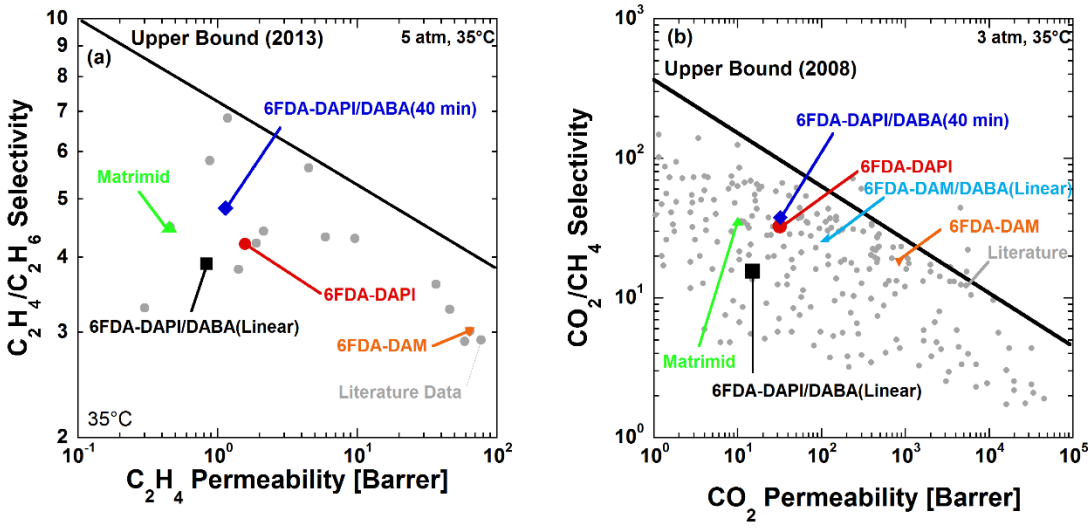

Figure 4.9. Upper bound plots for: (a) C_2H_4/C_2H_6 at 5 atm [13] and (b) CO_2/CH_4 at 3 atm [20] for 6FDA-DAPI [●], linear 6FDA-DAPI/DABA [■],6FDA-DAPI/DABA(40 min) [♦], data collected from literature [●] [13]. Matrimid® [▲] properties for C_2H_4/C_2H_6 (3.4 atm) and CO_2/CH_4 (4 atm) were obtained from [13] and [43], respectively [44]. Pressures for literature points vary slightly. 6FDA-DAM [▼] [29, 45, 46] and linear 6FDA-DAM/DABA [◣] [29, 47] data are from the literature.

4.3. CONCLUSIONS

6FDA-DAPI/DABA was cross-linked by thermal decarboxylation of DABA. The cross-linking mechanism was investigated by DSC, TGA-MS, FTIR, and ^{13}C CP/TOSS solid state NMR, revealing removal of the carboxylic acid group during the thermal treatment. No detectable change in FFV due to cross-linking was detected using experimental density values. However, WAXS revealed a slight increase in inter-chain d-spacing after thermal cross-linking, qualitatively trending with the observed increase in gas permeability in the cross-linked samples. As cross-linking conversion increased, pure gas permeability increased, with 6FDA-DAPI/DABA(40 min) having 30% higher pure gas permeability for most gases, with no significant loss in ideal selectivity relative to its uncross-linked analog. Compared to Matrimid®, the 6FDA unit increased gas permeability in 6FDA-DAPI and linear 6FDA-DAPI/DABA and 6FDA-DAPI/DABA(40 min).

4.4. ACKNOWLEDGMENTS

This material is based upon work supported in part by the National Science Foundation Graduate Research Fellowship under Grant No. DGE-1610403. The authors gratefully acknowledge partial support from the Division of Chemical Sciences, Geosciences, and Biosciences, Office of Basic Energy Sciences of the U.S. Department of Energy (DOE), USA through Grant DE-FG02-02ER15362 and partial support by the Australian-American Fulbright Commission for the award to BDF of the U.S. Fulbright Distinguished Chair in Science, Technology and Innovation sponsored by the Commonwealth Scientific and Industrial Research Organization (CSIRO). Additionally, this work is supported in part by the National Science Foundation under Cooperative Agreement No. EEC-1647722. Any opinions, findings and conclusions or recommendations expressed in this material are those of the authors and do not necessarily reflect the views of the National Science Foundation. NAL and MC thank the National

Science Foundation for partial support of this research (CBET-1706968). The authors acknowledge Steve Swinnea and Steve Sorey from The University of Texas at Austin for their assistance in measuring and interpreting WAXS and SS-NMR results, respectively.

4.5. REFERENCES

[1] R.W. Baker, Future Directions of Membrane Gas Separation Technology, Industrial & Engineering Chemistry Research, 41 (2002) 1393-1411.

[2] R.W. Baker, Membrane Technology and Applications, in: Membrane Technology, John Wiley & Sons, Ltd, Chichester, UK, 2004, pp. 545.

[3] S.A. Stern, Polymers for Gas Separationis: The Next Decade, Journal of Membrane Science, 94 (1994) 1-65.

[4] I.V. Farr, Synthesis and Characterization of Novel Polyimide Gas Separation Membrane Material Systems, Virginia Polytechnic Institute and State University 1999.

[5] I.V. Farr, D. Kratzner, T.E. Glass, D. Dunson, Q. Ji, J.E. McGrath, The Synthesis and Characterization of Polyimide Homopolymers Based on 5(6)-Amino-1-(4-Aminophenyl)1,3,3-Trimethylindane, Journal of Polymer Science Part A: Polymer Chemistry, 38 (2000) 2840-2854.

[6] T. Visser, M. Wessling, Auto and Mutual Plasticization in Single and Mixed Gas C3 Transport Through Matrimid-Based Hollow Fiber Membranes, Journal of Membrane Science, 312 (2008) 84-96.

[7] Z.P. Smith, Fundamentals of Gas Sorption and Transport in Thermally Rearranged Polyimides, Doctor of Philosophy, The University of Texas at Austin, Austin, TX, 2014.

[8] U.S. Shale Production, U.S. Energy Information Administration, https://www.eia.gov/dnav/ng/hist/res_epg0_r5302_nus_bcfa.htm, 2018.

[9] Hydrocarbon Gas Liquids Explained, U.S. Energy Information Administration, https://www.eia.gov/energyexplained/index.php?page=hgls_home, 2018.

[10] R.W. Baker, Membrane Technology and Applications, 3rd Edition ed., A John Wiley & Sons, Ltd., Publication, 2012.

[11] G.E. Keller, A.E. Marcinkowsky, S.K. Verma, K.D. Williamson, Olefin Recovery and Purification via Silver Comlexation, in: N.N. Li, J.M. Calo (Eds.) Separation and Purification Technology, Marcel Dekker, New York, 1992.

[12] D.J. Safarik, R.B. Eldridge, Olefin/Paraffin Separations by Reactive Absorption: A Review, Industrial & Engineering Chemistry Research, 37 (1998) 2571-2581.

[13] M. Rungta, C. Zhang, W.J. Koros, L. Xu, Membrane-Based Ethylene/Ethane Separation: The Upper Bound And Beyond, AIChE Journal, 59 (2013) 3475-3489.

[14] N. Du, M.M. Dal-Cin, G.P. Robertson, M.D. Guiver, Decarboxylation-Induced Cross-Linking of Polymers of Intrinsic Microporosity (PIMs) for Membrane Gas Separation, Macromolecules, 45 (2012) 5134-5139.

[15] A.M. Kratochvil, W.J. Koros, Decarboxylation-Induced Cross-Linking of a Polyimide for Enhanced CO_2 Plasticization Resistance, Macromolecules, 41 (2008) 7920-7927.

[16] C. Zhang, P. Li, B. Cao, Decarboxylation Crosslinking of Polyimides with High CO_2/CH_4 Separation Performance and Plasticization Resistance, Journal of Membrane Science, 528 (2017) 206-216.

[17] W. Qiu, C.-C. Chen, L. Xu, L. Cui, D.R. Paul, W.J. Koros, Sub-Tg Cross-Linking of a Polyimide Membrane for Enhanced CO_2 Plasticization Resistance for Natural Gas Separation, Macromolecules, 44 (2011) 6046-6056.

[18] S.A. Stern, Y. Mii, H. Yamamoto, Structure / Permeability Relationships of Polyimide Membranes. Applications to the Separation of Gas Mixtures, Journal of Polymer Science: Part B: Polymer Physics, 27 (1989) 1887-1909.

[19] S.A. Stern, V. Saxena, Concentration-Dependent Transport of Gases and Vapors in Glassy Polymers, Journal of Membrane Science, 7 (1980) 47-59.

[20] L.M. Robeson, The Upper Bound Revisited, Journal of Membrane Science, 320 (2008) 390-400.

[21] R.L. Scott, The Anomalous Behavior of Fluorocarbon Solutions, The Journal of Physical Chemistry, 62 (1958) 136 - 145.

[22] E.M.D. Siebert, C.M. Knobler, Interaction Virial Coefficients in Hydrocarbon-Fluorocarbon Mixtures, The Journal of Physical Chemistry, 75 (1971) 3863 - 3870.

[23] N.L. Le, Y. Wang, T.-S. Chung, Synthesis, Cross-linking Modifications of 6FDA-NDA/DABA Polyimide Membranes for Ethanol Dehydration via Pervaporation, Journal of Membrane Science, 415-416 (2012) 109-121.

[24] C. Staudt-Bickel, W. J. Koros, Improvement of CO_2/CH_4 Separation Characteristics of Polyimides by Chemical Crosslinking, Journal of Membrane Science, 155 (1999) 145-154.

[25] M.E. Dose, I. Hubacek, D.R. Paul, B.D. Freeman, CO_2, C_2H_4, and C_2H_6 Sorption and Mixed Gas Permeability of Thermally Cross-linked Diaminophenylindane (DAPI) Containing Polyimides, Journal of Membrane Science, Submitted (2018).

[26] M.E. Dose, J.D. Moon, I. Hubacek, D.R. Paul, B.D. Freeman, Fundamental Gas Transport and Dilation of Studies in Thermally Cross-linked Diaminophenylindane (DAPI) Containing Polyimides, Journal of Polymer Science Part B: Polymer Physics, In Preparation (2018).

[27] Z.P. Smith, D.F. Sanders, C.P. Ribeiro, R. Guo, B.D. Freeman, D.R. Paul, J.E. McGrath, S. Swinnea, Gas Sorption and Characterization of Thermally Rearranged Polyimides Based on 3,3′ -Dihydroxy-4,4′ -Diamino-Biphenyl (HAB) And 2,2′ -Bis-(3,4-Dicarboxyphenyl) Hexafluoropropane Dianhydride (6FDA), Journal of Membrane Science, 415-416 (2012) 558-567.

[28] R.R. Tiwari, Z.P. Smith, H. Lin, B.D. Freeman, D.R. Paul, Gas Permeation in Thin Films of "High Free-Volume" Glassy Perfluoropolymers: Part I. Physical Aging, Polymer, 55 (2014) 5788-5800.

[29] J.H. Kim, W.J. Koros, D.R. Paul, Physical Aging of Thin 6FDA-Based Polyimide Membranes Containing Carboxyl Acid Groups. Part I. Transport Properties, Polymer, 47 (2006) 3094-3103.

[30] P. Flory, J. Rehner, Statistical Mechanics of Cross-linked Polymer Chain Networks II: Swelling, The Journal of Chemical Physics, 11 (1943) 521 - 526.

[31] J.M. Salley, C.W. Frank, Charge Transfer in Aromatic Polyimdes, in: M. Ghosh (Ed.) Polyimide: Fundamentals and Applications, Marcel Dekker, New York, 1996.

[32] H. Kawakami, M. Mikawa, S. Nagaoka, Gas Transport Properties in Thermally Cured Aromatic Polyimide Membranes, Journal of Membrane Science, 118 (1996) 223-230.

[33] J.M. Cervantes-Uc, J.V. Cauich-Rodríguez, H. Vázquez-Torres, A. Licea-Claveríe, TGA/FTIR Study on Thermal Degradation of Polymethacrylates Containing Carboxylic Groups, Polymer Degradation and Stability, 91 (2006) 3312-3321.

[34] J.Y. Park, D.R. Paul, Correlation and Prediction of Gas Permeability in Glassy Polymer Membrane Materials via a Modified Free Volume Based Group Contribution Method, Journal of Membrane Science, 125 (1997) 23 - 39.

[35] M. Langsam, W. Burgoyne, Effects of Diamine Monomer Structure on the Gas Permeability of Polyimides. I. Bridged Diamines, Journal of Polymer Science Part A: Polymer Chemistry, 31 (1993) 909-921.

[36] D.R. Paul, Gas Sorption and Transport in Glassy Polymers, Reports of the Bunsen Society for Physical Chemistry, 83 (1979) 294-302.

[37] L.M. Robeson, M.E. Dose, B.D. Freeman, D.R. Paul, Analysis of the Transport Properties of Thermally Rearranged (TR) Polymers and Polymers of Intrinsic Microporosity (PIM) Relative to Upper Bound Performance, Journal of Membrane Science, 525 (2017) 18-24.

[38] L.M. Robeson, B.D. Freeman, D.R. Paul, B.W. Rowe, An Empirical Correlation of Gas Permeability and Permselectivity in Polymers and Its Theoretical Basis, Journal of Membrane Science, 341 (2009) 178-185.

[39] M.S. McCaig, D.R. Paul, Effect of UV Crosslinking and Physical Aging on the Gas Permeability of Thin Glassy Polyarylate Films, Polymer, 40 (1999) 7209-7225.

[40] C.T. Wright, D.R. Paul, Gas Sorption and Transport in UV-Irradiated Polyarylate Copolymers Based on Tetramethyl Bisphenol-A and Dihydroxybenzophenone, Journal of Membrane Science, 124 (1997) 161-174.

[41] Y. Huang, D. Paul, Experimental Methods for Tracking Physical Aging of Thin Glassy Polymer Films by Gas Permeation, Journal of Membrane Science, 244 (2004) 167-178.

[42] D. Punsalan, W.J. Koros, Thickness-Dependent Sorption and Effects of Physical Aging in a Polyimide Sample, Journal of Applied Polymer Science, 96 (2005) 1115-1121.

[43] M. Rungta, L. Xu, W.J. Koros, Carbon Molecular Sieve Dense Film Membranes Derived from Matrimid® for Ethylene/Ethane Separation, Carbon, 50 (2012) 1488-1502.

[44] A. Bos, I. Punt, H. Strathmann, M. Wessling, Suppression of Gas Separation Membrane Plasticization by Homogeneous Polymer Blending, AIChE Journal, 47 (2001) 1088 - 1093.

[45] L. Xu, M. Rungta, W.J. Koros, Matrimid® Derived Carbon Molecular Sieve Hollow Fiber Membranes for Ethylene/Ethane Separation, Journal of Membrane Science, 380 (2011) 138-147.

[46] W. Qiu, L. Xu, C.-C. Chen, D.R. Paul, W.J. Koros, Gas Separation Performance of 6FDA-based Polyimides with Different Chemical Structures, Polymer, 54 (2013) 6226-6235.

[47] J.D. Wind, D.R. Paul, W.J. Koros, Natural Gas Permeation in Polyimide Membranes, Journal of Membrane Science, 228 (2004) 227-236.

Chapter 5: CO_2, C_2H_4, and C_2H_6 Sorption and Mixed Gas Permeability of Thermally Cross-linked Diaminophenylindane (DAPI) Containing Polyimides

This study probes the influence of polymer structure and thermal cross-linking on plasticization resistance due to CO_2, C_2H_4, and C_2H_6. The polymer considered was a polyimide containing hexafluoroisopropylidene diphthalic anhydride (6FDA), diaminophenylindane (DAPI), and diaminobenzoic acid (DABA) in a molar ratio of 0.5/0.33/0.17, $6FDA_{0.5}$-$DAPI_{0.33}$/$DABA_{0.17}$. A polymer which did not contain the DABA cross-linking sites, $6FDA_{0.5}$-$DAPI_{0.5}$, was used as a control. $6FDA_{0.5}$-$DAPI_{0.33}$/$DABA_{0.17}$ thermally cross-linked at 353°C for 40 min showed improved plasticization resistance, relative to linear (i.e., uncross-linked) $6FDA_{0.5}$-$DAPI_{0.33}$/$DABA_{0.17}$, to pure CO_2, C_2H_4, and C_2H_6 at high pressure. However, with a 50:50 C_2H_4:C_2H_6 feed gas mixture, competitive sorption apparently suppressed C_2H_4 permeability and C_2H_4/C_2H_6 selectivity in $6FDA_{0.5}$-$DAPI_{0.5}$, while plasticization increased C_2H_6 permeability in $6FDA_{0.5}$-$DAPI_{0.5}$ and cross-linked $6FDA_{0.5}$-$DAPI_{0.33}$/$DABA_{0.17}$. Linear $6FDA_{0.5}$-$DAPI_{0.33}$/$DABA_{0.17}$ showed no significant differences between pure and mixed gas permeability and selectivity. Thus, cross-linking does not uniformly improve plasticization resistance in such materials, and the carboxylic acid group in DABA appears to improve plasticization resistance by C_2H_4 and C_2H_6 in mixed gas experiments. [4]

[4] This chapter has been adapted with permission from sections of M.E. Dose, I. Hubacek, D.R. Paul, B.D. Freeman, CO_2, C_2H_4, and C_2H_6 Sorption and Mixed Gas Permeability of Thermally Cross-linked Diaminophenylindane (DAPI) Containing Polyimides, Journal of Membrane Science, In Preparation (2018). I was the primary author, developed the

5.1. INTRODUCTION

Polymer based membrane gas separations are important in several commercial separations, including H_2/N_2, H_2/CO_2, O_2/N_2, CO_2/CH_4, and H_2O/air [1-6]. A disadvantage of polymer membranes is their susceptibility to undergo plasticization, or swelling, of the polymer matrix, which can decrease selectivity when membranes are exposed to highly condensable species. This shortcoming can limit the use of membranes for aggressive hydrocarbon based separations, including liquid-liquid separations, hydrocarbon contaminated natural gas, and olefin/paraffin separations.

Previous studies show improvements in CO_2 plasticization resistance by using thermal decarboxylation to cross-link carboxylic acid containing polyimides and polymers of intrinsic microporosity (PIM) [7-10]. Motivated by these reports, this study focuses on plasticization resistance of a thermally cross-linked polyimide synthesized from hexafluoroisopropylidene diphthalic anhydride (6FDA), diaminophenylindane (DAPI), and diaminobenzoic acid (DABA) in a molar ratio of 0.5/0.33/0.17, $6FDA_{0.5}$-$DAPI_{0.33}$/$DABA_{0.17}$. For this study, $6FDA_{0.50}$-$DAPI_{0.33}$/$DABA_{0.17}$ is abbreviated as 6FDA-DAPI/DABA. Previously, the inclusion of 6FDA in polymer backbones was shown to increase fractional free volume of the polymer matrix relative to other potential dianhydride monomer units. [11-13]. To determine the effect of including DABA in the polymer backbone on permeability and selectivity, transport of linear (i.e., uncross-linked) and cross-linked 6FDA-DAPI/DABA will be compared to

---

experimental design, conducted the experiments, and preformed most of the analysis. The co-authors from these papers contributed to the analysis and helped run supporting experiments.

6FDA0.5-DAPI0.5, which contains an equal molar ratio of 6FDA and DAPI and will be referred to as 6FDA-DAPI.

Pure gas permeability of 6FDA-DAPI, linear 6FDA-DAPI/DABA, and 6FDA-DAPI/DABA cross-linked at 353°C for 40 min was reported previously [13]. By heating 6FDA-DAPI/DABA above its glass transition temperature, thermogravimetric analysis coupled with mass spectroscopy (TGA-MS) and Fourier-transform infrared spectroscopy (FT-IR) revealed that the DABA –COOH moiety underwent decarboxylation, resulting in a cross-linked structure. After cross-linking 6FDA-DAPI/DABA at 353°C for 40 min, wide angle x-ray scattering (WAXS) revealed an increase in d-spacing, which correlated with a 30% increase in pure gas permeability for most gases. Additionally, while 6FDA-DAPI and cross-linked 6FDA-DAPI/DABA had similar FFV values, cross-linked 6FDA-DAPI/DABA had higher CO_2/CH_4 and C_2H_4/C_2H_6 pure gas selectivities than 6FDA-DAPI and polymers with similar structures. The cause for this increase in selectivity will be investigated further in this study and in a subsequent publication [14]. While cross-linking conversion of 6FDA-DAPI/DABA can be controlled by adjusting cross-linking time, this study focused on 6FDA-DAPI/DABA cross-linked at 353°C for 40 mins, which showed almost 100% decarboxylation and will be referred to as "cross-linked 6FDA-DAPI/DABA". Similarly, the uncross-linked precursor for cross-linked 6FDA-DAPI/DABA will be referred to as "linear 6FDA-DAPI/DABA".

Pure gas permeability of CO_2, C_2H_4, and C_2H_6 in 6FDA-DAPI, linear 6FDA-DAPI/DABA, and cross-linked 6FDA-DAPI/DABA is investigated, aiming to

understand the influence of thermal cross-linking on plasticization behavior of this polymer system. Additionally, pure gas sorption isotherms and diffusion data for N_2, CH_4, CO_2, C_2H_4, and C_2H_6 are reported to further inform the plasticization discussion. Mixed gas permeation data for a 50:50 C_2H_4:C_2H_6 feed will also be presented. A more detailed study of polymer dilation and diffusivity will be presented subsequently [14].

5.2. Results and Discussion

5.2.1. CO_2, C_2H_4, and C_2H_6 Plasticization and Conditioning Effects

As previously reported, pure gas permeability for all gases increased in the following order: linear 6FDA-DAPI/DABA < cross-linked 6FDA-DAPI/DABA < 6FDA:DAPI [1]. Additionally, gas transport in all three polymers followed dual-mode behavior, typical of glassy polymers, where permeability decreased at low feed pressure and approached a constant value at high fugacity for H_2, N_2, O_2, and CH_4 [1, 2]. At higher fugacity, 6FDA-DAPI and linear 6FDA-DAPI/DABA showed an increase in permeability for CO_2, C_2H_4, and C_2H_6, while these effects were minimal for cross-linked 6FDA-DAPI/DABA. This result is likely due to sorption of CO_2, C_2H_4, and C_2H_6 inducing plasticization, or swelling, of the polymer matrix. As the polymer plasticizes, gas diffusivity increases, thereby increasing gas permeability at high fugacity [3-6]. Typically, the pressure at which this upturn in permeability with pressure occurs is referred to as the "plasticization pressure", or "plasticization fugacity" for non-ideal gases [3-6]. This plasticization fugacity can depend on testing conditions (i.e., both upstream and downstream pressures, not just the pressure difference across the film), so we use the

plasticization fugacity as an arbitrary, but reasonable, point of comparison for plasticization resistance of films tested under similar conditions [7].

Due to differences in gas permeability between samples, extent of plasticization was compared by normalizing gas permeability coefficients with respect to the permeability at 3 atm, which was typically the lowest feed pressure considered (cf., Table 5.1). Normalized permeability coefficients for 6FDA-DAPI, linear 6FDA-DAPI/DABA, and cross-linked 6FDA-DAPI/DABA versus fugacity are plotted for CO_2, C_2H_4, and C_2H_6 in Figure 5.1 a-c. To analyze the relative extent of plasticization, the relative increase in permeability above the minimum permeability value, which defines the location of the plasticization fugacity, was compared between the three gases and the three polymers using the method shown in Figure C.3. Plasticization fugacity, f^*, and percent change in relative permeability, ΔP_{rel}, are recorded in Table C.1 of the SI. As shown in Figure 5.1, for all three samples, CO_2 induced the largest increase in relative permeability over the pressures tested, followed by C_2H_6, and C_2H_4. This trend is qualitatively consistent with the trend in solubility of CO_2, C_2H_6, and C_2H_4 in these materials, as will be discussed later.

	Permeability, P_i [Barrer] at 3 atm		
Polymer	**CO_2**	**C_2H_4**	**C_2H_6**
6FDA-DAPI	39 ± 6	1.6 ± 0.1	0.37 ± 0.03
6FDA-DAPI/DABA (linear)	16.4 ± 0.9	0.83 ± 0.3	0.232 ± 0.007
6FDA-DAPI/DABA (cross-linked)	34 ± 1	1.14 ± 0.04	0.237 ± 0.008

Table 5.1. Pure gas permeability of CO_2, C_2H_4, and C_2H_6 in 6FDA-DAPI, linear 6FDA-DAPI/DABA, and cross-linked 6FDA-DAPI/DABA at 3 atm and 35°C.

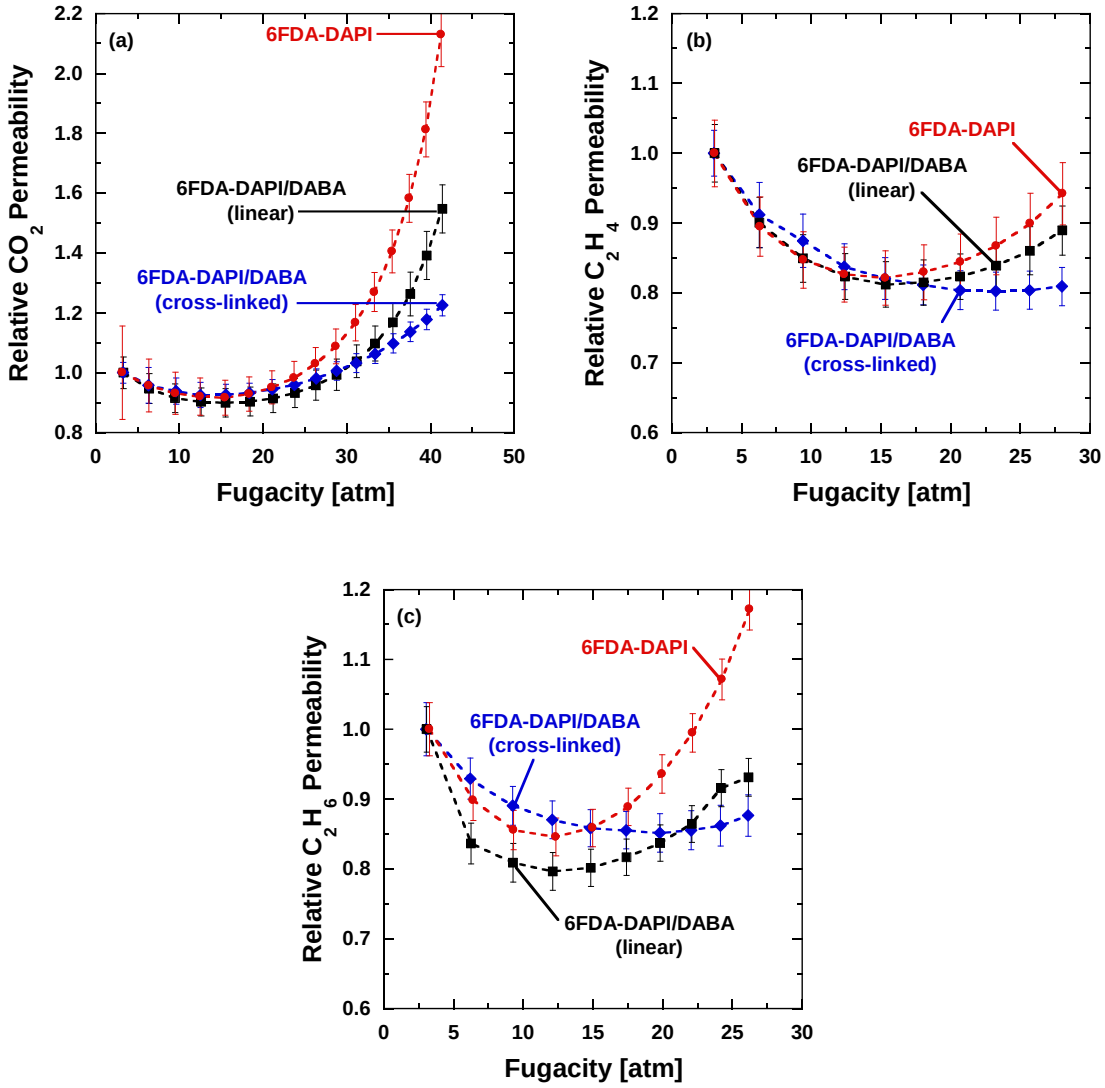

Figure 5.1. Relative pure gas permeability of: (a) CO_2, (b) C_2H_4, and (c) C_2H_6 in 6FDA-DAPI [●], linear 6FDA-DAPI/DABA [■], and 6FDA-DAPI/DABA cross-linked at 353°C for 40 min [♦], measured at 35°C versus pure gas fugacity. The pure gas permeability data are from the literature [1]. The values recorded in Table 5.1 were used to normalized the relative permeability at 3 atm and the permeability data was reported previously [1].

For pure CO_2, C_2H_4, and C_2H_6, the relative increases in permeability after the plasticization fugacity are presented in Figure 5.1 and recorded in Table C.1. For these

gases, relative permeability at the highest fugacity considered increased in the following order: cross-linked 6FDA-DAPI/DABA < linear 6FDA-DAPI/DABA < 6FDA-DAPI. At the highest fugacity considered, CO_2 permeability increased by approximately 120% in 6FDA-DAPI, C_2H_6 permeability increased by 32%, and C_2H_4 permeability increased by 12%. Linear 6FDA-DAPI/DABA plasticized less than 6FDA-DAPI for all gases, increasing only 65%, 14%, and 8.0% for CO_2, C_2H_6, and C_2H_4, respectively. The reduced extent of plasticization of linear 6FDA-DAPI/DABA, compared to 6FDA-DAPI, may be due to the polar –COOH groups in DABA facilitating inter-chain hydrogen bonding, possibly restricting polymer chain motion and increasing polymer cohesive energy density. Minimal plasticization was observed in cross-linked 6FDA-DAPI/DABA for all gases, and relative permeability increased only 29%, 2.0%, and 1.0%, for CO_2, C_2H_6, and C_2H_4, respectively. Increases in relative permeability for C_2H_6 and C_2H_4 in cross-linked 6FDA-DAPI/DABA fall within experimental uncertainty of the pure gas permeation measurements (cf., Figure 5.1). This negligible increase in pure C_2H_4 and C_2H_6 permeability at high pressure suggests cross-linking by thermal decarboxylation of DABA might limit plasticization, particularly for C_2H_4 and C_2H_6.

While there is a large database of studies investigating plasticization effects of CO_2 in many different polymers, there are very few studies investigating plasticization effects of C_2H_4 and C_2H_6. Thus, it could be difficult to assess the potential plasticization resistance of a polymer to such hydrocarbon gases if only plasticization resistance to CO_2 is known. Indeed, results from this study show that CO_2 is not a good proxy for C_2H_4 or C_2H_6 in terms of gauging plasticization resistance.

5.2.2. Conditioning by CO_2, C_2H_4, and C_2H_6

High levels of gas sorption in a glassy polymer can leave the polymer matrix in a low density state following the removal of the gas, a phenomenon known as conditioning [8-10]. Due to the rigid backbone, after conditioning occurs, the polymer is often kinetically trapped in a new non-equilibrium state, and it may only return to its initial state slowly, if at all, once the gas is removed [8-10]. Such conditioning is often observed via hysteresis in gas permeation experiments, where higher permeability is observed during depressurization following exposure to a condensable gas at high pressure [6].

For C_2H_4 and C_2H_6, a pressurization loop was performed with cross-linked 6FDA-DAPI/DABA, where permeability was measured as pressure was first increased and then decreased, the results of which are presented in Figure 5.2 a-b. While no significant increase in permeability occurred at fugacities beyond the plasticization pressure, some hysteresis was observed for both hydrocarbon gases as pressure decreased. After vacuum was pulled for at least 20 times the measured time lag of each gas, C_2H_4 permeability returned to the value measured on the first pressurization (cf., Figure 5.2-a). For C_2H_6, permeability on the second pressurization at low fugacity remained slightly higher than the values measured on first exposure, then approached the original values above 15 atm fugacity, as shown in Figure 5.2-b.

Similarly, permeability coefficients of CO_2 in cross-linked 6FDA-DAPI/DABA returned to their original values after degassing, despite a 29% increase in relative permeability for at 3 atm CO_2 after exposure to high pressure CO_2 (cf., Figure 5.2-c). These results suggest swelling induced by CO_2, C_2H_4, and C_2H_6 is not permanent and can be

reversed by degassing. We speculate that cross-links induced by thermal decarboxylation may facilitate the return of the material to its previous state upon degassing. To further study the extent of swelling and reversible nature of plasticization, dilation measurements have been performed and will be reported separately [11].

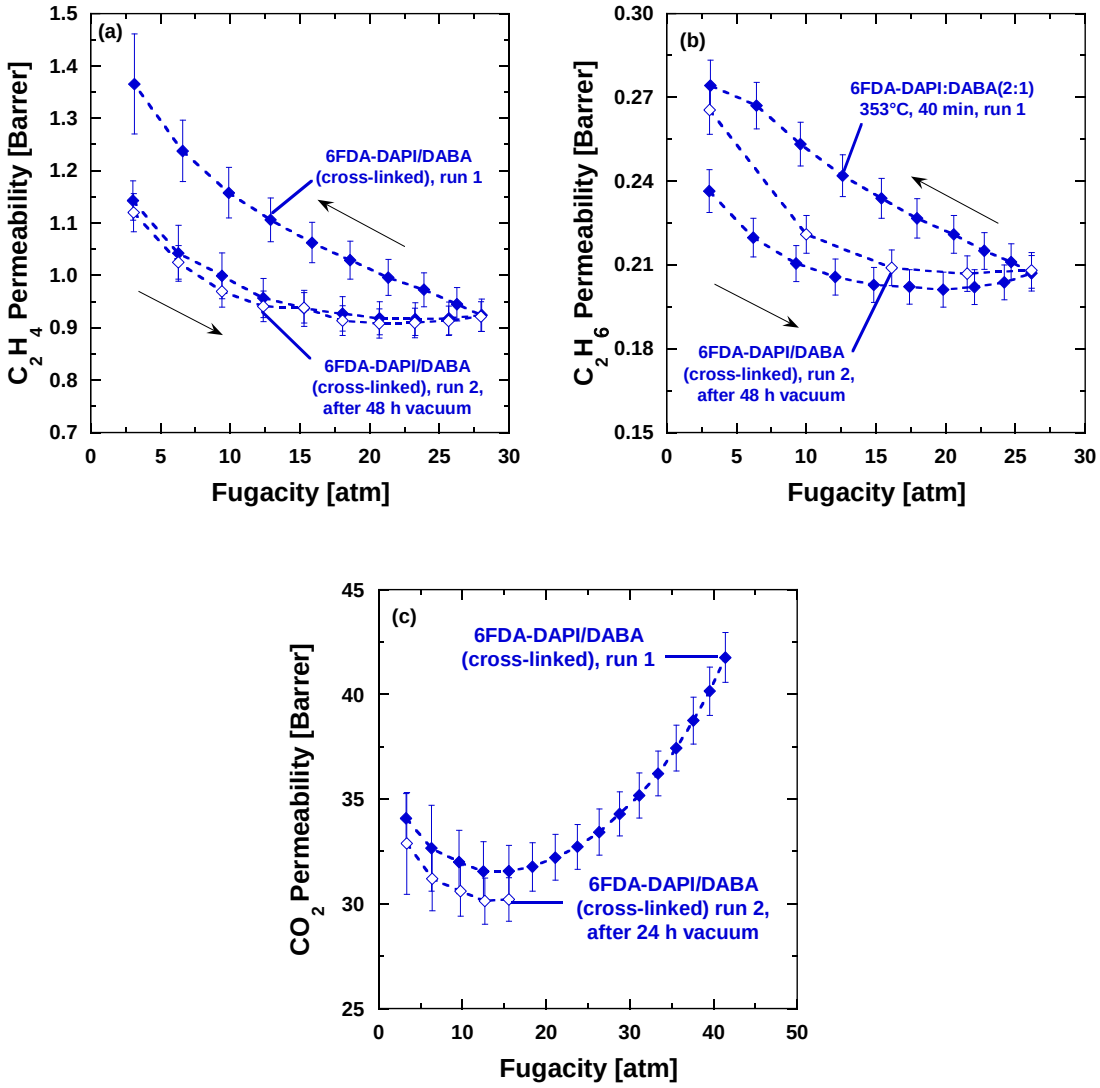

Figure 5.2. Conditioning from: (a) C_2H_4, and (b) C_2H_6 (c) CO_2, in 6FDA-DAPI/DABA cross-linked at 353°C for 40 min. For all three gases, the first pressurization loop is shown in ♦ and the second pressurization after degassing is shown in ◊. The arrows in (a) and (b) denote the direction of pressure change during the initial pressurization and depressurization loop. Permeability data from the pressurization steps of run 1 are from the literature [1].

5.2.3. Pure Gas Solubility

Sorption isotherms for C_2H_4, C_2H_6, and CO_2 in 6FDA-DAPI, linear 6FDA-DAPI/DABA, and cross-linked 6FDA-DAPI/DABA are presented in Figure 5.3 a-c. For brevity, the sorption isotherms for CH_4 and N_2 are presented in Figure C.4 a-c in the SI. Solubility coefficients were calculated using Eq. 2.10 and reported at 20 atm in Table 5.2. For CH_4, CO_2, C_2H_4, and C_2H_6, solubility isotherms were concave down with fugacity, consistent with dual-mode sorption in glassy polymers [2]. Due to its low solubility, N_2 uptake follows a linear trend with pressure. For all three polymers, gas solubility was similar and increased in the following order: $S_{N2} < S_{CH_4} < S_{C_2H_6} \approx S_{C_2H_4} < S_{CO_2}$. However, as shown in Figure 5.3-b, C_2H_6 solubility in linear 6FDA-DAPI/DABA was somewhat lower at high pressures than in 6FDA-DAPI and cross-linked 6FDA-DAPI/DABA.

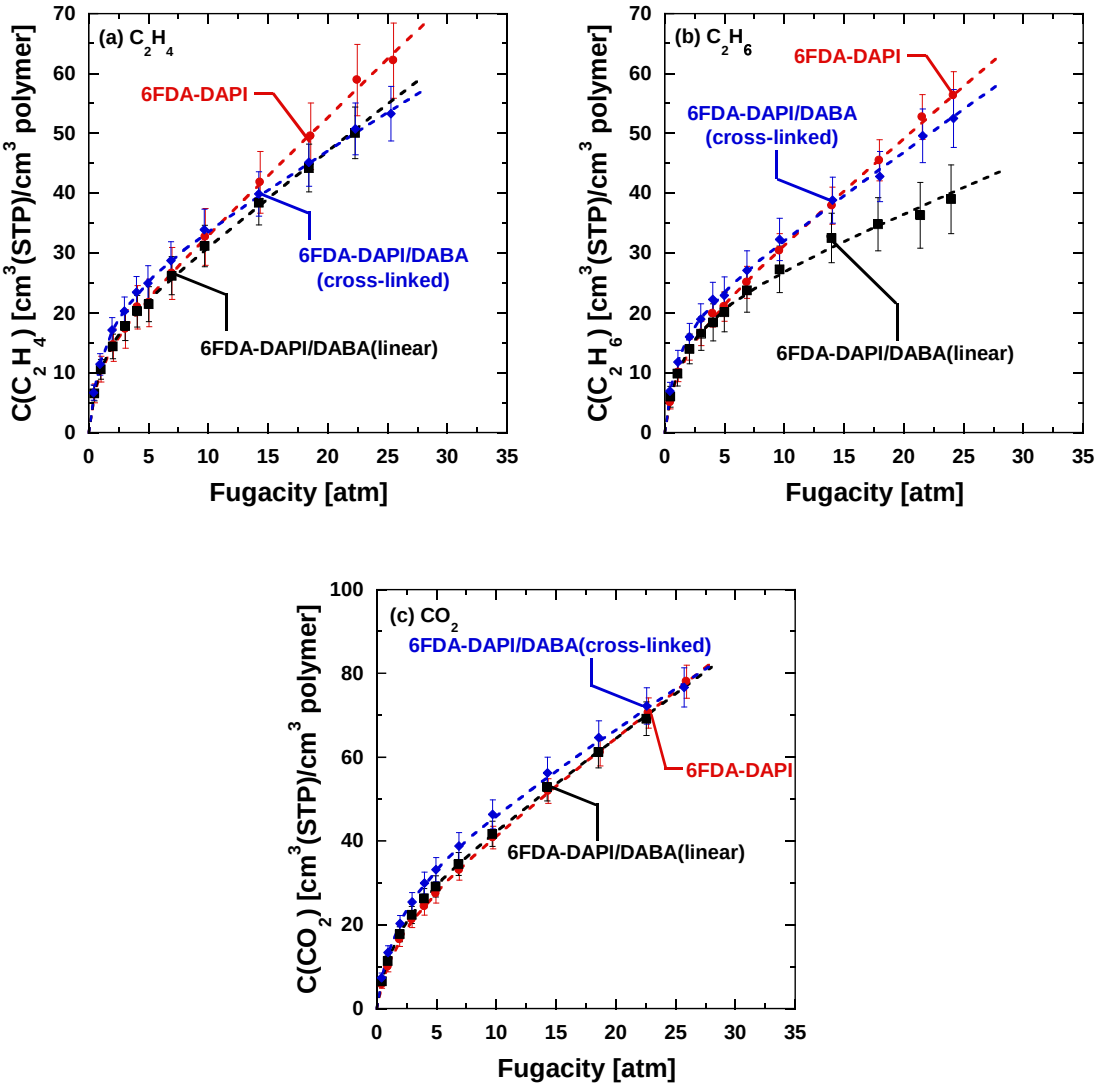

Figure 5.3. Pure gas sorption of: (a) C_2H_4, (b) C_2H_6, (c) CO_2, in 6FDA-DAPI (●), linear 6FDA-DAPI/DABA (■), and cross-linked 6FDA-DAPI/DABA (♦) at 35°C. The dashed lines represent the dual-mode fit.

Polymer	Pure Gas Solubility, S_i [cm^3(STP)/(cm^3 polymer atm)]				
	N_2	CH_4	C_2H_4	CO_2	C_2H_6
6FDA-DAPI	0.78 ± 0.1	1.3 ± 0.1	2.6 ± 0.2	3.2 ± 0.2	2.5 ± 0.2
6FDA-DAPI/DABA (linear)	0.79 ± 0.2	1.2 ± 0.2	2.4 ± 0.2	3.2 ± 0.2	1.8 ± 0.2
6FDA-DAPI/DABA (cross-linked)	0.71 ± 0.2	1.2 ± 0.1	2.4 ± 0.2	3.3 ± 0.2	2.4 ± 0.2
T_c [K]	126.1	190.7	282.5	304.2	305.3

Table 5.2. Pure gas solubility of N_2, CH_4, C_2H_4, C_2H_6, and CO_2 in 6FDA-DAPI, linear 6FDA-DAPI/DABA, cross-linked 6FDA-DAPI/DABA at 20 atm and 35°C. Critical temperatures, T_c, were obtained from the literature [12].

Dual-mode parameters for 6FDA-DAPI, linear 6FDA-DAPI/DABA, and cross-linked 6FDA-DAPI/DABA, recorded in Table C.2, were calculated by fitting the experimental sorption data to Eq. 2.9, using a non-linear least squares method, and the sorption isotherms were well described by the dual-mode model. However, due to the nature of the dual-mode model, values of b and C_H' are highly coupled [13-15]. Thus, changes in the value of b are often offset by changes in C_H' with only a minimal impact on quality of fit [13-15]. This is a well-recognized problem with fitting the dual-mode model to experimental data [13-15]. Thus, the dual-mode fit was primarily used as a curve fitting method to represent the shape of the sorption isotherms, and we assign no special physical significance to the parameter values themselves.

5.2.4. Pure Gas Diffusivity and Selectivity

Using pure gas permeability, reported elsewhere (c.f., Table C.3) [1], and pure gas solubility coefficients from this study, diffusivity coefficients were calculated using Eq. 2.11 Table 5.2 and Table 5.3 present representative sorption and diffusion coefficients for

N_2, CH_4, CO_2, C_2H_4, and C_2H_6 at 20 atm and 35°C. Due to higher uncertainty in gas sorption measurements at lower pressures, transport properties were compared at 20 atm. While there are only relatively small differences in pure gas solubility in 6FDA-DAPI, linear 6FDA-DAPI/DABA, and cross-linked 6FDA-DAPI/DABA, gas diffusivity differs significantly between the three polymers. Gas diffusion coefficients increased in the following order: $C_2H_6 < C_2H_4 < CH_4 < N_2 < CO_2$, which is consistent with the smaller penetrants having higher diffusion coefficients.

	Pure Gas Diffusivity, D_i [x10^{-10} cm^2/s]				
Polymer	**CO_2**	**N_2**	**CH_4**	**C_2H_4**	**C_2H_6**
6FDA-DAPI	850 ± 50	140 ± 90	50 ± 10	38 ± 4	11 ± 1
6FDA-DAPI/DABA (linear)	350 ± 20	100 ± 40	40 ± 10	22 ± 2	8.2 ± 0.6
6FDA-DAPI/DABA (cross-linked)	730 ± 40	150 ±10	50 ± 10	30 ± 2	6.5 ± 0.5
Gas Diameter, d_g [Å]	3.44	3.49	3.82	4.16	4.44

Table 5.3. Pure gas diffusivity of CO_2, N_2, CH_4, C_2H_4, and C_2H_6 at in 6FDA-DAPI, linear 6FDA-DAPI/DABA, and cross-linked 6FDA-DAPI/DABA at 20 atm and 35°C. The gas diameters were obtained from the literature [12, 16].

To better understand the influence of the polymer backbone on pure gas transport properties, fractional changes in permeability, solubility, and diffusivity of CO_2, N_2, CH_4, C_2H_4, and C_2H_6 were compared for 6FDA-DAPI and linear 6FDA-DAPI/DABA, calculated as follows:

$$Fractional\ Change\ in\ X = \left(\frac{X_{Linear\ 6FDA-DAPI/DABA}}{X_{6FDA-DAPI}} - 1\right) \qquad \text{Eq. 5.1}$$

where X is P, S, D, P_i/P_j, S_i/S_j, and D_i/D_j. The results of this analysis are presented in Figure 5.4. For all gases, diffusion coefficients in linear 6FDA-DAPI/DABA are less than in

6FDA-DAPI, resulting in lower permeabilities. Additionally, for all gases except C_2H_6, the decrease in diffusion coefficients in linear 6FDA-DAPI/DABA was the dominate contributor to the decrease in permeability [1]. Lower diffusion coefficients are consistent with the smaller d-spacings measured previously in linear 6FDA-DAPI/DABA than in 6FDA-DAPI [1].

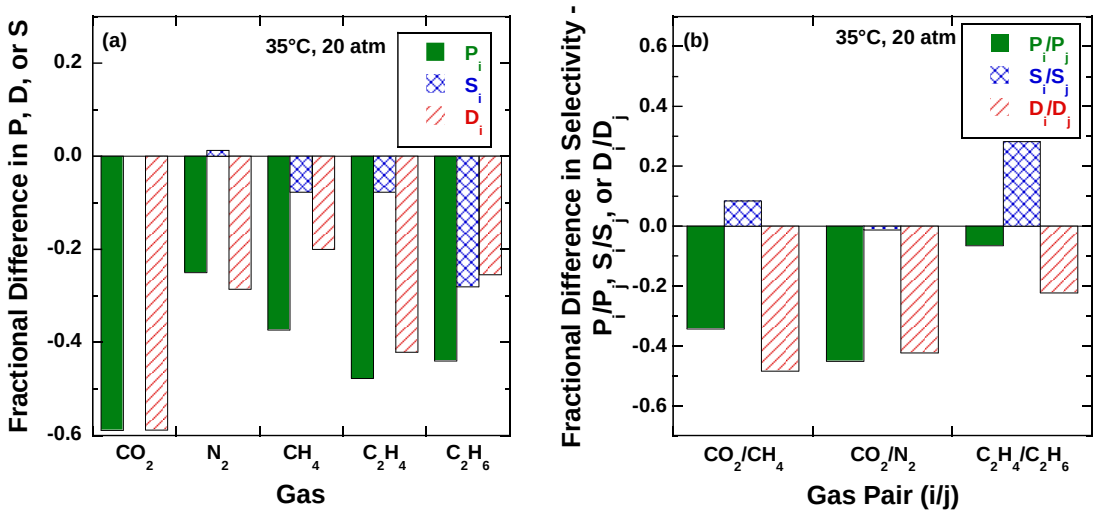

Figure 5.4. (a) Fractional difference in pure gas permeability, P_i (green), solubility, S_i (blue), and diffusivity, D_i (red), for CO_2, N_2, CH_4, C_2H_4, and C_2H_6 and (b) fractional difference in pure gas permeability selectivity, P_i/P_j (green), solubility selectivity, S_i/S_j (blue), and diffusivity selectivity, D_i/D_j (red), for CO_2/CH_4, CO_2/N_2, and C_2H_4/C_2H_6 gas pairs, comparing 6FDA-DAPI to linear 6FDA-DAPI/DABA. Values were calculated using Eq. 5.1.

Fractional changes in selectivity were compared for 6FDA-DAPI and linear 6FDA-DAPI/DABA. These values were calculated using Eq. 5.1 and are reported in Figure 5.4-b. Interestingly, the DABA-containing polymer had both lower permeability and diffusion coefficients and lower permeability and diffusion selectivity for all gases and gas pairs considered. This decrease in both diffusivity and diffusivity selectivity with the inclusion

of DABA in the polymer backbone is consistent with linear 6FDA-DAPI/DABA having not only smaller inter-chain spacing but perhaps also a broader distribution of free volume elements than 6FDA-DAPI. Both smaller d-spacing and a broader FFV distribution in linear 6FDA-DAPI/DABA could potentially explain the simultaneous decrease in both diffusivity and diffusion selectivity. In data reported elsewhere, there was a hint of such differences in WAXS, but there was no significant difference in density-based fractional free volume among these three polymers.

To better understand the effect of thermally induced cross-linking by decarboxylation on gas transport, the fractional change in P_i, S_i, and D_i for CO_2, N_2, CH_4, C_2H_4, and C_2H_6 and P_i/P_j, S_i/S_j, and D_i/D_j for CO_2/CH_4, CO_2/N_2, and C_2H_4/C_2H_6 gas pairs were compared for linear and cross-linked 6FDA-DAPI/DABA according to:

$$Fractional\ Change\ in\ X = \left(\frac{X_{cross-linked}}{X_{linear}} - 1\right) \qquad \text{Eq. 5.2}$$

where X is P_i, S_i, D_i, P_i/P_j, S_i/S_j, or D_i/D_j. ***Figure 5.5-a*** illustrates changes in P_i, D_i and S_i for CO_2, N_2, CH_4, C_2H_4, and C_2H_6. The substantial increases in CO_2, N_2, CH_4, and C_2H_4 permeability at 20 atm after cross-linking were largely due to increases in gas diffusivity, while the very modest increase in C_2H_6 permeability was due to an increase in solubility coupled with a reduction in diffusivity. Changes in P_i/P_j, S_i/S_j, and D_i/D_j for CO_2/CH_4, CO_2/N_2, and C_2H_4/C_2H_6 gas pairs are presented in Figure 5.5-b. In all cases, permeability selectivity increased, driven mainly by increases in diffusion selectivity. Remarkably, the cross-linked sample is both more permeable and more selective than its linear analog. Curiously, C_2H_6 solubility increased significantly after cross-linking, and this effect

resulted in a decrease in pure gas C_2H_4/C_2H_6 solubility selectivity, which partially counteracted the increase in pure gas diffusivity selectivity.

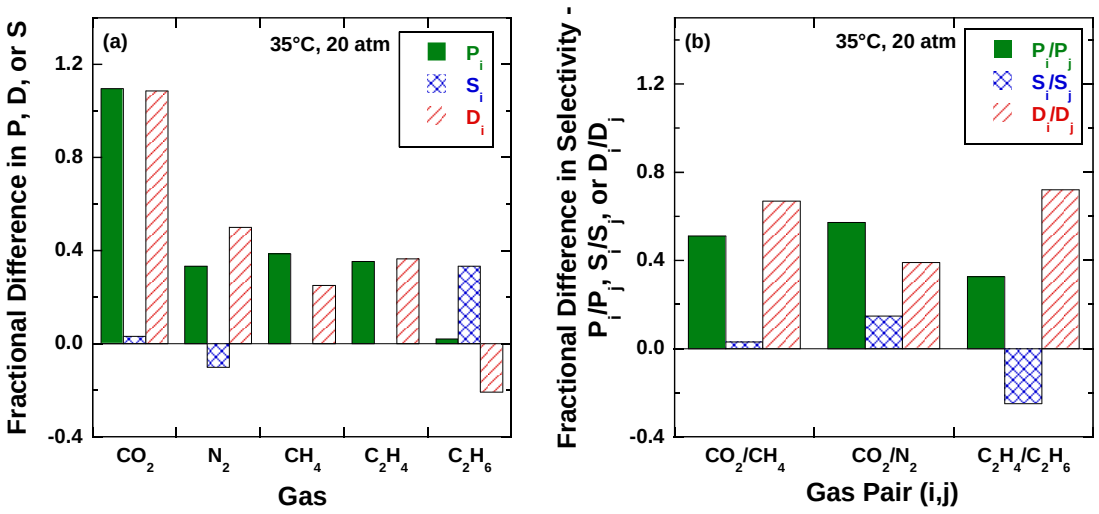

Figure 5.5. (a) Fractional difference in pure gas permeability, P_i (green), solubility, S_i (blue), and diffusivity, D_i (red), for CO_2, N_2, CH_4, C_2H_4, and C_2H_6 and (b) fractional difference in pure gas permeability selectivity, P_i/P_j (green), solubility selectivity, S_i/S_j (blue), and diffusivity selectivity, D_i/D_j (red), for CO_2/CH_4, CO_2/N_2, and C_2H_4/C_2H_6 gas pairs, comparing linear 6FDA-DAPI/DABA to cross-linked 6FDA-DAPI/DABA. Values were calculated using Eq. *5.2* and the permeability data listed in Table C.3, the solubility data listed Table 5.2, and the diffusion data listed in Table 5.3.

5.2.5. Ethylene/Ethane Mixed Gas Permeability

To better understand the impact of polymer structure and thermal cross-linking on plasticization resistance of DAPI containing polyimides, mixed gas permeability was measured using a 50:50 mixture of C_2H_4:C_2H_6. Pure and mixed gas permeability coefficients of 6FDA-DAPI, linear 6FDA-DAPI/DABA, and cross-linked 6FDA-DAPI/DABA are compared in Figure 5.6-a and Figure 5.6-b. Mixed gas C_2H_4/C_2H_6 selectivity was calculated using Eq. 2.7 and is compared to pure gas selectivity as a function

of fugacity in Figure 5.7. Mixed gas permeability and selectivity are plotted versus total fugacity, which is the sum of C_2H_4 and C_2H_6 partial fugacity, to better represent the total concentration of gas in the polymer. Similar to pure gas permeability, mixed gas permeability coefficients of C_2H_4 and C_2H_6 in all three polymers exhibit dual-mode behavior at low fugacity, with permeability decreasing slightly with increased fugacity. In 6FDA-DAPI at higher fugacity, mixed gas permeability coefficients of C_2H_4 and C_2H_6 exhibited a distinct increase at a mixture fugacity above about 13 atm, consistent with plasticization. For linear 6FDA-DAPI/DABA and cross-linked 6FDA-DAPI/DABA, C_2H_6 mixed gas permeability coefficients increased slightly at high fugacity while no significant increase in C_2H_4 mixed gas permeability was observed at high fugacity.

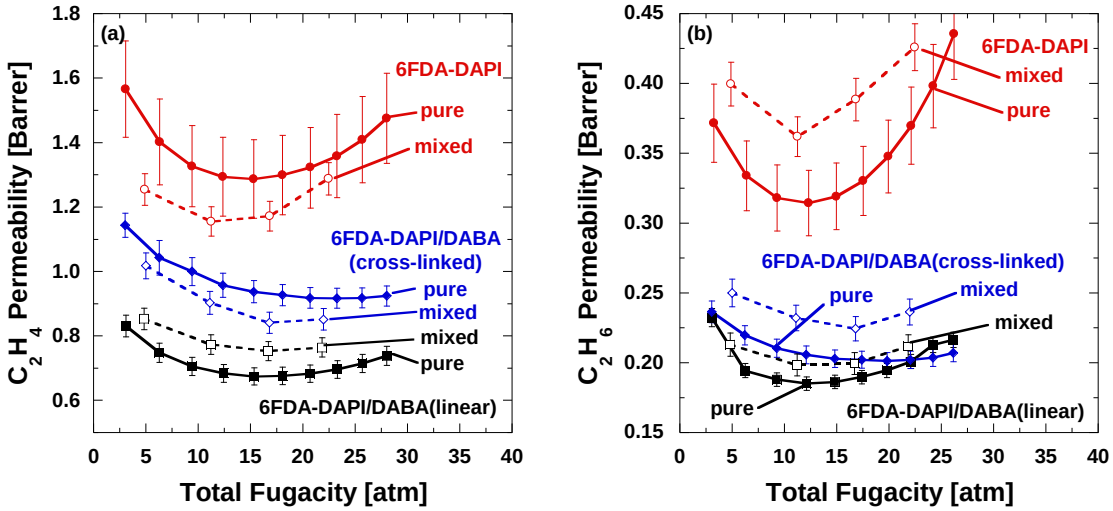

Figure 5.6. (a) C_2H_4 and (b) C_2H_6 permeability vs. total fugacity for 6FDA-DAPI (●), linear 6FDA-DAPI/DABA (■), cross-linked 6FDA-DAPI/DABA (♦), where filled markers are pure gas measurements and unfilled markers are mixed gas measurements for a 50:50 C_2H_4:C_2H_6 mixture. Mixed gas permeability data is plotted versus total fugacity (i.e., the sum of C_2H_6 and C_2H_4 fugacity in the mixture). The solid and dashed lines are drawn to guide the eye. The pure gas permeation data was reported previously [1].

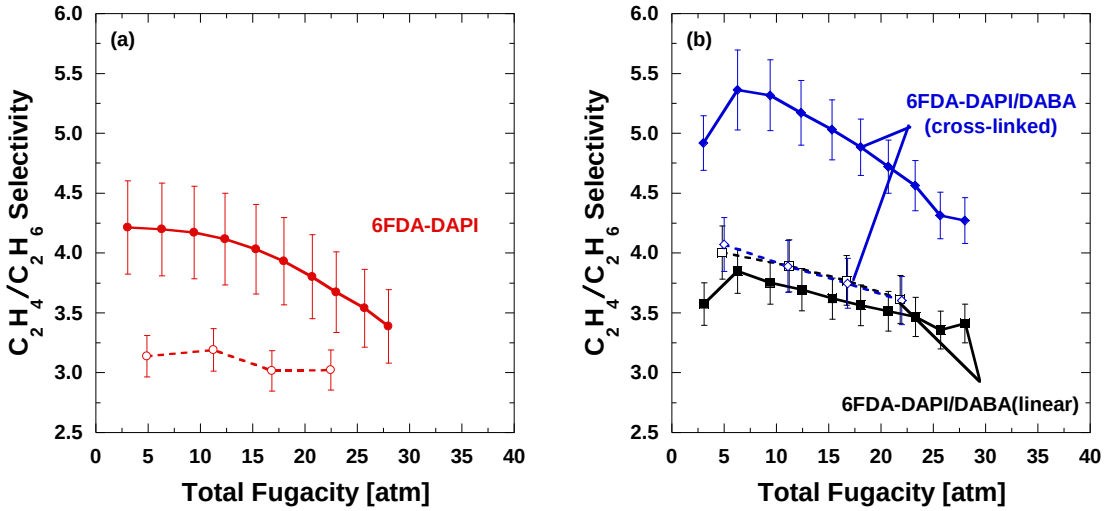

Figure 5.7. Ethylene/ethane selectivity vs. total fugacity for: (a) 6FDA-DAPI (●), and (b) linear 6FDA-DAPI/DABA (■) and cross-linked 6FDA-DAPI/DABA (♦). Filled markers are pure gas measurements and open markers are mixed gas measurements for a 50:50 C_2H_4:C_2H_6 mixture. Mixed gas data is plotted as total fugacity (i.e., the sum of ethane and ethylene fugacity in the mixture). The solid and dashed lines are drawn to guide the eye. The pure gas selectivity was calculated from previously reported pure gas permeation data [1].

Differences in pure and mixed gas permeability can arise from at least several factors including competitive sorption and plasticization. Competitive sorption is a dual-mode effect, where a limited number of Langmuir sites are available for gas sorption, and gases compete for sorption within these Langmuir sites [17, 18]. Preferential sorption of one gas over others reduces sorption, and thus permeability, of other species [17, 19]. Affinity for Langmuir sites tends to increase with increasing penetrant condensability, frequently characterized by critical temperature [13, 20]. If a larger, slower permeating species had a higher Langmuir affinity than a smaller, faster permeating species, competitive sorption might be expected to reduce permeability selectivity in mixed gas

conditions, relative to that expected based on pure gas permeation experiments, due to a reduction in solubility selectivity. If one or more of the penetrants induces plasticization, swelling of the polymer matrix under mixed gas conditions generally causes a larger proportional increase in diffusivity of larger species than smaller species, decreasing mixed gas selectivity more than expected based on pure gas permeability selectivity [13, 21, 22].

To help quantify the effects of competitive sorption and plasticization, the pure and mixed gas selectivities and permeabilities were compared as follows:

$$Fractional\ Change\ X = \left(\frac{X_{mixed}}{X_{pure}} - 1\right) \qquad \text{Eq. 5.3}$$

where X is C_2H_4/C_2H_6 selectivity, C_2H_4 permeability, or C_2H_6 permeability from pure and mixed gas experiments. Suppressed C_2H_4 permeability in mixed gas experiments suggests competitive sorption, while increased C_2H_6 permeability under mixed gas conditions suggests plasticization [13, 23].

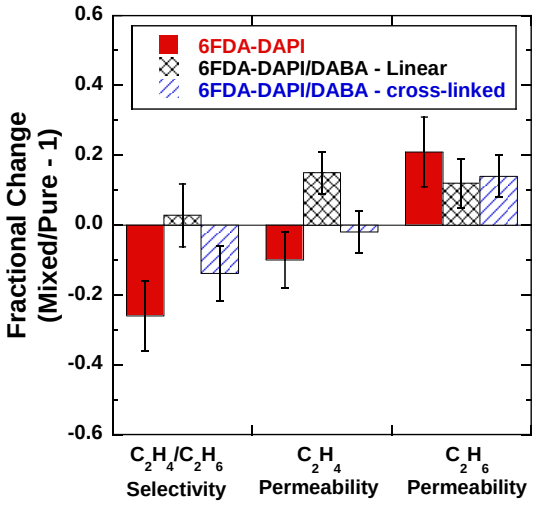

Figure 5.8. Fractional change in C_2H_4/C_2H_6 selectivity, C_2H_4 permeability, and C_2H_6 permeability for 6FDA-DAPI (red), linear 6FDA-DAPI/DABA (grey), and cross-linked 6FDA-DAPI/DABA (blue), comparing pure and mixed gas transport at 5 atm total fugacity and 35°C.

As shown in Figure 5.8 and Figure 5.6-b, all samples had slightly higher C_2H_6 mixed gas permeability than pure gas permeability. This result suggests a modest level of plasticization from exposure to the mixture of C_2H_4 and C_2H_6 in all three polymers, despite cross-linked 6FDA-DAPI/DABA showing no significant plasticization by either C_2H_4 or C_2H_6 in pure gas permeation experiments (cf., Figure 5.1). While cross-linking reduces plasticization by CO_2 in CO_2/CH_4 mixtures [13, 24-26], under the conditions considered in this study, cross-linking did not prevent some plasticization by the C_2H_4/C_2H_6 mixture. However, as indicated in Figure 5.7-b and Figure *5.8*, changes in selectivity with mixture fugacity for linear 6FDA-DAPI/DABA samples were small, essentially within the uncertainty of the measurements.

Additionally, as shown in Figure 5.6-a and Figure 5.8, 6FDA-DAPI had perhaps slightly lower C_2H_4 permeability under mixed gas conditions, while cross-linked 6FDA-DAPI/DABA showed no significant difference between pure and mixed gas C_2H_4 permeability at 5 atm. If C_2H_4 permeability in 6FDA-DAPI is indeed somewhat lower under mixed gas conditions, this result would suggest competitive sorption between C_2H_4 and C_2H_6, which could lower C_2H_4/C_2H_6 selectivity in mixed gas experiments (cf., Figure 5.7-a and Figure *5.8*). While pure gas solubility of C_2H_4 and C_2H_6 are similar in 6FDA-DAPI (c.f., Table 5.2 and Figure C.4-a), C_2H_6 has a higher critical temperature than C_2H_4 (c.f., Table 5.2), indicating C_2H_6 may have a higher Langmuir affinity than C_2H_4 [13, 20]. Higher Langmuir affinity for C_2H_6 might reduce C_2H_4 solubility under mixed gas conditions, consistent with lower C_2H_4 permeability in mixed gas experiments. However, these effects are modest at the experimental conditions considered.

Unlike 6FDA-DAPI and cross-linked 6FDA-DAPI/DABA, linear 6FDA-DAPI/DABA had a higher mixed gas permeability for both C_2H_4 and C_2H_6 (c.f., Figure 5.6), resulting in no significant difference in pure and mixed gas selectivity (c.f., Figure 5.7-b and Figure 5.8). To better understand plasticization resistance and the extent of competitive sorption within these materials, mixed gas sorption experiments would be useful.

The fugacity dependence of pure and mixed gas C_2H_4/C_2H_6 selectivity for all three polymers are illustrated in Figure *5.7*, with the selectivity at 5 atm total fugacity plotted on the C_2H_4/C_2H_6 upper bound in Figure 5.9. As fugacity increased, mixed gas C_2H_4/C_2H_6 selectivity generally decreased for all samples. These results further support the notion of

plasticization in all three polymers. Thus, thermal cross-linking of 6FDA-DAPI/DABA likely did not completely prevent swelling of the polymer matrix. The presence of plasticization after cross-linking is likely due to swelling induced by C_2H_4 and C_2H_6 between cross-linking sites. As the polymer matrix swells, diffusivity selectivity can be reduced. Apparent plasticization in cross-linked 6FDA-DAPI/DABA resulted in somewhat lower C_2H_4/C_2H_6 permeability selectivity in mixed gas experiments. Thus, cross-linking, in this particular polymer system, does not reduce plasticization effects of C_2H_4 and C_2H_6 under the experimental conditions considered. To better understand the effect of cross-linking on plasticization resistance, it would be of interest to investigate plasticization in polymers with higher cross-link densities (e.g., DAPI:DABA ratios of 2:3, 1:3, etc.).

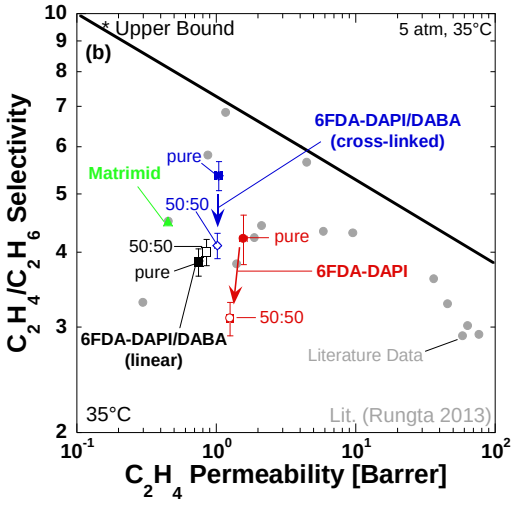

Figure 5.9. Ethylene/ethane selectivity vs. ethylene permeability at 5 atm, for 6FDA-DAPI (●), linear 6FDA-DAPI/DABA (■), and cross-linked 6FDA-DAPI/DABA (♦). Filled symbols are pure gas measurements, and open symbols are mixed gas measurements for a 50:50 C_2H_4:C_2H_6 mixture. Matrimid (▲) [27] and other literature data points (●) [27] have been added to as a reference points and the upper bound represents the boundary defined by Rungta et al. [27]

5.3. CONCLUSIONS

6FDA-DAPI/DABA cross-linked at 353°C for 40 min showed improved plasticization resistance to CO_2, C_2H_4, and C_2H_6, relative to 6FDA-DAPI and linear 6FDA-DAPI/DABA, in pure gas permeation experiments. While CO_2-induced plasticization occurred, no detectible plasticization or permanent conditioning was observed in cross-linked 6FDA-DAPI/DABA when exposed to 27 atm of pure C_2H_4 or C_2H_6.

Despite pure gas experiments indicating improved plasticization resistance due to thermal cross-linked, plasticization was still observed at high pressures in all three DAPI-containing polyimides when tested under mixed gas conditions with a gas feed of 50:50

C_2H_4:C_2H_6, based on increased C_2H_6 permeability in the mixed gas experiments than in ther pure gas experiments. However, linear 6FDA-DAPI/DABA showed somewhat higher C_2H_4 and C_2H_6 permeability with no significant change in selectivity in mixed gas experiments, for reasons that are poorly understood. Cross-linking is not necessarily needed to prevent plasticization by C_2H_4 and C_2H_6 in the materials and experimental conditions considered in this study.

5.4. ACKNOWLEDGMENTS

This material is based upon work supported in part by the National Science Foundation Graduate Research Fellowship under Grant No. DGE-1610403. The authors gratefully acknowledge partial support from the Division of Chemical Sciences, Geosciences, and Biosciences, Office of Basic Energy Sciences of the U.S. Department of Energy (DOE), USA through Grant DE-FG02-02ER15362 and partial support by the Australian-American Fulbright Commission for the award to BDF of the U.S. Fulbright Distinguished Chair in Science, Technology and Innovation sponsored by the Commonwealth Scientific and Industrial Research Organization (CSIRO). Additionally, this work is supported in part by the National Science Foundation under Cooperative Agreement No. EEC-1647722. Any opinions, findings, and conclusions or recommendations expressed in this material are those of the authors and do not necessarily reflect the views of the National Science Foundation.

5.5. REFERENCES

[1] M.E. Dose, M. Chwatko, I. Hubacek, N.A. Lynd, D.R. Paul, B.D. Freeman, Thermally Cross-linked Diaminophenylindane (DAPI) Containing Polyimides for Membrane Based Gas Separations, Polymer, Submitted (2018).

[2] D.R. Paul, Gas Sorption and Transport in Glassy Polymers, Reports of the Bunsen Society for Physical Chemistry, 83 (1979) 294-302.

[3] M. Wessling, S. Schoeman, T. van der Boomgaard, C.A. Smolders, Plasticization of Gas Separation Membranes, Gas Separation & Purification, 5 (1991) 222 - 228.

[4] W.J. Koros, D.R. Paul, Design Considerations for Measurement of Gas Sorption in Polymers by Pressure Decay, Journal of Polymer Science Part B: Polymer Physics, 14 (1976) 1903 - 1907.

[5] J.H. Petropoulos, Mechanisms and Theories for Sorption and Diffusion of Gases in Polymers, in: Polymeric Gas Separation Membranes, CRC Press, Inc, Boca Raton, FL, 1994.

[6] A.F. Ismail, W. Lorna, Penetrant-Induced Plasticization Phenomenon in Glassy Polymers for Gas Separation Membrane, Separation and Purification Technology, 27 (2002) 173 - 194.

[7] M. Minelli, M.G. De Angelis, G.C. Sarti, Predictive Calculations of Gas Solubility and Permeability in Glassy Polymeric Membranes: An Overview, Frontiers of Chemical Science and Engineering, 11 (2017) 405-413.

[8] G.K. Fleming, W.J. Koros, Dilation of Polymers by Sorption of Carbon Dioxide at Elevated Pressures 1. Silicone Rubber and Unconditioned Polycarbonate, Macromolecules, 19 (1986) 2285-2291.

[9] J.D. Wind, S.M. Sirard, D.R. Paul, P.F. Green, K.P. Johnston, W.J. Koros, Carbon Dioxide-Induced Plasticization of Polyimide Membranes: Pseudo-Equilibrium Relationships of Diffusion, Sorption, and Swelling, Macromolecules, 36 (2003) 6433-6441.

[10] A.G. Wonders, D.R. Paul, Effect of CO_2 Exposure History on Sorption and Transport in Polycaronate, Journal of Membrane Science, 5 (1979) 63 - 75.

[11] M.E. Dose, J.D. Moon, I. Hubacek, D.R. Paul, B.D. Freeman, Fundamental Gas Transport and Dilation of Studies in Thermally Cross-linked Diaminophenylindane (DAPI) Containing Polyimides, Journal of Polymer Science Part B: Polymer Physics, In Preparation (2018).

[12] E.W. Lemmon, M.O. McLinden, D.G. Friend, Thermophysical Properties of Fluid Systems, in: P.J. Linstrom, W.G. Mallard (Eds.) NIST Chemistry WebBook, NIST Standard Reference Database Number 69, National Institute of Standards and Technology, Gaithersburg MD, 2018.

[13] K.L. Gleason, Z.P. Smith, Q. Liu, D.R. Paul, B.D. Freeman, Pure- and Mixed-Gas Permeation of CO_2 and CH_4 in Thermally Rearranged Polymers Based on 3,3′ -Dihydroxy-4,4′ -Diamino-Biphenyl (HAB) and 2,2′ -Bis-(3,4-Dicarboxyphenyl) Hexafluoropropane Dianhydride (6FDA), Journal of Membrane Science, 475 (2015) 204-214.

[14] Z.P. Smith, D.F. Sanders, C.P. Ribeiro, R. Guo, B.D. Freeman, D.R. Paul, J.E. McGrath, S. Swinnea, Gas Sorption and Characterization of Thermally Rearranged Polyimides Based on 3,3′ -Dihydroxy-4,4′ -Diamino-Biphenyl (HAB) And 2,2′ -Bis-(3,4-Dicarboxyphenyl) Hexafluoropropane Dianhydride (6FDA), Journal of Membrane Science, 415-416 (2012) 558-567.

[15] L.M. Robeson, Q. Liu, B.D. Freeman, D.R. Paul, Comparison of Transport Properties of Rubbery and Glassy Polymers and the Relevance to the Upper Bound Relationship, Journal of Membrane Science, 476 (2015) 421-431.

[16] L.M. Robeson, B.D. Freeman, D.R. Paul, B.W. Rowe, An Empirical Correlation of Gas Permeability and Permselectivity in Polymers and Its Theoretical Basis, Journal of Membrane Science, 341 (2009) 178-185.

[17] E.S. Sanders, High-Pressure Sorption of Pure and Mixed Gases in Glassy Polymers, Doctor of Philosophy, North Carolina State University, Raleigh, NC, 1983.

[18] R. Raharjo, B. Freeman, E. Sanders, Pure and Mixed Gas CH_4 and n-C_4H_{10} Sorption and Dilation in Poly(dimethylsiloxane), Journal of Membrane Science, 292 (2007) 45-61.

[19] J.E. Bachman, Z.P. Smith, T. Li, T. Xu, J.R. Long, Enhanced Ethylene Separation and Plasticization Resistance in Polymer Membranes Incorporating Metal-Organic Framework Nanocrystals, Nature Materials, 15 (2016) 845-849.

[20] L.M. Robeson, Z.P. Smith, B.D. Freeman, D.R. Paul, Contributions of Diffusion and Solubility Selectivity to the Upper Bound Analysis for Glassy Gas Separation Membranes, Journal of Membrane Science, 453 (2014) 71-83.

[21] W.R. Vieth, J.M. Howell, J.H. Hsieh, Dual Sorption Theory, Journal of Membrane Science, 1 (1976) 177 - 220.

[22] W.J. Koros, R.T. Chern, V. Stannett, H.B. Hopfenberg, A Model for Permeation of Mixed Gases and Vapors in Glassy Polymers, Journal of Polymer Science: Polymer Physics Edition, 19 (1981) 1513 - 1530.

[23] T. Visser, M. Wessling, Auto and Mutual Plasticization in Single and Mixed Gas C3 Transport Through Matrimid-Based Hollow Fiber Membranes, Journal of Membrane Science, 312 (2008) 84-96.

[24] A.M.W. Hillock, S.J. Miller, W.J. Koros, Crosslinked Mixed Matrix Membranes for the Purification of Natural Gas: Effects of Sieve Surface Modification, Journal of Membrane Science, 314 (2008) 193-199.

[25] N. Du, M.M. Dal-Cin, G.P. Robertson, M.D. Guiver, Decarboxylation-Induced Cross-Linking of Polymers of Intrinsic Microporosity (PIMs) for Membrane Gas Separation, Macromolecules, 45 (2012) 5134-5139.

[26] C. Zhang, P. Li, B. Cao, Decarboxylation Crosslinking of Polyimides with High CO_2/CH_4 Separation Performance and Plasticization Resistance, Journal of Membrane Science, 528 (2017) 206-216.

[27] M. Rungta, C. Zhang, W.J. Koros, L. Xu, Membrane-Based Ethylene/Ethane Separation: The Upper Bound And Beyond, AIChE Journal, 59 (2013) 3475-3489.

Chapter 6: Fundamental Gas Transport and Dilation Studies in Thermally Cross-linked Diaminophenylindane (DAPI) Containing Polyimides

The dilation and diffusion of CO_2, C_2H_4, and C_2H_6 in diaminophenylindane (DAPI) containing polyimides were studied at 35°C and at fugacities up to 30 atm. To study the influence of thermal cross-linking on plasticization, 6FDA$_{0.5}$-DAPI$_{0.33}$/DABA$_{0.17}$, a polyimide containing hexafluoroisopropylidene diphthalic anhydride (6FDA), diaminophenylindane (DAPI), and diaminobenzoic acid (DABA), was cross-linked at 353°C for 40 min under inert atmosphere, and its transport properties were compared to those of uncross-linked (i.e., linear) 6FDA$_{0.5}$-DAPI$_{0.33}$/DABA$_{0.17}$, and 6FDA$_{0.5}$-DAPI$_{0.5}$, which does not contain the cross-linkable DABA units. All three polymers swelled by about 4 vol% when exposed to 25 atm of CO_2, C_2H_4, or C_2H_6. The higher partial molar volume of C_2H_6 in linear 6FDA$_{0.5}$-DAPI$_{0.33}$/DABA$_{0.17}$ than in the other polymers suggests that C_2H_6 is more readily excluded from free volume elements in linear 6FDA$_{0.5}$-DAPI$_{0.33}$/DABA$_{0.17}$.[5]

[5] This chapter has been adapted with permission from sections of [1] M.E. Dose, J.D. Moon, I. Hubacek, D.R. Paul, B.D. Freeman, Fundamental Gas Transport and Dilation Studies in Thermally Cross-linked Diaminophenylindane (DAPI) Containing Polyimides, Journal of Polymer Science Part B: Polymer Physics, In Preparation (2018). I was the primary author, developed the experimental design, conducted the experiments, and preformed most of the analysis. The co-authors from these papers contributed to the analysis and helped run supporting experiments.

6.1. INTRODUCTION

The rapid growth of shale gas production has catalyzed efforts to develop energy efficient separation techniques capable of processing light hydrocarbons [1, 2]. Polymer membrane based separation processes offer several advantages over traditional separation techniques for hydrocarbon separations but have yet to be used in commercial hydrocarbon separations. Plasticization and swelling induced by hydrocarbon sorption into the polymer matrix, which reduces the polymer's size sieving ability and permeability selectivity, are challenges membranes face in such applications [3, 4]. Additionally, plasticization may appear minimal when materials are evaluated under ideal pure gas conditions, but when tested using more realistic mixed gas conditions, the separation performance can be significantly lower than predicted by pure gas experiments [5, 6].

While significant work has focused on understanding the fundamentals of CO_2-induced plasticization in various polymers [7-13], few studies have investigated plasticization caused by light hydrocarbons, such as ethane and ethylene [14-17]. To better understand how light hydrocarbons interact with the polymers, it is important to consider gas solubility, sorption-induced dilation, and penetrant diffusivity.

This study used a polyimide containing **hexaf**luoroisopropylidene **d**iphthalic **a**nhydride (6FDA), **d**i**a**mino**p**heny**l**indane (DAPI), and **d**i**a**mino**b**enzoic **a**cid (DABA) in a molar ratio of 0.5/0.33/0.17 (i.e., $6FDA_{0.5}$-$DAPI_{0.33}$/$DABA_{0.17}$) and a polyimide where 6FDA and DAPI are present in equal molar ratios (i.e., $6FDA_{0.5}$-$DAPI_{0.5}$). For this work, $6FDA_{0.5}$-$DAPI_{0.33}$/$DABA_{0.17}$ is abbreviated "6FDA-DAPI/DABA", and $6FDA_{0.5}$-$DAPI_{0.5}$ is abbreviated "6FDA-DAPI". Polymer structures are given in Figure 6.1. The carboxylic acid group in DABA allows 6FDA-DAPI/DABA to be thermally cross-linked by

decarboxylation [9, 11, 18, 19]. Previously, cross-linking 6FDA-DAPI/DABA at 353°C for 40 min increased polymer chain d-spacing, which correlated with a 30% increase in pure gas permeability for most gases relative to linear 6FDA-DAPI/DABA [19]. Minimal differences in pure gas solubility were observed between 6FDA-DAPI, linear 6FDA-DAPI/DABA, and cross-linked 6FDA-DAPI/DABA. Additionally, increases in diffusivity selectivity were observed for the CO_2/CH_4, CO_2/N_2, and C_2H_4/C_2H_6 gas pairs, suggesting a narrowing of the fractional free volume distribution upon cross-linking 6FDA-DAPI/DABA [20].

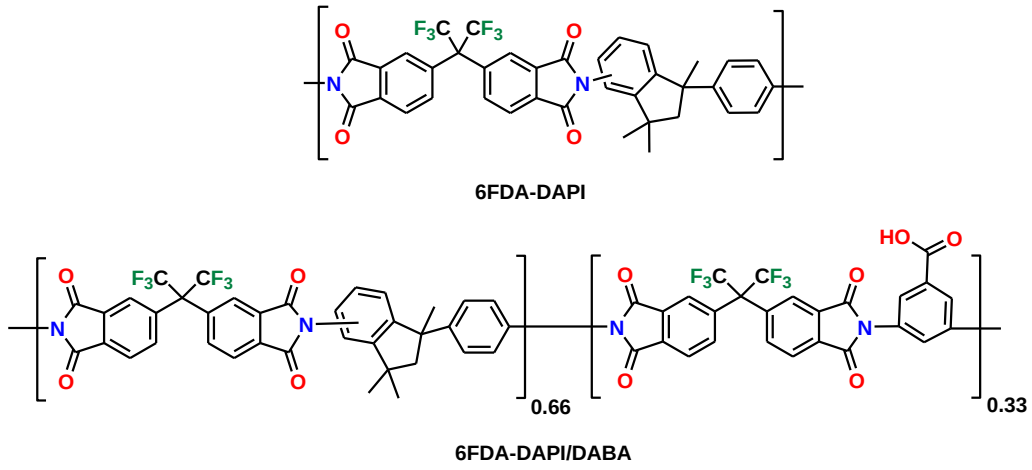

Figure 6.1. Structure of 6FDA-DAPI and linear (i.e., uncross-linked) 6FDA-DAPI/DABA. Linear 6FDA-DAPI/DABA can be thermally cross-linked by decarboxylation of the DABA moiety [19, 20].

Despite pure gas experiments indicating improved plasticization resistance, evidence of plasticization was still present at high fugacity in all three DAPI containing polyimides when tested under mixed gas conditions with a 50:50 C_2H_4:C_2H_6 mixture [20]. Apparent competitive sorption lowered C_2H_4 permeability and C_2H_4/C_2H_6 selectivity while plasticization increased C_2H_6 permeability under mixed gas conditions in 6FDA-DAPI and

cross-linked 6FDA-DAPI/DABA. However, linear 6FDA-DAPI/DABA showed a slight increase in C_2H_4 and C_2H_6 permeability in mixed gas experiments and no significant change in C_2H_4/C_2H_6 selectivity relative to pure gas experiments. Linear 6FDA-DAPI/DABA was more resistant to plasticization than either 6FDA-DAPI or cross-linked 6FDA-DAPI/DABA, resulting in no significant difference between pure and mixed gas permeation results. To better understand how potentially plasticizing gases interact with 6FDA-DAPI, linear 6FDA-DAPI/DABA, and cross-linked 6FDA-DAPI/DABA, this study focuses on the dilation and pressure dependence of gas diffusivity when exposed to high fugacity CO_2, C_2H_4, and C_2H_6.

6.2. Results and Discussion

6.2.1. Pure Gas Dilation

Volumetric dilation from CO_2, C_2H_4, and C_2H_6 was measured at fugacities up to 30 atm in 6FDA-DAPI, linear 6FDA-DAPI/DABA, and cross-linked 6FDA-DAPI/DABA. The dilation isotherms are presented in Figure 6.2 a-i. All polymers dilated about 4% by volume at 25 atm for all three gases, with the exception of 6FDA-DAPI, which dilated about 5% when exposed to CO_2 at about 25 atm. The dilation by C_2H_6 in all three polymers is consistent with plasticization, which was observed in mixed gas permeation experiments [20].

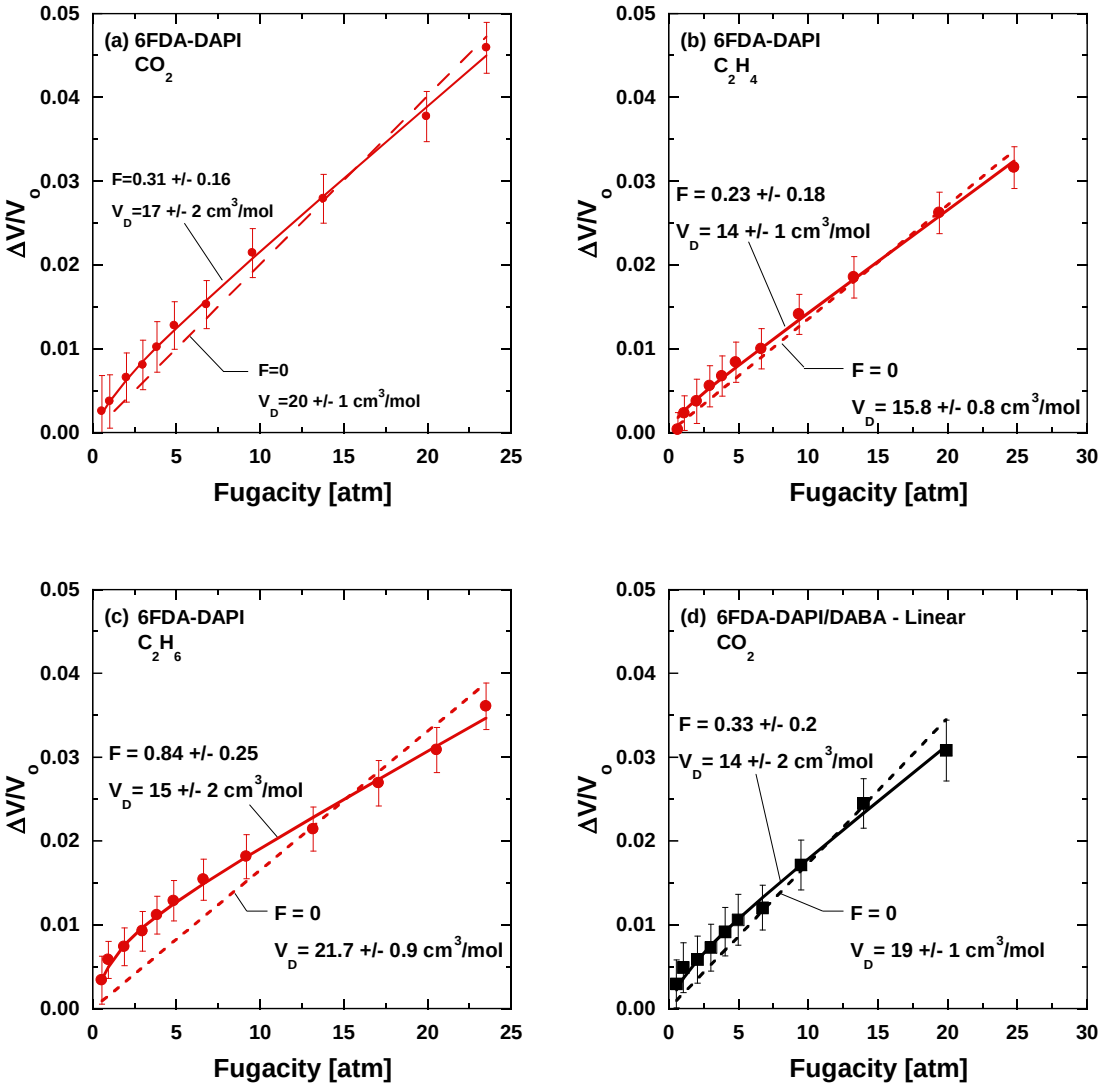

Figure 6.2. Dilation of 6FDA-DAPI (●), linear 6FDA-DAPI/DABA (■), and cross-linked 6FDA-DAPI/DABA (♦) by CO_2, C_2H_4, and C_2H_6 at 35°C. The dilation data is fit to two models based off Eq. 6.1: 1) assuming Langmuir sites do not contribute to dilation (F = 0, dashed line), and 2) assuming Langmuir sites contribute to dilation ($F \neq 0$, solid line).

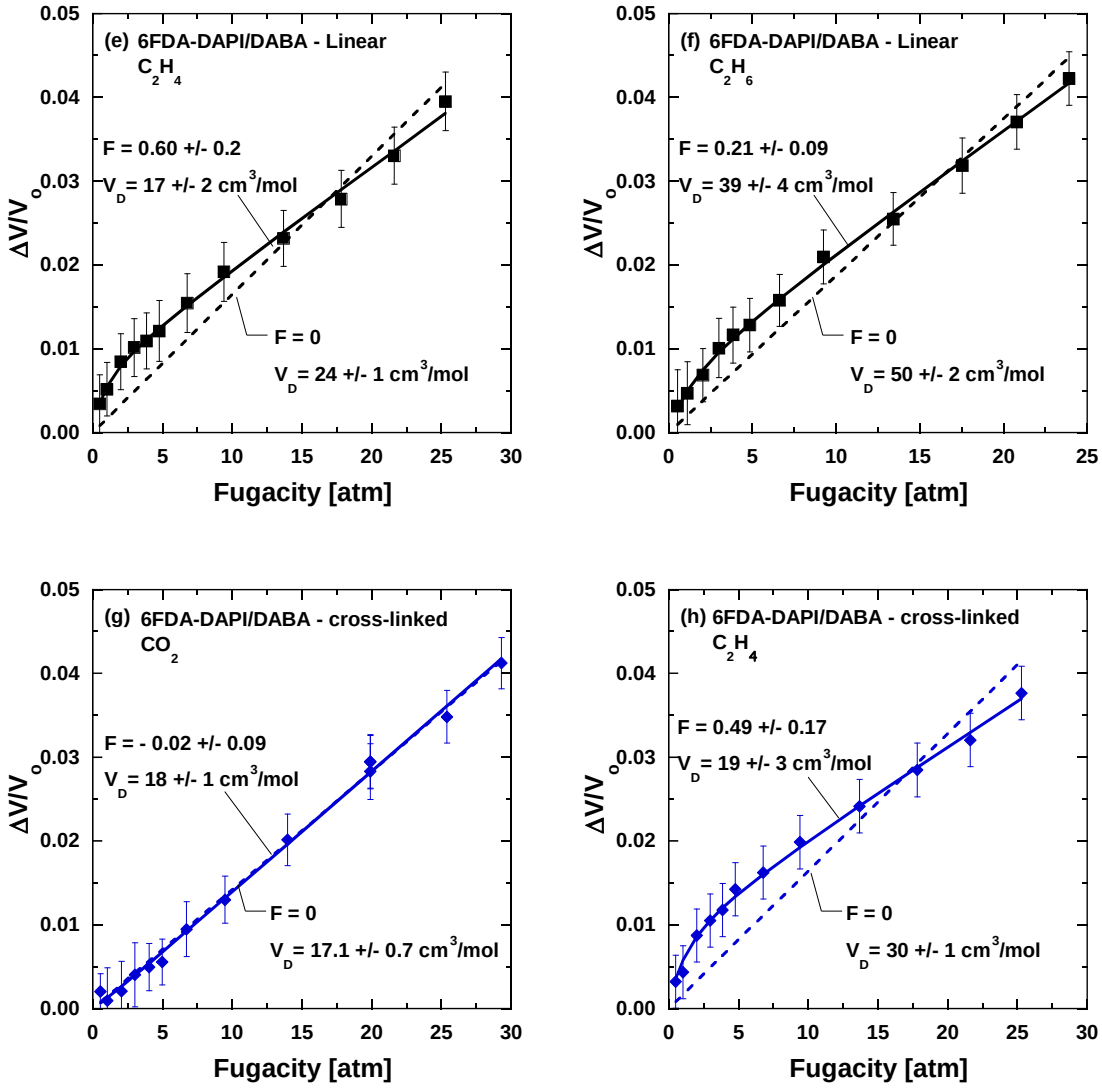

Figure 6.2. (Continued) Dilation of 6FDA-DAPI (●), linear 6FDA-DAPI/DABA (■), and cross-linked 6FDA-DAPI/DABA (♦) by CO_2, C_2H_4, and C_2H_6 at 35°C. The dilation data is fit to two models based off *Eq. 6.1*: 1) assuming Langmuir sites do not contribute to dilation (F = 0, dashed line), and 2) assuming Langmuir sites contribute to dilation (F ≠ 0, solid line).

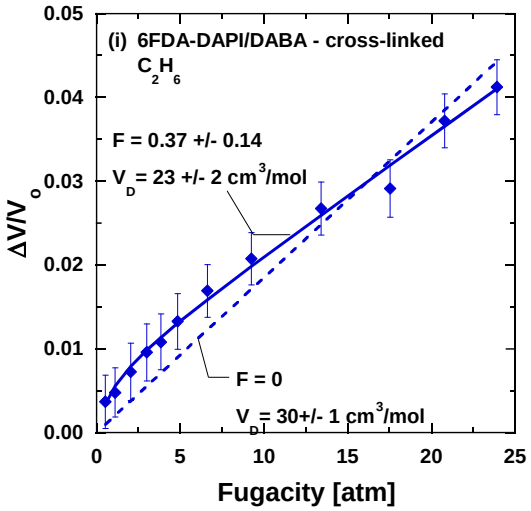

Figure 6.2. (Continued) Dilation of 6FDA-DAPI (●), linear 6FDA-DAPI/DABA (■), and cross-linked 6FDA-DAPI/DABA (♦) by CO_2, C_2H_4, and C_2H_6 at 35°C. The dilation data is fit to two models based off *Eq. 6.1*: 1) assuming Langmuir sites do not contribute to dilation (F = 0, dashed line), and 2) assuming Langmuir sites contribute to dilation (F ≠ 0, solid line).

Kamiya et al. and others [21-24] have described the dilation of penetrants in glassy polymers using the following expression:

$$\frac{\Delta V}{V_o} = V_D\left(k_D f + F\frac{C'_H b f}{1+bf}\right) \qquad \text{Eq. 6.1}$$

where F is the average fraction of Langmuir sorption sites contributing to dilation ($0 \leq F \leq 1$) [22, 23, 25], and the constants k_D, C'_H, and b are dual-mode parameters derived from pure gas sorption data [20]. Small values of F indicate dilation occurs primarily via Henry's Law sorption, while larger F values suggest significant dilation of Langmuir sites is necessary to accommodate penetrants. For rubbery and some glassy polymers, penetrant induced dilation increases linearly with fugacity (i.e., $F=0$), suggesting dilation occurred

only in the Henry's Law sites and the dissolved penetrant had a partial molar volume that is independent of pressure [26, 27].

As shown in Figure 6.2, sorption induced dilation in 6FDA-DAPI, linear 6FDA-DAPI/DABA, and cross-linked 6FDA-DAPI/DABA showed non-linear dilation, particularly for C_2H_4 and C_2H_6 at low fugacity. To obtain the V_D and F values recorded in Table 6.1, the dilation isotherms were fit to Eq. 6.1 using a weighted least squares non-linear fit in Wolfram Mathematica software (WolframAlpha, Chamaign, IL USA) and the dual-mode parameters reported previously [20]. Both dilation parameters are dependent on dual-mode sorption parameters, with V_D strongly coupled to k_D and F coupled to C_H' and b. However, in our previous analysis, we determined the values of k_D, C_H', and b were not uniquely different for the sorption data and no special physical significance was assigned to the values themselves [6, 28, 29]. Additionally, the high relative uncertainty in the dilation isotherm at low fugacities, which is due to instrument limitations, makes it difficult to place any confidence in the value of F. Thus, it is difficult to determine if V_D and F are uniquely different for each polymer-penetrant pair. While a statistical analysis suggests $F \neq 0$ is a better fit to the dilation data, the remainder of our analysis uses V_D and F values merely as fitting parameters. The values of F and V_D may correlate with some physical polymer-penetrant interactions, but not obvious correlations were observed in this work.

Polymer	CO_2		C_2H_4		C_2H_6	
	V_D [cm^3/mol]	F	V_D [cm^3/mol]	F	V_D [cm^3/mol]	F
6FDA-DAPI	17 ± 2	0.3 ± 0.2	14 ± 1	0.2 ± 0.2	15 ± 2	0.8 ± 0.3
6FDA-DAPI/DABA (linear)	14 ± 2	0.3 ± 0.2	17 ± 2	0.6 ± 0.2	39 ± 4	0.2 ± 0.1
6FDA-DAPI/DABA (cross-linked)	18 ± 1	0.02 ± 0.09	19 ± 3	0.5 ± 0.2	23 ± 2	0.4 ± 0.1

Table 6.1. Volumetric dilation parameters for 6FDA-DAPI, linear 6FDA-DAPI/DABA, and cross-linked 6FDA-DAPI/DABA determined by fitting dilation isotherms to Eq. 6.1.

6.2.2. Partial Molar Volume

By combining volumetric dilation and gas sorption data, the penetrant partial molar volumes in the polymers, $\bar{V}_i$, can be estimated using the definition [22, 30, 31]:

$$\bar{V}_i = \left(\frac{\partial V}{\partial n_i}\right)_{T,p,n_j} \quad \text{Eq. 6.2}$$

where V is the total volume of the mixture and n_i is the moles of penetrant i. For dilation of a polymer-penetrant mixture, penetrant partial molar volume can be calculated using Eq. 6.3 [32, 33]:

$$\bar{V}_i = \left[\frac{\partial}{\partial f}\left(\frac{\Delta V}{V_o}\right) + \beta\right]\frac{\partial f}{\partial C} \quad \text{Eq. 6.3}$$

where β is the polymer isothermal compressibility, and C is the penetrant concentration expressed in cm^3(STP)/(cm^3 polymer). Since penetrant-induced swelling is more significant than isothermal compressibility in rigid glassy polymers, β can be neglected in Eq. 6.3 [32, 33]. For this work, partial molar volumes were calculated using Eq. 6.4, which is derived from Eq. 6.3, Eq. D.2, the dual-mode sorption model, and dilation expressions (i.e., Eq. 6.1) [24]:

$$\bar{V}_i = V_D \left[\frac{k_D + F \dfrac{C'_H b}{(1+bf)^2}}{k_D + \dfrac{C'_H b}{(1+bf)^2}} \right] \qquad \text{Eq. 6.4}$$

where k_D, b, and C'_H are the dual-mode parameters determined previously [20], and V_D and F are dilation model parameters from Eq. 6.1 [24]. The partial molar volume can also be determined graphically by taking the tangent of dilation data plotted versus penetrant concentration (cf., Figure 6.3). While no physical significance is associated with the values of V_D and F, the values of V_D, F, and the dual-mode parameters are used as fitting parameters to accurately calculate the slopes represented in Figure 6.3 a-c (i.e., the partial molar volumes). Partial molar volumes are reported in Figure 6.4 a-c. In all cases, $\bar{V}_i$ increases at low fugacity and approaches a constant value at high fugacity.

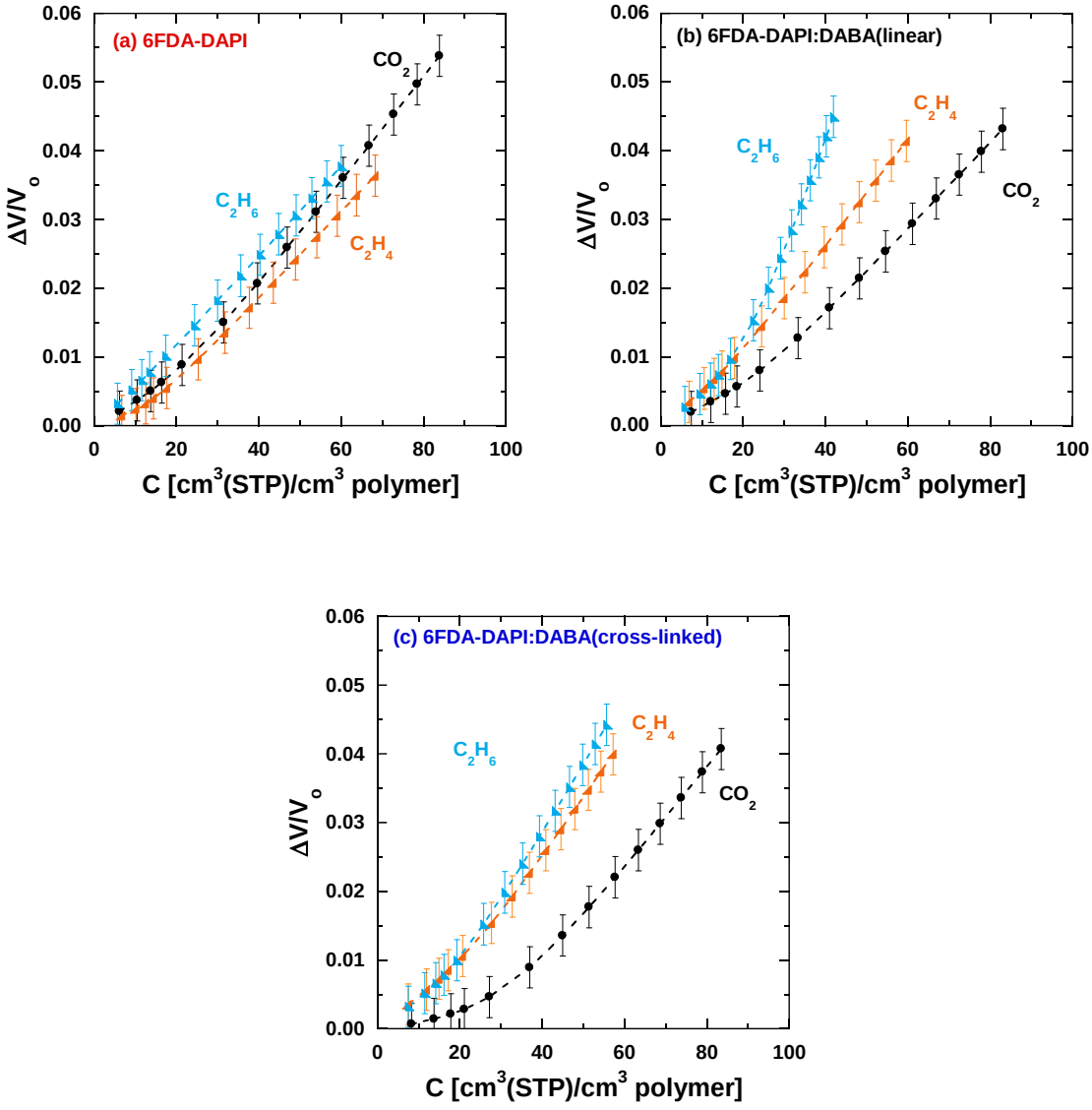

Figure 6.3. Polymer dilation versus gas concentration for CO_2 (●), C_2H_4 (◢), and C_2H_6 (◣) in (a) 6FDA-DAPI, (b) linear 6FDA-DAPI/DABA, and (c) cross-linked 6FDA-DAPI/DABA. The slope of these plots is the penetrant partial molar volume.

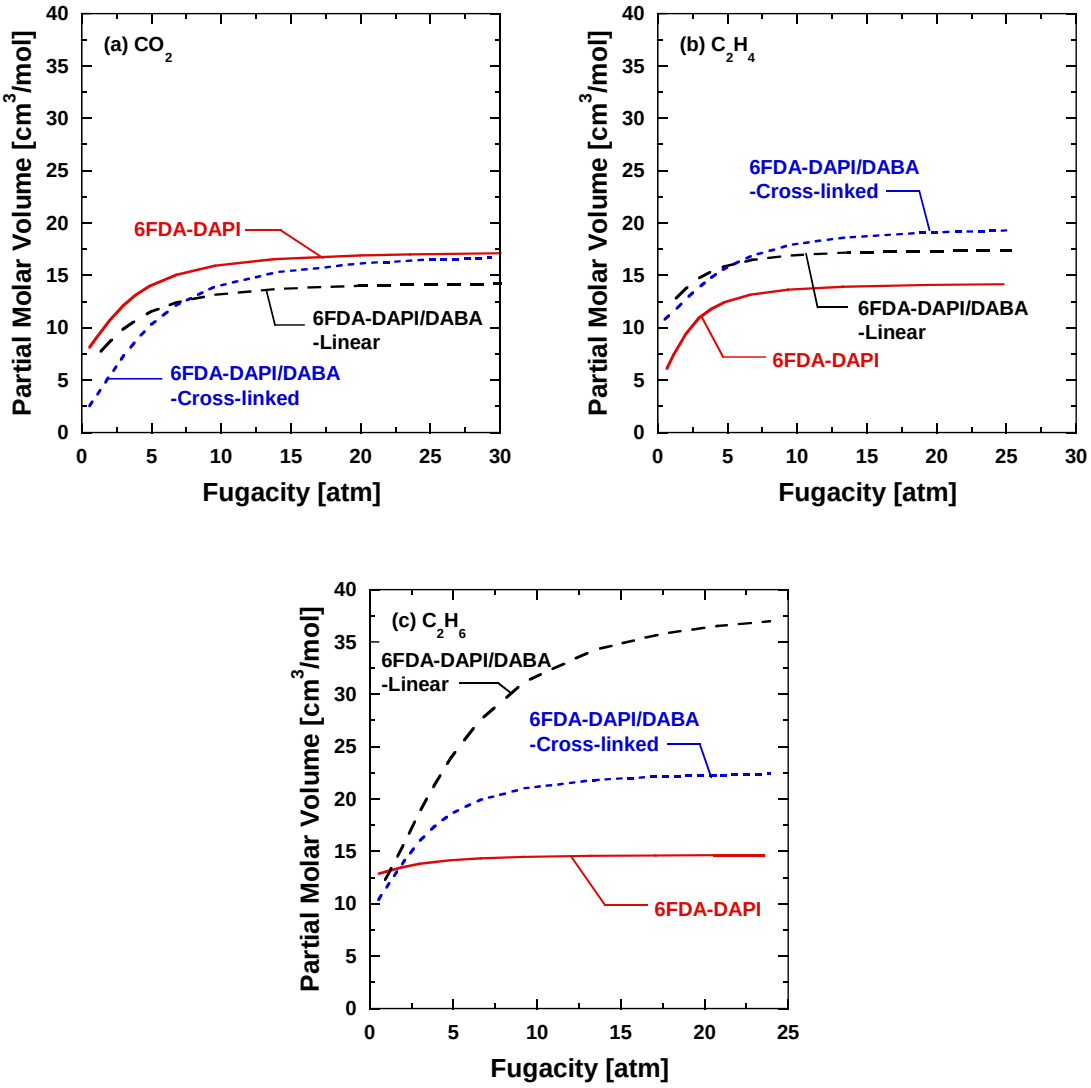

Figure 6.4. Partial molar volume of: (a) CO_2, (b) C_2H_4, and (c) C_2H_6 in 6FDA-DAPI (red, solid line), linear 6FDA-DAPI/DABA (black, long dashed line), and cross-linked 6FDA-DAPI/DABA (blue, short dashed line).

As shown in Figure 6.3-a, dilation of 6FDA-DAPI increased linearly with concentration and exhibited similar dilation for CO_2, C_2H_4, and C_2H_6, despite the penetrants having different gas diameters. While there was no significant difference in the dilation of linear 6FDA-DAPI/DABA at concentrations less than 20 $cm^3(STP)/cm^3$ polymer, Figure

6.3-b shows the dilation of linear 6FDA-DAPI/DABA increased in the following order: CO_2 (d_g = 3.44 Å) < C_2H_4 (d_g =4.16 Å) < C_2H_6 (d_g = 4.44 Å), increasing with increasing gas diameter [34, 35]. Similarly, dilation of cross-linked 6FDA-DAPI/DABA was somewhat dependent on penetrant size, with C_2H_4 and C_2H_6 dilating the cross-linked polymer more than CO_2 at a given penetrant concentration (c.f., Figure 6.3-c).

The partial molar volume of CO_2, $\bar{V}_{CO_2}$, in all three polymers are reported in Figure 6.4-a, where $\bar{V}_{CO_2}$ increased at low fugacity and approached a constant value, or $\bar{V}_{CO_2}^{sat}$, of about 16 cm^3/mol at high fugacity. Lower values of $\bar{V}_{CO_2}$ at low fugacity and low penetrant concentration can be attributed to a significant fraction of CO_2 dissolving in the existing free volume elements, (i.e., the Langmuir sites of the polymer matrix) and sorption in those sites contributing little, if at all, to polymer swelling. At higher fugacity and higher penetrant concentration, when Langmuir sorption sites have been saturated, the polymer must swell in order to accommodate the penetrants. The $\bar{V}_{CO_2}^{sat}$ in all three polymers are significantly lower than the $\bar{V}_{CO_2}^{sat}$ dissolved in silicon rubber and organic liquids, 46 cm^3/mol [23]. Similar trends and depression of the saturated partial molar volume has been observed for other polymer-penetrant pairs, such as when water dissolves into both rigid polybenzimidizole (PBI) polymers and bulky solvents [24, 36]. Additionally, the depression of the $\bar{V}_{CO_2}^{sat}$ in the DAPI-containing polyimides is more significant than that observed in polycarbonate, where $\bar{V}_{CO_2}$ approached 36 cm^3/mol at high pressures [23]. This result may be due to higher fractional free volume, FFV, and Langmuir sorption in 6FDA-DAPI (FFV = 0.179), linear 6FDA-DAPI/DABA (FFV = 0.180), and cross-linked 6FDA-DAPI/DABA (FFV = 0.177) [19] than in polycarbonate (FFV = 0.164) [26].

The partial molar volume of C_2H_4, $\bar{V}_{C_2H_4}$, was very similar to that of CO_2 and approached values of 17 cm^3/mol and 19 cm^3/mol for linear 6FDA-DAPI/DABA and cross-linked 6FDA-DAPI/DABA at high fugacity, respectively (cf. Figure 6.4-b*)*. However, $\bar{V}_{C_2H_4}$approached 14 cm^3/mol in 6FDA-DAPI, slightly lower than the values observed in the other two polymers in this study. Additionally, the partial molar volume at high fugacity, $\bar{V}_{C_2H_4}^{sat}$, in all three polymers are significantly lower than the C_2H_4 liquid molar volume of 50 cm^3/mol at 170 K or the saturated partial molar volume of 52 cm^3/mol dissolved in polybutadiene at 35°C [30, 37]. Similar to CO_2, the depression of$\bar{V}_{C_2H_4}^{sat}$ in 6FDA-DAPI, linear 6FDA-DAPI/DABA, and cross-linked 6FDA-DAPI/DABA is likely due to a large fraction of C_2H_4 dissolving in the Langmuir sites that contribute minimally to volumetric dilation.

As shown in Figure 6.4-c, the partial molar volume of C_2H_6, at high fugacity, $\bar{V}_{C_2H_6}^{sat}$, varied significantly between the three polymers, increasing in the following order: 6FDA-DAPI (15 cm^3/mol) < cross-linked 6FDA-DAPI/DABA (23 cm^3/mol) < linear 6FDA-DAPI/DABA (39 cm^3/mol). Similar to $\bar{V}_{CO_2}^{sat}$ and $\bar{V}_{C_2H_4}^{sat}$, $\bar{V}_{C_2H_6}^{sat}$ values in all polymers in this study are lower than the liquid molar volume of C_2H_6 and its saturated partial molar volume in rubbery polybutadiene, 65 cm^3/mol and 57 cm^3/mol, respectively, at 35°C [30, 37]. Higher $\bar{V}_{C_2H_6}^{sat}$was observed in linear 6FDA-DAPI, which has the smallest d-spacing value (5.63Å), and may reflect fewer non-swelling Langmuir sorption sites available for C_2H_6 to occupy [19]. This effect is observed most strongly with C_2H_6, probably due to its gas diameter being larger than that of CO_2 or C_2H_4. Larger penetrants require larger free volume elements for sorption to occur. Additionally, a previous study showed that linear 6FDA-

DAPI/DABA has a smaller d-spacing (5.63 Å) than its cross-linked counterpart (5.73 Å) and may also have broader free volume distribution [20]. A broader free volume distribution could be consistent with a larger fraction of free volume elements in linear 6FDA-DAPI/DABA being too small for C_2H_6 to access without swelling, resulting in more swelling and higher C_2H_6 partial molar volume in linear 6FDA-DAPI/DABA than in 6FDA-DAPI or cross-linked 6FDA-DAPI/DABA.

6.2.3. Penetrant Mobility Versus Gas Diameter

Gas diffusion coefficients for both rubbery and glassy polymers often trend linearly with gas diameter squared, according to Eq. 6.11:

$$\ln(D) = \alpha - \gamma d_g^2 \qquad \text{Eq. 6.11}$$

where d_g is the effective gas diameter [29], and α and γ are empirical constants for a given polymer [50]. With this correlation, γ serves as a measure of the size sieving ability of the polymer, where larger γ values indicate that the polymer has greater size sieving ability. Infinite dilution diffusion coefficients of CO_2, C_2H_4, C_2H_6, CH_4, and N_2 were correlated with their corresponding gas diameters (cf., Table D.1 and Table D.7). The infinite dilution diffusion coefficient values, D_o, for CO_2, C_2H_4, and C_2H_6 were estimated using the empirical parameters from Eq. 6.8 and the penetrant free FFV values reported previously [19]. Due to the lack of dilation data for CH_4 and N_2, $D_{w,o}$ values from Eq. 6.6 were used for CH_4 and N_2. The use of diffusion coefficients extrapolated to infinite dilution prevented the analysis from being influenced by plasticization.

As shown in *Figure 6.9, D_o* values of the gases followed an exponential trend with d_g^2 as predicted by Eq. 6.11. However, the γ-values for all three polymers are similar, with

significant scatter occurring in the D_o values for 6FDA-DAPI. However, the γ value for cross-linked 6FDA-DAPI/DABA is slightly larger than the γ value for linear 6FDA-DAPI/DABA. This trend suggests the free volume distribution of cross-linked 6FDA-DAPI/DABA may be slightly more narrow than linear 6FDA-DAPI/DABA, possibly contributing to the increase in diffusion selectivity with cross-linking, as previous diffusion and permeability experiments have suggested [19, 20]. At higher pressures, the scatter in data around the fit to Eq. 6.11 (c.f., Figure D.12) increased, suggesting other factors, like plasticization, may be contributing to a loss in the size sieving ability of the polymer.

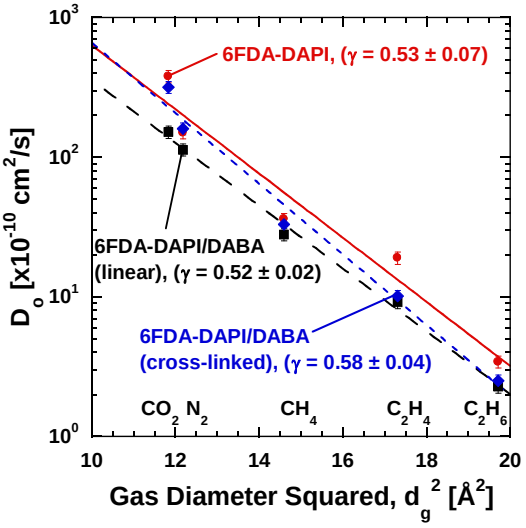

Figure 6.5. Diffusion coefficients at infinite dilution, D_o, in 6FDA-DAPI (●), linear 6FDA-DAPI/DABA (■), and cross-linked 6FDA-DAPI/DABA (♦) versus effective gas diameter squared, d_g^2. The values for CO_2, C_2H_4, and C_2H_4 were from the polymer penetrant free FFV using Eq. 6.8. Due to the lack of dilation data for CH_4 and N_2, infinite dilution values were estimated at zero weight fraction using Eq. 6.6. The solid lines represent the exponential trend, as described by Eq. 6.11.

6.3. CONCLUSIONS

All three DAPI containing polyimides showed similar dilation level for three gases up to 25 atm and exhibited non-linear dilation at low fugacity for C_2H_4 and C_2H_6. These results indicate a fraction of the Langmuir sites are too small to accommodate the larger gas molecules and must swell to accommodate the penetrants. The partial molar volume of C_2H_6 varied the most between the three polymers, following the order: 6FDA-DAPI < cross-linked 6FDA-DAPI/DABA < linear 6FDA-DAPI/DABA. The larger partial molar volume in linear 6FDA-DAPI/DABA is likely due to a larger fraction of the free volume elements in linear 6FDA-DAPI/DABA being too small for C_2H_6 to access without swelling.

Weight fraction based exponential factors for the diffusion coefficients, $\beta_{D,w}$, of CO_2, C_2H_4, and C_2H_6 did not correlate with the pressure dependent swelling, k_{sw}, or increase with the increase in relative permeability after the plasticization fugacity, ΔP_{rel}, observed in pure gas experiments. However, it was observed that $\beta_{D,w}$ increased with increasing saturated partial molar volume of the penetrant, $\bar{V}^{sat}$. Additionally, the accessible free volume, FFV_a, of the polymers were found increase with increasing penetrant concentration, contributing to the increase in diffusion coefficients observed for CO_2, C_2H_4, and C_2H_6.

6.4. ACKNOWLEDGMENTS

This material is based upon work supported in part by the National Science Foundation Graduate Research Fellowship under Grant No. DGE-1610403. The authors gratefully acknowledge partial support from the Division of Chemical Sciences, Geosciences, and Biosciences, Office of Basic Energy Sciences of the U.S. Department of

Energy (DOE), USA through Grant DE-FG02-02ER15362 and partial support by the Australian-American Fulbright Commission for the award to BDF of the U.S. Fulbright Distinguished Chair in Science, Technology and Innovation sponsored by the Commonwealth Scientific and Industrial Research Organization (CSIRO). Additionally, this work is supported in part by the National Science Foundation under Cooperative Agreement No. EEC-1647722. Any opinions, findings, and conclusions or recommendations expressed in this material are those of the authors and do not necessarily reflect the views of the National Science Foundation.

6.5. NOMENCLATURE

Symbol	Meaning
$\Delta V_i/V_o$	Fractional change in sample volume
L_o	Initial length of penetrant free polymer sample
L_i	Sample length after equilibrating at target pressure
k_D	Dual-mode Henry's law constant
f	fugacity
V_D	Effective condensed penetrant molar volume
F	Fraction of Langmuir sites contributing to dilation
C'_H	Dual-mode Langmuir capacity constant
b	Dual-mode ffinity constant
β	Isothermal compressibility factor
C	Penetrant concentration
$\bar{V}_i$	Partial molar volume of penetrant *i*
$\bar{V}_i^{sat}$	Saturated partial molar volume of penetrant *i*, or the partial molar volume of penetrant *i* at the maximum fugacity tested in this work.
P_i	Permeability coefficient of penetrant *i*
S_i	Solubility coefficient of penetrant *i*
D_i	Diffusion coefficient of penetrant *i*

w_i	Weight fraction of penetrant *i*
M_i	Molecular weight of penetrant *i*
ρ_{poly}	Penetrant-free polymer density
k_{sw}	Swelling constant from the NELF model
Q_i	Thermodynamic factor of penetrant *i*
L_i	Mobility factor of penetrant *i*
D_o	Penetrant free diffusion coefficient (at either penetrant free fractional free volume or zero penetrant weight fraction)
$D_{w,o}$	Penetrant diffusion coefficient at zero penetrant weight fraction
$\beta_{D,w}$	Weigh fraction based exponential factor for diffusion coefficients
$\beta_{D,C}$	Concentration based exponential factor for diffusion coefficients
$\beta_{L,w}$	Weight fraction based exponential factor for mobility coefficients
$\beta_{L,C}$	Concentration based exponential factor for mobility coefficients
A	Pre-exponential factor for Eq. 6.10
B	"B-value", exponential factor for Eq. 6.10
FFV_a	Accessible fractional free volume
$\hat{V}_{total}$	Total specific volume of polymer/penetrant mixture
$V_{occupied}$	Specific volume occupied by polymer chains
α	Empirical constant for Eq. 6.13
γ	Size sieving ability of a polymer, exponential factor for *Eq. 6.13*

6.6. REFERENCES

[1] U.S. Shale Production, U.S. Energy Information Administration, https://www.eia.gov/dnav/ng/hist/res_epg0_r5302_nus_bcfa.htm, 2018.

[2] Hydrocarbon Gas Liquids Explained, U.S. Energy Information Administration, https://www.eia.gov/energyexplained/index.php?page=hgls_home, 2018.

[3] R.W. Baker, B.T. Low, Gas Separation Membrane Materials: A Perspective, Macromolecules, 47 (2014) 6999-7013.

[4] M. Brayden, W.J. Koros, L. Xu, M. Martinez, B. Stears, G. Barbay, Carbon Molecular Sieve Hollow Fiber Membranes for Olefin/Paraffin Separations, AIChE National Meeting, San Antonio, TX, 2013, 140C.

[5] C. Staudt-Bickel, W.J. Koros, Olefin/paraffin gas separations with 6FDA-based polyimide membranes, Journal of Membrane Science, 170 (2000) 205-214.

[6] K.L. Gleason, Z.P. Smith, Q. Liu, D.R. Paul, B.D. Freeman, Pure- and Mixed-Gas Permeation of CO_2 and CH_4 in Thermally Rearranged Polymers Based on 3,3′ -Dihydroxy-4,4′ -Diamino-Biphenyl (HAB) and 2,2′ -Bis-(3,4-Dicarboxyphenyl) Hexafluoropropane Dianhydride (6FDA), Journal of Membrane Science, 475 (2015) 204-214.

[7] M. Calle, H.J. Jo, C.M. Doherty, A.J. Hill, Y.M. Lee, Cross-Linked Thermally Rearranged Poly(benzoxazole-co-imide) Membranes Prepared from ortho-Hydroxycopolyimides Containing Pendant Carboxyl Groups and Gas Separation Properties, Macromolecules, 48 (2015) 2603-2613.

[8] A. Bos, I. Punt, H. Strathmann, M. Wessling, Suppression of Gas Separation Membrane Plasticization by Homogeneous Polymer Blending, AIChE Journal, 47 (2001) 1088 - 1093.

[9] A.M. Kratochvil, W.J. Koros, Decarboxylation-Induced Cross-Linking of a Polyimide for Enhanced CO_2 Plasticization Resistance, Macromolecules, 41 (2008) 7920-7927.

[10] S.H. Han, N. Misdan, S. Kim, C.M. Doherty, A.J. Hill, Y.M. Lee, Thermally Rearranged (TR) Polybenzoxazole: Effects of Diverse Imidization Routes on Physical Properties and Gas Transport Behaviors, Macromolecules, 43 (2010) 7657-7667.

[11] W. Qiu, C.-C. Chen, L. Xu, L. Cui, D.R. Paul, W.J. Koros, Sub-Tg Cross-Linking of a Polyimide Membrane for Enhanced CO_2 Plasticization Resistance for Natural Gas Separation, Macromolecules, 44 (2011) 6046-6056.

[12] Y. Liu, R. Wang, T.-S. Chung, Chemical Cross-linking Modification of Polyimide Membranes for Gas Separation, Journal of Membrane Science, 189 (2001) 231–239.

[13] C. Staudt-Bickel, W. J. Koros, Improvement of CO_2/CH_4 Separation Characteristics of Polyimides by Chemical Crosslinking, Journal of Membrane Science, 155 (1999) 145-154.

[14] S.S. Chan, T.-S. Chung, Y. Liu, R. Wang, Gas and Hydrocarbon (C2 and C3) Transport Properties of Co-Polyimides Synthesized From 6FDA and 1,5-NDA (Naphthalene)/Durene diamines, Journal of Membrane Science, 218 (2003) 235-245.

[15] J.E. Bachman, Z.P. Smith, T. Li, T. Xu, J.R. Long, Enhanced Ethylene Separation and Plasticization Resistance in Polymer Membranes Incorporating Metal-Organic Framework Nanocrystals, Nature Materials, 15 (2016) 845-849.

[16] L. Xu, M. Rungta, W.J. Koros, Matrimid® Derived Carbon Molecular Sieve Hollow Fiber Membranes for Ethylene/Ethane Separation, Journal of Membrane Science, 380 (2011) 138-147.

[17] M. Rungta, L. Xu, W.J. Koros, Carbon Molecular Sieve Dense Film Membranes Derived from Matrimid® for Ethylene/Ethane Separation, Carbon, 50 (2012) 1488-1502.

[18] N. Du, M.M. Dal-Cin, G.P. Robertson, M.D. Guiver, Decarboxylation-Induced Cross-Linking of Polymers of Intrinsic Microporosity (PIMs) for Membrane Gas Separation, Macromolecules, 45 (2012) 5134-5139.

[19] M.E. Dose, M. Chwatko, I. Hubacek, N.A. Lynd, D.R. Paul, B.D. Freeman, Thermally Cross-linked Diaminophenylindane (DAPI) Containing Polyimides for Membrane Based Gas Separations, Polymer, Submitted (2018).

[20] M.E. Dose, I. Hubacek, D.R. Paul, B.D. Freeman, CO_2, C_2H_4, and C_2H_6 Sorption and Mixed Gas Permeability of Thermally Cross-linked Diaminophenylindane (DAPI) Containing Polyimides, Journal of Membrane Science, Submitted (2018).

[21] Y. Kamiya, T. Hirose, Y. Naito, K. Mizoguchi, Sorptive Dilation of Polysulfone and Poly(ethylene terephthalate) Films by High-pressure Carbon Dioxide, Journal of Polymer Science Part B: Polymer Physics, 26 (1988) 159-177.

[22] D. Punsalan, W.J. Koros, Drifts in penetrant partial molar volumes in glassy polymers due to physical aging, Polymer, 46 (2005) 10214-10220.

[23] G.K. Fleming, W.J. Koros, Carbon Dioxide Conditioning Effects on Sorption and Volume Dilation Behavior for Bisphenol A-Polycarbonate, Macromolecules, 23 (1990) 1353-1360.

[24] J.D. Moon, M. Galizia, H. Borjigin, R. Liu, J.S. Riffle, B. Freeman, D. Paul, Water Vapor Sorption, Diffusion, and Dilation in Polybenzimidazoles, Macromolecules, 51 (2018) 7197 - 7208.

[25] Y. Kamiya, K. Mizoguchi, T. Hirose, Y. Naito, Sorption and Dilation in Poly(ethyl methacrylate) -Carbon Dioxide System, Journal of Polymer Science: Part B: Polymer Physics, 27 (1989) 879-892.

[26] G.K. Fleming, W.J. Koros, Dilation of Polymers by Sorption of Carbon Dioxide at Elevated Pressures 1. Silicone Rubber and Unconditioned Polycarbonate, Macromolecules, 19 (1986) 2285-2291.

[27] D. Pope, W.J. Koros, Gas Sorption-Induced Dilation of Poly(4-methyl-1-pentene), Journal of Polymer Science Part B: Polymer Physics, 34 (1996) 1861-1868.

[28] Z.P. Smith, D.F. Sanders, C.P. Ribeiro, R. Guo, B.D. Freeman, D.R. Paul, J.E. McGrath, S. Swinnea, Gas Sorption and Characterization of Thermally Rearranged Polyimides Based on 3,3′ -Dihydroxy-4,4′ -Diamino-Biphenyl (HAB) And 2,2′ -Bis-(3,4-Dicarboxyphenyl) Hexafluoropropane Dianhydride (6FDA), Journal of Membrane Science, 415-416 (2012) 558-567.

[29] L.M. Robeson, Q. Liu, B.D. Freeman, D.R. Paul, Comparison of Transport Properties of Rubbery and Glassy Polymers and the Relevance to the Upper Bound Relationship, Journal of Membrane Science, 476 (2015) 421-431.

[30] Y. Kamiya, Y. Naito, K. Mizoguchi, Sorption and Partial Molar Volume of Gases in Polybutadiene, Journal of Polymer Science Part B: Polymer Physics, 27 (1989) 2243.

[31] R. Kirchheim, Partial Molar Volume of Small Molecules in Glassy Polymers, Journal of Polymer Science: Part B Polymer Physics, 31 (1993) 1373-1382.

[32] R. Raharjo, B. Freeman, E. Sanders, Pure and Mixed Gas CH_4 and n-C_4H_{10} Sorption and Dilation in Poly(dimethylsiloxane), Journal of Membrane Science, 292 (2007) 45-61.

[33] D. Pope, The University of Texas at Austin, 1991.

[34] L.M. Robeson, B.D. Freeman, D.R. Paul, B.W. Rowe, An Empirical Correlation of Gas Permeability and Permselectivity in Polymers and Its Theoretical Basis, Journal of Membrane Science, 341 (2009) 178-185.

[35] M. Rungta, C. Zhang, W.J. Koros, L. Xu, Membrane-Based Ethylene/Ethane Separation: The Upper Bound And Beyond, AIChE Journal, 59 (2013) 3475-3489.

[36] J.R. Scherer, B. Bolton, Water in Polymer Membranes. 5. On the Existence of Pores and Voids, Journal of Physical Chemistry, 89 (1985) 3535 - 3540.

[37] R. Reich, W.T. Ziegler, K.A. Rogers, Adsorption of Methane, Ethane, and Ethylene Gases and Their Binary and Ternary Mixtures and Carbon Dioxide on Activated Carbon at 212-301 K and Pressures to 35 Atmospheres, Industrial & Engineering Chemistry Process Design and Development, 19 (1980) 336-344.

[38] J.G. Wijmans, R.W. Baker, The Solution-Diffustion Model: A Review, Journal of Membrane Science, 107 (1995) 1-21.

[39] M. Minelli, M.G. De Angelis, G.C. Sarti, Predictive Calculations of Gas Solubility and Permeability in Glassy Polymeric Membranes: An Overview, Frontiers of Chemical Science and Engineering, 11 (2017) 405-413.

[40] E. Favre, P. Schaetzel, Q.T. Nguygen, R. Clement, J. Neel, Sorption, Diffusion and Vapor Permeation of Various Penetrants Through Dense Poly(dimethylsiloxane) Membranes: A Transport Analysis, Journal of Membrane Science, 92 (1994) 16-184.

[41] M. Galizia, M.G. De Angelis, E. Finkelshtein, Y.P. Yampolskii, G.C. Sarti, Sorption and Transport of Hydrocarbons and Alcohols in Addition-Type Poly(trimethyl Silyl Norbornene). I: Experimental Data, Journal of Membrane Science, 385-386 (2011) 141-153.

[42] M. Minelli, G.C. Sarti, Thermodynamic Model for the Permeability of Light Gases in Glassy Polymers, AIChE Journal, 61 (2015) 2776-2788.

[43] T.C. Merkel, V.I. Bondar, K. Nagai, B. Freeman, Sorption and Transport of Hydrocarbon and Perfluorocarbon Gases in Poly(1-trimthylsilyl-1-propyne), Journal of Polymer Science: Part B Polymer Physics, 38 (2000) 273 - 296.

[44] M. Galizia, C. Daniel, G. Fasano, G. Guerra, G. Mensitieri, Gas Sorption and Diffusion in Amorphous and Semicrystalline Nanoporous Poly(2,6-dimethyl-1,4-phenylene)oxide, Macromolecules, 45 (2012) 3604-3615.

[45] M. Minelli, G.C. Sarti, Elementary Prediction of Gas Permeability in Glassy Polymers, Journal of Membrane Science, 521 (2017) 73-83.

[46] M. Minelli, F. Doghieri, Predictive Model for Gas and Vapor Sorption and Swelling in Glassy Polymers: II. Effect of Sample Previous History, Fluid Phase Equilibria, 444 (2017) 47-55.

[47] M. Minelli, G.C. Sarti, Permeability and Solubility of Carbon Dioxide in Different Glassy Polymer Systems with and without Plasticization, Journal of Membrane Science, 444 (2013) 429-439.

[48] J.S. Vrentas, J.L. Duda, Diffusion in Polymer-Solvent Systems. I. Reexamination of the Free-Volume Theory, Journal of Polymer Science Part B: Polymer Physics, 15 (1977) 403-416.

[49] J.Y. Park, D.R. Paul, Correlation and Prediction of Gas Permeability in Glassy Polymer Membrane Materials via a Modified Free Volume Based Group Contribution Method, Journal of Membrane Science, 125 (1997) 23 - 39.

[50] L.M. Robeson, M.E. Dose, B.D. Freeman, D.R. Paul, Analysis of the Transport Properties of Thermally Rearranged (TR) Polymers and Polymers of Intrinsic Microporosity (PIM) Relative to Upper Bound Performance, Journal of Membrane Science, 525 (2017) 18-24.

Chapter 7: Conclusions and Recommendations

This dissertation investigated the fundamental transport of gases in thermally rearranged (TR) polymers and polymers of intrinsic microporosity (PIM) to gain an understanding of why these materials tend to perform at or beyond the Robeson Upper Bound for select gas pairs (Chapter 3). This in depth analysis of the literature determined that high diffusion coefficients, high diffusion selectivity, and high solubility are critical for a polymer to have both high permeability and permeability selectivity. Additionally, this dissertation studied how thermal cross-linking effects the plasticization resistance of polyimides to CO_2, C_2H_4, and C_2H_6. A novel polyimide containing diaminophenylindane (DAPI), hexafluoroisopropylidene (6FDA), and diaminobenzoic acid (DABA), referred to as 6FDA-DAPI/DABA, was synthesized and characterized (Chapter 4). While thermal cross-linking showed improved plasticization resistance to pure CO_2, C_2H_4, and C_2H_6, mixed gas permeation experiments revealed linear 6FDA-DAPI/DABA was more resistant to plasticization than its cross-linked analog (Chapter 5). By studying sorption induced dilation in the DAPI-containing polyimides, we concluded that linear 6FDA-DAPI/DABA more readily excluded C_2H_6 from the free volume elements, correlating with the minimal plasticization effects observed in the mixed gas permeation experiments (Chapters 5 and 6). Additionally, the diffusion coefficients correlated with accessible fractional free volume (FFV_a), which was estimated using volumetric dilation and sorption data (Chapter 6).

7.1. CONCLUSIONS

PIM and TR polymers have been shown to perform at or beyond the upper bound for several gas pairs (i.e., a combination of high permeability and permeability selectivity). To better understand what fundamental transport properties contribute to PIM and TR polymers upper bound performance, several TR polymer structures and PIM structures were compared to a large literature database. A critical analysis of the diffusion selectivity, solubility selectivity, diffusion coefficients, and solubility coefficients was performed in Chapter 3. TR polymers and PIM materials both have high gas solubility coefficients as a consequence of high free volume combined with high glass transition temperature. Relative to other polymers at a given selectivity, this elevated solubility increased the permeability of PIM and TR polymers. Additionally, both PIM and TR polymers exhibited higher gas diffusion coefficients compared to polymers with similar size sieving ability. This suggests that high diffusion coefficients, high diffusion selectivity, and high solubility are critical for a polymer to have both high permeability and permeability selectivity [1].

Chapter 4 focused on the synthesis and characterization of a polyimide containing hexafluoroisopropylidene diphthalic anhydride (6FDA), diaminophenylindane (DAPI), and diaminobenzoic acid (DABA) in a molar ratio of 0.5/0.33/0.17, abbreviated 6FDA-DAPI/DABA. By heating the linear polyimide above its glass transition temperature, the DABA moiety underwent thermal decarboxylation and resulted in a cross-linked structure. After cross-linking, pure gas permeability increased by about 30%, which correlated with an apparent increase in polymer chain d-spacing, measured by wide angle x-ray scattering (WAXS). Additionally, an increase in CO_2/CH_4 and C_2H_4/C_2H_6 pure gas selectivities was observed, suggesting a narrowing of the fractional free volume size distribution occurred with cross-linking [2].

Chapter 5 extended the study developed in Chapter 4, probing the influence of polymer structure and thermal cross-linking on the plasticization resistance due to CO_2, C_2H_4, and C_2H_6. As a control, the transport properties of linear and cross-linked 6FDA-DAPI/DABA were compared to 6FDA-DAPI, a polymer which did not contain any cross-linking sites. In pure gas conditions, extent of plasticization from CO_2, C_2H_4, and C_2H_6 increased in the following order: cross-linked 6FDA-DAPI/DABA < linear 6FDA-DAPI/DABA < 6FDA-DAPI. While a slight increase in CO_2 permeability at high pressure was observed in cross-linked 6FDA-DAPI/DABA, no detectible plasticization was observed when the cross-linked polymer was exposed to 27 atm of pure C_2H_4 or C_2H_6. Additionally, no significant difference in pure gas sorption was detected between the three DAPI-containing polyimides, except for linear 6FDA-DAPI/DABA, which had slightly lower C_2H_6 uptake than 6FDA-DAPI and cross-linked 6FDA-DAPI/DABA. However, mixed gas permeation experiments using a 50:50 (mol:mol) C_2H_4:C_2H_6 feed gas showed evidence of plasticization occurring in all three DAPI-containing polyimides. For 6FDA-DAPI and cross-linked 6FDA-DAPI/DABA, C_2H_4 permeability was lower and C_2H_6 permeability was higher in mixed gas permeation experiments, resulting in lower C_2H_4/C_2H_6 mixed gas selectivity. However, both C_2H_4 and C_2H_6 permeability coefficients increased in linear 6FDA-DAPI/DABA in mixed gas experiments, resulting in no significant difference between pure and mixed gas C_2H_4/C_2H_6 selectivity. These results suggest that cross-linking is not necessarily needed to prevent plasticization from C_2H_4 and C_2H_6 [3].

Chapter 6 extended the study developed in Chapter 4 and Chapter 5 by investigating the volumetric dilation and diffusion in 6FDA-DAPI, linear 6FDA-DAPI/DABA, and cross-linked 6FDA-DAPI/DABA. All three polymers dilated about 4 – 5% when exposed to 25 atm of pure CO_2, C_2H_4, and C_2H_6. While the partial molar volume of dissolved CO_2

and C_2H_4 was very similar in the polymers studied, the partial molar volume C_2H_6 was significantly higher in linear 6FDA-DAPI/DABA than in 6FDA-DAPI and cross-linked 6FDA-DAPI/DABA. This suggests that C_2H_6 is more readily excluded from the free volume elements in linear 6FDA-DAPI/DABA. Additionally, the dilation and sorption data were used to estimate the accessible free volume in the polymer-penetrant mixture.

The appendices of this dissertation provide supplemental information for several chapters of this dissertation, as well as two additional studies that were not published elsewhere. Appendix A provides additional information used to analyze the fundamental transport properties of PIM and TR polymers. Appendix B details additional characterization results used analyze the structure and transport properties of 6FDA-DAPI, linear 6FDA-DAPI/DABA, and cross-linked 6FDA-DAPI/DABA in Chapter 4. Appendix C and Appendix D include additional transport results from the work discussed in Chapter 5 and Chapter 6.

Appendix E discusses the effect of casting solvent and procedure on the transport properties of TR polymers. The observed 50% variation in CO_2 and CH_4 permeability of the same TR polymer structure cast using different methods was attributed to free volume variations due to the solvent content remaining in the film when the solvent-mixture passes through the mixture glass transition temperature. The solvent content as the mixture transitions to the glass is believed to cause free volume variations that cannot be thermally "reset" due to the thermal rearrangement process.

Finally, Appendix F discusses using UV cross-linked poly(arylene ether ketone)s (PAEKs) for olefin/paraffin separations. However, due to non-uniform UV exposure through the film thickness, it was difficult to separate the effects of cross-linking and plasticization. Due to these issues and apparent low permeability and C_2H_4/C_2H_6 selectivity, this study was not continued.

7.2. RECOMMENDATIONS FOR FUTURE WORK

7.2.1. Conduct a structure property study with thermally cross-linked polyimides

The work presented in this dissertation focused primarily on one thermally cross-linked polyimide, 6FDA-DAPI/DABA, with a monomer molar ratio of 0.5/0.33/0.17 for 6FDA/DAPI/DABA. Due to this monomer molar ratio, one carboxylic acid cross-linking site is present for every three repeat units. To better understand the structure-property relationships with the carboxylic acid moity and the effect of cross-link density, it is recommended that polyimides with different ratios of 6FDA, DAPI, and DABA be studied. In particular, it would be interesting to investigate polyimides with ratios of 0.5/0.25/0.25, or 0.5/0.375/0.125, where the DABA monomer would occur every other repeat unit and every four repeat units, respectively. This would allow for the polymers in this dissertation to be compared to polymers with similar structures, but with both higher and lower cross-link densities. Due to the increase in permeability with cross-linking reported in Chapter 4 of this dissertation, it would be interesting to see how both permeability and plasticization resistance change with changes in cross-link density. Previous studies have suggested that higher cross-link densities may reduce polymer chain motions and increase resistance to plasticization [5-9].

Additional structure-property studies can be conducted on thermally cross-linked polyimides by substituting different anhydrides structures for 6FDA and/or different diamine structures for DAPI, while keeping the ratio of monomers the same (i.e., anhydride/diamine/DABA in a 0.5/0.33/0.17 molar ratio). Based on existing studies, it would be interesting to substitute 2,4,6-trimethyl-1,3-phenylenediamine (DAM) in the place of DAPI in one polymer structure (6FDA-DAM/DABA) and substitute 3,3’,4,4’-benzophenonetetracarboxylic dianhydride (BTDA) in place of 6FDA in another polymer structure (BTDA-DAPI/DABA). DAM is more bulky and rigid than DAPI and

has been shown to provide additional fractional free volume and increase the glass transition temperature of the polymer [4, 10, 11]. Additionally, substituting BTDA for 6FDA will serve two purposes: 1) using the benzophenone moiety in place of the 6F-group will allow for the effect of the fluorine functionality on hydrocarbon transport to be investigated, and 2) the properties of BTDA-DAPI/DABA can be compared to Matrimid®, which contains BTDA and DAPI monomers in equal molar ratios, to investigate how thermal cross-linking effects the plasticization resistance of a structure similar to Matrimid® [12-15]. The first task for studying these materials would be measuring pure gas permeability of H_2, N_2, CH_4, O_2, CO_2, C_2H_4, and C_2H_6 in both the linear and thermally cross-linked analogs of these polyimides. Further studies would involve measuring the sorption isotherms for these materials so the gas permeability can be separated into solubility and diffusivity contributions.

7.2.2. Positron Annihilation Lifetime Spectroscopy on thermally cross-linked polyimides

Chapters 4 through Chapter 6 of this dissertation probed the effects of thermally cross-linking on 6FDA-DAPI/DABA. From these studies, both wide angle x-ray scattering (WAXS) and changes in diffusivity selectivity suggested a change in polymer chain spacing and free volume distribution may occur during thermal cross-linking [2-4]. To probe these differences more directly, it is recommended that positron annihilation lifetime spectroscopy (PALS) be used to determine both the size and size distribution of the free volume elements in these materials. In previous studies, PALS has been able to probe the changes in free volume structure that occur during the thermal rearrangement process of various TR polymers [16-19]. Conducting similar studies on thermally cross-linked polyimides would help directly probe the changes that occur during thermal cross-linking

and provide further evidence for the changes in gas transport and WAXS results that are discussed in this dissertation.

7.2.3. NELF Modeling of C_2H_4 and C_2H_6 transport

As was discussed in Chapter 5, there are several challenges associated with modeling gas sorption using the dual-mode model. Other models, such as the Non-Equilibrium Lattice Fluid (NELF) model, have been shown to accurately represent sorption isotherms of light gases in several different glassy polymers [20-25]. In particular, others have reported the NELF model is capable of predicting plasticization behavior from high pressure CO_2 in several different glassy polymers [20-23]. However, the use of the NELF model for predicting sorption of hydrocarbons, like ethane and ethylene, has yet to be thoroughly explored. With the permeation, sorption, diffusion, and dilation data presented in this manuscript, the NELF model can be implored to investigate transport of CO_2, C_2H_4, and C_2H_6 in 6FDA-DAPI, linear 6FDA-DAPI/DABA, and cross-linked 6FDA-DAPI/DABA.

7.2.4. Transport of higher hydrocarbons

Finally, it would be interesting to investigate the transport of higher hydrocarbons, like propane (C_3H_6) and propylene (C_3H_8), in thermally cross-linked polyimides. Like ethane and ethylene, C_3H_6 and C_3H_8 have very similar gas diameters and critical temperatures, making the separation of these components very difficult and energy intensive. Additionally, C_3H_6 and C_3H_8 have been shown to induce plasticization in polymer membranes. Due to the results presented in this dissertation, DABA containing polyimides and thermally cross-linked polyimides may be capable of reducing plasticization effects from C_3H_6 and C_3H_8. The first step to investigating this would be to preform pure gas permeation experiments on both the linear and thermally cross-linked

polyimides. Then, due to the non-ideal behavior of olefins and paraffins, it would be imperative to perform mixed gas permeation experiments to determine if cross-linking improved the plasticization resistance to C_3H_6 and C_3H_8.

7.3. REFERENCES

[1] L.M. Robeson, M.E. Dose, B.D. Freeman, D.R. Paul, Analysis of the Transport Properties of Thermally Rearranged (TR) Polymers and Polymers of Intrinsic Microporosity (PIM) Relative to Upper Bound Performance, Journal of Membrane Science, 525 (2017) 18-24.

[2] M.E. Dose, M. Chwatko, I. Hubacek, N.A. Lynd, D.R. Paul, B.D. Freeman, Thermally Cross-linked Diaminophenylindane (DAPI) Containing Polyimides for Membrane Based Gas Separations, Polymer, Submitted (2018).

[3] M.E. Dose, I. Hubacek, D.R. Paul, B.D. Freeman, CO_2, C_2H_4, and C_2H_6 Sorption and Mixed Gas Permeability of Thermally Cross-linked Diaminophenylindane (DAPI) Containing Polyimides, Journal of Membrane Science, Submitted (2018).

[4] M.E. Dose, J.D. Moon, I. Hubacek, D.R. Paul, B.D. Freeman, Fundamental Gas Transport and Dilation Studies in Thermally Cross-linked Diaminophenylindane (DAPI) Containing Polyimides, Journal of Polymer Science Part B: Polymer Physics, In Preparation (2018).

[5] S.D. Kelman, S. Matteucci, C.W. Bielawski, B.D. Freeman, Crosslinking Poly(1-Trimethylsilyl-1-Propyne) and Its Effect On Solvent Resistance and Transport Properties, Polymer, 48 (2007) 6881-6892.

[6] M.S. McCaig, D.R. Paul, Effect of UV Crosslinking and Physical Aging on the Gas Permeability of Thin Glassy Polyarylate Films, Polymer, 40 (1999) 7209-7225.

[7] B.J. Sundell, A.T. Shaver, Q. Liu, A. Nebipasagil, P. Pisipati, S.J. Mecham, J.S. Riffle, B.D. Freeman, J.E. McGrath, Synthesis, Oxidation and Crosslinking of Tetramethyl Bisphenol F (TMBPF)-Based Polymers for Oxygen/Nitrogen Gas Separations, Polymer, 55 (2014) 5623-5634.

[8] B. Kraftschik, W.J. Koros, Cross-Linkable Polyimide Membranes for Improved Plasticization Resistance and Permselectivity in Sour Gas Separations, Macromolecules, 46 (2013) 6908-6921.

[9] H. Eguchi, D.J. Kim, W.J. Koros, Chemically Cross-linkable Polyimide Membranes for Improved Transport Plasticization Resistance for Natural Gas Separation, Polymer, 58 (2015) 121-129.

[10] A.M. Kratochvil, W.J. Koros, Decarboxylation-Induced Cross-Linking of a Polyimide for Enhanced CO_2 Plasticization Resistance, Macromolecules, 41 (2008) 7920-7927.

[11] W. Qiu, C.-C. Chen, L. Xu, L. Cui, D.R. Paul, W.J. Koros, Sub-Tg Cross-Linking of a Polyimide Membrane for Enhanced CO_2 Plasticization Resistance for Natural Gas Separation, Macromolecules, 44 (2011) 6046-6056.

[12] L. Xu, M. Rungta, W.J. Koros, Matrimid® Derived Carbon Molecular Sieve Hollow Fiber Membranes for Ethylene/Ethane Separation, Journal of Membrane Science, 380 (2011) 138-147.

[13] M. Rungta, L. Xu, W.J. Koros, Carbon Molecular Sieve Dense Film Membranes Derived from Matrimid® for Ethylene/Ethane Separation, Carbon, 50 (2012) 1488-1502.

[14] X. Ning, W.J. Koros, Carbon Molecular Sieve Membranes Derived from Matrimid® Polyimide for Nitrogen/Methane Separation, Carbon, 66 (2014) 511-522.

[15] S.M. Davoodi, M. Sadeghi, M. Naghsh, A. Moheb, Olefin–Paraffin Separation Performance of Polyimide Matrimid®/Silica Nanocomposite Membranes, RSC Advances, 6 (2016) 23746-23759.

[16] P. Budd, N. McKeown, B. Ghanem, K. Msayib, D. Fritsch, L. Starannikova, N. Belov, O. Sanfirova, Y. Yampolskii, V. Shantarovich, Gas Permeation Parameters and Other Physicochemical Properties of a Polymer of Intrinsic Microporosity: Polybenzodioxane PIM-1, Journal of Membrane Science, 325 (2008) 851-860.

[17] S.H. Han, N. Misdan, S. Kim, C.M. Doherty, A.J. Hill, Y.M. Lee, Thermally Rearranged (TR) Polybenzoxazole: Effects of Diverse Imidization Routes on Physical Properties and Gas Transport Behaviors, Macromolecules, 43 (2010) 7657-7667.

[18] Y. Jiang, F.T. Willmore, D. Sanders, Z.P. Smith, C.P. Ribeiro, C.M. Doherty, A. Thornton, A.J. Hill, B.D. Freeman, I.C. Sanchez, Cavity Size, Sorption and Transport Characteristics of Thermally Rearranged (TR) Polymers, Polymer, 52 (2011) 2244-2254.

[19] D.F. Sanders, Z.P. Smith, C.P. Ribeiro, R. Guo, J.E. McGrath, D.R. Paul, B.D. Freeman, Gas Permeability, Diffusivity, and Free Volume of Thermally Rearranged Polymers Based on 3,3'-Dihydroxy-4,4'-Diamino-Biphenyl (HAB) and 2,2'-Bis-(3,4-Dicarboxyphenyl) Hexafluoropropane Dianhydride (6FDA), Journal of Membrane Science, 409-410 (2012) 232-241.

[20] M. Minelli, F. Doghieri, Predictive Model for Gas and Vapor Solubility and Swelling in Glassy Polymers I: Application to Different Polymer/Penetrant Systems, Fluid Phase Equilibria, 381 (2014) 1-11.

[21] M. Minelli, F. Doghieri, Predictive Model for Gas and Vapor Sorption and Swelling in Glassy Polymers: II. Effect of Sample Previous History, Fluid Phase Equilibria, 444 (2017) 47-55.

[22] M. Minelli, M.G. De Angelis, G.C. Sarti, Predictive Calculations of Gas Solubility and Permeability in Glassy Polymeric Membranes: An Overview, Frontiers of Chemical Science and Engineering, 11 (2017) 405-413.

[23] M. Minelli, G.C. Sarti, Permeability and Solubility of Carbon Dioxide in Different Glassy Polymer Systems with and without Plasticization, Journal of Membrane Science, 444 (2013) 429-439.

[24] M. Minelli, M.G. De Angelis, D. Hofmann, A Novel Multiscale Method for the Prediction of the Volumetric and Gas Solubility Behavior of High-Tg Polyimides, Fluid Phase Equilibria, 333 (2012) 87-96.

[25] M.G. De Angelis, F. Doghieri, G.C. Sarti, B.D. Freeman, Modeling Gas Sorption in Amorphous Teflon Through the Non Equilibrium Thermodynamics for Glassy Polymers (NET-GP) Approach, Desalination, 193 (2006) 82-89.

Appendices

APPENDIX A: SUPPLEMENTARY INFORMATION FOR THE ANALYSIS OF THE TRANSPORT PROPERTIES OF THERMALLY REARRANGED (TR) POLYMERS AND POLYMERS OF INTRINSIC MICROPOROSITY (PIM) RELATIVE TO UPPER BOUND PERFORMANCE (CHAPTER 3)

A.1. Least-Squares Fitting Analysis for Polynomials

A least-squares fit was performed to determine the parameters and parameter uncertainties for correlating the natural log of diffusion coefficients with either the square of the gas diffusion diameters, d_g^2, or the square of the Teplyakov-Meares diameters, $d_{T\text{-}M}^2$. The models considered were:

$$lnD = \alpha + \beta d_i^2 \qquad \text{Eq. A.1}$$

$$lnD = a + bd_i^2 + c(d_i^2)^2 \qquad \text{Eq. A.2}$$

A least-squares fit analysis was used to estimate the parameters in these equations according to the procedure described in Bevington and Robinson [1]. Each diffusion coefficient was assumed to have an estimated ±10% uncertainty to ensure the fitting incorporated typical experimental uncertainties in reported diffusion coefficients. The results of the fits are recorded in Table A.1.

Linear Fit (Eq. A1)					
Material	d_i	**α**	**β**	R^2	χ^2
PIM-1	d_g	-5.3 ± 0.2	-0.75 ± 0.1	0.97	88.1
	$d_{T\text{-}M}$	-7.1 ± 0.1	-0.81 ± 0.01	0.97	95.4
TR-450	d_g	-5.2 ± 0.2	-0.74 ± 0.02	0.95	67.1
	$d_{T\text{-}M}$	-6.7 ± 0.2	-0.82 ± 0.02	0.86	205

Quadratic Fit (Eq. A2)						
Material	d_i	**a**	**b**	**c**	R_2	χ^2
PIM-1	d_g	-3.0 ± 0.6	-1.2 ± 0.1	0.023 ± 0.006	0.97	72.3
	$d_{T\text{-}M}$	-11.1 ± 0.4	-0.6 ± 0.1	-0.11 ± 0.01	0.99	3.76
TR-450	d_g	-5.4 ± 0.9	-0.7 ± 0.2	-0.002 ± 0.008	0.95	67.1
	$d_{T\text{-}M}$	-15.9 ± 0.8	-2.0 ± 0.3	-0.20 ± 0.02	0.94	81.6

Table A.1. Best fit parameters used to correlate diffusion coefficients (cm^2/s) for PIM-1 and TR-450 with gas diffusion (d_g^2) and T-M ($d_{T\text{-}M}^2$) diameters.

To determine the significance of the additional term in Eq. A.2, an F Test for the additional term was performed. According to Bevington and Robinson. [2], the F_χ value is defined as follows:

$$F_\chi = \frac{\chi^2(m) - \chi^2(m+1)}{\frac{\chi^2(m+1)}{N-m-1}} = \frac{\Delta\chi^2}{\chi_v^2} \qquad \text{Eq. A.3}$$

where N is the number of data points for each data set, m is the number of fitted parameters in the model (i.e., m = 2 for a linear fit), and the χ^2 values correspond to the respective linear (i.e., $\chi^2(m)$) and quadratic (i.e., $\chi^2(m+1)$) fits for each data set. F_χ characterizes the significance of an additional term in a fitted equation and should be large if the fitting equation containing the additional term (i.e., Eq. A.2) represents a significant improvement over the base fitting equation (i.e., Eq. A.1). The statistical significance of the additional term can be evaluated using a one-tailed F-test. If F_χ exceeds the test value for F, the additional term (i.e., the quadratic term in Eq. A.2 in this case) likely substantially improves the quality of the fit and should be included. The degrees of freedom for the denominator

(dF = N – m – 1) are listed in Table S2 along with the p-values corresponding to a one-tailed F-test. The degree of freedom for the test case was set to 1 due to the one degree of freedom difference between the linear and quadratic fits (i.e., $\chi^2(m) - \chi^2(m+1)$). The p-values were calculated using the Microsoft Excel F.DIST.RT(F_χ, 1, dF) function.

Material	d_i	F_χ	dF^*	***p-value***
PIM-1	d_g	0.659	3	0.476
	$d_{T\text{-}M}$	73.1	3	0.003
TR-450	d_g	0.001	2	0.977
	$d_{T\text{-}M}$	3.043	2	0.223

Table A.2. Results of F-Test to determine the statistical significance of adding a quadratic term to the linear correlation between diffusion coefficients and gas diameters squared. (* *dF* = degrees of freedom for quadratic fit).

For the additional term to be statistically significant (i.e., for Eq. A.2 to more effectively correlate d_i^2 and *lnD* than Eq. A.1), the probability (p-value) of rejecting the null hypothesis that there is no significant difference between the linear and quadratic fits (i.e., that $F_\chi < F_{critical}$, or c=0), when it is actually true should be small (e.g., < 0.05 or < 0.01) . Using this criterion, Eq. A.1 is the best fit for correlating the gas diffusion diameter squared, d_g^2, with the diffusion coefficients of PIM-1 and TR-450, while Eq. A.2 best correlates the Teplyakov-Meares diameters squared, $d_{T\text{-}M}^2$, for the diffusion coefficients of PIM-1. While the addition of the quadratic term (i.e., Eq A.2) to the correlation of $d_{T\text{-}M}^2$ with the diffusion coefficients of TR-450 was not statistically significant (i.e., p = 0.223), the fit was improved. The fits are presented visually in Figure A.1.

The better linear fit, e.g., Eq. A.1, of the TR and PIM diffusivities with d_g^2 than with other diameters appears to be a consequence of the larger relative gas diameter difference between O_2, N_2, and CH_4 in d_g than in the other correlations. The linearity of

these correlations of *lnD* with d_g^2 allows for an improved prediction of diffusion coefficients using d_g than can be obtained using other measures of gas molecule size [3].

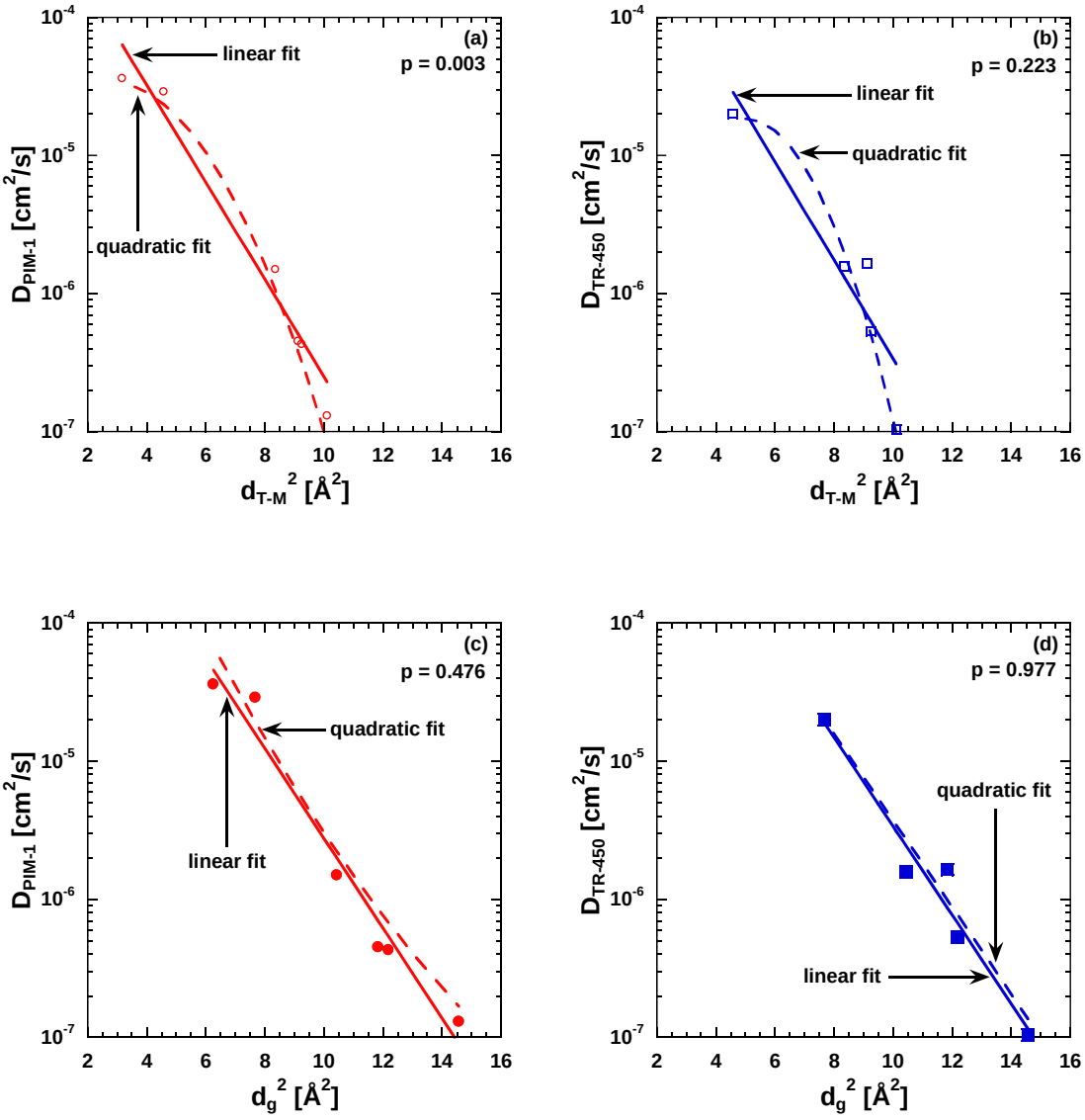

Figure A.1(a-d). Comparison between the linear (i.e., Eq. A.1) and quadratic (i.e., Eq. A.2) fits for PIM-1 (red circles) and TR-450 (blue squares) using Teplyakov-Meares diameters ($d_{T\text{-}M}^2$, unfilled markers) and gas diffusion diameters (d_g^2, filled markers). The p-values listed are the results from the F-test.

A.2. References

[1] P.R. Bevington, D.K. Robinson, Least-Squares Fit to a Polynomial, in: Data Reduction and Error Analysis for the Physical Sciences, McGraw Hill, Boston, MA, 2003, pp. 116 - 141.

[2] P.R. Bevington, D.K. Robinson, 11.4 F Test, in: Data Reduction and Error Analysis for the Physical Sciences, McGraw Hill, Boston, MA, 2003, pp. 207 - 208.

[3] L.M. Robeson, Z.P. Smith, B.D. Freeman, D.R. Paul, Contributions of Diffusion and Solubility Selectivity to the Upper Bound Analysis for Glassy Gas Separation Membranes, Journal of Membrane Science, 453 (2014) 71-83.

APPENDIX B: SUPPLEMENTARY INFORMATION FOR THERMALLY CROSS-LINKED DIAMINOPHENYLINDANE (DAPI) CONTAINING POLYIMIDES FOR MEMBRANE BASED GAS SEPARATIONS (CHAPTER 4)

Gas	Gas Diameter, d_g [Å]	Critical Temperature, T_c [K]
H_2	2.77	33.18
O_2	3.23	154.4
CO_2	3.44	304.2
N_2	3.49	126.1
CH_4	3.82	190.7
C_2H_4	4.16	282.5
C_2H_6	4.44	305.3

Table B.1. Gas diameter and critical temperature. Gas diameters [1] and critical temperatures [2] were obtained from the literature.

B.1. Structure Characterization

Linear 6FDA-DAPI and linear 6FDA-DAPI/DABA were dissolved in chloroform and THF, respectively, for molecular weight analysis (cf. Table B.2). 6FDA-DAPI had a weight average molecular weight (M_w) of 42,400 g/mol (~48 repeat units per chain, 674 g/mol repeat unit, cf., Figure 2.1) with a PDI of 1.31. 6FDA-DAPI/DABA had a M_w of 41,000 g/mol (~30 repeat units per chain, where one repeat unit is 636 g/mol repeat unit, cf., Figure 2.1) with a PDI of 2.16. The repeat unit for 6FDA-DAPI was defined as the sum of 1 6FDA and 1 DAPI unit, and the repeat unit for 6FDA-DAPI/DABA was defined as 1 6FDA unit, 2/3rds of DAPI, and 1/3rd DABA units by weight. The low PDI of 6FDA-DAPI is presumably due to low molecular weight species remaining in solution during the precipitation process. This effect was evident by the methanol used for precipitation taking on a light brown/yellow color when 6FDA-DAPI was precipitated, but not when 6FDA-DAPI/DABA was precipitated. The intrinsic viscosity, $[\eta]_n$ and the Mark-Houwink-Sakurada (M-H-S) parameters (cf., Table B.2) were determined using the viscosity data

obtained from Wyatt Technologies viscometer connected to the effluent of the SEC column [3].

Polymer	dn/dc [mL/g]	M_w [g/mol]	PDI	Repeat Units, n	Intrinsic Viscosity, [η] [mL/g]	M-H-S Parameters	
						a	K [mL/g]
6FDA-DAPI [a]	0.163	42400	1.31	48	29.7	0.767	1.10×10^{-2}
6FDA-DAPI/DABA [b]	0.345	41000	2.16	30	53.7	0.661	9.43×10^{-2}

Table B.2. Molecular weight, intrinsic viscosity, and Mark-Houwink-Sakurada (M-H-S) parameters for linear 6FDA-DAPI and 6FDA-DAPI/DABA [a] Solvent: Chloroform, [b] Solvent: THF

Polymer	$CHCl_3$	CH_2Cl_2	THF	Toluene	NMP	DMAc
6FDA-DAPI	++	++	++	++	++	++
6FDA-DAPI/DABA linear	+-	+-	++	--	++	++
6FDA-DAPI/DABA 353°C, 40 min	--	--	--	--	--	--

Table B.3. Solubility of 6FDA-DAPI and linear 6FDA-DAPI/DABA in common solvents. Soluble: ++ ; Swollen: +- ; Not Soluble: --

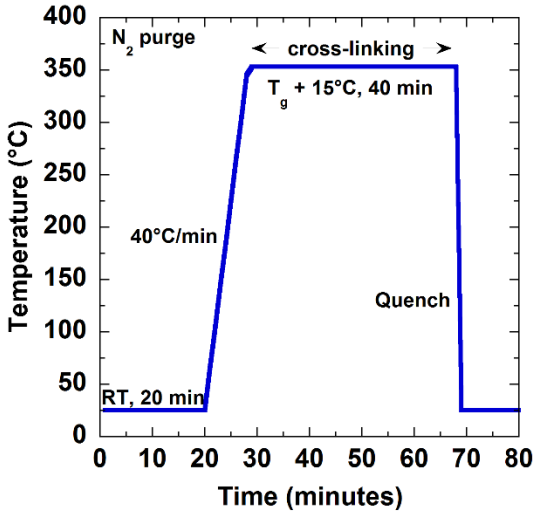

Figure B.1. Thermal treatment for cross-linking 6FDA-DAPI/DABA. To achieve partial cross-linking, the samples were held at 353°C for either 10, 20, 30, or 40 min. A N_2 purge of ~90 cm^3/min was used to keep an inert environment.

6FDA-DAPI and linear 6FDA-DAPI/DABA structures were confirmed by ^{1}H and COSY solution NMR, reference Figure B.2 and Figure B.3**,** respectively. The ratio of DAPI to DABA was 2:1 based on integrations of peaks at 1.12 ppm and 8.21 ppm in ^{1}H NMR, corresponding to the H-27 and H-33/35 moieties in DAPI and DABA, respectively To help determine peak assignments, COSY NMR (cf., Figure B.3) was used to determine which protons were coupled. The peaks in the 1D COSY spectra correspond to the same peaks labeled in the ^{1}H NMR spectra in Figure B.2.

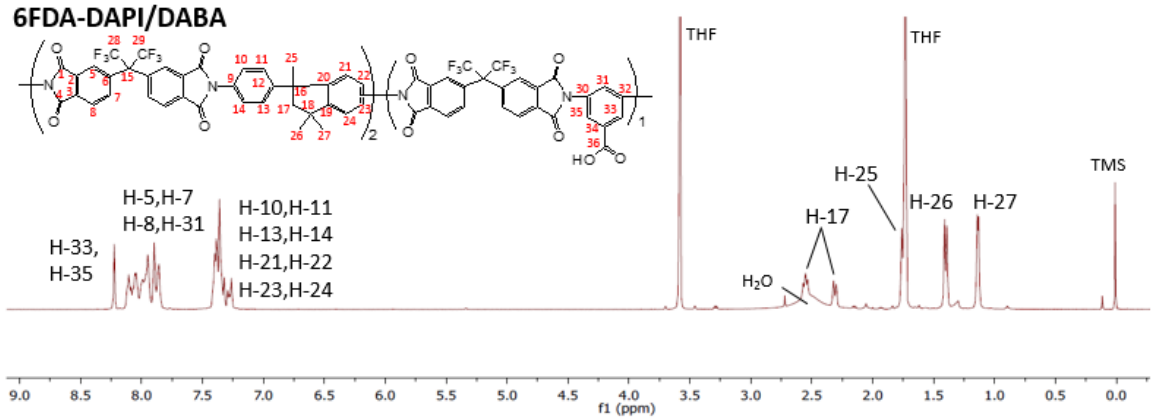

Figure B.2. Proton NMR spectra for linear 6FDA-DAPI/DABA with peak assignments.

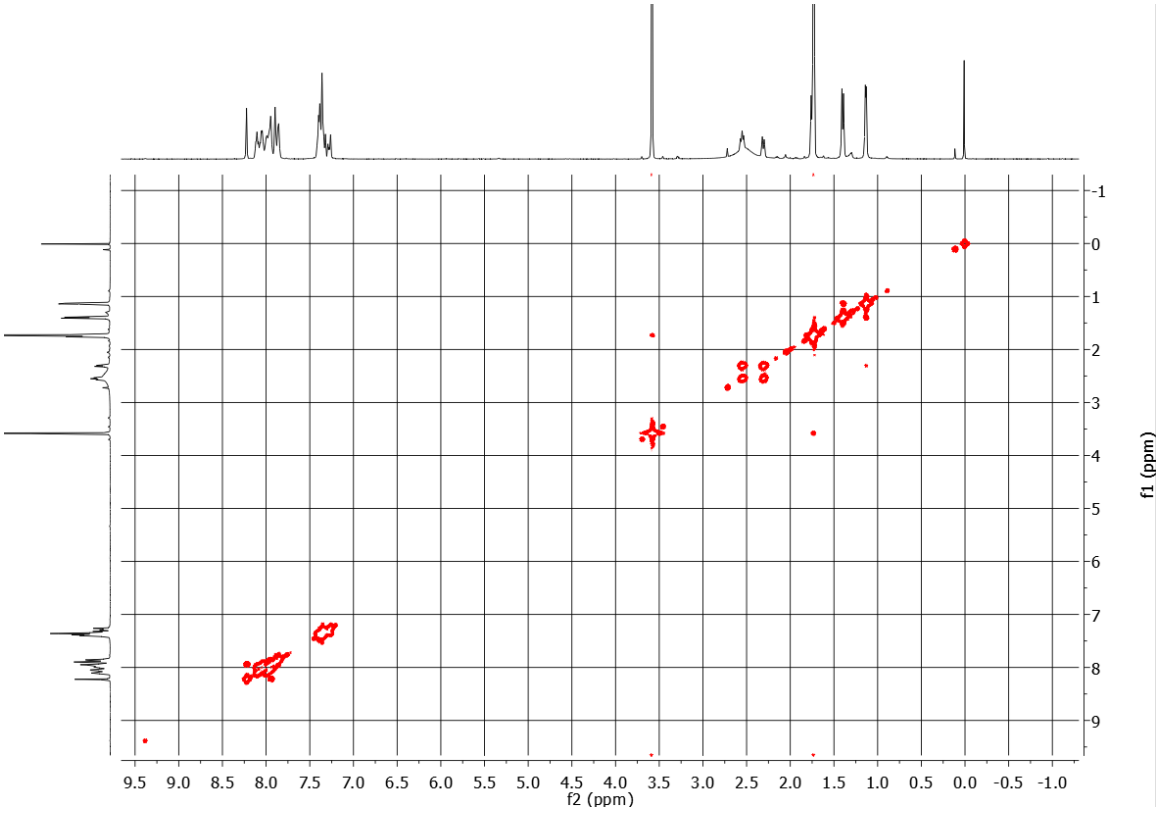

Figure B.3. COSY spectrum of linear 6FDA-DAPI/DABA in THF, illustrating the ^{1}H-^{1}H correlations.

FT-IR was performed in ATR mode, and absorbance spectra were collected from 500 – 4000 cm^{-1}. The spectra were each normalized to the imide stretch at 720 cm^{-1} based on the number of imide rings present per unit volume of the polymer, calculated using the specific volume, or inverse density (cf., Table B.4) [4]. The normalized spectra are presented in Figure B.4. The characteristic polyimide FT-IR peaks were observed for 6FDA-DAPI and linear 6FDA-DAPI/DABA at 1785 cm^{-1}, 1725 cm^{-1}, and 720 cm^{-1}, corresponding to symmetric C=O stretching vibration, asymmetric C=O stretching vibration, and C-N-C deformation of imide ring, respectively. After cross-linking for 40 min at 353°C, the broad peak observed at 3300 – 3500 cm^{-1}, associated with –OH stretching in linear 6FDA-DAPI/DABA, disappeared, supporting the cross-linking mechanism detailed in Figure 2.3. Additionally, the linear 6FDA-DAPI/DABA spectrum contains a doublet at 1720 cm^{-1}, whereas 6FDA-DAPI and 6FDA-DAPI/DABA(40 min) only have a singlet at 1720 cm^{-1}. The extra peak is likely associated with the additional C=O group associated with the DABA carboxylic acid in linear 6FDA-DAPI/DABA, which is lost during thermal cross-linking.

Polymer	Thermal Treatment	C-N-C [units/repeat]	Specific Volume [cm^3/mol repeat unit]	Imide Conc. [units/cm^3]	Normalizing Factor
6FDA-DAPI	None	2	520	0.00385	0.89
6FDA-DAPI/DABA	None	2	476	0.00421	0.98
	353°C, 10 min	2	473	0.00423	0.98
	353°C, 20 min	2	471	0.00425	0.99
	353°C, 40 min	2	464	0.00431	1.00

Table B.4. Normalization procedure for FT-IR ATR spectra presented in Figure B.4.

The values in Table B.4 were calculated using the following equations:

$$Imide\ Conc. = \frac{imide\ units\ per\ repeat}{Specific\ Volume\ per\ repeat} \quad \text{Eq. B.1}$$

$$Normalizing\ Factor = \frac{(Imide\ Conc.)_i}{(Imide\ Conc.)_{40min}} \quad \text{Eq. B.2}$$

$$I_{Normalized} = I_{measured} * (Normalizing\ Factor) \quad \text{Eq. B.3}$$

where $I_{measured}$ is the absorbance intensity measured by the instrument and $I_{Normalized}$ is the absorbance intensity corrected for the concentration of imide units.

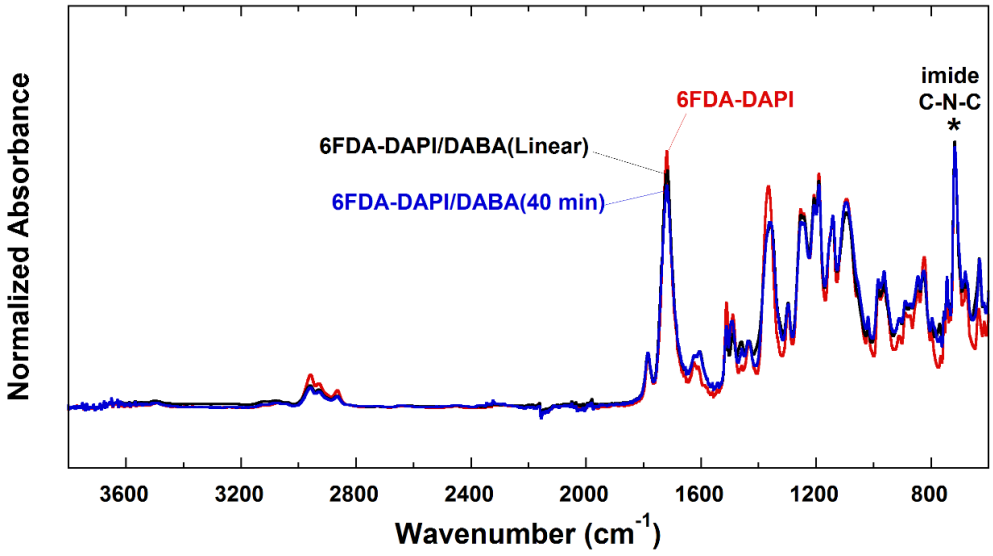

Figure B.4. ATR FT-IR spectra for 6FDA-DAPI (red), linear 6FDA-DAPI/DABA, and 6FDA-DAPI/DABA(40 min). Each spectrum was normalized to the peak at 720 cm^{-1}, corresponding to the C-N-C imide ring stretch and adjusted for the polymer molar density.

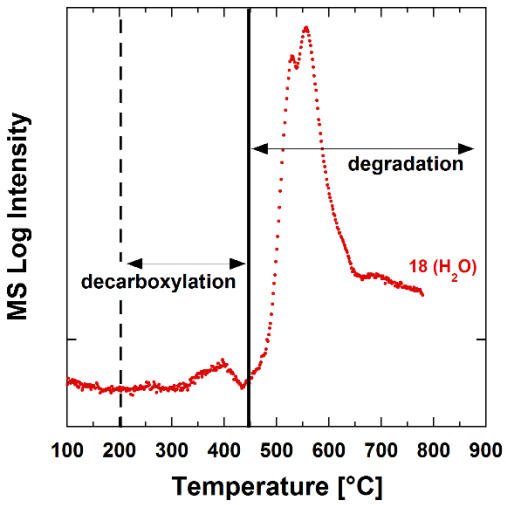

Figure B.5. Mass spec signal of evolved gases of linear 6FDA-DAPI/DABA during TGA for m/z = 18, corresponding to H_2O.

B.2. Fractional Free Volume Analysis

B.2.1. Density Measurements and Group Contribution Theory

The polymer densities were measured using Archimedes' Principal, using *n*-heptane as the buoyancy liquid (cf., Table 4.1). To obtain a reasonable experimental uncertainty, a minimum of 8 samples were measured, and the error was propagated appropriately though the various calculations, assuming no error associated with occupied volume (V_o) determined by group contribution theory [5]. V_o values were calculated assuming either only cross-linking by radical coupling (Route *d* in Figure 2.3) or only cross-linking by methyl hydrogen abstraction (Route *a* and *b* in Figure 2.3), as recorded in Figure B.6. The fractional free volume was calculated using Eq. B.4,

$$FFV = \frac{V - V_o}{V} \qquad \text{Eq. B.4}$$

where V is the total specific volume of the sample, which is the inverse of the measured polymer density, the results of which are recorded in Table 4.1 of the main manuscript [5]. To account for partial conversion to the cross-linked structures, the occupied volume, V_o, was estimated using Eq. B.5:

$$V_o = cV_{o,XL} + (1 - c)V_{o,linear} \qquad \text{Eq. B.5}$$

where $V_{o,XL}$ is the estimated occupied volume of the cross-linked structure, $V_{o,linear}$ is the occupied volume of the linear polymer, and c is the fractional mass conversion determined using Eq. 4.1. $V_{o,XL}$ was calculated for both potential cross-linked structures, assuming either 100% cross-linking by radical combination (Route *d* in Figure 2.3) or 100% methyl hydrogen abstraction (Route *a* and *b* in Figure 2.3).

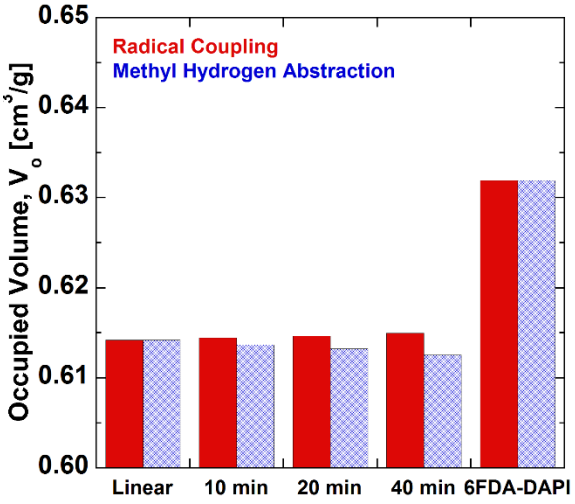

Figure B.6. Free volume analysis for 6FDA-DAPI, 6FDA-DAPI/DABA linear, and 6FDA-DAPI/DABA cross-linked at 353°C for 10, 20, and 40 min. **(b)** occupied volume (V_o) calculated using Eq. B.5.

As shown in Figure B.6, there is no significant difference between the V_o values of the potential cross-linked structures, so the distinction between cross-linking routes is not needed to estimate the FFV of the cross-linked polymers. For all cross-linked polymers in this study, the change in density after cross-linking is minimal and falls within the experimental uncertainty, and, due to the minimal differences in V_o for the two cross-linking routes, the changes in FFV fall within experimental uncertainly (cf. Table 4.1).

For the thermally cross-linked samples, several factors can potentially contribute to the density, or specific volume, of a polymer sample, including: 1) heating the sample above the glass transition temperature, 2) how long the sample is held above the T_g, 3) the cooling rate of the sample after cross-linking, 4) the solvent used for casting the film, and 5) restriction of polymer chain motion due to cross-links forming during the heating process. Due to these multiple factors, it is difficult to ascertain which/if one factor has the strongest effect on the specific polymer volume (or density).

B.2.2. Wide Angle X-ray Scattering

The Xenocs Ganesha small angle scattering instrument allowed for WAXS to be collected down to 2°, which is a significantly lower scattering angle than typically measured on other wide angle diffractometers (which have lower limits of ~7°). These results revealed a scattering peak with a maximum at 2θ of about 5°, corresponding to a d-spacing of about 17Å (cf. Figure 4.5-a and Figure B.7-b). Based on molecular dynamic simulations and MM2 energy minimizations in ChemDraw 3D using two repeat units (i.e., 6FDA-DAPI-6FDA-DAPI) to simulate a polymer chain, an average distance of 16.1Å was measured between intra-chain 6F units (cf. Figure B.8). WAXS peaks in this range have been observed in both experimental and molecular modeling studies and attributed to intra-molecular scattering [6, 7]. By incorporating a DABA monomer unit for every three repeat units into the 6FDA-DAPI backbone, the average distance between the intra-chain 6F units

would be expected to increase. An increase in intra-molecular scattering is consistent with the WAXS results, where linear 6FDA-DAPI/DABA and the corresponding cross-linked structures have larger intra-chain d-spacing than 6FDA-DAPI (Figure B.7-b and Table B.5). Additionally, the scattering intensity for 6FDA-DAPI in this region is significantly higher than that of 6FDA-DAPI/DABA, indicating the scattering species at this length scale are more ordered in 6FDA-DAPI.

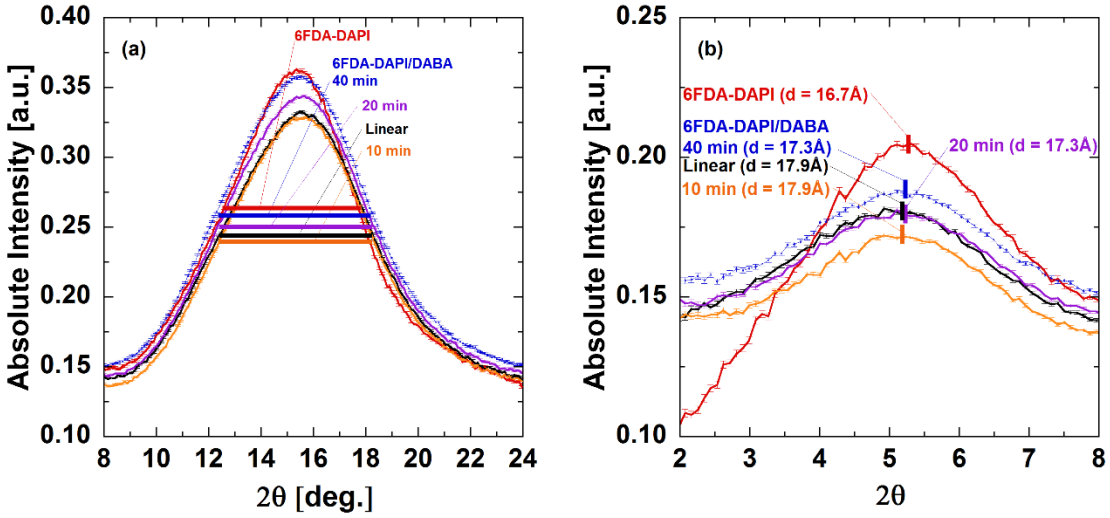

Figure B.7. WAXS data for 6FDA-DAPI [red], linear 6FDA-DAPI/DABA [black], and 6FDA-DAPI/DABA cross-linked at 353°C for 10 min [orange], 20 min [purple], and 40 min [blue]. (a) The large scattering peak, showing the width at peak half maximum, $w_{1/2}$, and (b) the small scattering peak at low 2θ showing the d-spacing calculated using the 2θ at the maximum scattering intensity.

The shift in the scattering peak around 15° was measured on 2 different sets of samples. Some studies on 6F containing polyimides have associated this peak with inter-chain spacing (i.e., the average distance between neighboring polymer chains) [8], while others have attributed this scattering to intra-molecular distances [6, 7]. Due to the increase in permeability with the increase in calculated d-spacing at the peak maximum (cf., Figure

4.7-b, Figure B.12, and Figure B.13), it is likely this peak is associated with inter-chain spacing. To investigate any potential differences in the free-volume distribution, the width at half maximum of the large scattering peak was calculated for each polymer (cf., Figure B.7-a). Previously, it has been asserted that the scattering peak width can be influenced by the FFV distribution, where a more narrow peak reflects a more narrow distribution of free volume elements [9]. The 6FDA-DAPI peak width is slightly more narrow than that of the other polymers, followed by 6FDA-DAPI/DABA cross-linked for 40 min. Linear 6FDA-DAPI/DABA as well as 6FDA-DAPI/DABA crosslinked for 10 and 20 min have the same peak width. This result suggests that 6FDA-DAPI and cross-linked 6FDA-DAPI/DABA may have a slightly more narrow free volume distribution than the other polymers.

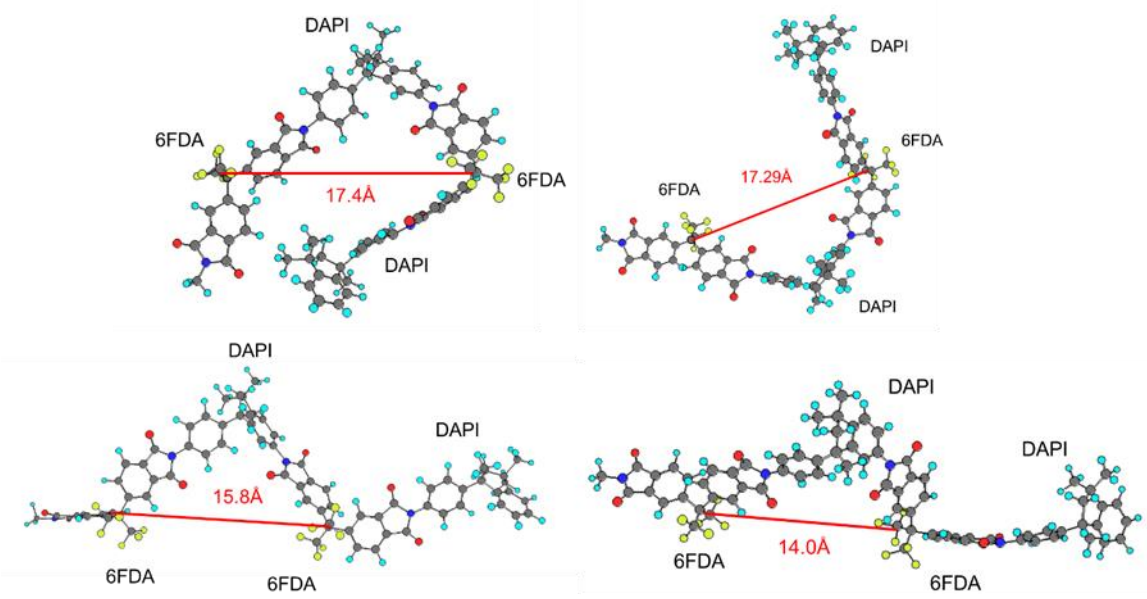

Figure B.8. Representative ChemDraw 3D simulations of 6FDA-DAPI-6FDA-DAPI units, using MM2 energy minimizations and molecular dynamic simulations to estimate potential polymer chain orientations.

Polymer	Thermal Treatment Time at 353°C	I at Half Max [a.u.]	d-spacing at Large Peak Maximum [Å]	Large Peak Width at Half Max, $W_{1/2}$ [degrees]	d-spacing at Small Peak Maximum [Å]	O_2/N_2 Selectivity
6FDA-DAPI	None	0.255	5.76	5.382	16.7	5.4 ± 0.5
6FDA-DAPI/DABA	None	0.235	5.63	6.311	17.9	5.6 ± 0.4
	10 min	0.232	5.63	6.311	17.9	5.5 ± 0.8
	20 min	0.243	5.66	6.311	17.3	5.6 ± 0.5
	40 min	0.255	5.73	6.218	17.3	5.5 ± 0.3

Table B.5. WAXS analysis for the small peak at low 2θ and the large peak at higher 2θ. The d-spacing values for each peak were calculated using the 2θ at the peak maximum, and the width at peak half maximum was determined for the large peak.

B.3. Pure Gas Permeability and Plasticization

Pure gas permeabilities of H_2, CH_4, N_2, O_2, CO_2, C_2H_4, and C_2H_6 were measured using a constant volume, variable pressure method [10]. The permeability of each gas was determined using Eq. B.6,

$$P_i = \frac{V\ell}{fRTA}\left[\left(\frac{dp}{dt}\right)_{SS} - \left(\frac{dp}{dt}\right)_{leak}\right] \qquad \text{Eq. B.6}$$

where V is the downstream volume, ℓ is the sample thickness, f is the fugacity of the gas feed calculated from the REFPROP equation of state [2], T is the absolute temperature, A is the sample area, $(dp/dt)_{SS}$ is the steady state pressure rise in the downstream volume, and $(dp/dt)_{leak}$ is the system leak rate [10]. The fugacity was calculated using Eq. B.7 and Eq. B.8, where Figure B.9 presents the compressibility factors, Z_i, for CO_2, C_2H_4, and C_2H_6 calculated using the REFPROP equation of state.

$$\ln(\phi_i) = \int_0^p (Z_i - 1)\frac{dp}{p} \qquad \text{Eq. B.7}$$

$$f_i = \phi_i p_i \qquad \text{Eq. B.8}$$

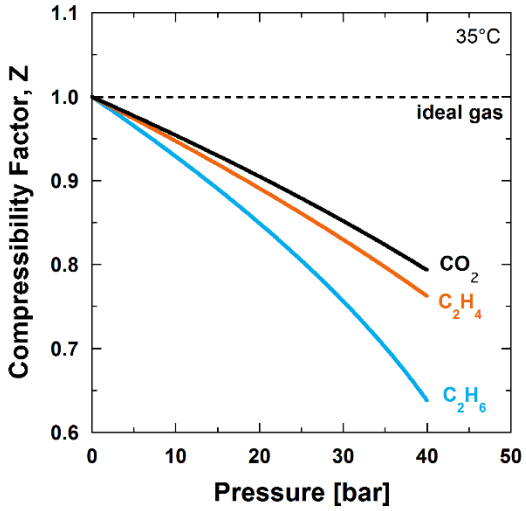

Figure B.9. Influence of pressure on ompressibility factors, Z_i, vs pressure for CO_2 [black], C_2H_4 [orange], and C_2H_6 [light blue], determined using the REFPROP equation of state at 35°C [2]. The dashed line marks unit compressibility associated with the ideal gas assumption.

The upstream pressure was monitored using a 1000 psig STJE pressure transducer (Honeywell Sensotec, Columbus, OH USA), and the downstream pressure was monitored using a capacitance manometer (Baratron 626A, MKS Instruments, Andover, MA USA). Membranes were masked using a brass disk and sealed with epoxy (Devcon, No. 145250, Danvers, MA USA) to provide a well-defined area [10]. All measurements were made at 35°C with UHP grade gases (Airgas, Radnor, PA USA), and each pressure point was held for 6 times the time lag to ensure steady state was achieved [10].

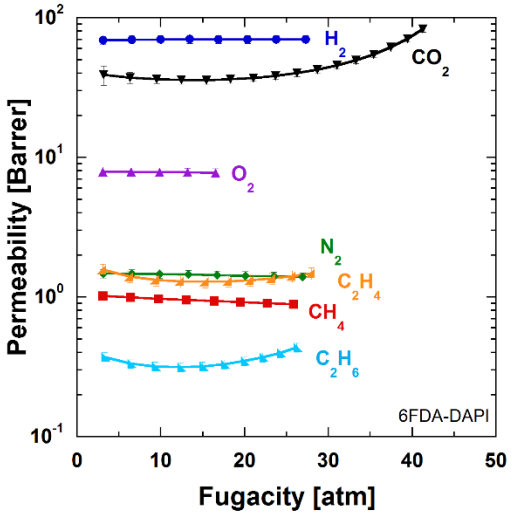

Figure B.10. Pure gas permeability of H_2 [●], CO_2 [▼], O_2 [▲], N_2 [♦], C_2H_4 [◢], CH_4 [■], and C_2H_6 [◣] in 6FDA-DAPI at 35°C. Fugacity was used to calculate permeability of CO_2, C_2H_4, and C_2H_6 and pressure was used to calculate permeability of N_2 and CH_4.

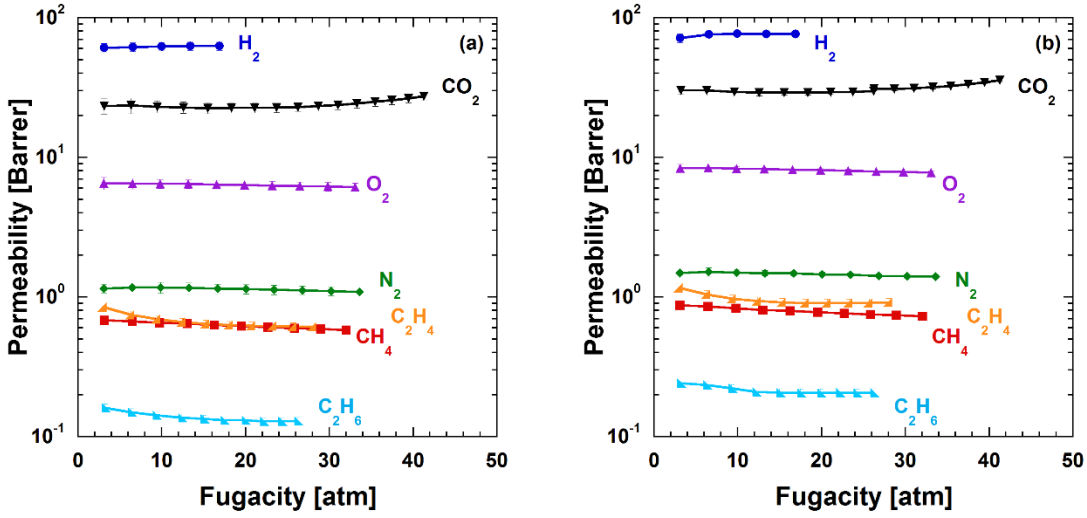

Figure B.11. Pure gas permeability of H_2 [●], CO_2 [▼], O_2 [▲], N_2 [♦], C_2H_4 [◢], CH4 [■], and C_2H_6 [◣] in (a) 6FDA-DAPI/DABA(10 min) and (b) 6FDA-DAPI/DABA(20 min) measured at 35°C. Fugacity was used to calculate permeability of CO_2, C_2H_4, and C_2H_6 and pressure was used to calculate permeability of N_2 and CH_4.

Polymer	Thermal Treatment	Pure Gas Permeability [Barrer]						
		H_2	O_2	CO_2	N_2	CH_4	C_2H_4	C_2H_6
6FDA-DAPI	None	73 ± 6	7.9 ± 0.5	32 ± 2	1.5 ±0.1	0.99 ± 0.07	1.4 ± 0.1	0.33 ± 0.03
6FDA-DAPI/DABA	None	61 ± 5	6.1 ± 0.4	15.6 ± 0.8	1.1 ± 0.1	0.63 ± 0.02	0.74 ± 0.03	0.19 ± 0.01
	353°C, 10 min	62 ± 4	6.5 ± 0.5	24 ± 3	1.2 ± 0.1	0.67 ± 0.05	0.74 ± 0.04	0.15 ± 0.01
	353°C, 20 min	76 ± 3	8.4 ± 0.4	30 ± 2	1.5 ± 0.1	0.86 ± 0.02	1.04 ± 0.07	0.23 ± 0.01
	353°C, 40 min	72 ± 4	7.9 ± 0.3	33 ± 2	1.43 ± 0.04	0.89 ± 0.03	1.04 ± 0.05	0.22 ± 0.01
Matrimid [11, 12]	None	17.5	1.46	7.29	0.22	0.21	0.45	0.10
6FDA-DAM [12-14]	None	--	191	842	55	46.8	64	21.3
6FDA-DAM/DABA [13, 15]	None	--	18	113	4.36	4.17	--	--
[16]	389°C, 40 min	--	--	325	--	--	--	--

Table B.6. Pure gas permeability of 6FDA-DAPI and 6FDA-DAPI/DABA cross-linked at 353°C for 0, 10, 20, 40 min, measured at 35°C and 5 atm.

Polymer	Thermal Treatment	Ideal Selectivity								
		H_2/ CO_2	H_2/ C_2H_4	H_2/ C_2H_6	O_2/ N_2	N_2/ CH_4	N_2/ C_2H_4	CO_2/ CH_4	CO_2/ N_2	C_2H_4/ C_2H_6
6FDA-DAPI	None	2.3 ± 0.2	52 ± 6	220 ± 20	5.4 ± 0.5	1.5 ± 0.2	1.0 ± 0.1	32 ± 3	21 ±2	4.2 ± 0.5
6FDA-DAPI/DABA	None	3.9 ± 0.4	81 ± 7	310 ± 30	5.6 ± 0.4	1.7 ± 0.1	1.5 ± 0.1	25 ± 2	14 ±1	3.9 ± 0.2
	353°C, 10 min	2.6 ± 0.4	83 ± 8	410 ± 40	5.5 ± 0.8	1.7 ± 0.2	1.6 ± 0.2	35 ± 5	20 ± 3	5.0 ± 0.4
	353°C, 20 min	2.5 ± 0.2	73 ± 6	320 ± 20	5.6 ± 0.5	1.8 ± 0.2	1.4 ± 0.1	35 ±3	20 ± 2	4.4 ± 0.4
	353°C, 40 min	2.2 ± 0.2	69 ± 5	330 ± 20	5.5 ± 0.3	1.6 ± 0.1	1.4 ± 0.1	37 ± 3	23 ± 2	4.7 ± 0.3
Matrimid [11, 12]	None	2.40	38.8	175	6.64	1.05	0.49	34.71	33.1	4.50
6FDA-DAM [12]	None				3.5	1.2	0.86	18	15.3	3.0
6FDA-DAM/DABA [13, 15]	None				4.1	1.04		27	25.9	

Table B.7. Pure gas selectivity of 6FDA-DAPI and 6FDA-DAPI/DABA cross-linked at 353°C for 0, 10, 20, 40 min, measured at 35°C and 5 atm.

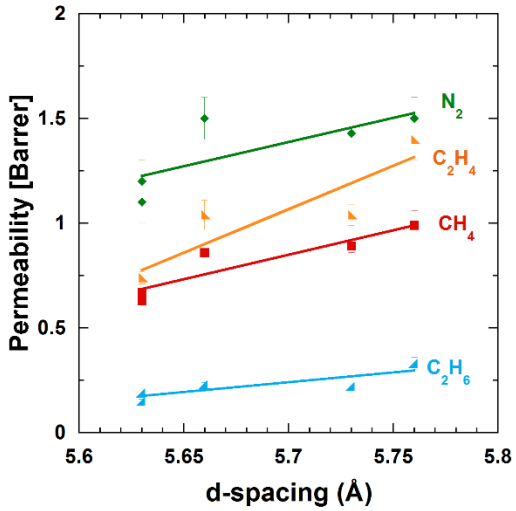

Figure B.12. Pure gas permeability at 5 atm versus inter-chain d-spacing (cf., Table B.1 and Table B.6) for N_2 (♦), C_2H_4 (◣), CH_4 (■), and C_2H_6 (◢).

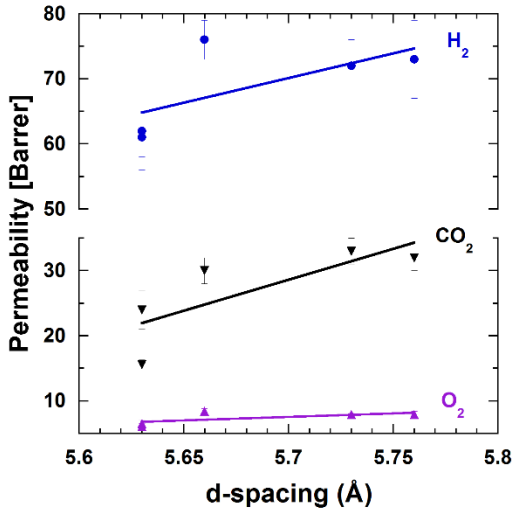

Figure B.13. Pure gas permeability at 5 atm versus inter-chain d-spacing (cf., Table B.1 and Table B.6) for H_2 (●), CO_2 (▼), and O_2 (▲).

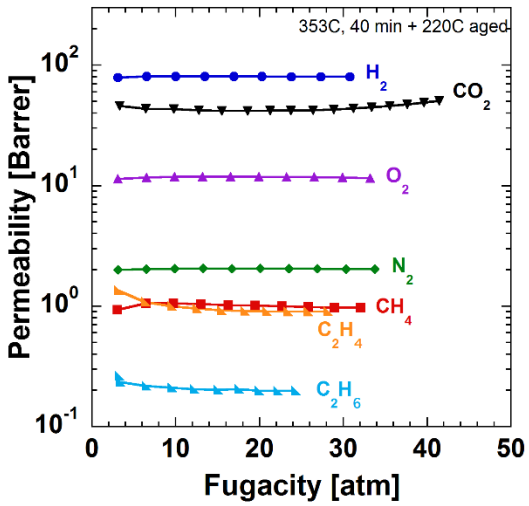

Figure B.14. Pure gas permeability of H_2 [●], CO_2 [▼], O_2 [▲], N_2 [♦], C_2H_4 [◢], CH4 [■], and C_2H_6 [◣] in 6FDA-DAPI/DABA crosslinked at 353°C for 40 min, quenched rapidly to room temperature, then aged at 220°C for 24 h under vacuum.

B.4 References

[1] L.M. Robeson, B.D. Freeman, D.R. Paul, B.W. Rowe, An Empirical Correlation of Gas Permeability and Permselectivity in Polymers and Its Theoretical Basis, Journal of Membrane Science, 341 (2009) 178-185.

[2] E.W. Lemmon, M.O. McLinden, D.G. Friend, Thermophysical Properties of Fluid Systems, in: P.J. Linstrom, W.G. Mallard (Eds.) NIST Chemistry WebBook, NIST Standard Reference Database Number 69, National Institute of Standards and Technology, Gaithersburg MD, 2018.

[3] P.C. Hiemenz, T.P. Lodge, Polymer Chemistry, Second ed., CRC Press, New York, 2007.

[4] J.D. Ingle, S.R. Crouch, Spectrochemical Analysis, Printice Hall, Englewood Cliffs, NJ, 1988.

[5] J.Y. Park, D.R. Paul, Correlation and Prediction of Gas Permeability in Glassy Polymer Membrane Materials via a Modified Free Volume Based Group Contribution Method, Journal of Membrane Science, 125 (1997) 23 - 39.

[6] A. Shimazu, T. Miyazaki, K. Ikeda, Interpretation of d-Spacing Determined by Wide Angle X-Ray Scattering in 6FDA-Based Polyimide by Molecular Modeling, Journal of Membrane Science, 166 (2000) 113-118.

[7] S. Jacobson, Molecular Modeling Studies of Polymeric Gas Separation and Barrier Materials: Structure and Transport Mechanisms, Polymers for Advanced Technologies, 5 (1993) 724-732.

[8] M. Langsam, W. Burgoyne, Effects of Diamine Monomer Structure on the Gas Permeability of Polyimides. I. Bridged Diamines, Journal of Polymer Science Part A: Polymer Chemistry, 31 (1993) 909-921.

[9] D.F. Sanders, Z.P. Smith, C.P. Ribeiro, R. Guo, J.E. McGrath, D.R. Paul, B.D. Freeman, Gas Permeability, Diffusivity, and Free Volume of Thermally Rearranged Polymers Based on 3,3'-Dihydroxy-4,4'-Diamino-Biphenyl (HAB) and 2,2'-Bis-(3,4-Dicarboxyphenyl) Hexafluoropropane Dianhydride (6FDA), Journal of Membrane Science, 409-410 (2012) 232-241.

[10] H. Lin, B.D. Freeman, Chapter 7: Permeation and Diffusion, in: Springer Handbook of Materials Measurement Methods, 2006, pp. 371-387.

[11] Y. Zhang, I.H. Musselman, J.P. Ferraris, K.J. Balkus, Gas Permeability Properties of Matrimid® Membranes Containing the Metal-Organic Framework Cu–BPY–HFS, Journal of Membrane Science, 313 (2008) 170-181.

[12] M. Rungta, L. Xu, W.J. Koros, Carbon Molecular Sieve Dense Film Membranes Derived from Matrimid® for Ethylene/Ethane Separation, Carbon, 50 (2012) 1488-1502.

[13] J.H. Kim, W.J. Koros, D.R. Paul, Physical Aging of Thin 6FDA-Based Polyimide Membranes Containing Carboxyl Acid Groups. Part I. Transport Properties, Polymer, 47 (2006) 3094-3103.

[14] W. Qiu, L. Xu, C.-C. Chen, D.R. Paul, W.J. Koros, Gas Separation Performance of 6FDA-based Polyimides with Different Chemical Structures, Polymer, 54 (2013) 6226-6235.

[15] J.D. Wind, D.R. Paul, W.J. Koros, Natural Gas Permeation in Polyimide Membranes, Journal of Membrane Science, 228 (2004) 227-236.

[16] A.M. Kratochvil, W.J. Koros, Decarboxylation-Induced Cross-Linking of a Polyimide for Enhanced CO_2 Plasticization Resistance, Macromolecules, 41 (2008) 7920-7927.

APPENDIX C: SUPPLEMENTARY INFORMATION FOR CO_2, C_2H_4, AND C_2H_6 SORPTION AND MIXED GAS PERMEABILITY OF THERMALLY CROSS-LINKED DIAMINOPHENYLINDANE (DAPI) CONTAINING POLYIMIDES (CHAPTER 5)

C.1. Gas Properties and Pure Gas Permeability

Pure gas permeability coefficients, P_i, were calculated as follows:

$$P_i = \frac{V\ell}{fRTA}\left[\left(\frac{dp}{dt}\right)_{SS} - \left(\frac{dp}{dt}\right)_{leak}\right] \qquad \text{Eq. C.1}$$

where V is the downstream volume, ℓ is the sample thickness, f is the fugacity of the gas feed calculated from the REFPROP equation of state [1], T is the absolute temperature, A is the sample area, $(dp/dt)_{SS}$ is the steady state pressure rise in the downstream volume, and $(dp/dt)_{leak}$ is the system leak rate [2].

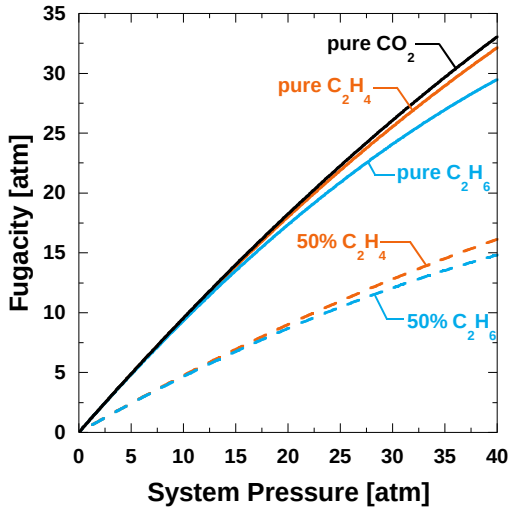

Figure C.1. Pure (solid) and mixed (dashed) gas fugacity for C_2H_4 (orange), C_2H_6 (blue), and CO_2 (black) verses system (i.e., total) pressure at 35°C, determined using the REFPROP equation of state [3].

C.2. Mixed Gas Permeation Measurements

A schematic of the mixed gas permeation system is presented in Figure C.2. The membrane was first degassed for a minimum of 18 h by pulling vacuum on the upstream and downstream faces of the sample, leaving V1, V2, V4, V11, and V12 closed, placing the crossover valve such that the permeation cell was open to vacuum, and the remaining valves were open. Depending on the expected flux through the sample, the auxiliary volumes were left open or closed as needed. The system leak rate was measured by closing valves V1, V2, V3, V4, V5, V6, and V9 for at least 1 h, measuring the rate of the upstream and downstream pressure rise. To start a permeation measurement, the cross-over valve was set to bypass, valves V2, V3, V5, V6, and V9 were closed, and V1 and V10 were opened. The feed pressure was then set at the cylinder. Then V2 was opened, using the regulating valve to set the feed flowrate. After setting the feed pressure and flowrate, the cross-over valve was switched to expose the upstream face of the sample to the test gas, starting the permeability experiment. The upstream and downstream pressures were recorded using LABVIEW. To ensure steady state was achieved, the pressure steps were held for 6θ, where θ is the time lag determined for pure C_2H_6 permeation. After 1.5θ, the downstream was evacuated by opening V6 for 5 min to ensure all non-steady state permeate was removed from the downstream. Then V6 was closed, and steady state permeate was collected in the downstream for the remaining 4.5θ. After the permeation measurement was complete, the permeate was transferred to the evacuated GC sample charging volume by closing V7 and V8 and opening V9. The GC sample charging volume pressure, P3, was monitored using a 10 Torr capacitation manometer. Once pressure

equilibrated between the downstream and the GC charging volume, V9 was closed and V8 was opened to feed a portion of the sample gas to the evacuated TCD sample loop, and the concentration was measured using the GC. A total of 5 GC measurements were made on each permeate sample.

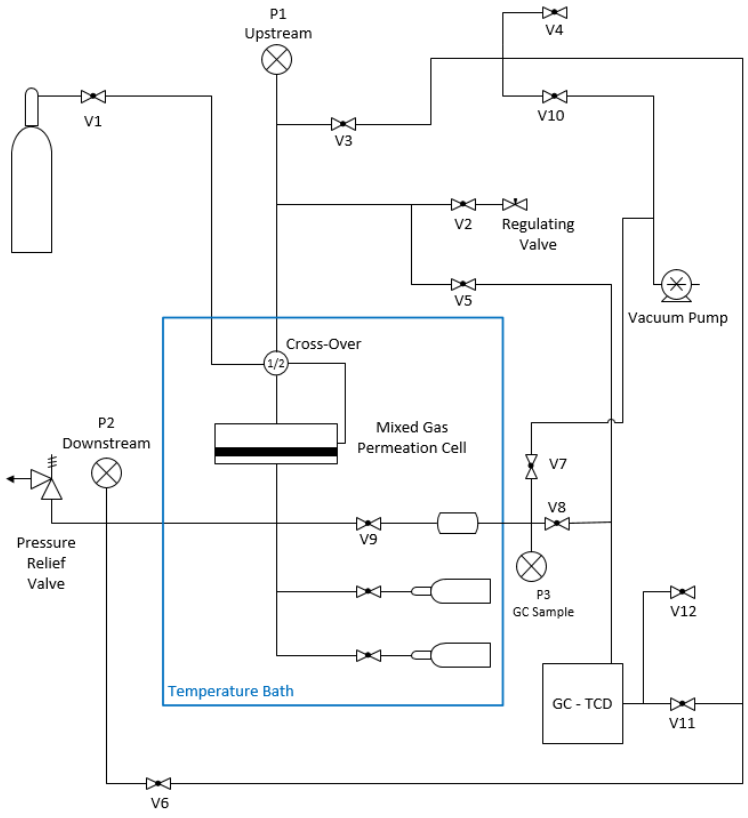

Figure C.2. Mixed gas permeation equipment.

C.3. Pure gas plasticization characterization

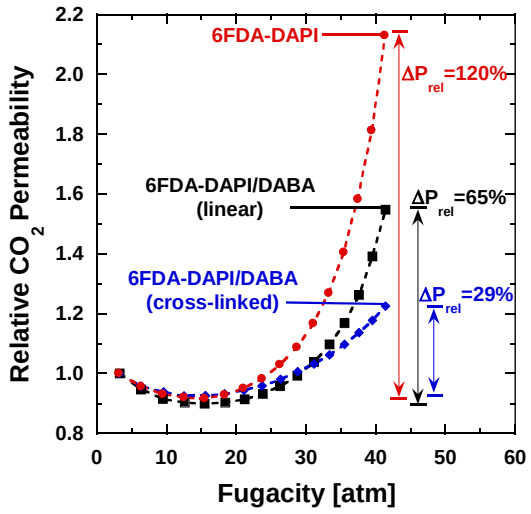

Figure C.3. Relative CO_2 permeability in 6FDA-DAPI [●], linear 6FDA-DAPI/DABA [■], and 6FDA-DAPI/DABA cross-linked at 353°C for 40 min [♦], indicating the percent change in relative permeability after the plasticization fugacity (i.e., fugacity at which permeability reaches a minimum).

Polymer	CO_2		C_2H_6		C_2H_4	
	f^* [atm]	ΔP_{rel} (%)	f^* [atm]	ΔP_{rel} (%)	f^* [atm]	ΔP_{rel} (%)
6FDA-DAPI	16	120	12	32	15	12
6FDA-DAPI/DABA(linear)	15	65	15	14	15	8.0
6FDA-DAPI/DABA(cross-linked)	16	29	20	2.0	23	1.0

Table C.1. Plasticization fugacity, f^*, [4] and percent increase in relative permeability, ΔP_{rel}, after the plasticization fugacity for CO_2, C_2H_4, and C_2H_6 in 6FDA-DAPI, linear 6FDA-DAPI/DABA, and 6FDA-DAPI/DABA cross-linked at 353°C for 40 min.

C.4. Pure gas solubility

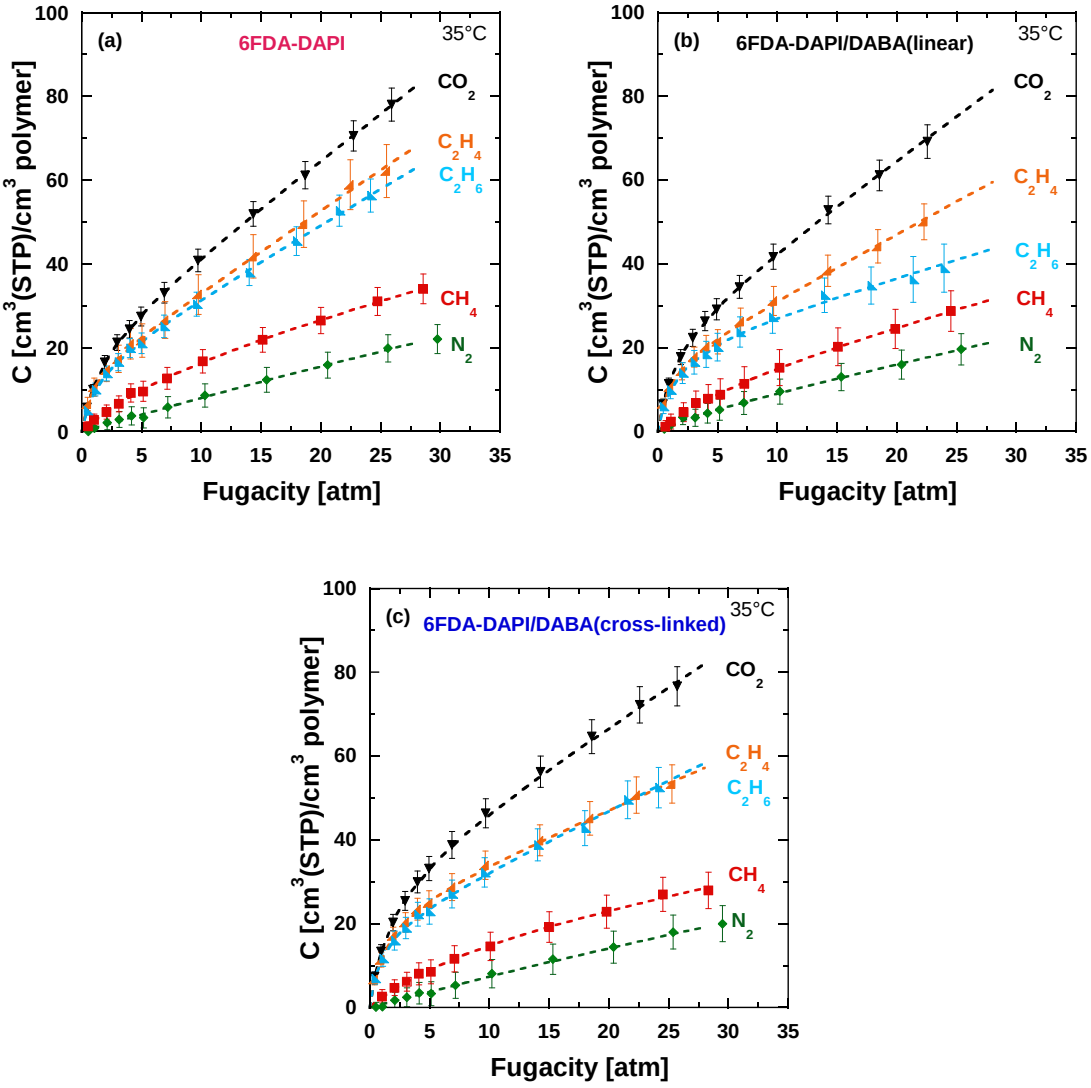

Figure C.4. Pure gas solubility at 35°C in: (a) 6FDA-DAPI, (b) linear 6FDA-DAPI/DABA, and (c) cross-linked 6FDA-DAPI/DABA for CO_2 (▼), C_2H_4 (◢), C_2H_6 (◣), CH_4 (■), and N_2 (♦). The dashed lines represent the dual mode fit for each gas.

Polymer	Gas	k_D [cm^3(STP)/(cm^3 polymer atm)]	C'_H [cm^3(STP)/(cm^3 polymer)]	b [atm^{-1}]
6FDA-DAPI	N_2*	0.8 ± 0.2	--	--
	CH_4	0.7 ± 0.5	17 ± 2	0.1 ± 0.2
	C_2H_4	1.9 ± 0.3	15 ± 4	1.2 ± 0.9
	C_2H_6	1.7 ± 0.2	16 ± 4	0.9 ± 0.4
	CO_2	2.2 ± 0.2	22 ± 4	0.6 ± 0.2
6FDA-DAPI/DABA(linear)	N_2*	0.8 ± 0.2	--	--
	CH_4	0.7 ± 1.0	13 ± 3	0.1 ± 0.4
	C_2H_4	1.5 ± 0.2	17 ± 4	1.1 ± 0.6
	C_2H_6	0.8 ± 0.3	21 ± 6	0.7 ± 0.4
	CO_2	2.1 ± 0.3	25 ± 5	0.7 ± 0.2
6FDA-DAPI/DABA(cross-linked)	N_2*	0.7 ± 0.2	--	--
	CH_4	0.5 ± 0.8	19 ± 2	0.1 ± 0.2
	C_2H_4	1.2 ± 0.2	24 ± 4	0.8 ± 0.3
	C_2H_6	1.4 ± 0.2	20 ± 4	1.0 ± 0.5
	CO_2	1.8 ± 0.3	32 ± 5	0.6 ± 0.2

Table C.2**.** Dual-mode parameters for CH_4, C_2H_4, C_2H_6, and CO_2 in 6FDA-DAPI, linear 6FDA-DAPI/DABA, and cross-linked 6FDA-DAPI/DABA. The parameters and corresponding uncertainties were determined by weighted least-squares optimization. Due to experimental uncertainty and the low N_2 solubility in each polymer, dual-mode parameters could not be determined for N_2. *Note: For N_2, effective Henry's Law coefficients are reported as the slope of the sorption isotherms.

For most of the gases considered, solubility coefficients in all three polymers increased with increasing critical temperature, T_c, as shown in Figure C.5, which is often used as a measure of gas solubility, with only C_2H_6 deviating from this trend. The slope of $\ln(S_i)$ versus T_c for 6FDA-DAPI, linear 6FDA-DAPI/DABA, and cross-linked 6FDA-DAPI/DABA was about 0.008 K^{-1}. This slope is less than the average slope for 6FDA-containing polyimides (0.016 – 0.019 K^{-1}), but similar to the trends in penetrant solubility measured in perfluorinated polymers (0.007 – 0.011 K^{-1}) [5-7].

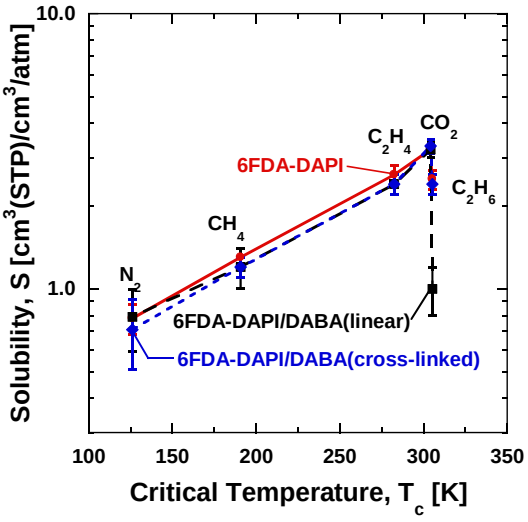

Figure C.5. Solubility coefficients of N_2, CH_4, C_2H_4, CO_2, and C_2H_6 in 6FDA-DAPI (●), linear 6FDA-DAPI/DABA (■), and cross-linked 6FDA-DAPI/DABA (♦), at 20 atm and 35°C. The errors bars represent the experimental uncertainty of the measurement. T_c values are included in Table 5.2.

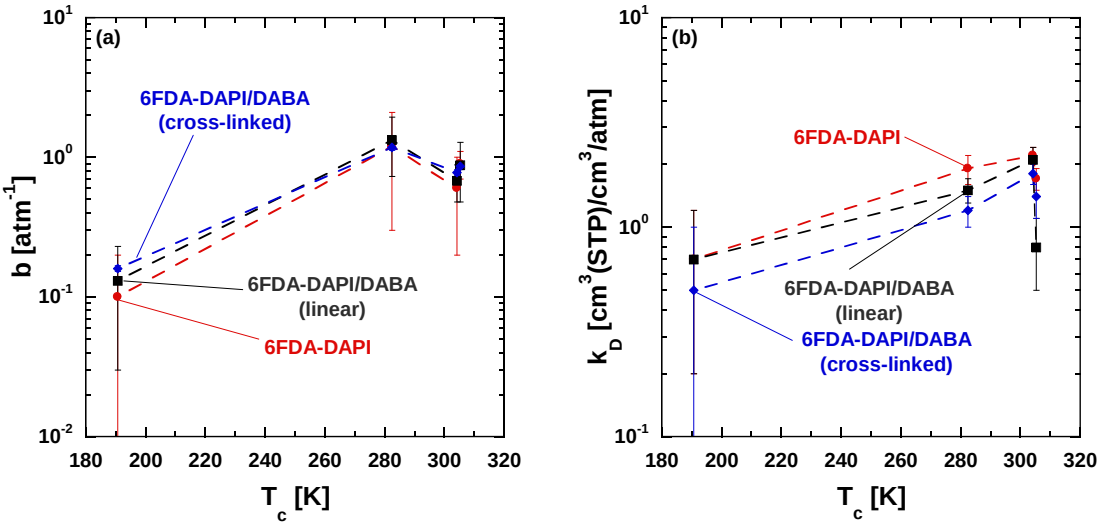

Figure C.6. Dual mode parameters, (a) b, and (b) k_D, for CH_4, C_2H_4, C_2H_6, and CO_2 in 6FDA-DAPI (●), linear 6FDA-DAPI/DABA (■), and cross-linked 6FDA-DAPI/DABA (♦) versus penetrant T_c (cf., Table 5.2).

	Pure Gas Permeability, P_i [Barrer]				
Polymer	**CO_2**	**N_2**	**CH_4**	**C_2H_4**	**C_2H_6**
6FDA-DAPI	36 ± 2	1.4 ± 0.5	0.91 ± 0.05	1.3 ± 0.05	0.35 ± 0.01
6FDA-DAPI/DABA (linear)	14.8 ± 0.5	1.05 ± 0.07	0.57 ± 0.03	0.68 ± 0.04	0.20 ± 0.01
6FDA-DAPI/DABA (cross-linked)	31 ± 2	1.4 ± 0.1	0.79 ± 0.04	0.92 ± 0.05	0.20 ± 0.01

Table C.3. Pure gas permeability of N_2, CH_4, C_2H_4, C_2H_6, and CO_2 in 6FDA-DAPI, linear 6FDA-DAPI/DABA, cross-linked 6FDA-DAPI/DABA at 20 atm and 35°C. These values were reported previously [8].

C.5. References

[1] E.W. Lemmon, M.O. McLinden, D.G. Friend, Thermophysical Properties of Fluid Systems, in: P.J. Linstrom, W.G. Mallard (Eds.) NIST Chemistry WebBook, NIST Standard Reference Database Number 69, National Institute of Standards and Technology, Gaithersburg MD, 2018.

[2] H. Lin, B.D. Freeman, Chapter 7: Permeation and Diffusion, in: Springer Handbook of Materials Measurement Methods, 2006, pp. 371-387.

[3] E.W. Lemmon, I.H. Bell, M.L. Huber, M.O. McLinden, Standard Reference Data Program, in: NIST Standard Reference Database 23: Reference Fluid Thermodynamic and Transport Properties - REFPROP, Version 10.0, National Institute of Standards and Technology, Gaithersburg, 2018.

[4] A.F. Ismail, W. Lorna, Penetrant-Induced Plasticization Phenomenon in Glassy Polymers for Gas Separation Membrane, Separation and Purification Technology, 27 (2002) 173 - 194.

[5] Z.P. Smith, D.F. Sanders, C.P. Ribeiro, R. Guo, B.D. Freeman, D.R. Paul, J.E. McGrath, S. Swinnea, Gas Sorption and Characterization of Thermally Rearranged Polyimides Based on 3,3′ -Dihydroxy-4,4′ -Diamino-Biphenyl (HAB) And 2,2′ -Bis-(3,4-Dicarboxyphenyl) Hexafluoropropane Dianhydride (6FDA), Journal of Membrane Science, 415-416 (2012) 558-567.

[6] Z.P. Smith, Fundamentals of Gas Sorption and Transport in Thermally Rearranged Polyimides, Doctor of Philosophy, The University of Texas at Austin, Austin, TX, 2014.

[7] Z.P. Smith, R.R. Tiwari, M.E. Dose, K.L. Gleason, T.M. Murphy, D.F. Sanders, G. Gunawan, L.M. Robeson, D.R. Paul, B.D. Freeman, Influence of Diffusivity and Sorption on Helium and Hydrogen Separations in Hydrocarbon, Silicon, and Fluorocarbon-Based Polymers, Macromolecules, 47 (2014) 3170-3184.

[8] M.E. Dose, M. Chwatko, I. Hubacek, N.A. Lynd, D.R. Paul, B.D. Freeman, Thermally Cross-linked Diaminophenylindane (DAPI) Containing Polyimides for Membrane Based Gas Separations, Polymer, Submitted (2018).

APPENDIX D: SUPPLEMENTAL INFORMATION FOR FUNDAMENTAL GAS TRANSPORT AND DILATION STUDIES IN THERMALLY CROSS-LINKED DIAMINOPHENYLINDANE (DAPI) CONTAINING POLYIMIDES (CHAPTER 6)

D.1. Pure gas properties

Gas	Gas Diameter, d_g [Å]	Critical Temperature, T_c [K]
CO_2	3.44	304.2
N_2	3.49	126.1
CH_4	3.82	190.7
C_2H_4	4.16	282.5
C_2H_6	4.44	305.3

Table D.1. Effective gas diameters and critical temperature values. Gas diameters and critical temperatures were obtained from the literature [1, 2], respectively.

D.2. Non-linear dilation

To determine the significance of the $F \neq 0$ versus $F=0$ in Eq. 6.2, an F-Test for the additional term was performed. According to Bevington and Robinson. [2], the F_χ value is defined as follows:

$$F_\chi = \frac{\chi^2(m) - \chi^2(m+1)}{\chi^2(m+1)/(N-m-1)} \qquad \text{Eq. D.1}$$

where N is the number of data points for each data set, m is the number of fitted parameters in the model, and the χ^2 values correspond to the $F=0$ (i.e., $\chi^2(m)$) and $F \neq 0$ (i.e., $\chi^2(m+1)$) fits for each data set. F_χ characterizes the significance of an additional term in a fitted equation and should be large if the fitting equation where $F \neq 0$ represents a significant improvement over the equation where $F=0$. The statistical significance of the additional term can be evaluated using a one-tailed F-test. If F_χ exceeds the test value for F_{test}, the additional term (i.e., the quadratic term in Eq. D.2 in this case) likely substantially improves

the quality of the fit and should be included. The p-values in Table D.2 were calculated using the Microsoft Excel ***F.DIST.RT(***F_χ*, 1, dF)* function.

	Probability, *p*, of F_χ exceeding F_{test}		
Polymer	**CO_2**	**C_2H_4**	**C_2H_6**
6FDA-DAPI	9.4×10^{-6}	1.8×10^{-3}	4.6×10^{-8}
6FDA-DAPI/DABA -linear	2.3×10^{-4}	5.7×10^{-8}	3.8×10^{-8}
6FDA-DAPI/DABA -cross-linked	0.44	8.2×10^{-9}	4.7×10^{-6}

Table D.2. Probability of Fχ exceeding Ftest. Probability values less than 0.05 indicate the fit to Eq. 2 with F≠ 0 is statistically a better fit to the data than Eq. 2 with F=0.

D.3. Partial Molar Volume Calculations:

$$\bar{V}_i = \frac{\partial}{\partial f}\left(\frac{\Delta V}{V_o}\right)\left(\frac{\partial C}{\partial f}\right)^{-1} \qquad \text{Eq. D.2}$$

D.4. Correlation of diffusion coefficients with fugacity and penetrant concentration

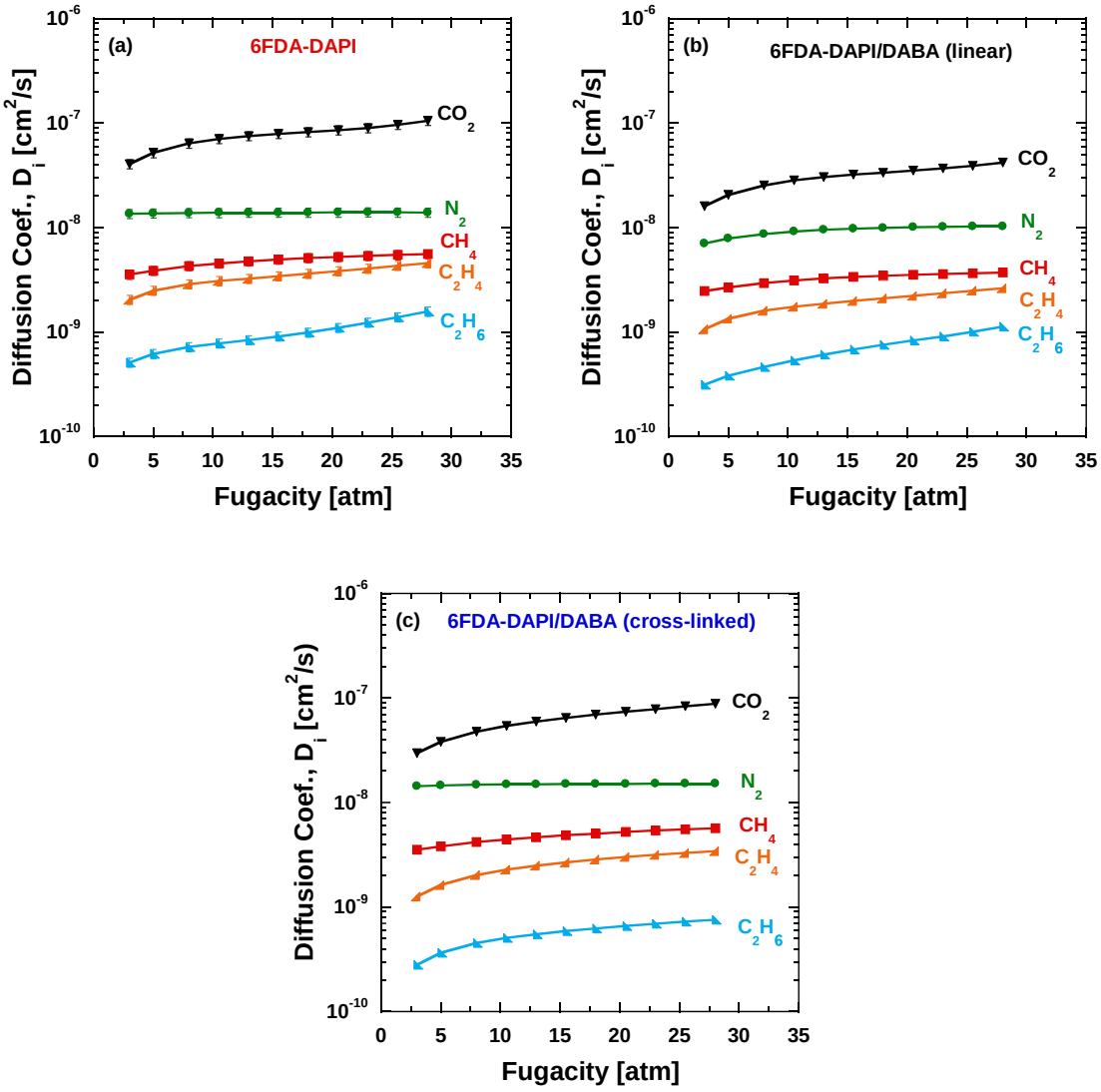

Figure D.1. Diffusion coefficients of N_2 (green), CH_4 (red), CO_2 (black), C_2H_4 (orange), and C_2H_6 (blue) in: (a) 6FDA-DAPI, (b) 6FDA-DAPI/DABA (linear), and (c) 6FDA-DAPI/DABA (cross-linked) versus penetrant fugacity at 35°C.

$$D_i = D_{C,o}\exp(\beta_{D,C}C_i) \qquad \text{Eq. D.3}$$

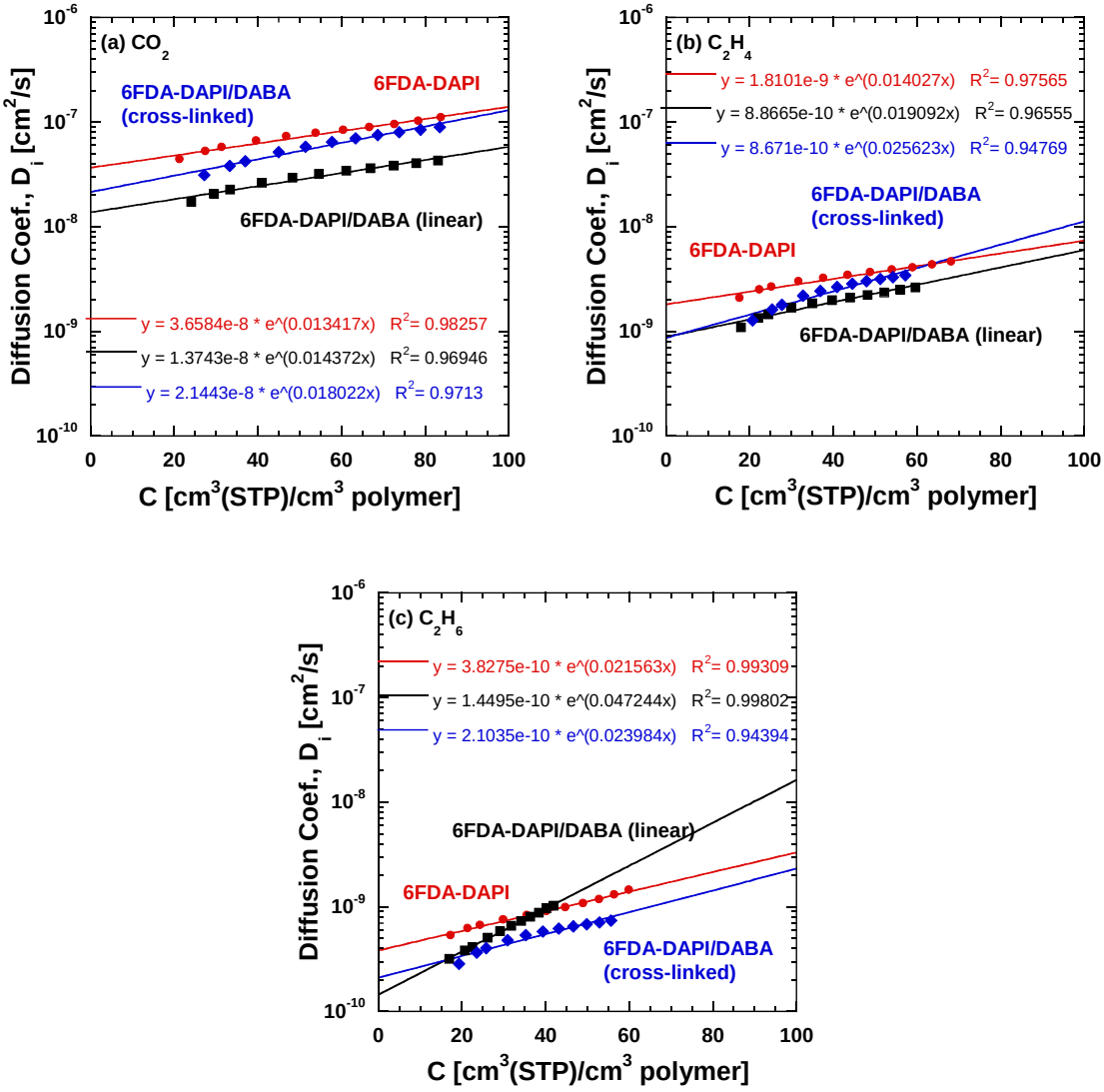

Figure D.2. Diffusion coefficients of: (a) CO_2, (b), C_2H_4, and (c) C_2H_6 in 6FDA-DAPI (●), linear 6FDA-DAPI/DABA (■), and cross-linked 6FDA-DAPI/DABA (♦), versus penetrant concentration.

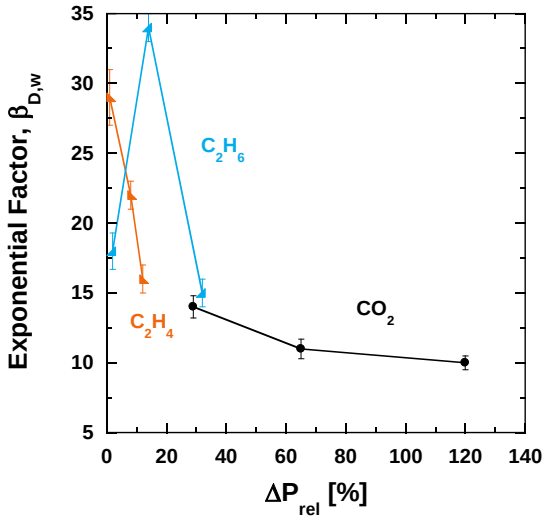

Figure D.3. Relative increase in pure gas permeability above the plasticization fugacity, ΔP_{rel}, versus the weight fraction based exponential factor for diffusion coefficients, $\beta_{D,w}$, for CO_2 (●), C_2H_4 (◢), and C_2H_6 (◣). The lines are drawn to guide the eye. The ΔP_{rel} values were reported previously [3].

	CO_2			C_2H_4			C_2H_6			CH_4			N_2		
Polymer	$D_{C,o}$ [x10^{-10} cm^2/s]	$\beta_{D,C}$	R^2	$D_{C,o}$ [x10^{-10} cm^2/s]	$\beta_{D,C}$	R^2	$D_{C,o}$ [x10^{-10} cm^2/s]	$\beta_{D,C}$	R^2	$D_{C,o}$ [x10^{-10} cm^2/s]	$\beta_{D,C}$	R^2	$D_{C,o}$ [x10^{-10} cm^2/s]	$\beta_{D,C}$	R^2
6FDA-DAPI	370	0.013	0.97	18	0.014	0.96	3.8	0.020	0.99	36	0.016	0.98	150	-0.003	0.97
6FDA-DAPI/DABA (linear)	140	0.014	0.96	8.9	0.019	0.95	1.4	0.047	0.99	28	0.013	0.94	110	-0.003	0.98
6FDA-DAPI/DABA (cross-linked)	210	0.018	0.97	8.7	0.026	0.95	2.1	0.024	0.94	33	0.020	0.99	160	-0.003	0.88

Table D.3. Infinite dilution diffusion coefficients, $D_{Co,i}$, plasticization factors, $\beta_{D,C}$, and R^2 values for CO_2, C_2H_4, C_2H_6, CH_4, and N_2 in 6FDA-DAPI, linear 6FDA-DAPI/DABA, and cross-linked 6FDA-DAPI/DABA, fit using Eq. D.3.

D.5. Thermodynamic Factor:

The driving force for the diffusive flux of species i, J_i, in one dimension is the chemical potential gradient, $\nabla\mu_i$:

$$J_i = -\frac{L_i \rho w_i}{RT} \nabla\mu_i \qquad \text{Eq. D.4}$$

where ρ is the mixture density, w_i is the penetrant weight fraction, R is the universal gas constant, T is the temperature, and L_i is the mobility of the penetrant in the system [4-8]. Fick's first law can be written as [6, 9-12]:

$$J_i = -D_i \rho \nabla w_i \qquad \text{Eq. D.5}$$

From Eq. D.4 and Eq. D.5, the diffusion coefficient of a penetrant, D_i, can be separated into two different contributions: a penetrant mobility coefficient, L_i, which describes the purely kinetic contribution to diffusion, and a thermodynamic factor, Q_i, which describes polymer-penetrant interactions. D_i can be expressed by:

$$D_i = L_i Q_i \qquad \text{Eq. D.6}$$

where Q_i is the weight fraction based thermodynamic factor. Q_i is defined as [5, 6, 10-13]:

$$Q_i = \frac{1}{RT} \frac{\partial(\mu_i)}{\partial \ln(w_i)} \qquad \text{Eq. D.7}$$

From Eq. D.7, Q_i values can be calculated from solubility data and expressed in terms of the dual-mode and dilation fitting parameters, and L_i can then be calculated using Eq. D.6.

Penetrant activity, a_i in the polymer is given by [14]:

$$\frac{\mu_i}{RT} = \ln(a) = \ln\left(\frac{f}{f_o}\right) \qquad \text{Eq. D.8}$$

where f_o is a reference fugacity for the penetrant.

Derivatives based on the dual-mode model useful for these calculations are as follows:

$$\frac{\partial C}{\partial f} = C' = k_D + \frac{C'_H b}{(1+bf)^2} \quad \text{Eq. D.9}$$

$$\frac{\partial C}{\partial a} = f_o C' \quad \text{Eq. D.10}$$

$$\frac{\partial^2 C}{\partial f^2} = C'' = -\frac{2C'_H b^2}{(1+bf)^3} \quad \text{Eq. D.11}$$

The weight fraction based thermodynamic factor is defined as:

$$Q_i = \frac{\partial a}{\partial ln(w_i)} = \left[\frac{\partial C}{\partial a}\right]^{-1}\left[\frac{\partial w}{\partial C}\right]^{-1} \quad \text{Eq. D.12}$$

In terms of dual-mode parameters, Q_{wi} can be expressed as:

$$Q_i = \frac{C\left(\frac{M_i C}{22414} + \rho_{poly}\right)}{C' f \rho_{poly}} \quad \text{Eq. D.13}$$

The weight fraction based thermodynamic factors, Q_i, for CO_2, C_2H_4, and C_2H_6 in 6FDA-DAPI, linear 6FDA-DAPI/DABA, and cross-linked 6FDA-DAPI/DABA are presented in *Figure D.5*. All three gases follow the same trend, starting at 1.0 at infinite dilution, increased to a maximum value of about 2-2.5 at around 5 atm, and then decreasing slightly to a constant value of about 1.5. As shown in *Figure D.**6***, this results in L_i being lower than the diffusion coefficients at low fugacity and exponential factors for mobility coefficients being larger than exponential factors for diffusion coefficients.

Using penetrant weight fraction as the driving force for Fickian diffusion (i.e., weight fraction based thermodynamic factors and mobilities) offers the advantage of only requiring solubility data for calculation. Consequently, a significant portion of existing studies use this method [5, 6, 10-13]. However, it has been noted that the rate at which gas mobility changes is not only a function of the weight fraction of the dissolved penetrant, but also the size of the penetrant molecule [5, 7, 15].

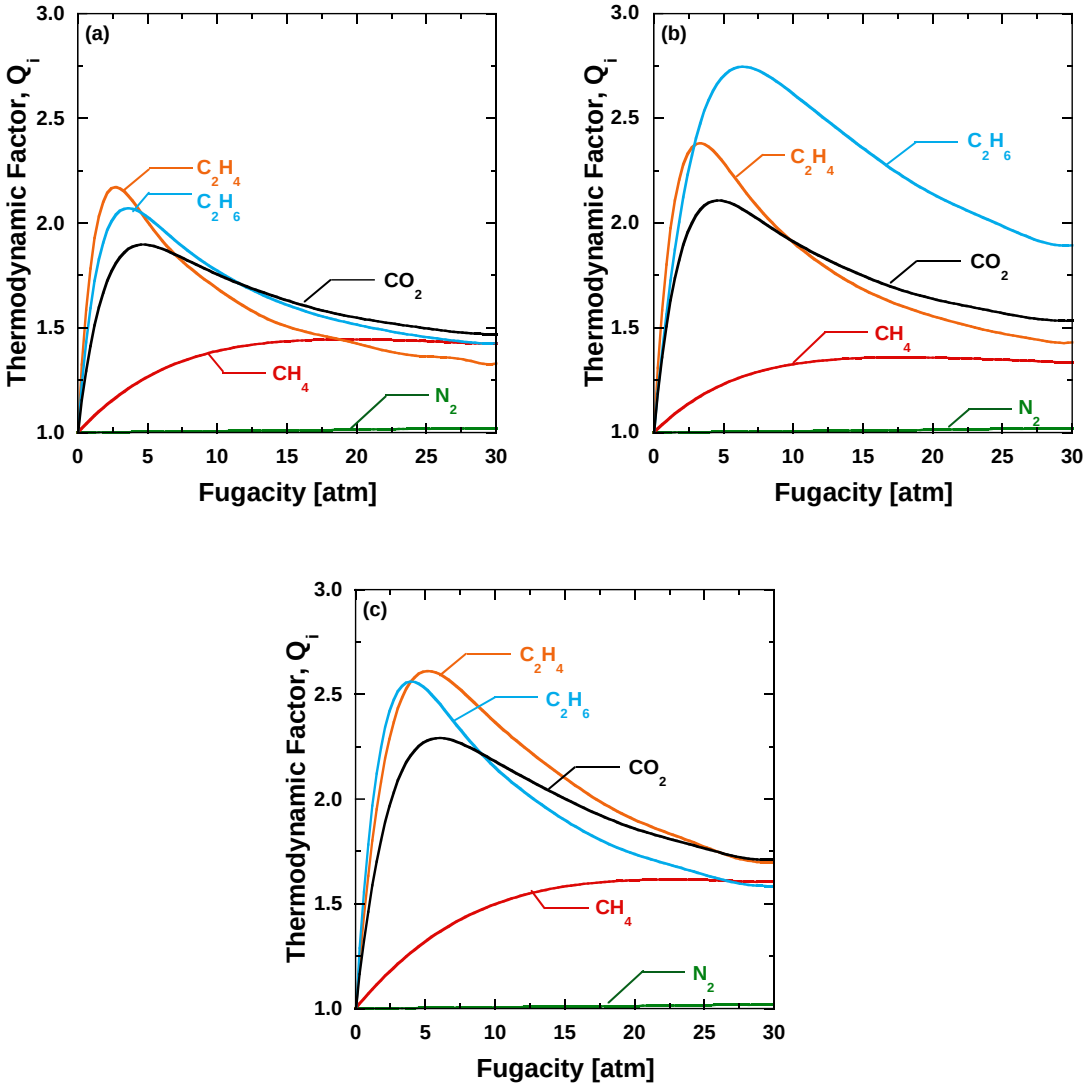

Figure D.4. Thermodynamic factor, Q_i, calculated using weight fraction for N_2 (green), CH_4 (red), C_2H_4 (orange), C_2H_6(blue) and CO_2 (black) in (a) 6FDA-DAPI, (b) linear 6FDA-DAPI/DABA, and (c) cross-linked 6FDA-DAPI/DABA.

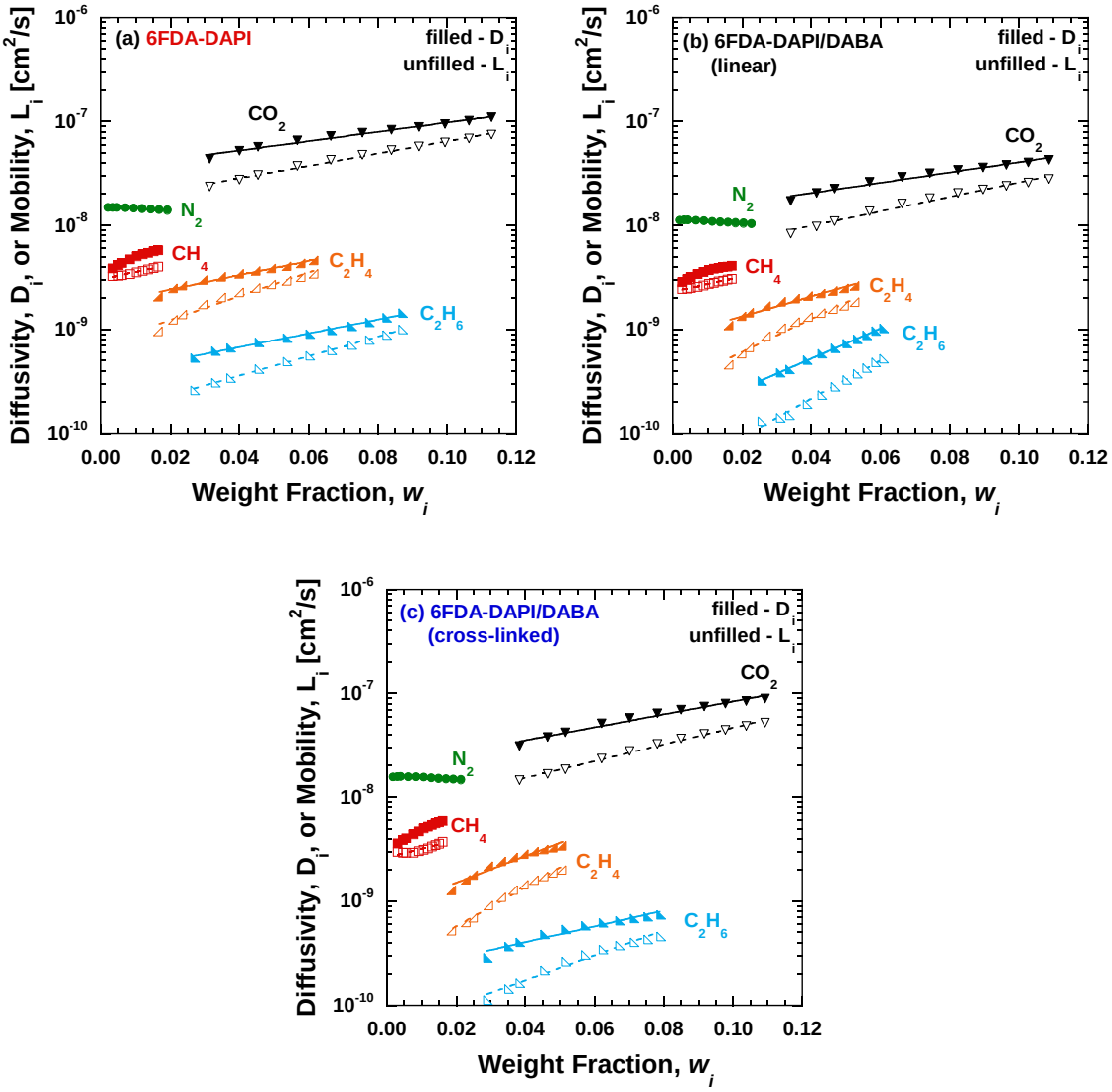

Figure D.5. Diffusion (filled markers) and mobility (unfilled markers) of N_2 (green), CH_4 (red), C_2H_4 (orange), C_2H_6 (blue) and CO_2 (black) versus penetrant weight fraction in: (a) 6FDA-DAPI, (b) linear 6FDA-DAPI/DABA, and (c) cross-linked 6FDA-DAPI/DABA. The solid and dashed lines represent exponential fits of D_i and L_i with weight fraction.

Similar to diffusion coefficients, the mobility coefficients, L_i, increases exponentially with weight fraction of penetrant:

$$L_i = L_{i,o} \exp\left(\beta_{L,w} w_i\right) \quad \text{Eq. D.14}$$

where $L_{i,o}$ is the infinite dilution mobility coefficient of the penetrant, and β_w is the plasticization factor [6, 10-13]. The mobility data and exponential trends reported in Figure D.5 a-c are replotted in Figure D.6 a-c to better compare the mobility of CO_2, C_2H_4, and C_2H_6 in 6FDA-DAPI. Linear 6FDA-DAPI/DABA, and cross-linked 6FDA-DAPI/DABA. $L_{i,o}$, $\beta_{L,w}$, and the R^2 values determined by fitting the mobility data to Eq. D.14 are shown in Table D.4.

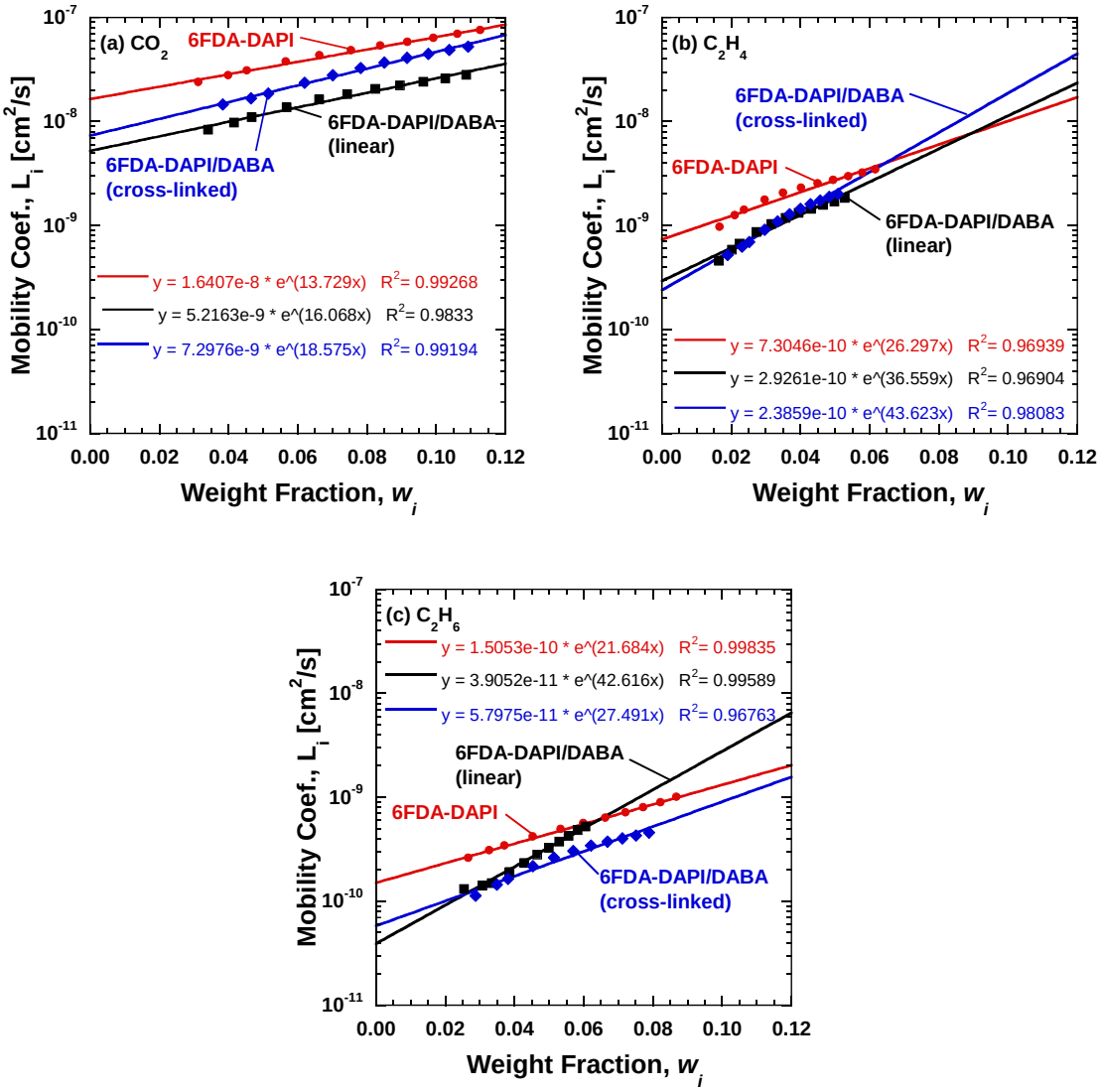

Figure D.6. Mobility coefficients of: (a) CO_2, (b), C_2H_4, and (c) C_2H_6 in 6FDA-DAPI (●), linear 6FDA-DAPI/DABA (■), and cross-linked 6FDA-DAPI/DABA (♦), versus penetrant weight fraction

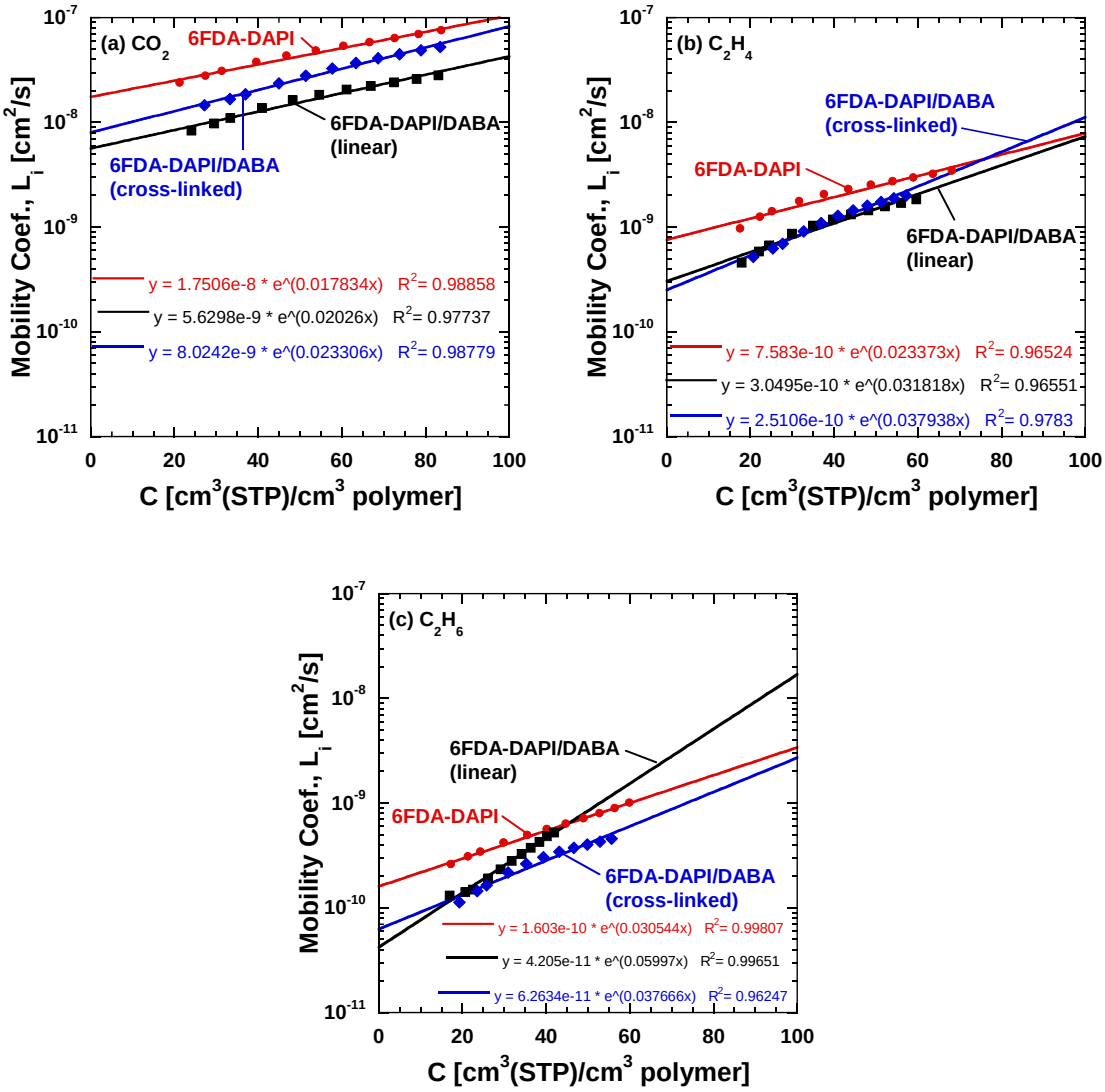

Figure D.7. Mobility coefficients of: (a) CO_2, (b), C_2H_4, and (c) C_2H_6 in 6FDA-DAPI (●), linear 6FDA-DAPI/DABA (■), and cross-linked 6FDA-DAPI/DABA (♦), versus penetrant concentration.

	CO_2			C_2H_4			C_2H_6			CH_4			N_2		
Polymer	$L_{i,o}$ [x10^{-10} cm^2/s]	$\beta_{L,w}$	R^2	$L_{i,o}$ [x10^{-10} cm^2/s]	$\beta_{L,w}$	R^2	$L_{i,o}$ [x10^{-10} cm^2/s]	$\beta_{L,w}$	R^2	$L_{i,o}$ [x10^{-10} cm^2/s]	$\beta_{L,w}$	R^2	$L_{i,o}$ [x10^{-10} cm^2/s]	$\beta_{L,w}$	R^2
6FDA-DAPI	160	13.7	0.99	7.3	26	0.97	1.5	21.7	0.99	30	16	0.98	150	-4.3	0.98
6FDA-DAPI/DABA (linear)	53	16	0.98	3.0	36	0.97	0.40	42	0.99	23	17	0.99	113	-4.7	0.99
6FDA-DAPI/DABA (cross-linked)	75	18	0.99	2.5	43	0.98	0.60	27	0.97	27	19	0.88	160	-4.0	0.92

Table D.4. Infinite dilution mobility coefficients, $L_{w,o}$, plasticization factors, $\beta_{L,w,}$ and R^2 values for CO_2, C_2H_4, C_2H_6, CH_4, and N_2 in 6FDA-DAPI, linear 6FDA-DAPI/DABA, and cross-linked 6FDA-DAPI/DABA, fit using Eq. D.14.

	CO_2			C_2H_4			C_2H_6			CH_4			N_2		
Polymer	$L_{i,o}$ [x10^{-10} cm^2/s]	$\beta_{L,C}$	R^2	$L_{i,o}$ [x10^{-10} cm^2/s]	$\beta_{L,C}$	R^2	$L_{i,o}$ [x10^{-10} cm^2/s]	$\beta_{L,C}$	R^2	$L_{i,o}$ [x10^{-10} cm^2/s]	$\beta_{L,C}$	R^2	$L_{i,o}$ [x10^{-10} cm^2/s]	$\beta_{L,C}$	R^2
6FDA-DAPI	175	0.017	0.98	7.6	0.023	0.96	1.6	0.031	0.99	30	0.009	0.97	150	-0.004	0.98
6FDA-DAPI/DABA (linear)	56	0.020	0.98	3.0	0.032	0.96	0.42	0.060	0.99	23	0.009	0.99	110	-0.004	0.99
6FDA-DAPI/DABA (cross-linked)	80	0.023	0.99	2.5	0.037	0.98	0.63	0.038	0.97	27	0.010	0.88	160	-0.004	0.93

Table D.5. Infinite dilution mobility coefficients, $L_{i,o}$, plasticization factors, $\beta_{L,C,}$ and R^2 values for CO_2, C_2H_4, C_2H_6, CH_4, and N_2 in 6FDA-DAPI, linear 6FDA-DAPI/DABA, and cross-linked 6FDA-DAPI/DABA, fit using Eq. D.14, using concentration in place of weight fraction.

D.6. Mobility coefficients versus accessible fractional free volume, FFV_a

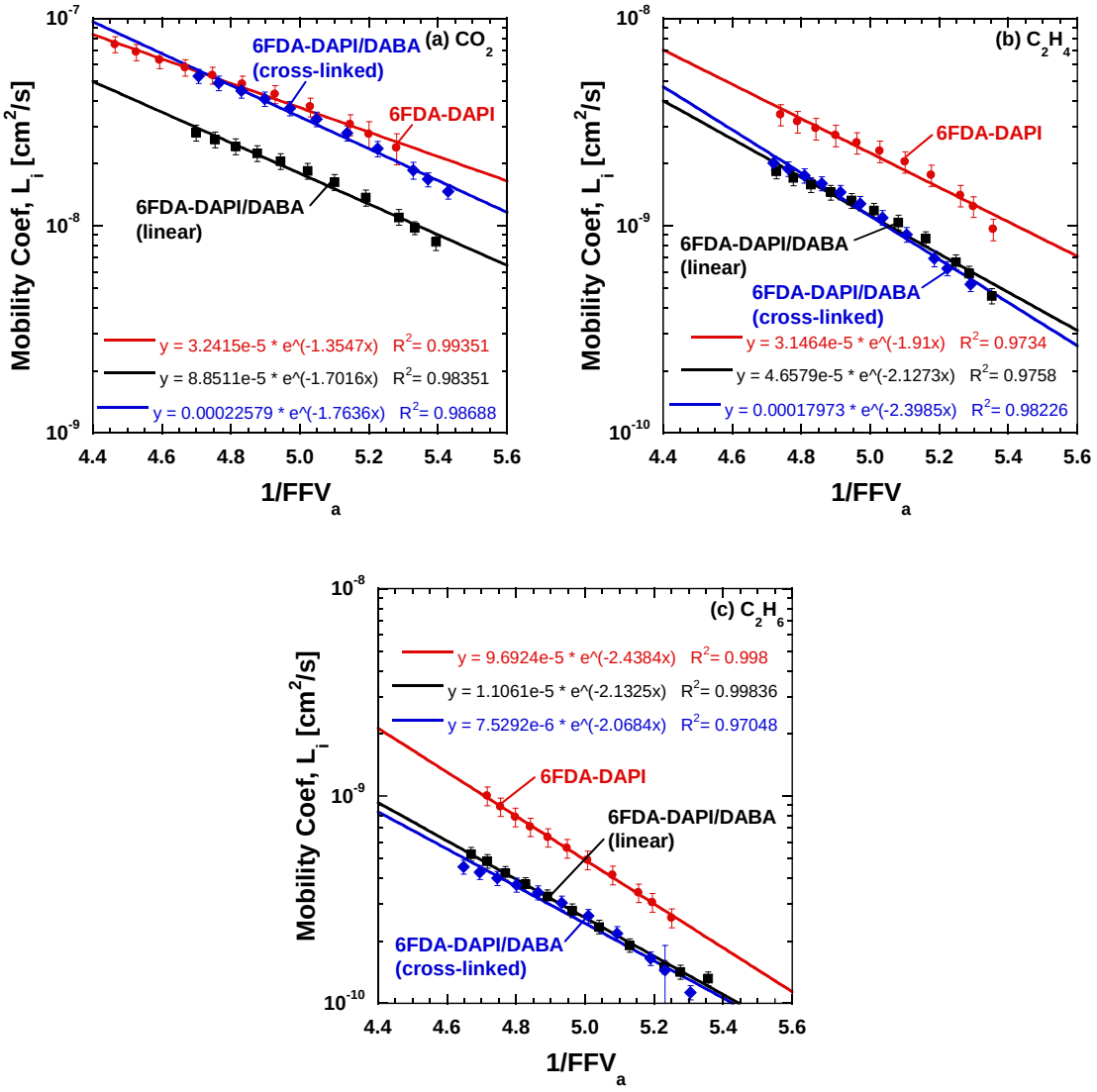

Figure D.8. Mobility coefficients of: (a) CO_2, (b), C_2H_4, and (c) C_2H_6 in 6FDA-DAPI (●), linear 6FDA-DAPI/DABA (■), and cross-linked 6FDA-DAPI/DABA (♦), versus accessible fractional free volume.

D.7. Diffusivity and Mobility Versus Gas Diameter

		D_o(x10^{-10} cm^2/s)				
	FFV$_o$	CO$_2$	C$_2$H$_4$	C$_2$H$_6$	CH$_4$	N$_2$
6FDA-DAPI	0.181±0.003	380	19	3.4	36	150
6FDA-DAPI/DABA -linear	0.179±0.002	150	9.2	2.3	28	110
6FDA-DAPI/DABA -cross-linked	0.181±0.002	310	10	2.5	33	160

Table D.6. Diffusion coefficients at penetrant free fractional free volume, D_o, for CO_2, C_2H_4, and C_2H_6, calculated using Eq. 10. Infinite dilution diffusion coefficients at zero weight fraction, $D_{w,o}$, were used for CH_4 and N_2, using Eq. 8. FFV$_o$ is the penetrant free fractional free volume, which was reported previously [16].

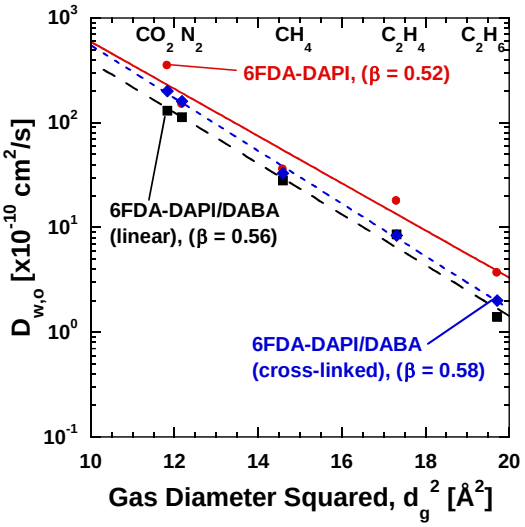

Figure D.9. Diffusion coefficients at infinite dilution, $D_{w,o}$ in 6FDA-DAPI (●), linear 6FDA-DAPI/DABA (■), and cross-linked 6FDA-DAPI/DABA (♦) versus the effective penetrant gas diameter squared, d_g^2. The solid lines represent the exponential trend in Eq. 13.

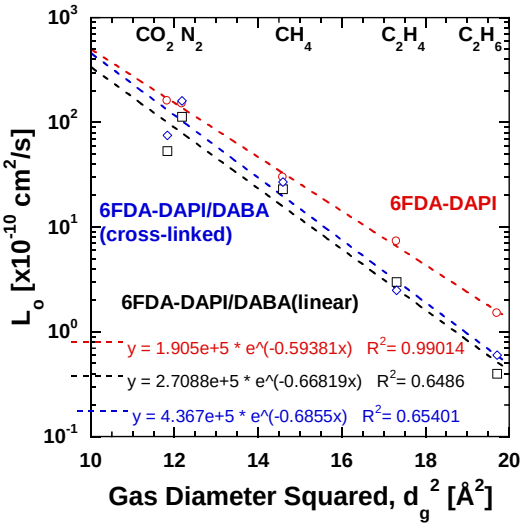

Figure D.10. Infinite dilution mobility coefficients in 6FDA-DAPI (●), linear 6FDA-DAPI/DABA (■), and cross-linked 6FDA-DAPI/DABA (♦), versus penetrant effective gas diameter squared, d_g^2.

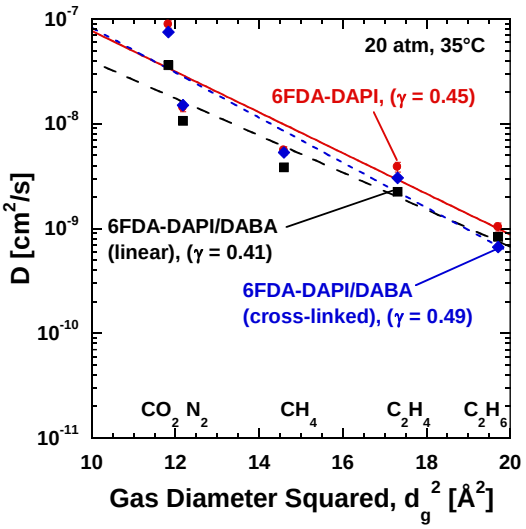

Figure D.11. Diffusion coefficients at 20 atm, in 6FDA-DAPI (●), linear 6FDA-DAPI/DABA (■), and cross-linked 6FDA-DAPI/DABA (♦) versus the effective penetrant gas diameter squared, d_g^2. The solid lines represent the exponential trend in Eq. 13.

D.8. References

[1] L.M. Robeson, B.D. Freeman, D.R. Paul, B.W. Rowe, An Empirical Correlation of Gas Permeability and Permselectivity in Polymers and Its Theoretical Basis, Journal of Membrane Science, 341 (2009) 178-185.

[2] E.W. Lemmon, M.O. McLinden, D.G. Friend, Thermophysical Properties of Fluid Systems, in: P.J. Linstrom, W.G. Mallard (Eds.) NIST Chemistry WebBook, NIST Standard Reference Database Number 69, National Institute of Standards and Technology, Gaithersburg MD, 2018.

[3] M.E. Dose, I. Hubacek, D.R. Paul, B.D. Freeman, CO_2, C_2H_4, and C_2H_6 Sorption and Mixed Gas Permeability of Thermally Cross-linked Diaminophenylindane (DAPI) Containing Polyimides, Journal of Membrane Science, Submitted (2018).

[4] R.B. Bird, W.E. Stewart, E.N. Lightfoot, Transport Phenomena, 2nd ed., John Wiley & Sons, 1961.

[5] J.S. Vrentas, J.L. Duda, Diffusion in Polymer-Solvent Systems. I. Reexamination of the Free-Volume Theory, Journal of Polymer Science Part B: Polymer Physics, 15 (1977) 403-416.

[6] M. Galizia, M.G. De Angelis, E. Finkelshtein, Y.P. Yampolskii, G.C. Sarti, Sorption and Transport of Hydrocarbons and Alcohols in Addition-Type Poly(trimethyl Silyl Norbornene). I: Experimental Data, Journal of Membrane Science, 385-386 (2011) 141-153.

[7] J.S. Vrentas, J.L. Duda, H.-C. Ling, Free-Volume Theories for Self-Diffusion in Polymer-Solvent Systems. I. Conceptual Differences in Theories, Journal of Polymer Science Part B: Polymer Physics, 23 (1985) 275-288.

[8] J.S. Vrentas, J.L. Duda, H.-C. Ling, C.-C. Hou, Free-Volume Theories for Self-Diffusion in Polymer-Solvent Systems. II. Predictive Capabilities, Journal of Polymer Science Part B: Polymer Physics, 23 (1985) 289-304.

[9] F. Doghieri, D. Biavati, G.C. Sarti, Solubility and Diffusivity of Ethanol in PTMSP: Effects of Activity and of Polymer Aging, Industrial & Engineering Chemistry Process Design and Development, 35 (1996) 2420-2430.

[10] M. Galizia, C. Daniel, G. Fasano, G. Guerra, G. Mensitieri, Gas Sorption and Diffusion in Amorphous and Semicrystalline Nanoporous Poly(2,6-dimethyl-1,4-phenylene)oxide, Macromolecules, 45 (2012) 3604-3615.

[11] M. Galizia, K.A. Stevens, D.R. Paul, B.D. Freeman, Modeling Gas Permeability and Diffusivity in HAB-6FDA Polyimide and Its Thermally Rearranged Analogs, Journal of Membrane Science, 537 (2017) 83-92.

[12] J.D. Moon, M. Galizia, H. Borjigin, R. Liu, J.S. Riffle, B. Freeman, D. Paul, Water Vapor Sorption, Diffusion, and Dilation in Polybenzimidazoles, Macromolecules, 51 (2018) 7197 - 7208.

[13] N. Ramesh, P.K. Davis, J.M. Zielinski, R.P. Danner, J.L. Duda, Application of Free-Volume Theory to Self Diffusion of Solvents in Polymers Below the Glass Transition Temperature: A Review, Journal of Polymer Science Part B: Polymer Physics, 49 (2011) 1629-1644.

[14] J.M. Smith, H.C. Van Ness, M.M. Abbott, Introduction to Chemical Engineering Thermodynamics, 7th ed., McGraw-Hill Education, New York, 2004.

[15] E. Favre, P. Schaetzel, Q.T. Nguygen, R. Clement, J. Neel, Sorption, Diffusion and Vapor Permeation of Various Penetrants Through Dense Poly(dimethylsiloxane) Membranes: A Transport Analysis, Journal of Membrane Science, 92 (1994) 16-184.

[16] M.E. Dose, M. Chwatko, I. Hubacek, N.A. Lynd, D.R. Paul, B.D. Freeman, Thermally Cross-linked Diaminophenylindane (DAPI) Containing Polyimides for Membrane Based Gas Separations, Polymer, Submitted (2018).

APPENDIX E: SOLVENT AND THERMAL HISTORY EFFECTS ON GAS TRANSPORT IN THERMALLY REARRANGED (TR) POLYMERS AND THEIR PRECURSORS

HAB-6FDA polyimide was synthesized by a two-step polycondensation method with chemical imidization. Dense polymer films were solution cast from tetrahydrofuran (THF), acetone, and N,N-dimethylacetamide (DMAc). Films cast from THF and acetone were cast in a solvent saturated glove bag then dried at 200°C for 24 h. Two separate films were cast from DMAc in a vacuum oven using different heating and vacuum protocols, with one utilizing a gas purge and the other a temperature ramp under partial vacuum. Each precursor film was used to prepare thermally rearranged (TR) polymers. The rearrangement reaction was performed at 400°C and resulted in a 54% conversion to the polybenzoxazole TR product. Pure CH_4 and CO_2 gas permeability measurements were made on both the precursor and the TR polymer. While the ideal CH_4/CO_2 selectivity remained constant for all four polyimide films, the different casting procedures resulted in a 40% difference in permeability coefficients, with the film prepared from DMAc under partial vacuum having the lowest permeability coefficients for both gases and the DMAc film cast using a gas purge having the highest. The respective TR polymer films exhibited the same trend in permeability with a 37% variation with only minimal differences in selectivity. These trends have been attributed to free volume variations due to the different casting techniques and the inability to thermally "reset" the history of the polyimide precursor.

E.1. Introduction

Thermally rearranged polymers, or TR polymers, have been investigated for several different gas separation applications, with particular interest in CO_2 removal from natural gas (CO_2/CH_4) [1-8]. TR polymers are polybenzoxazoles (PBOs) formed by a thermal solid-sate reaction of an ortho-functional polyimide or polyamide precursor [1, 7]. As shown in Figure E.1, TR polymers often exceed upper bound performance, particularly for CO_2/CH_4 mixtures, largely due to high free volume, narrow free volume distribution, and the rigid structure of the PBO backbone. Additionally, TR polymers have been shown to be resistant to swelling, or plasticization, from high pressure CO_2 [1, 3].

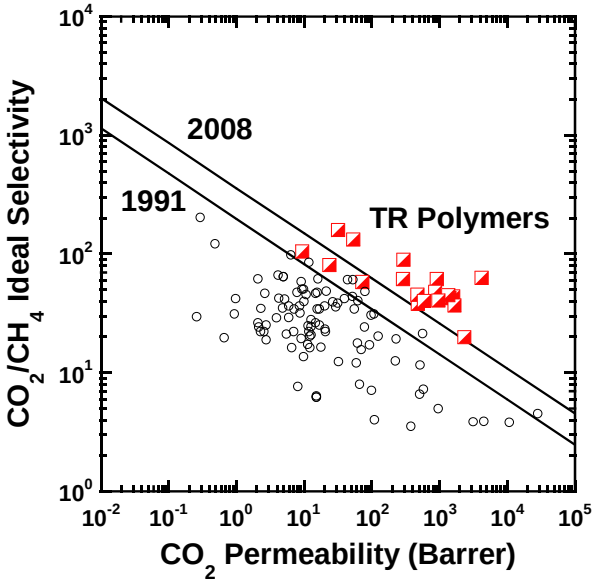

Figure E.1. CO_2/CH_4 upper bound plot, where the 1991 [9] and 2008 [10] permeability-selectivity tradeoff boundaries are indicated by the solid lines. Various TR polymers (◪), and other polymers (○) are indicated. [11-13]

Some of the most widely studied TR polymers are based on the polyimide precursor containing 3,3'-dihydroxy-4,4'-diamino-biphenyl (HAB) and 2,2'-bis-(3,4-dicarboxyphenyl) hexafluoropropane dianhydride (6FDA), synthesized by chemical

imidiziation and referred to as HAB-6FDA-CI. The structure and TR reaction for HAB-6FDA-CI are detailed in Figure E.2, where chemical imidization resulted in an acetate ortho-functional group. To thermally rearrange HAB-6FDA-CI, the solution-cast polyimide films were heated from room temperature to 300°C at 5°C/min in a tube furnace with flowing nitrogen (90 cm^3/min), and held for 60 min to ensure complete imidization of the polyimide. Then, the films were heated to the final treatment temperature, 400°C, held for the desired treatment time (60 min), then cooled at 10°C/min to room temperature [5-8, 14]. As the thermal treatment time and temperature increases, so does the conversion to the PBO structure, where the percent conversion is defined as ratio of the actual mass loss during thermal treatment to the theoretical mass loss associated with the conversion to the PBO structure [14].

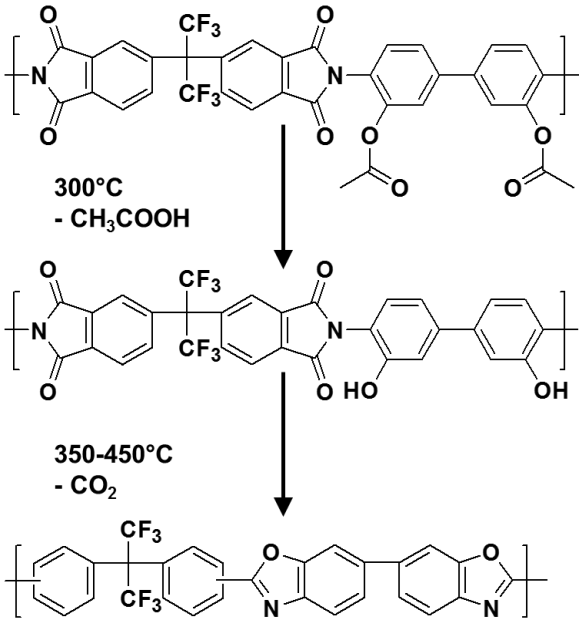

Figure E.2. Thermal rearrangement of HAB-6FDA-CI. Samples for this study were heated at 400°C for 1 h [7, 8].

E.2. Variable Transport Properties of TR Polymers

While TR polymers derived from HAB-6FDA-CI have shown CO_2/CH_4 separation performance beyond the upper bound, there is a significant variability in pure gas CO_2 and CH_4 permeability values reported in the literature, with permeability values varying by almost 40% [3, 5, 6, 8, 15]. These differences in transport properties are often attributed to different solvent and casting procedures used to prepare the dense polyimide precursor films. Within six publications, five different solution-casting procedures are reported:

(1) Casting from n-methyl-2-pyrrolidone (NMP), removing the bulk of the solvent at 80°C under atmospheric conditions for 24 h, then removing residual solvent by heating at 200°C under full vacuum for 18 h [6].

(2) Casting from NMP, removing the bulk of the solvent by placing the casting plate under an IR lamp at 60°C for 24 h, then removing residual solvent by heating at 190°C under full vacuum for at least 24 h [15].

(3) Casting from dimethylacetamide (DMAc), removing the bulk of the solvent at 80°C under atmospheric conditions for 24 h, then removing residual solvent by heating at 200°C under full vacuum for 18 h [8].

(4) Casting from DMAc, drying at 80°C at -10 inHg for 24 h in a vacuum oven, purging the oven with dry air to remove the bulk of the solvent, drying at 80°C under full vacuum for 24 h, then heating at 200°C for 24 h to remove residual solvent [5].

(5) Casting from DMAc, drying at 80°C at -10 inHg for 24 h in a vacuum oven, heating to 100°C at -10 inHg for 24 h, pulling full vacuum and holding at 100°C for 12 h to remove the bulk of the solvent, then drying at 200°C under full at vacuum for 24 h to remove residual solvent [3].

Both Sanders et al. [5] and Gleason et al. [3] reported using the same casting procedure, (4-a) and (4-b). However, they reported a 10% difference in CO_2 permeabilities, as detailed in Table E.1.

Procedure:	**(1)**	**(2)**	**(3)**	**(4-a)**	**(4-b)**	**(5)**
Reference	[6]	[15]	[8]	[5]		[3]
Solvent:	NMP	NMP	DMAc	DMAc	DMAc	DMAc
Step 1:	80°C, atm, 24 h	60°C, IR lamp, 24 h	80°C, atm, 24 h	80°C, -10 inHg, 24 h	80°C, -10 inHg, 24 h	80°C, -10 inHg, 24 h
Step 2:	200°C, full vac, 18 h	190°C, full vac, >24 h	200°C, full vac, 18 h	Purge w/ dry air	Purge w/ dry air	100°C, -10 inHg, 24 h
Step 3:	--	--	--	80°C, full vac, 24 h	80°C, full vac, 24 h	100°C, full vac, 12 h
Step 4:	--	--	--	200°C, full vac, 24 h	200°C, full vac, 24 h	200°C, full vac, 24 h
$P(CH_4)$ [Barrer]	0.31	0.26	0.313	0.31	0.34	0.23
$P(CO_2)$ [Barrer]	12.6	11	12.0	11.7	13.0	8.5
Selectivity CO_2/CH_4	40.6	42	38.3	37.7	38.2	37.5

Table E.1. Various casting procedures used for preparing HAB-6FDA-CI polyimide precursor films from the literature with their resulting CO_2 and CH_4 transport properties for 35°C at 5 atm.

The pressure dependence of CO_2 and CH_4 permeability in HAB-6FDA-CI polyimide precursor cast using the various procedures are recorded in Figure E.3. The error bars noted represent the uncertainty values reported in the respective publications. Both

CO_2 and CH_4 permeability decreased slightly with increasing pressure, consistent with dual mode transport behavior.

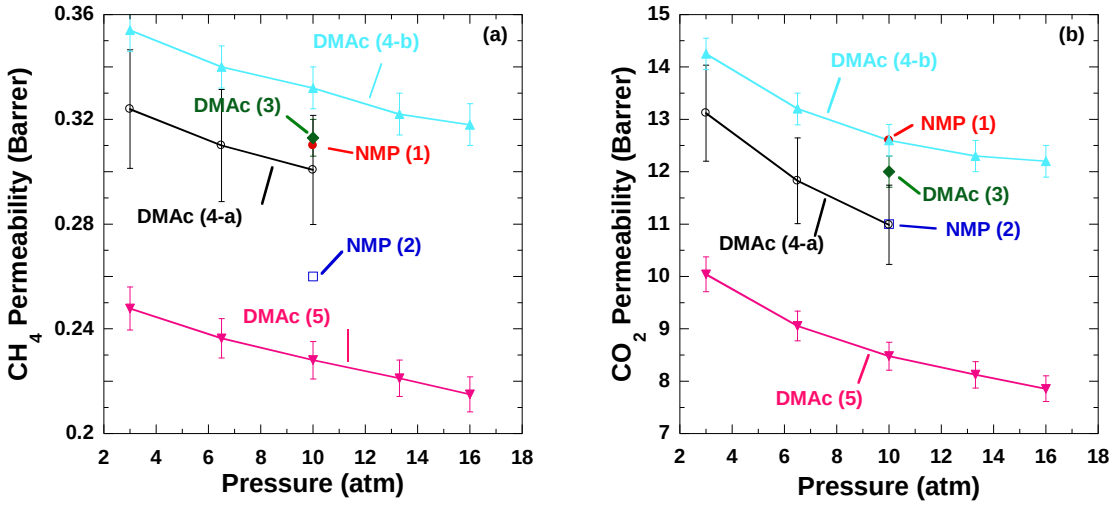

Figure E.3. (a) CH_4 permeability and (b) CO_2 permeability in HAB-6FDA-CI precursor polyimide, measured at 35°C and solution cast using different solvents and casting procedures. See Table E.1 for details of the casting protocols.

However, despite the differences in gas permeability, all publications reported similar CO_2/CH_4 selectivities, as noted in Figure E.4. The differences in permeability are believed to be associated with the use of different casting solvents and thermal histories of the HAB-6FDA-CI polyimide. For non-TR polymers, the thermal, solvent, and aging history of non-equilibrium glassy polymers can often be reset by heating the polymer above its glass transition temperature (T_g) and then rapidly cooling to room temperature [16, 17]. Due to the onset of the TR process in the vicinity of the T_g, it is not possible to heat the TR polymer precursors above their glass transition temperature to "erase" thermal and processing history. Thus, using different solvents and casting procedures can result in TR polyimide precursors with different fractional free volumes and free volume distributions.

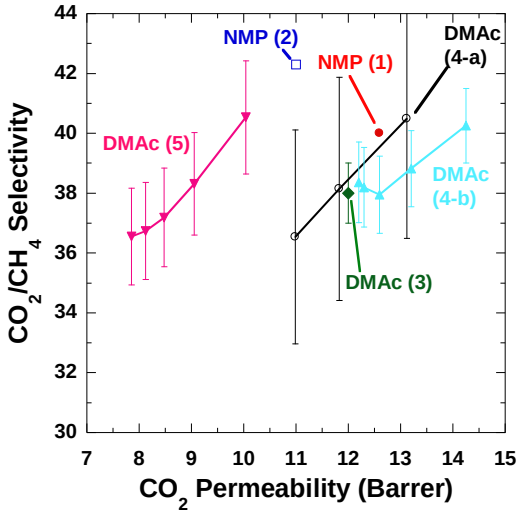

Figure E.4. CO_2/CH_4 selectivity versus CO_2 permeability in HAB-6FDA-CI polyimide precursor cast using different solvents and casting procedures.

This work will focus on investigating the effect of casting solvent and casting procedure to determine the effect processing history has on TR polymers and their precursors. For this work, HAB-6FDA-CI polyimide precursor and HAB-6FDA-TR400 will be used, where HAB-6FDA-TR400 was thermally rearranged at 400°C for 60 min to achieve a 54% conversion to the PBO structure. The polyimide used in this work was synthesized using the polycondensation method with chemical imidization, as described previously [7]. The structure and complete imidization with acetate ortho-functionality was confirmed with FT-IR and ^{1}H-NMR using a ~5% solution in dimethyl sulfoxide-d6. HAB-6FDA-TR400 was chosen to minimize any potential effects of thermal degradation, which are often observed in TR polymers thermally rearranged at 450°C for 30 min [7]. Pure gas permeabilities of CO_2 and CH_4 were measured using a constant volume, variable pressure method, as described in Chapter 2.

E.3. Effect of Solvent and Thermal Processing on TR Polymers

To vary the solvent and processing history of HAB-6FDA-CI polyimide precursor, DMAc, acetone, and tetrahydrofuran (THF) were used as casting solvents in the following casting procedures:

- **DMAc(100°C)** – Casting a 2 wt% polymer solution in DMAc, using casting procedure (5).
- **DMAc(80°C)** – Casting a 2 wt% polymer solution in DMAc, using casting procedure (4-b).
- **Acetone** – Casting a 2 wt% polymer solution in acetone onto a glass plate in an acetone saturated glove bag at room temperature to allow for slow solvent evaporation. Residual solvent was removed by drying the resulting film at 200°C under full vacuum for 24 h.
- **THF** – Casting a 2 wt% polymer solution in THF onto a glass plate in THF saturated glove bag at room temperature. Residual solvent was removed by drying the resulting film at 200°C under full vacuum for 24 h.

These casting procedures are briefly described in Table E.2. Thermal gravimetric analysis (TGA) and differential scanning calorimetry (DSC) were used to confirm complete solvent removal. The target thickness of all the TR precursor films was 30 μm.

	Casting Procedure			
	DMAc (100°C),(5)	**DMAc (80°C),(4-b)**	**THF**	**Acetone**
Casting Conditions	vacuum oven	vacuum oven	glove bag, partially saturated	glove bag, partially saturated
Bulk Solvent Removed	80°C, -10 inHg, 24 h	80°C, -10 inHg, 24 h	ambient, 24 h	ambient, 24 h
Solid Film Formed	100°C, -10inHg, 24 h	80°C, Purge w/ dry air		
Residual Solvent Removal	100°C, full vac, 12 h	80°C, full vac, 24 h	200°C, full vac, 24 h	200°C, full vac, 24 h
	200°C, full vac, 24 h	200°C, full vac, 24 h		

Table E.2. Casting procedures used for this work for DMAc, THF, and acetone based solvent castings. All films were cast from a 2 wt% solvent solution, filtered with a 1.2 micrometer syringe filter.

As was observed previously in Figure E.3, CO_2 and CH_4 permeability in HAB-6FDA-CI polyimide precursor decreased slightly with increasing pressure, following dual-mode behavior. Films cast using THF and DMAc(100°C) had the lowest CO_2 and CH_4 permeabilities measured in this work, followed by the films cast from acetone and DMAc(80°C), as shown in Figure E.5. Despite the polyimide cast from DMAc(100°C) and DMAc (80°C) both using DMAc as the casting solvent, DMAc(80°C) had CO_2 and CH_4 permeabilities about 40% higher than DMAc(100°C). Additionally, both samples using acetone and THF as the solvents were cast at room temperature and then dried at 200°C under vacuum for 24 h, but the films cast from acetone had about 18% higher CO_2 and CH_4 permeability than the films cast from THF. However, despite the differences in gas permeability when using different casting procedures, there was no significant difference in CO_2/CH_4 selectivity between casting methods (cf., Figure E.6).

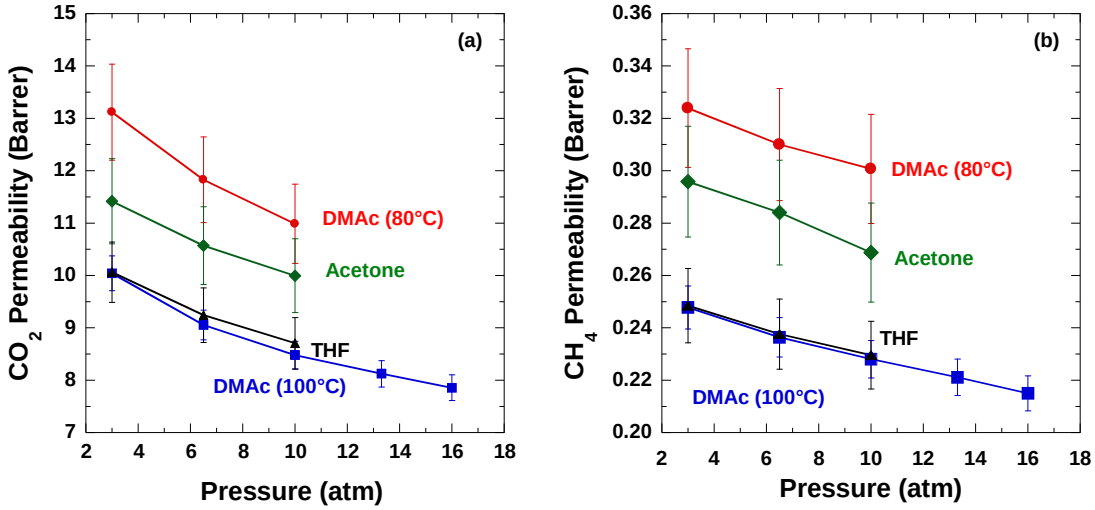

Figure E.5. (a) CO_2 permeability and (b) CH_4 permeability in HAB-6FDA-CI polyimide cast using acetone (♦), THF (▲), and DMAc at 80°C (●), and DMAc at 100°C (■).

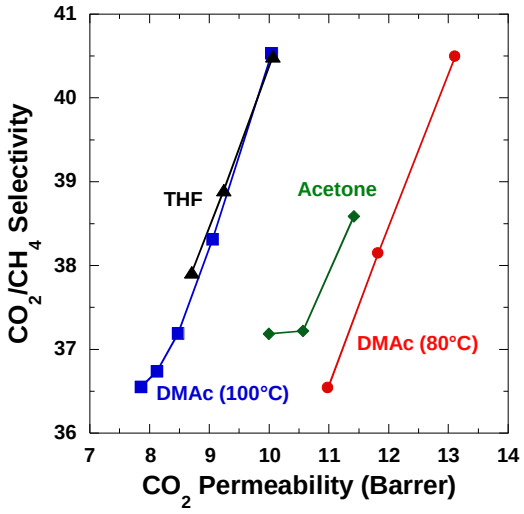

Figure E.6. CO_2/CH_4 selectivity versus CO_2 permeability in HAB-6FDA-CI polyimide cast using acetone (♦), THF (▲), and DMAc at 80°C (●), and DMAc at 100°C (■).

Permeability of CO_2 and CH_4 was higher in HAB-6FDA-TR400 than in the polyimide precursor, consistent with previous reports [8]. As shown in Figure E.7, CO_2 and CH_4 permeability showed no significant pressure dependence. Additionally, CO_2 permeability varied about 40% between the different castings and CH_4 permeability varied about 80%. CO_2 and CH_4 permeability increased in the following order: THF < DMAc(100°C) < Acetone < DMAc(80°C). This indicates that the processing conditions that affect transport properties of the polyimide also have an effect on the transport properties of the corresponding TR polymers. While the polyimide precursor films showed no significant differences in CO_2/CH_4 selectivity, the CO_2/CH_4 selectivity in the HAB-6FDA-TR400 decreased slightly with increasing CO_2 permeability across the film casting procedures (cf. Figure E.8).

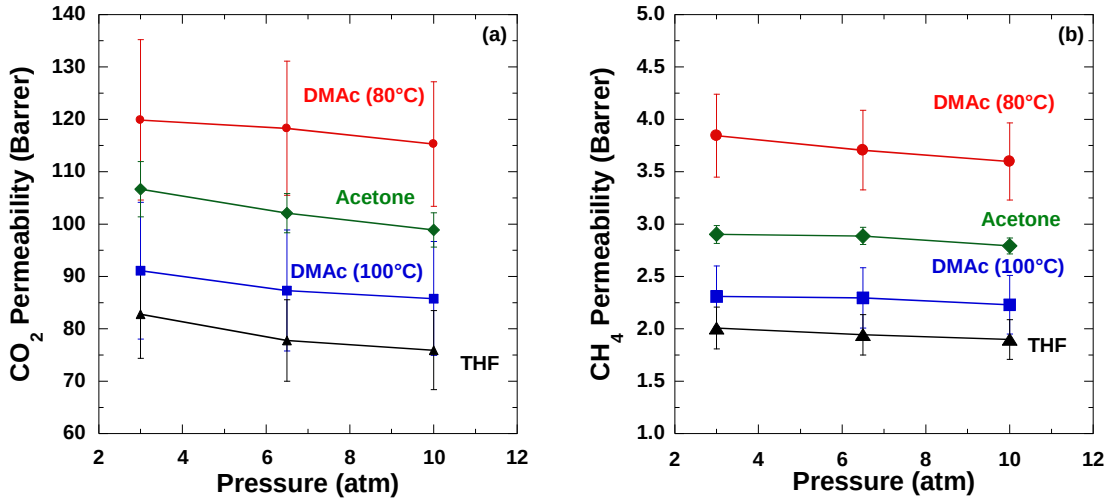

Figure E.7. (a) CO_2 permeability and (b) CH_4 permeability in HAB-6FDA-TR400, where the precursor was cast using acetone (♦), THF (▲), and DMAc at 80°C (●), and DMAc at 100°C (■).

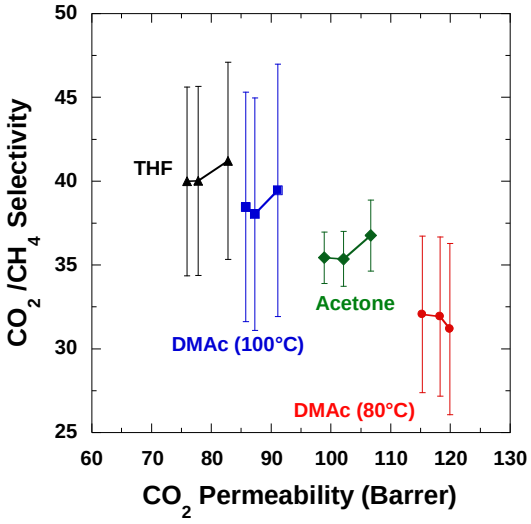

Figure E.8. CO_2/CH_4 selectivity versus CO_2 permeability in HAB-6FDA-TR400, where the precursor was cast using acetone (♦), THF (▲), and DMAc at 80°C (●), and DMAc at 100°C (■).

In an attempt to probe the difference between the four casting procedures, the densities of the polyimide precursor and HAB-6FDA-TR400 were measured using Archimedes' Principle. The fractional free volume (FFV) was calculated using group contribution theory with the occupied volume estimated by percent conversion to the PBO structure, as described previously [8]. The density and FFV values of the precursor and HAB-6FDA-TR400 films are reported in Table E.3 and are similar to values reported previously [3, 5, 6, 8, 15]. However, due to the uncertainty associated with the density measurement, no significant differences in density or fractional free volume was observed between the different casting procedures for both the polyimide precursor and HAB-6FDA-TR400. To better understand the difference in polymer structure, it is suggested that wide angle x-ray scattering (WAXS) be used to better detect differences in inter-chain d-spacing for samples with different processing histories.

Polymer	Casting Procedure	Density [cm^3/g]	FFV
Polyimide	DMAc(100°C)	1.417 ± 0.009	0.152 ± 0.002
	DMAc(80°C)	1.420 ± 0.009	0.151 ± 0.002
	Acetone	1.421 ± 0.007	0.150 ± 0.002
	THF	1.410 ± 0.007	0.156 ± 0.002
TR400	DMAc(100°C)	1.343 ± 0.007	0.195 ± 0.002
	DMAc(80°C)	1.332 ± 0.009	0.202 ± 0.002
	Acetone	1.339 ± 0.007	0.198 ± 0.002
	THF	1.334 ± 0.008	0.201 ± 0.002

Table E.3. Density and FFV of polyimide precursor and TR-400 samples of HAB-6FDA-CI. Values were measured using Archimedes' Principle, using *n*-heptane as the buoyancy liquid.

E.4. Solvent Weight Fraction at the Glass Transition

Because both the casting solvent and processing temperature affect the transport properties of the polyimide precursor and the corresponding TR polymer, it is believed that the different transport properties are due to the quantity of residual solvent in the polymer when a solid film is formed. As described by Weill and Dechenaux, a solution-cast polymer is formed by evaporation of the solvent through the process described in Figure E.9 [18]. As the solvent evaporates from the surface, a concentration gradient forms, with the highest polymer concentration at the solution surface (steps A and B in Figure E.9). The polymer concentration at the surface eventually reaches a critical concentration where a solid "crust" forms over the viscous solution (step C in Figure E.9). The formation of the crust during evaporation is believed to be related to the point at which the solvent-polymer mixture transitions from behaving as a rubber, or gel, to behaving and possessing the physical properties of a glass. The thickness of the crust increases as solvent evaporation continues, resulting in a uniform film that still retains a small amount of residual solvent [18, 19].

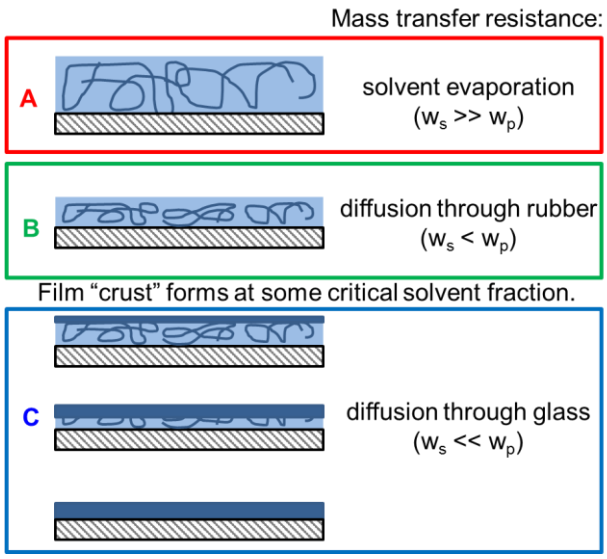

Figure E.9. Steps of film formation during solution casting where w_s and w_p represent the weight fraction in the solvent and polymer, respectively [18].

The critical polymer concentration at which the crust forms and the amount of residual solvent in the film can be estimated using the Fox equation, which estimates the glass transition temperature of a mixture, $T_{g,mix}$, based on the polymer and solvent T_g's, according to Eq. E.1,

$$\frac{1}{T_{g,mix}} = \frac{w_p}{T_{g,p}} + \frac{w_s}{T_{g,s}} \qquad \text{Eq. E.1}$$

where w_p is the polymer weight fraction, w_s is the solvent weight fraction, $T_{g,p}$ is the polymer glass transition temperature, and $T_{g,s}$ is the solvent glass transition temperature. The glass transition temperature of the mixture for this work is considered to be the temperature at which a solid film is formed during the casting procedure, T_{solid}. The T_g values for THF, acetone, DMAc, and HAB-6FDA-CI are recorded in Table E.4, along with the estimated solvent weight fraction at the glass transition. The solvent weight fraction at the mixture T_g in HAB-6FDA-CI polyimide precursor increases in the following order: THF < DMAc(100°C) < Acetone < DMAc(80°C).

Solvent/Polymer	T_g [K]	T_{solid} [K]	w_s
THF [20]	85	298	0.155
Acetone [21]	100	298	0.190
DMAc [22]	150	353	0.210
		373	0.180
HAB-6FDA-CI [7]	553	--	--

Table E.4. Glass transition temperature of the solvents used in this study, casting temperature at which a solid film is formed (T_{solid}), and estimated solvent weight fraction, w_s, in the film when the solvent-polymer mixture transitions to a glass (i.e., when $T_{g,mix} = T_{solid}$).

As shown in Figure E.10-a and Figure E.10-b, CO_2 permeability in both HAB-6FDA-CI polyimide precursor and HAB-6FDA-TR400 increased with increasing residual solvent weight fraction. Although the residual solvent had been completely removed from the polyimide when permeation measurements were made, we speculate that the amount of residual solvent affects FFV and the distribution of the free volume elements in the polyimide precursor. While no measureable difference in FFV was detected using experimental density values, we previously showed slight differences in FFV can fall within experimental uncertainty while still resulting in different gas transport properties (cf., Chapter 4). After the polymer-solvent mixture passes through its glass transition, polymer chain motion slows enormously [23]. This makes it likely that the FFV and free volume distribution of the solvent-free polyimide is dependent on the presence of residual solvent during the transition of the mixture from a gel to a glass. Additionally, since the thermal rearrangement starts to occur around the T_g of the polyimide precursor (280°C), the differences in FFV and free volume distribution are also reflected in the corresponding TR polymers (cf., Figure E.10-b).

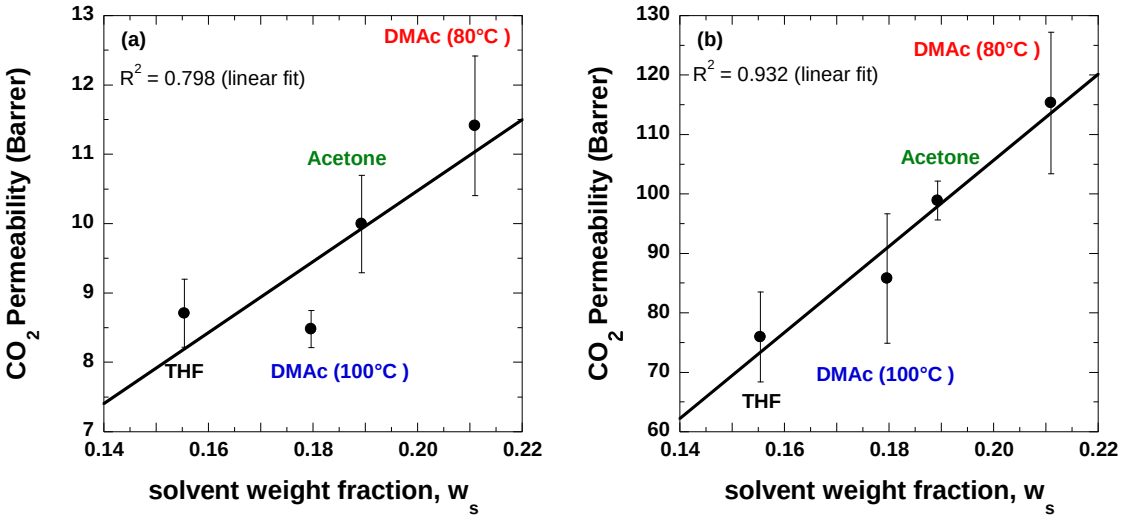

Figure E.10. CO_2 permeability in (a) HAB-6FDA-CI polyimide and (b) HAB-6FDA-TR400 versus weight fraction of solvent, w_s, remaining in the film during the solvent-polymer glass transition during casting of the film. The solid lines represent the linear trend of permeability with w_s.

E.5. Conclusions

HAB-6FDA-CI polyimide precursor was cast from DMAc, THF, and acetone, using three different casting procedures. Due to the differences in the casting solvent and temperature at which a solid film was formed, CO_2 and CH_4 permeability in HAB-6FDA-CI polyimide varied by about 40% between the different castings. Additionally, after thermal rearrangement, CO_2 permeability in HAB-6FDA-TR400 varied about 50% between the different castings, and CH_4 permeability varied about 80%. While no significant differences in FFV were measured using experimental density values, the transport properties correlate qualitatively with the solvent remaining in the polymer when a solid film is formed during casting. Due to the glass transition and thermal rearrangement occurring around the same temperature, the differences in the polyimide transport properties were still present after thermal rearrangement.

E.6. References

[1] H.B. Park, S.H. Han, C.H. Jung, Y.M. Lee, A.J. Hill, Thermally Rearranged (TR) Polymer Membranes for CO_2 Separation, Journal of Membrane Science, 359 (2010) 11-24.

[2] J.I. Choi, C.H. Jung, S.H. Han, H.B. Park, Y.M. Lee, Thermally Rearranged (TR) Poly(benzoxazole-co-pyrrolone) Membranes Tuned for High Gas Permeability and Selectivity, Journal of Membrane Science, 349 (2010) 358-368.

[3] K.L. Gleason, Z.P. Smith, Q. Liu, D.R. Paul, B.D. Freeman, Pure- and Mixed-Gas Permeation of CO_2 and CH_4 in Thermally Rearranged Polymers Based on 3,3′ -Dihydroxy-4,4′ -Diamino-Biphenyl (HAB) and 2,2′ -Bis-(3,4-Dicarboxyphenyl) Hexafluoropropane Dianhydride (6FDA), Journal of Membrane Science, 475 (2015) 204-214.

[4] R. Guo, D.F. Sanders, Z.P. Smith, B.D. Freeman, D.R. Paul, J.E. McGrath, Synthesis and Characterization of Thermally Rearranged (TR) polymers: Influence of Ortho-Positioned Functional Groups of Polyimide Precursors on TR process and Gas Transport Properties, Journal of Materials Chemistry A, 1 (2013) 262-272.

[5] D. Sanders, The Effect of Synthesis Route and ortho-Position Functional Group on Thermally Rearranged Polymer Thermal and Transport Properties, Docor of Philosophy, The University of Texas at Austin, 2013.

[6] D.F. Sanders, R. Guo, Z.P. Smith, K.A. Stevens, Q. Liu, J.E. McGrath, D.R. Paul, B.D. Freeman, Influence of Polyimide Precursor Synthesis Route and Ortho-Position Functional Group on Thermally Rearranged (TR) Polymer Properties: Pure gas Permeability and Selectivity, Journal of Membrane Science, 463 (2014) 73-81.

[7] Z.P. Smith, D.F. Sanders, C.P. Ribeiro, R. Guo, B.D. Freeman, D.R. Paul, J.E. McGrath, S. Swinnea, Gas Sorption and Characterization of Thermally Rearranged Polyimides Based on 3,3′ -Dihydroxy-4,4′ -Diamino-Biphenyl (HAB) And 2,2′ -Bis-(3,4-Dicarboxyphenyl) Hexafluoropropane Dianhydride (6FDA), Journal of Membrane Science, 415-416 (2012) 558-567.

[8] D.F. Sanders, Z.P. Smith, C.P. Ribeiro, R. Guo, J.E. McGrath, D.R. Paul, B.D. Freeman, Gas Permeability, Diffusivity, and Free Volume of Thermally Rearranged Polymers Based on 3,3'-Dihydroxy-4,4'-Diamino-Biphenyl (HAB) and 2,2'-Bis-(3,4-

Dicarboxyphenyl) Hexafluoropropane Dianhydride (6FDA), Journal of Membrane Science, 409-410 (2012) 232-241.

[9] L.M. Robeson, Correlation of Separation Factor Versus Permeability for Polymeric Membranes, Journal of Membrane Science, 62 (1991) 165-185.

[10] L.M. Robeson, The Upper Bound Revisited, Journal of Membrane Science, 320 (2008) 390-400.

[11] H.B. Park, C.H. Jung, Y.M. Lee, A.J. Hill, S.J. Pas, S.T. Mudie, E. Van Wagner, B.D. Freeman, D.J. Cookson, Polymers with Cavities Tuned for Fast Selective Transport of Small Molecules and Ions, Science, 318 (2007) 254-258.

[12] L.M. Robeson, B.D. Freeman, D.R. Paul, B.W. Rowe, An Empirical Correlation of Gas Permeability and Permselectivity in Polymers and Its Theoretical Basis, Journal of Membrane Science, 341 (2009) 178-185.

[13] W.J. Koros, G.K. Fleming, Membrane-Based Gas Separation, Journal of Membrane Science, 83 (1993) 1-80.

[14] Y. Jiang, F.T. Willmore, D. Sanders, Z.P. Smith, C.P. Ribeiro, C.M. Doherty, A. Thornton, A.J. Hill, B.D. Freeman, I.C. Sanchez, Cavity Size, Sorption and Transport Characteristics of Thermally Rearranged (TR) Polymers, Polymer, 52 (2011) 2244-2254.

[15] R. Guo, D.F. Sanders, Z.P. Smith, B.D. Freeman, D.R. Paul, J.E. McGrath, Synthesis and Characterization of Thermally Rearranged (TR) Polymers: Effect of Glass Transition Temperature of Aromatic Poly(hydroxyimide) Precursors on TR Process and Gas Permeation Properties, Journal of Materials Chemistry A, 1 (2013) 6063-6072.

[16] Y. Huang, D. Paul, Experimental Methods for Tracking Physical Aging of Thin Glassy Polymer Films by Gas Permeation, Journal of Membrane Science, 244 (2004) 167-178.

[17] J.H. Kim, W.J. Koros, D.R. Paul, Physical Aging of Thin 6FDA-Based Polyimide Membranes Containing Carboxyl Acid Groups. Part I. Transport Properties, Polymer, 47 (2006) 3094-3103.

[18] A. Weill, E. Dchenaux, The Spin-Coating Process Mechanism Related to Polymer Solution Properties, Polymer Engineering and Science, 28 (1988) 945 - 948.

[19] R.B. Bird, W.E. Stewart, E.N. Lightfoot, Transport Phenomena, 2nd ed., John Wiley & Sons, 1961.

[20] O. Yamamuro, M. Oguni, T. Matsuo, H. Suga, Calorimetric Study of Pure and KOH-doped Tetrahydrofuran Clathrate Hydrate, Journal of Physics and Chemsitry of Solids, 49 (1988) 425 - 434.

[21] A.V. Lesikar, Effect of Association Complexes on the Glass Transition in Organic Halide Mixtures, The Journal of Physical Chemistry, 80 (1976) 1005 - 1011.

[22] E.J. Sare, C.A. Angell, Glass-Forming Composition Regions and Glass Transition Temperature in Nonaqueous Electrolyte Solutions, Journal of Solution Chemistry, 2 (1973) 53 - 57.

[23] J.H. Gibbs, E.A. DiMarzio, Nature of the Glass Transition and the Glassy State, The Journal of Chemical Physics, 28 (1958) 373.

APPENDIX F: UV CROSS-LINKED POLY(ARYLENE ETHER KETONE)S FOR OLEFIN PARAFFIN SEPARATIONS

This study focuses on the permeability of C_2H_4 and C_2H_6 in UV cross-linked poly(arylene ether ketones) (PAEKs). Initial results show PAEKs cross-linked with 365 nm light have improved ethylene/ethane selectivity over their linear analogs, but significant plasticization at high pressures (up to 27 atm) still occurs after cross-linking. These results have been attributed to non-uniform cross-linking throughout the thickness (15 μm) of the membrane. UV-vis spectroscopy and FT-IR analysis indicate UV intensity (and thus likely cross-linking), can vary as much as 60% in a 27 μm thick film and 10% in an 8 μm thick film. Due to the non-uniform cross-linking, it is difficult to isolate how UV cross-linking affects the plasticization resistance PAEKs to C_2H_4 and C_2H_6.

F.1. Introduction

Poly(arylene ether ketone)s, or PAEKs, were chosen as the initial polymer system for this study due to the commercial availability of several different monomer units, ability to crosslink over a wide range of UV light wavelengths, and their amorphous, glassy properties. Tetramethyl-bisphenol A benzophenone (TMBPA-BP) and dimethyl-phenylflorene benzophenone (DMPF-BP) were selected as the starting structures.

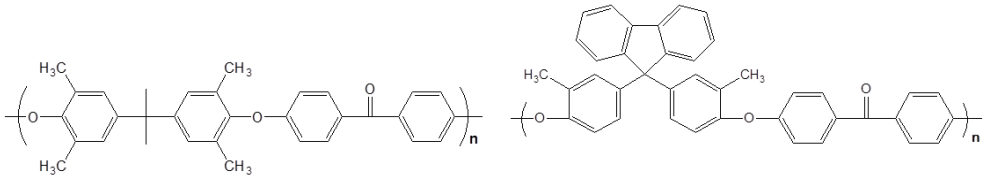

Figure F.1. Structures of the PAEKs proposed for this study, with TMBPA-BP on left and DMPF-BP on the right.

PAEKs contain both benzylic and aliphatic hydrogens as well as benzophenone (BP) group(s). The photochemical crosslinking mechanism for these polymer moieties has been widely studied due to their prominence in adhesives, UV-curable coatings, and protein engineering [1, 2]. Upon radiation by UV light, the BP group is excited, and two radicals are generated. Subsequently, the radicals can abstract a neighboring benzylic or aliphatic hydrogen to yield a ketyl radical and a carbon-centered radical [3, 4]. The radicals can then either form crosslinks or potentially undergo an oxidation reaction if oxygen is present. This crosslinking mechanism for TMBPA-BP is given in Figure F**.2** below.

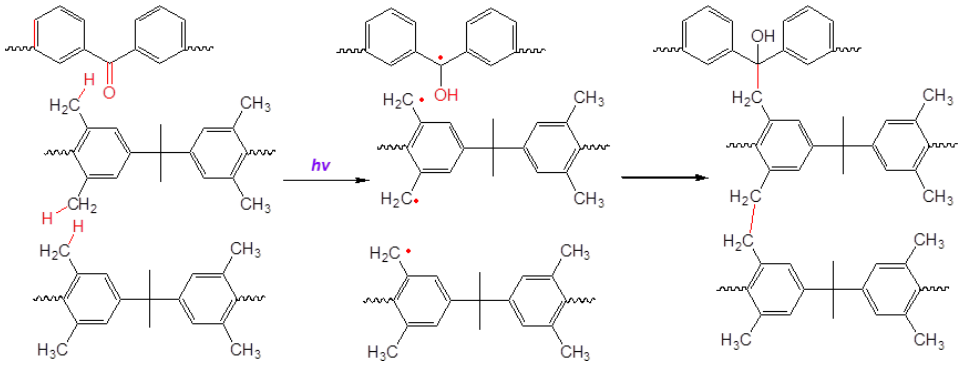

Figure F.2. UV induced cross-linking mechanism of PAEKs, demonstrated with TMBPA-BP, through the excitement of the benzophenone group, abstraction of neighboring benzylic or aliphatic hydrogens, and eventual cross-linking [4, 5].

F.2. Materials and Methods

F.2.1. PEAK Synthesis

TMBA-BP and DMHPF-BP were synthesized using the same method. A 250 mL three neck flask was equipped with a mechanical stirring rod, a Dean-Stark apparatus, a condenser, and a nitrogen purge. TMBPA and DFBP monomers (25 mmol each) were added to the reaction flask with K_2CO_3 (60 mmol), 60 mL of DMAc, and 25 mL of toluene. While stirring slowly, the solution was heated to 155°C using an aluminum heating block and maintained at this temperature for 16 h. After cooling to 90°C, the resulting viscous solution was precipitated in a water and acetic acid solution (4:1 by volume), washed and soaked in water for 24 h. After filtering, the resulting polymer was dried at 100°C under vacuum for 24 h to remove any residual solvent. Dense films, with target thicknesses of 10-20 μm, were formed by casting the PAEKs from a 2 wt% solution of toluene. The toluene was allowed to evaporate under ambient conditions, then residual solvent was removed by drying the samples at 120°C for 24 h under vacuum.

F.2.2. UV Cross-linking

Crosslinking was performed by irradiating polymer films in air under a 100 W high intensity, long-wave UV lamp equipped with a 365-nm light filter (Blak-Ray B-100, UVP). Films prepared for gas permeation were placed about 3.5 cm from the UV lamp and irradiated for one hour on each side. At this distance, the UV intensity was measured to be 19.7 mW/cm^2. For FT-IR experiments, the irradiation time was varied from 10 – 60 min per side.

F.2.3. UV-Vis Spectroscopy

UV-vis spectroscopy was performed on dense, flat films of varying thickness using a Cary 5000UV-VIS NIR over a spectral range of 175 – 3300 nm using a single beam. Three separate films of each thickness were tested and the averages are reported.

F.2.4. Gel Fraction

Gel fractions were measured using Soxhlet extraction, as described in Chapter 2, using toluene as the solvent. The non-UV treated samples were completely soluble and the PAEK films cross-linked for 60 min/side had gel fractions >99%.

F.3. Results and Discussion

F.3.1. Plasticization resistance to C_2H_4 and C_2H_6

As a first step, the pure gas permeability of ethane and ethylene in TMBPA-BP and DMHPF-BP were measured at 35°C between 3 – 30 atm. To determine the effect of UV cross-linking, a 13.5 μm thick TMBPA-BP film was exposed to 365 nm light for 1 h on each side (68 J/cm^2 per side). UV-crosslinking TMBPA-BP slightly increased the ethylene/ethane selectivity while decreasing the ethylene permeability (cf., Figure F.3). However, significant decreases in selectivity and increase in permeability were observed

as pressure increased for the cross-linked PAEK films, indicating plasticization is occurring after cross-linking.

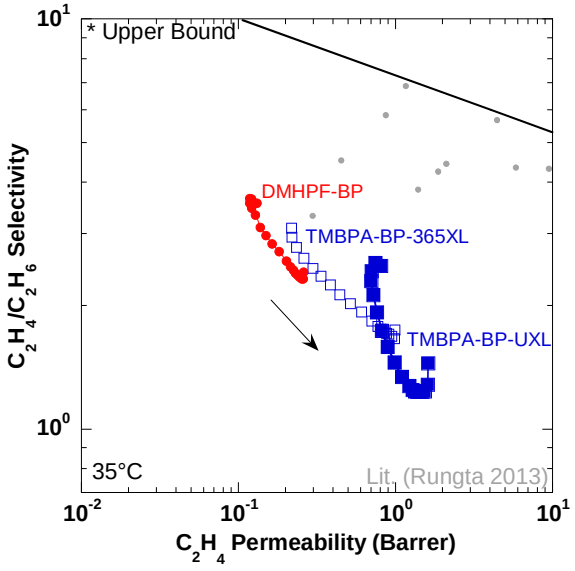

Figure F.3. Upper bound plot for ideal ethylene/ethane selectivity at 35°C. Blue squares indicate uncross-linked (filled) and crosslinked (open) TMBPA-BP films. Red circles indicate DMBPA-BP films. The arrow denotes the direction of increasing feed pressure.

F.3.2. Testing Cross-linking Uniformity with UV-vis Spectroscopy

To help isolate the source of the apparent plasticization after cross-linking, UV-vis spectroscopy was performed on two uncross-linked TMBPA-BP films, 27 µm and 8 µm thick. As shown in Figure F.4-a, the TMBPA-BP films have high absorbance in the UV range (<400 nm), with the 27 µm thick film being greater than that of the 8 µm thick film. The extent of crosslinking at any point in a film could potentially depend on the UV intensity reaching that location. As radiation is absorbed by a film, the radiation intensity naturally decreases as UV penetrates deeper into the film. If there is a sharp gradient of UV intensity between the surface and the center of a film, crosslinking may not be uniform. A profile of UV intensity within a film can be described by the Beer-Lambert Law and the

relative intensity of 365 nm light as a function of the normalized film thickness is shown in Figure F.4 [6]. From these results, even a film 8 μm thick will have at least 10% variation in UV exposure, which could contribute to non-homogeneous crosslinking throughout the film thickness.

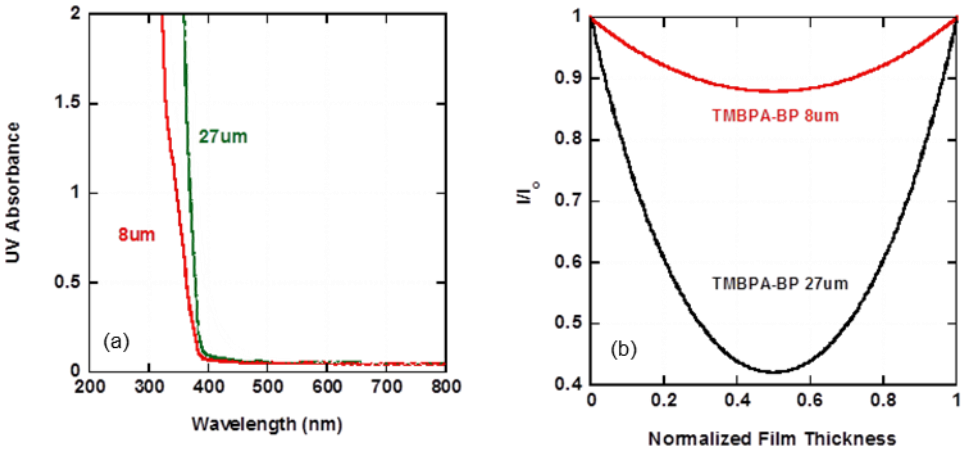

Figure F.4. (a) UV-vis absorbance of TMBPA-BP films versus the radiation wavelength and (b) the calculated intensity of irradiation with 365 nm wavelength, I, relative to the surface intensity, I_o, as a function of the distance from the film surface for films irradiated on both sides. These calculations were performed as reported previously [6].

F.3.3. Testing Cross-linking Uniformity and UV-induced Oxidation with FT-IR

These results are further supported by an FT-IR study (cf., Figure F.5), where ATR and transmission mode FT-IR spectra indicated non-homogeneous cross-linking throughout the films. The effect on UV-exposure time was investigated by exposing 15 μm thick TMBPA-BP films to 365 nm light with 19.7 mW/cm^2 intensity from 0-60 min per side and monitoring signature peaks in the FT-IR sepectra using both ATR and transmission modes. The FTIR spectra were normalized to the aromatic C=C peak at 1600 cm^{-1}. The ATR mode monitors changes in the surface of the film while transmission mode monitors changes throughout the film. Cross-linking can be tracked via evolution of the hydroxyl peak, 3660 – 3000 cm^{-1}, corresponding to the –OH group formed during

crosslinking and the decrease in the C=O peak at 1650 cm^{-1}, corresponding to disappearance of benzophenone groups. As shown in Figure F.5, the ATR mode spectra show a significant increase in the hydroxyl peak, but transmission mode reveals only a modest increase in absorbance in this region. This result further supports that significant crosslinking is occurring at the surface of the film, but likely less UV-induced crosslinking is taking place at the center of the film. It would be of interest to study even thinner films (< 1 μm) to ensure uniform cross-linking throughout the film.

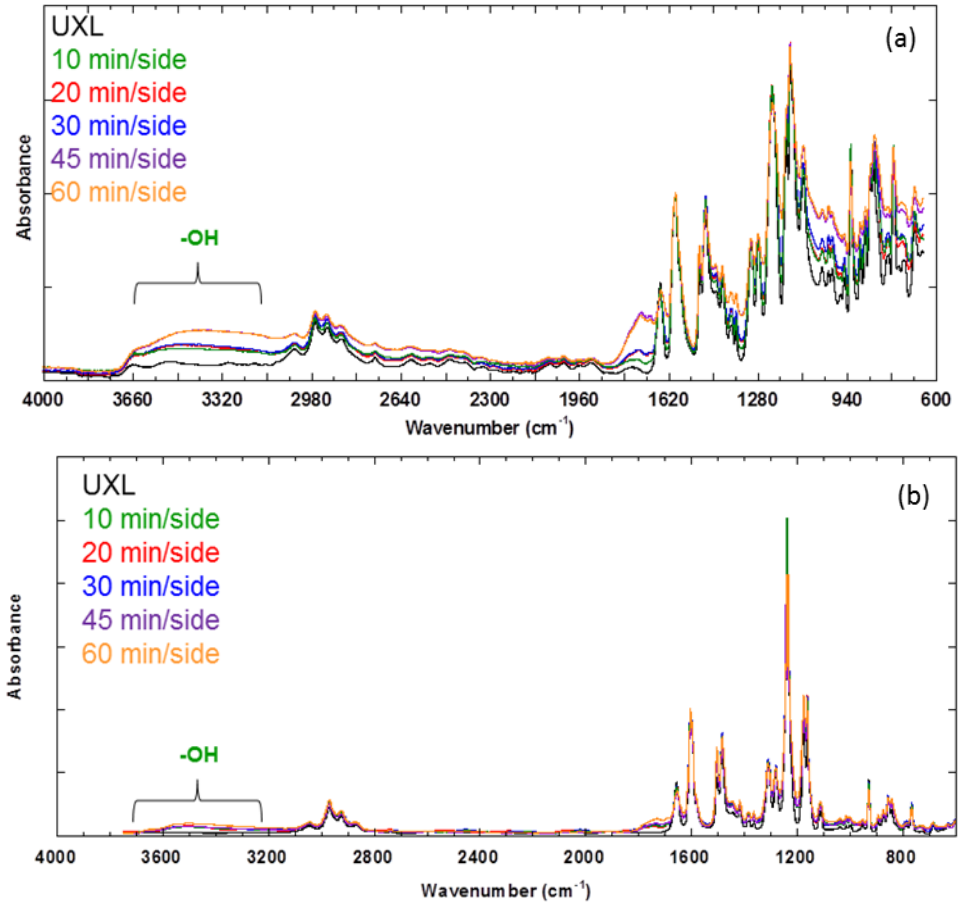

Figure F.5. FT-IR spectra in (a) ATR and (b) transmission modes of TMBPA-BP film (15 μm thick) exposed to 0 min/side (UXL), 10 min/side (green), 20 min/side (red), 30 min/side (blue), 45 min/side (purple), and 60 min/side (orange) of 365 nm light at 19.7 mW/cm^2.

F.4. Conclusions

After cross-linking TMBPA-BP by exposing to 365 nm light for 1 h on each side, C_2H_4 permeability decreased and C_2H_4/C_2H_6 selectivity decreased significantly with increasing pressure. While cross-linking decreased the permeability, the decrease in selectivity suggesting plasticization was occurring in the cross-linked membrane. UV-vis and FT-IR of the cross-linked films revealed UV-exposure, and thus potentially cross-linking, was not uniform throughout the film thickness. This suggests that plasticization may be occurring in the center of the film, potentially reducing the C_2H_4/C_2H_6 selectivity, while the cross-linking at the surface of the film possibly reduced the overall permeability of TMBPA-BP, as has been observed previously with other gases [6]. To further investigate how UV cross-linking affects plasticization resistance of PAEKs, it is suggested films less than 1 μm are used to ensure uniform cross-linking. Due to the low permeability and low C_2H_4/C_2H_6 selectivity of these materials, this study was not continued.

F.5. References

[1] S.K. Christensen, M.C. Chiappelli, R.C. Hayward, Gelation of Copolymers with Pendent Benzophenone Photo-cross-linkers, Macromolecules, 45 (2012) 5237-5246.

[2] G. Eisele, J.P. Fouassier, R. Reeb, Kinetics of Photocrosslinking Reactions of a DCPA/EA Matrix in the Presence of Thiols and Acrylates, Journal of Polymer Science, Part A: Polymer Chemistry, 35 (1997) 2333-2345.

[3] A.A. Lin, V.R. Sastri, G. Tesoro, A. Reiser, R. Eachus, On the Crosslinking mechanism of Benzophenone-Containing Polyimides, Macromolecules, 21 (1988) 1165-1169.

[4] G. Porter, F. Wilkinson, Primary Photochemical Processes in Aromatic Molecules. Part 5. Flash Photolysis of Benzophenone in Solution, Transactions of the Faraday Society, 57 (1961) 1686-1686.

[5] A.A. Lin, V.R. Sastri, Giuliana Tesoro, A. Reiser, On the Cross-Linking Mechanism of Benzophenone-Containing Polyimides, Macromolecules, 21 (1988) 1165 - 1169.

[6] B.J. Sundell, A.T. Shaver, Q. Liu, A. Nebipasagil, P. Pisipati, S.J. Mecham, J.S. Riffle, B.D. Freeman, J.E. McGrath, Synthesis, Oxidation and Crosslinking of Tetramethyl Bisphenol F (TMBPF)-Based Polymers for Oxygen/Nitrogen Gas Separations, Polymer, 55 (2014) 5623-5634.

Bibliography

Chapter 1

A. Bos, I.G.M. Pu, M. Wessling, S. H, Suppression of CO2 Plasticization by Semiinterpenetrating Polymer Network Formation, Journal of Polymer Science Part B: Polymer Physics, 36 (1997) 1547-1556.

A. Bos, I. Pünt, H. Strathmann, M. Wessling, Suppression of Gas Separation Membrane Plasticization by Homogeneous Polymer Blending, AIChE Journal, 47 (2001) 1088-1093.

R.L. Burns, W.J. Koros, Defining the Challenges for C3H6/C3H8 Separation Using Polymeric Membranes, Journal of Membrane Science, 211 (2003) 299-309.

M.E. Dose, M. Chwatko, I. Hubacek, N.A. Lynd, D.R. Paul, B.D. Freeman, Thermally Cross-linked Diaminophenylindane (DAPI) Containing Polyimides for Membrane Based Gas Separations, Polymer, Submitted (2018).

M.E. Dose, I. Hubacek, D.R. Paul, B.D. Freeman, CO2, C2H4, and C2H6 Sorption and Mixed Gas Permeability of Thermally Cross-linked Diaminophenylindane (DAPI) Containing Polyimides, Journal of Membrane Science, Submitted (2018).

M.E. Dose, J.D. Moon, I. Hubacek, D.R. Paul, B.D. Freeman, Fundamental Gas Transport and Dilation of Studies in Thermally Cross-linked Diaminophenylindane (DAPI) Containing Polyimides, Journal of Polymer Science Part B: Polymer Physics, In Submission (2018).

N. Du, M.M. Dal-Cin, G.P. Robertson, M.D. Guiver, Decarboxylation-Induced Cross-Linking of Polymers of Intrinsic Microporosity (PIMs) for Membrane Gas Separation, Macromolecules, 45 (2012) 5134-5139.

B.R. Eldridge, Olefin/Paraffin Separation Technology: A Review Industrial & Engineering Chemistry Research, 32 (1993) 2208-2212.

I.V. Farr, Synthesis and Characterization of Novel Polyimide Gas Separation Membrane Material Systems, Virginia Polytechnic Institute and State University 1999.

I.V. Farr, D. Kratzner, T.E. Glass, D. Dunson, Q. Ji, J.E. McGrath, The Synthesis and Characterization of Polyimide Homopolymers Based on 5(6)-Amino-1-(4-Aminophenyl)1,3,3-Trimethylindane, J Polym Sci Pol Chem, 38 (2000) 2840-2854.

B.D. Freeman, Basis of Permeability/Selectivity Tradeoff Relations in Polymeric Gas Separation Membranes, Macromolecules, 32 (1999) 375-380.

A.M. Kratochvil, W.J. Koros, Decarboxylation-Induced Cross-Linking of a Polyimide for Enhanced CO2 Plasticization Resistance, Macromolecules, 41 (2008) 7920-7927.

N.L. Le, Y. Wang, T.-S. Chung, Synthesis, Cross-linking Modifications of 6FDA-NDA/DABA Polyimide Membranes for Ethanol Dehydration via Pervaporation, Journal of Membrane Science, 415-416 (2012) 109-121.

J.H. Petropoulos, Mechanisms and Theories for Sorption and Diffusion of Gases in Polymers, in: Polymeric Gas Separation Membranes, CRC Press, Inc, Boca Raton, FL, 1994.

W. Qiu, C.-C. Chen, L. Xu, L. Cui, D.R. Paul, W.J. Koros, Sub-Tg Cross-Linking of a Polyimide Membrane for Enhanced CO2 Plasticization Resistance for Natural Gas Separation, Macromolecules, 44 (2011) 6046-6056.

L.M. Robeson, Correlation of Separation Factor Versus Permeability for Polymeric Membranes, Journal of Membrane Science, 62 (1991) 165-185.

L.M. Robeson, The Upper Bound Revisited, Journal of Membrane Science, 320 (2008) 390-400.

L.M. Robeson, M.E. Dose, B.D. Freeman, D.R. Paul, Analysis of the Transport Properties of Thermally Rearranged (TR) Polymers and Polymers of Intrinsic Microporosity (PIM) Relative to Upper Bound Performance, Journal of Membrane Science, 525 (2017) 18-24.

C. Staudt-Bickel, W. J. Koros, Improvement of CO2/CH4 Separation Characteristics of Polyimides by Chemical Crosslinking, Journal of Membrane Science, 155 (1999) 145-154.

K. Tanaka, A. Taguchi, J. Hao, H. Kita, K. Okamoto, Permeation and Separation Properties of Polyimide Membranes to Olefins and Paraffins, Journal of Membrane Science, 121 (1996) 197-207.

C. Zhang, P. Li, B. Cao, Decarboxylation Crosslinking of Polyimides with High CO2/CH4 Separation Performance and Plasticization Resistance, Journal of Membrane Science, 528 (2017) 206-216.

C. Zhou, The Accelerated CO2 Plasticization of Ultra-Thin Polyimide Films and the Effect of Surface Chemical Cross-linking on Plasticization and Physical Aging, Journal of Membrane Science, 225 (2003) 125-134.

Chapter 2

P.R. Bevington, D.K. Robinson, Error Analysis, in: Data Reduction and Error Analysis, McGraw-Hill, New York, NY, 2003, pp. 36-50.

N. Du, M.M. Dal-Cin, G.P. Robertson, M.D. Guiver, Decarboxylation-Induced Cross-Linking of Polymers of Intrinsic Microporosity (PIMs) for Membrane Gas Separation, Macromolecules, 45 (2012) 5134-5139.

S.H. Han, N. Misdan, S. Kim, C.M. Doherty, A.J. Hill, Y.M. Lee, Thermally Rearranged (TR) Polybenzoxazole: Effects of Diverse Imidization Routes on Physical Properties and Gas Transport Behaviors, Macromolecules, 43 (2010) 7657-7667.

C.P.R. Jr., B.D. Freeman, Sorption, Dilation, and Partial Molar Volumes of Carbon Dioxide and Ethane in Cross-Linked Poly(ethylene oxide), Macromolecules, 41 (2008) 9458-9468.

A.M. Kratochvil, W.J. Koros, Decarboxylation-Induced Cross-Linking of a Polyimide for Enhanced CO2 Plasticization Resistance, Macromolecules, 41 (2008) 7920-7927.

N.L. Le, Y. Wang, T.-S. Chung, Synthesis, Cross-linking Modifications of 6FDA-NDA/DABA Polyimide Membranes for Ethanol Dehydration via Pervaporation, Journal of Membrane Science, 415-416 (2012) 109-121.

E.W. Lemmon, M.O. McLinden, D.G. Friend, Thermophysical Properties of Fluid Systems, in: P.J. Linstrom, W.G. Mallard (Eds.) NIST Chemistry WebBook, NIST Standard Reference Database Number 69, National Institute of Standards and Technology, Gaithersburg MD, 2018.

H. Lin, B.D. Freeman, Chapter 7: Permeation and Diffusion, in: Springer Handbook of Materials Measurement Methods, 2006, pp. 371-387.

K.C. O'Brien, W.J. Koros, T.A. Barbari, A New Technique for the Measurement of Multicomponent Gas Transport Through Polymeric Films, Journal of Membrane Science, 29 (1986) 229-238.

D.R. Paul, Gas Sorption and Transport in Glassy Polymers, Reports of the Bunsen Society for Physical Chemistry, 83 (1979) 294-302.

W. Qiu, C.-C. Chen, L. Xu, L. Cui, D.R. Paul, W.J. Koros, Sub-Tg Cross-Linking of a Polyimide Membrane for Enhanced CO2 Plasticization Resistance for Natural Gas Separation, Macromolecules, 44 (2011) 6046-6056.

R. Raharjo, B. Freeman, E. Sanders, Pure and Mixed Gas CH4 and n-C4H10 Sorption and Dilation in Poly(dimethylsiloxane), Journal of Membrane Science, 292 (2007) 45-61.

C. Staudt-Bickel, W. J. Koros, Improvement of CO2/CH4 Separation Characteristics of Polyimides by Chemical Crosslinking, Journal of Membrane Science, 155 (1999) 145-154.

[14] J.G. Wijmans, R.W. Baker, The Solution-Diffustion Model: A Review, Journal of Membrane Science, 107 (1995) 1-21.

C. Zhang, P. Li, B. Cao, Decarboxylation Crosslinking of Polyimides with High CO2/CH4 Separation Performance and Plasticization Resistance, Journal of Membrane Science, 528 (2017) 206-216.

Chapter 3

A. Alentiev, Y. Yampolskii, Correlation of Gas Permeability and Diffusivity with Selectivity: Orientations of the Clouds of the Data Points and the Effects of Temperature, Industrial & Engineering Chemistry Research, 52 (2013) 8864-8874.

R.W. Baker, Membrane Technology and Applications, in: Membrane Technology, John Wiley & Sons, Ltd, Chichester, UK, 2004, pp. 545.

R.W. Baker, B.T. Low, Gas Separation Membrane Materials: A Perspective, Macromolecules, 47 (2014) 6999-7013.

R.B. Bird, W.E. Stewart, E.N. Lightfoot, Transport Phenomena, 2nd ed., John Wiley & Sons, 1961.

W.A. Bollinger, D.L. MacLean, R.S. Narayan, Separation Systems For Oil Refining And Production, Chemical Engineering Progress, 78 (1982) 27-32.

D.W. Breck, Zeolite molecular sieves: structure, chemistry, and use, Wiley, New York, 1974.

P. Budd, N. McKeown, B. Ghanem, K. Msayib, D. Fritsch, L. Starannikova, N. Belov, O. Sanfirova, Y. Yampolskii, V. Shantarovich, Gas Permeation Parameters and Other Physicochemical Properties of a Polymer of Intrinsic Microporosity: Polybenzodioxane PIM-1, Journal of Membrane Science, 325 (2008) 851-860.

P. Budd, K. Msayib, C. Tattershall, B. Ghanem, K. Reynolds, N. McKeown, D. Fritsch, Gas separation membranes from polymers of intrinsic microporosity, Journal of Membrane Science, 251 (2005) 263-269.

P.M. Budd, E.S. Elabas, B.S. Ghanem, S. Makhseed, N.B. McKeown, K.J. Msayib, C.E. Tattershall, D. Wang, Solution-Processed, Organophilic Membrane Derived from a Polymer of Intrinsic Microporosity, Advanced Materials, 16 (2004) 456-459.

P.M. Budd, B. Ghanem, K. Msayib, N.B. McKeown, C. Tattershall, A nanoporous network polymer derived from hexaazatrinaphthylene with potential as an adsorbent and catalyst support, Journal of Materials Chemistry, 13 (2003) 2721-2726.

P.M. Budd, B.S. Ghanem, S. Makhseed, N.B. McKeown, K.J. Msayib, C.E. Tattershall, Polymers of intrinsic microporosity (PIMs): robust, solution-processable, organic nanoporous materials, Chemical Communications, (2004) 230-231.

P.M. Budd, N.B. McKeown, D. Fritsch, Free volume and intrinsic microporosity in polymers, Journal of Materials Chemistry, 15 (2005) 1977-1986.

M. Calle, Y.M. Lee, Thermally Rearranged (TR) Poly(ether−benzoxazole) Membranes for Gas Separation, Macromolecules, 44 (2011) 1156-1165.

M. Carta, P. Bernardo, G. Clarizia, J.C. Jansen, N.B. McKeown, Gas Permeability of Hexaphenylbenzene Based Polymers of Intrinsic Microporosity, Macromolecules, 47 (2014) 8320-8327.

M. Carta, M. Croad, R. Malpass-Evans, J.C. Jansen, P. Bernardo, G. Clarizia, K. Friess, M. Lanc, N.B. McKeown, Triptycene induced enhancement of membrane gas selectivity for microporous Troger's base polymers, Adv Mater, 26 (2014) 3526-3531.

M. Carta, R. Malpass-Evans, M. Croad, Y. Rogan, J.C. Jansen, P. Bernardo, F. Bazzarelli, N.B. McKeown, An efficient polymer molecular sieve for membrane gas separations, Science, 339 (2013) 303-307.

J.S. Chiou, D.R. Paul, Gas transport in a thermotropic liquid-crystalline polyester, Journal of Polymer Science Part B: Polymer Physics, 25 (1987) 1699-1707.

Y.J. Cho, H.B. Park, High Performance Polyimide with High Internal Free Volume Elements, Macromolecular Rapid Communications, 32 (2011) 579-586.

B. Comesaña-Gándara, M. Calle, H.J. Jo, A. Hernández, J.G. de la Campa, J. de Abajo, A.E. Lozano, Y.M. Lee, Thermally rearranged polybenzoxazoles membranes with biphenyl moieties: Monomer isomeric effect, Journal of Membrane Science, 450 (2014) 369-379.

M.M. Dal-Cin, A. Kumar, L. Layton, Revisiting the experimental and theoretical upper bounds of light pure gas selectivity–permeability for polymeric membranes, Journal of Membrane Science, 323 (2008) 299-308.

Y.S. Do, J.G. Seong, S. Kim, J.G. Lee, Y.M. Lee, Thermally rearranged (TR) poly(benzoxazole-co-amide) membranes for hydrogen separation derived from 3,3′-dihydroxy-4,4′-diamino-biphenyl (HAB), 4,4′-oxydianiline (ODA) and isophthaloyl chloride (IPCl), Journal of Membrane Science, 446 (2013) 294-302.

N. Du, G.P. Robertson, I. Pinnau, M.D. Guiver, Polymers of Intrinsic Microporosity with Dinaphthyl and Thianthrene Segments, Macromolecules, 43 (2010) 8580-8587.

N. Du, G.P. Robertson, J. Song, I. Pinnau, S. Thomas, M.D. Guiver, Polymers of Intrinsic Microporosity Containing Trifluoromethyl and Phenylsulfone Groups as Materials for Membrane Gas Separation, Macromolecules, 41 (2008) 9656-9662.

B.D. Freeman, Basis of Permeability/Selectivity Tradeoff Relations in Polymeric Gas Separation Membranes, Macromolecules, 32 (1999) 375-380.

D. Fritsch, G. Bengtson, M. Carta, N.B. McKeown, Synthesis and Gas Permeation Properties of Spirobischromane-Based Polymers of Intrinsic Microporosity, Macromolecular Chemistry and Physics, 212 (2011) 1137-1146.

[26] B.S. Ghanem, N.B. McKeown, P.M. Budd, D. Fritsch, Polymers of Intrinsic Microporosity Derived from Bis(phenazyl) Monomers, Macromolecules, 41 (2008) 1640-1646.

B.S. Ghanem, R. Swaidan, E. Litwiller, I. Pinnau, Ultra-microporous triptycene-based polyimide membranes for high-performance gas separation, Adv Mater, 26 (2014) 3688-3692.

B.S. Ghanem, R. Swaidan, X. Ma, E. Litwiller, I. Pinnau, Energy-efficient hydrogen separation by AB-type ladder-polymer molecular sieves, Adv Mater, 26 (2014) 6696-6700.

F. Grün, Diffusionsmessungen an Kautschuk, Experientia, 3 (1947) 490-492.

R. Guo, D.F. Sanders, Z.P. Smith, B.D. Freeman, D.R. Paul, J.E. McGrath, Synthesis and Characterization of Thermally Rearranged (TR) Polymers: Effect of Glass Transition Temperature of Aromatic Poly(hydroxyimide) Precursors on TR Process and Gas Permeation Properties, Journal of Materials Chemistry A, 1 (2013) 6063-6072.

S.H. Han, N. Misdan, S. Kim, C.M. Doherty, A.J. Hill, Y.M. Lee, Thermally Rearranged (TR) Polybenzoxazole: Effects of Diverse Imidization Routes on Physical Properties and Gas Transport Behaviors, Macromolecules, 43 (2010) 7657-7667.

M.W. Hellums, W.J. Koros, G.R. Husk, D.R. Paul, Gas transport in halogen-containing aromatic polycarbonates, Journal of Applied Polymer Science, 43 (1991) 1977-1986.

J.M.S. Henis, Commercial and Practical Aspects of Gas Separation Membranes, in: D.R. Paul, Y.P. Yampol'skii (Eds.) Polymeric Gas Separation Membranes, CRC Press, Boca Raton, FL, 1994, pp. 442-468.

Y. Jiang, F.T. Willmore, D. Sanders, Z.P. Smith, C.P. Ribeiro, C.M. Doherty, A. Thornton, A.J. Hill, B.D. Freeman, I.C. Sanchez, Cavity Size, Sorption and Transport Characteristics of Thermally Rearranged (TR) Polymers, Polymer, 52 (2011) 2244-2254.

I. Kardash, A.N. Pravednikov, Aromatic polyimides containing hydroxy and methyl groups, Vysokomol Soyed, 9 (1967) 873-876.

S. Kim, H.J. Jo, Y.M. Lee, Sorption and transport of small gas molecules in thermally rearranged (TR) polybenzoxazole membranes based on 2,2-bis(3-amino-4-hydroxyphenyl)-hexafluoropropane (bisAPAF) and 4,4′-hexafluoroisopropylidene diphthalic anhydride (6FDA), Journal of Membrane Science, 441 (2013) 1-8.

S. Kim, K.T. Woo, J.M. Lee, J.R. Quay, M. Keith Murphy, Y.M. Lee, Gas sorption, diffusion, and permeation in thermally rearranged poly(benzoxazole-co-imide) membranes, Journal of Membrane Science, 453 (2014) 556-565.

J.C.I. Lara-Estévez, C. Camacho-Zuñiga, F.A. Ruiz-Treviño, E. Bucio, P.E. Cassidy, C.J. Booth, Gas Transport Properties of Some Fluorine-Containing Polyethers, Industrial & Engineering Chemistry Research, 49 (2010) 11948-11953.

S. Li, H.J. Jo, S.H. Han, C.H. Park, S. Kim, P.M. Budd, Y.M. Lee, Mechanically robust thermally rearranged (TR) polymer membranes with spirobisindane for gas separation, Journal of Membrane Science, 434 (2013) 137-147.

W. Liu, W. Xie, Acetate-Functional Thermally Rearranged Polyimides Based on 2,2-Bis(3-amino-4-hydroxyphenyl)hexafluoropropane and Various Dianhydrides for Gas Separations, Industrial & Engineering Chemistry Research, 53 (2014) 871-879.

C.R. Mason, L. Maynard-Atem, N.M. Al-Harbi, P.M. Budd, P. Bernardo, F. Bazzarelli, G. Clarizia, J.C. Jansen, Polymer of Intrinsic Microporosity Incorporating

Thioamide Functionality: Preparation and Gas Transport Properties, Macromolecules, 44 (2011) 6471-6479.

N.B. McKeown, P.M. Budd, Exploitation of Intrinsic Microporosity in Polymer-Based Materials, Macromolecules, 43 (2010) 5163-5176.

N.B. McKeown, S. Hanif, K. Msayib, C.E. Tattershall, P.M. Budd, Porphyrin-based nanoporous network polymers, Chemical Communications, (2002) 2782-2783.

H.B. Park, C.H. Jung, Y.M. Lee, A.J. Hill, S.J. Pas, S.T. Mudie, E. Van Wagner, B.D. Freeman, D.J. Cookson, Polymers with Cavities Tuned for Fast Selective Transport of Small Molecules and Ions, Science, 318 (2007) 254-258.

N.A. Plate, S.G. Durgarjan, V.S. Khotimskii, V.V. Teplyakov, Y.P. Yampol'skii, Novel poly(silicon olefins) for gas separations, Journal of Membrane Science, 52 (1990) 289-304.

R.C. Reid, J.M. Prausnitz, T.K. Sherwood, The Properties of Gases and Liquids, McGraw Hill Book Co.,New York, NY, 1977.

L.M. Robeson, Correlation of Separation Factor Versus Permeability for Polymeric Membranes, Journal of Membrane Science, 62 (1991) 165-185.

L.M. Robeson, The Upper Bound Revisited, Journal of Membrane Science, 320 (2008) 390-400.

L.M. Robeson, B.D. Freeman, D.R. Paul, B.W. Rowe, An Empirical Correlation of Gas Permeability and Permselectivity in Polymers and Its Theoretical Basis, Journal of Membrane Science, 341 (2009) 178-185.

L.M. Robeson, Q. Liu, B.D. Freeman, D.R. Paul, Comparison of Transport Properties of Rubbery and Glassy Polymers and the Relevance to the Upper Bound Relationship, Journal of Membrane Science, 476 (2015) 421-431.

L.M. Robeson, Z.P. Smith, B.D. Freeman, D.R. Paul, Contributions of Diffusion and Solubility Selectivity to the Upper Bound Analysis for Glassy Gas Separation Membranes, Journal of Membrane Science, 453 (2014) 71-83.

Y. Rogan, R. Malpass-Evans, M. Carta, M. Lee, J.C. Jansen, P. Bernardo, G. Clarizia, E. Tocci, K. Friess, M. Lanč, N.B. McKeown, A highly permeable polyimide with enhanced selectivity for membrane gas separations, Journal of Materials Chemistry A, 2 (2014) 4874.

I. Rose, M. Carta, R. Malpass-Evans, M.-C. Ferrari, P. Bernardo, G. Clarizia, J.C. Jansen, N.B. McKeown, Highly Permeable Benzotriptycene-Based Polymer of Intrinsic Microporosity, ACS Macro Letters, 4 (2015) 912-915.

D.F. Sanders, Z.P. Smith, R. Guo, L.M. Robeson, J.E. McGrath, D.R. Paul, B.D. Freeman, Energy-Efficient Polymeric Gas Separation Membranes For A Sustainable Future: A Review, Polymer, 54 (2013) 4729-4761.

C.A. Scholes, C.P. Ribeiro, S.E. Kentish, B.D. Freeman, Thermal rearranged poly(benzoxazole-co-imide) membranes for CO2 separation, Journal of Membrane Science, 450 (2014) 72-80.

J.-J. Shieh, T.-S. Chung, Gas permeability, diffusivity, and solubility of poly(4-vinylpyridine) film, Journal of Polymer Science Part B: Polymer Physics, 37 (1999) 2851-2861.

R. Swaidan, M. Al-Saeedi, B. Ghanem, E. Litwiller, I. Pinnau, Rational Design of Intrinsically Ultramicroporous Polyimides Containing Bridgehead-Substituted Triptycene for Highly Selective and Permeable Gas Separation Membranes, Macromolecules, 47 (2014) 5104-5114.

R. Swaidan, B. Ghanem, I. Pinnau, Fine-Tuned Intrinsically Ultramicroporous Polymers Redefine the Permeability/Selectivity Upper Bounds of Membrane-Based Air and Hydrogen Separations, ACS Macro Letters, 4 (2015) 947-951.

K. Tanaka, H. Kita, K.-i. Okamoto, Permeability and permselectivity of gases in fluorinated polyimides., Sen'i Gakkaishi, 46 (1990) 541-547.

K. Tanaka, M. Okano, H. Toshino, H. Kita, K.-I. Okamoto, Effect of methyl substituents on permeability and permselectivity of gases in polyimides prepared from methyl-substituted phenylenediamines, Journal of Polymer Science Part B: Polymer Physics, 30 (1992) 907-914.

V. Teplyakov, P. Meares, Correlation aspects of the selective gas permeabilities of polymeric materials and membranes, Gas Separation & Purification, 4 (1990) 66-74.

K. Terada, K. Mizoguchi, T. Hirose, Gas transport in poly(vinyl methylbenzoates), Journal of Polymer Science Part B: Polymer Physics, 30 (1992) 539-548.

G. Tullos, L. Mathias, Unexpected thermal conversion of hydroxy-containing polyimides to polybenzoxazoles, Polymer, 40 (1999) 3463-3468.

H. Wang, T.-S. Chung, The Evolution of Physicochemical and Gas Transport Properties of Thermally Rearranged Polyhydroxyamide (Pha), Journal of Membrane Science, 385-386 (2011) 86-95.

Z. Wang, D. Wang, J. Jin, Microporous Polyimides with Rationally Designed Chain Structure Achieving High Performance for Gas Separation, Macromolecules, 47 (2014) 7477-7483.

D.H. Weinkauf, D.R. Paul, Gas Transport Properties of Liquid Crystalline Poly(Ethylene Terephthalate-co-p-Oxybenzoate), Journal of Polymer Science Part B: Polymer Physics, 29 (1991) 329-340.

D.H. Weinkauf, D.R. Paul, Gas Transport Properties of Thermotropic Liquid-Crystalline Copolyesters. I. The Effects of Orientation and Annealing, Journal of Polymer Science Part B: Polymer Physics, 30 (1992) 817-835.

Y. Yampolskii, Polymeric Gas Separation Membranes, Macromolecules, 45 (2012) 3298-3311.

Y.F. Yeong, H. Wang, K. Pallathadka Pramoda, T.-S. Chung, Thermal induced structural rearrangement of cardo-copolybenzoxazole membranes for enhanced gas transport properties, Journal of Membrane Science, 397-398 (2012) 51-65.

Y. Zhuang, J.G. Seong, Y.S. Do, H.J. Jo, Z. Cui, J. Lee, Y.M. Lee, M.D. Guiver, Intrinsically Microporous Soluble Polyimides Incorporating Tröger's Base for Membrane Gas Separation, Macromolecules, 47 (2014) 3254-3262.

C.M. Zimmerman, W.J. Koros, Polypyrrolones for membrane gas separations. I. Structural comparison of gas transport and sorption properties, Journal of Polymer Science Part B: Polymer Physics, 37 (1999) 1235-1249.

Chapter 4

Hydrocarbon Gas Liquids Explained, U.S. Energy Information Administration, https://www.eia.gov/energyexplained/index.php?page=hgls_home, 2018.

U.S. Shale Production, U.S. Energy Information Administration, https://www.eia.gov/dnav/ng/hist/res_epg0_r5302_nus_bcfa.htm, 2018.

R.W. Baker, Future Directions of Membrane Gas Separation Technology, Industrial & Engineering Chemistry Research, 41 (2002) 1393-1411.

R.W. Baker, Membrane Technology and Applications, in: Membrane Technology, John Wiley & Sons, Ltd, Chichester, UK, 2004, pp. 545.

R.W. Baker, Membrane Technology and Applications, 3rd Edition ed., A John Wiley & Sons, Ltd., Publication, 2012.

A. Bos, I. Punt, H. Strathmann, M. Wessling, Suppression of Gas Separation Membrane Plasticization by Homogeneous Polymer Blending, AIChE Journal, 47 (2001) 1088 - 1093.

J.M. Cervantes-Uc, J.V. Cauich-Rodríguez, H. Vázquez-Torres, A. Licea-Claveríe, TGA/FTIR Study on Thermal Degradation of Polymethacrylates Containing Carboxylic Groups, Polymer Degradation and Stability, 91 (2006) 3312-3321.

M.E. Dose, I. Hubacek, D.R. Paul, B.D. Freeman, CO2, C2H4, and C2H6 Sorption and Mixed Gas Permeability of Thermally Cross-linked Diaminophenylindane (DAPI) Containing Polyimides, Journal of Membrane Science, Submitted (2018).

M.E. Dose, J.D. Moon, I. Hubacek, D.R. Paul, B.D. Freeman, Fundamental Gas Transport and Dilation of Studies in Thermally Cross-linked Diaminophenylindane (DAPI) Containing Polyimides, Journal of Polymer Science Part B: Polymer Physics, In Submission (2018).

N. Du, M.M. Dal-Cin, G.P. Robertson, M.D. Guiver, Decarboxylation-Induced Cross-Linking of Polymers of Intrinsic Microporosity (PIMs) for Membrane Gas Separation, Macromolecules, 45 (2012) 5134-5139.

I.V. Farr, Synthesis and Characterization of Novel Polyimide Gas Separation Membrane Material Systems, Virginia Polytechnic Institute and State University 1999.

I.V. Farr, D. Kratzner, T.E. Glass, D. Dunson, Q. Ji, J.E. McGrath, The Synthesis and Characterization of Polyimide Homopolymers Based on 5(6)-Amino-1-(4-Aminophenyl)1,3,3-Trimethylindane, J Polym Sci Pol Chem, 38 (2000) 2840-2854.

P. Flory, J. Rehner, Statistical Mechanics of Cross-linked Polymer Chain Networks II: Swelling, The Journal of Chemical Physics, 11 (1943) 521 - 526.

Y. Huang, D. Paul, Experimental Methods for Tracking Physical Aging of Thin Glassy Polymer Films by Gas Permeation, Journal of Membrane Science, 244 (2004) 167-178.

H. Kawakami, M. Mikawa, S. Nagaoka, Gas Transport Properties in Thermally Cured Aromatic Polyimide Membranes, Journal of Membrane Science, 118 (1996) 223-230.

G.E. Keller, A.E. Marcinkowsky, S.K. Verma, K.D. Williamson, Olefin Recovery and Purification via Silver Comlexation, in: N.N. Li, J.M. Calo (Eds.) Separation and Purification Technology, Marcel Dekker, New York, 1992.

J.H. Kim, W.J. Koros, D.R. Paul, Physical Aging of Thin 6FDA-Based Polyimide Membranes Containing Carboxyl Acid Groups. Part I. Transport Properties, Polymer, 47 (2006) 3094-3103.

A.M. Kratochvil, W.J. Koros, Decarboxylation-Induced Cross-Linking of a Polyimide for Enhanced CO2 Plasticization Resistance, Macromolecules, 41 (2008) 7920-7927.

M. Langsam, W. Burgoyne, Effects of Diamine Monomer Structure on the Gas Permeability of Polyimides. I. Bridged Diamines, Journal of Polymer Science Part A: Polymer Chemistry, 31 (1993) 909-921.

N.L. Le, Y. Wang, T.-S. Chung, Synthesis, Cross-linking Modifications of 6FDA-NDA/DABA Polyimide Membranes for Ethanol Dehydration via Pervaporation, Journal of Membrane Science, 415-416 (2012) 109-121.

M.S. McCaig, D.R. Paul, Effect of UV Crosslinking and Physical Aging on the Gas Permeability of Thin Glassy Polyarylate Films, Polymer, 40 (1999) 7209-7225.

J.Y. Park, D.R. Paul, Correlation and Prediction of Gas Permeability in Glassy Polymer Membrane Materials via a Modified Free Volume Based Group Contribution Method, Journal of Membrane Science, 125 (1997) 23 - 39.

D.R. Paul, Gas Sorption and Transport in Glassy Polymers, Reports of the Bunsen Society for Physical Chemistry, 83 (1979) 294-302.

D. Punsalan, W.J. Koros, Thickness-Dependent Sorption and Effects of Physical Aging in a Polyimide Sample, Journal of Applied Polymer Science, 96 (2005) 1115-1121.

W. Qiu, C.-C. Chen, L. Xu, L. Cui, D.R. Paul, W.J. Koros, Sub-Tg Cross-Linking of a Polyimide Membrane for Enhanced CO2 Plasticization Resistance for Natural Gas Separation, Macromolecules, 44 (2011) 6046-6056.

W. Qiu, L. Xu, C.-C. Chen, D.R. Paul, W.J. Koros, Gas Separation Performance of 6FDA-based Polyimides with Different Chemical Structures, Polymer, 54 (2013) 6226-6235.

L.M. Robeson, The Upper Bound Revisited, Journal of Membrane Science, 320 (2008) 390-400.

L.M. Robeson, M.E. Dose, B.D. Freeman, D.R. Paul, Analysis of the Transport Properties of Thermally Rearranged (TR) Polymers and Polymers of Intrinsic Microporosity (PIM) Relative to Upper Bound Performance, Journal of Membrane Science, 525 (2017) 18-24.

L.M. Robeson, B.D. Freeman, D.R. Paul, B.W. Rowe, An Empirical Correlation of Gas Permeability and Permselectivity in Polymers and Its Theoretical Basis, Journal of Membrane Science, 341 (2009) 178-185.

M. Rungta, L. Xu, W.J. Koros, Carbon Molecular Sieve Dense Film Membranes Derived from Matrimid® for Ethylene/Ethane Separation, Carbon, 50 (2012) 1488-1502.

M. Rungta, C. Zhang, W.J. Koros, L. Xu, Membrane-Based Ethylene/Ethane Separation: The Upper Bound And Beyond, AIChE Journal, 59 (2013) 3475-3489.

D.J. Safarik, R.B. Eldridge, Olefin/Paraffin Separations by Reactive Absorption: A Review, Industrial & Engineering Chemistry Research, 37 (1998) 2571-2581.

J.M. Salley, C.W. Frank, Charge Transfer in Aromatic Polyimdes, in: M. Ghosh (Ed.) Polyimide: Fundamentals and Applications, Marcel Dekker, New York, 1996.

R.L. Scott, The Anomalous Behavior of Fluorocarbon Solutions, The Journal of Physical Chemistry, 62 (1958) 136 - 145.

E.M.D. Siebert, C.M. Knobler, Interaction Virial Coefficients in Hydrocarbon-Fluorocarbon Mixtures, The Journal of Physical Chemistry, 75 (1971) 3863 - 3870.

Z.P. Smith, Fundamentals of Gas Sorption and Transport in Thermally Rearranged Polyimides, The University of Texas at Austin, Austin, TX, 2014.

Z.P. Smith, D.F. Sanders, C.P. Ribeiro, R. Guo, B.D. Freeman, D.R. Paul, J.E. McGrath, S. Swinnea, Gas Sorption and Characterization of Thermally Rearranged Polyimides Based on 3,3′-Dihydroxy-4,4′-Diamino-Biphenyl (HAB) And 2,2′-Bis-(3,4-Dicarboxyphenyl) Hexafluoropropane Dianhydride (6FDA), Journal of Membrane Science, 415-416 (2012) 558-567.

C. Staudt-Bickel, W. J. Koros, Improvement of CO2/CH4 Separation Characteristics of Polyimides by Chemical Crosslinking, Journal of Membrane Science, 155 (1999) 145-154.

S.A. Stern, Polymers for Gas Separationis: The Next Decade, Journal of Membrane Science, 94 (1994) 1-65.

S.A. Stern, Y. Mii, H. Yamamoto, Structure / Permeability Relationships of Polyimide Membranes. Applications to the Separation of Gas Mixtures, Journal of Polymer Science: Part B: Polymer Physics, 27 (1989) 1887-1909.

S.A. Stern, V. Saxena, Concentration-Dependent Transport of Gases and Vapors in Glassy Polymers, Journal of Membrane Science, 7 (1980) 47-59.

R.R. Tiwari, Z.P. Smith, H. Lin, B.D. Freeman, D.R. Paul, Gas Permeation in Thin Films of "High Free-Volume" Glassy Perfluoropolymers: Part I. Physical Aging, Polymer, 55 (2014) 5788-5800.

T. Visser, M. Wessling, Auto and Mutual Plasticization in Single and Mixed Gas C3 Transport Through Matrimid-Based Hollow Fiber Membranes, Journal of Membrane Science, 312 (2008) 84-96.

J.D. Wind, D.R. Paul, W.J. Koros, Natural Gas Permeation in Polyimide Membranes, Journal of Membrane Science, 228 (2004) 227-236.

C.T. Wright, D.R. Paul, Gas Sorption and Transport in UV-Irradiated Polyarylate Copolymers Based on Tetramethyl Bisphenol-A and Dihydroxybenzophenone, Journal of Membrane Science, 124 (1997) 161-174.

L. Xu, M. Rungta, W.J. Koros, Matrimid® Derived Carbon Molecular Sieve Hollow Fiber Membranes for Ethylene/Ethane Separation, Journal of Membrane Science, 380 (2011) 138-147.

C. Zhang, P. Li, B. Cao, Decarboxylation Crosslinking of Polyimides with High CO2/CH4 Separation Performance and Plasticization Resistance, Journal of Membrane Science, 528 (2017) 206-216.

Chapter 5

R.W. Baker, Membrane Technology and Applications 2nd Edition ed., John Wiley & Sons Ltd, T, West Sussex, England, 2004.

W.A. Bollinger, D.L. MacLean, R.S. Narayan, Separation Systems For Oil Refining And Production, Chemical Engineering Progress, 78 (1982) 27-32.

M.E. Dose, M. Chwatko, I. Hubacek, N.A. Lynd, D.R. Paul, B.D. Freeman, Thermally Cross-linked Diaminophenylindane (DAPI) Containing Polyimides for Membrane Based Gas Separations, Polymer, Submitted (2018).

M.E. Dose, J.D. Moon, I. Hubacek, D.R. Paul, B.D. Freeman, Fundamental Gas Transport and Dilation of Studies in Thermally Cross-linked

Diaminophenylindane (DAPI) Containing Polyimides, Journal of Polymer Science Part B: Polymer Physics, In Submission (2018).

N. Du, M.M. Dal-Cin, G.P. Robertson, M.D. Guiver, Decarboxylation-Induced Cross-Linking of Polymers of Intrinsic Microporosity (PIMs) for Membrane Gas Separation, Macromolecules, 45 (2012) 5134-5139.

G.K. Fleming, W.J. Koros, Dilation of Polymers by Sorption of Carbon Dioxide at Elevated Pressures 1. Silicone Rubber and Unconditioned Polycarbonate, Macromolecules, 19 (1986) 2285-2291.

K.L. Gleason, Z.P. Smith, Q. Liu, D.R. Paul, B.D. Freeman, Pure- and Mixed-Gas Permeation of CO2 and CH4 in Thermally Rearranged Polymers Based on 3,3′-Dihydroxy-4,4′-Diamino-Biphenyl (HAB) and 2,2′-Bis-(3,4-Dicarboxyphenyl) Hexafluoropropane Dianhydride (6FDA), Journal of Membrane Science, 475 (2015) 204-214.

J.M.S. Henis, Commercial and Practical Aspects of Gas Separation Membranes, in: D.R. Paul, Y.P. Yampol'skii (Eds.) Polymeric Gas Separation Membranes, CRC Press, Boca Raton, FL, 1994, pp. 442-468.

A.M.W. Hillock, S.J. Miller, W.J. Koros, Crosslinked Mixed Matrix Membranes for the Purification of Natural Gas: Effects of Sieve Surface Modification, Journal of Membrane Science, 314 (2008) 193-199.

A.F. Ismail, W. Lorna, Penetrant-Induced Plasticization Phenomenon in Glassy Polymers for Gas Separation Membrane, Separation and Purification Technology, 27 (2002) 173 - 194.

W.J. Koros, R.T. Chern, V. Stannett, H.B. Hopfenberg, A Model for Permeation of Mixed Gases and Vapors in Glassy Polymers, Journal of Polymer Science: Polymer Physics Edition, 19 (1981) 1513 - 1530.

W.J. Koros, D.R. Paul, Design Considerations for Measurement of Gas Sorption in Polymers by Pressure Decay, Journal of Polymer Science Part B: Polymer Physics, 14 (1976) 1903 - 1907.

A.M. Kratochvil, W.J. Koros, Decarboxylation-Induced Cross-Linking of a Polyimide for Enhanced CO2 Plasticization Resistance, Macromolecules, 41 (2008) 7920-7927.

M. Minelli, M.G. De Angelis, G.C. Sarti, Predictive Calculations of Gas Solubility and Permeability in Glassy Polymeric Membranes: An Overview, Frontiers of Chemical Science and Engineering, 11 (2017) 405-413.

D.R. Paul, Gas Sorption and Transport in Glassy Polymers, Reports of the Bunsen Society for Physical Chemistry, 83 (1979) 294-302.

J.H. Petropoulos, Mechanisms and Theories for Sorption and Diffusion of Gases in Polymers, in: Polymeric Gas Separation Membranes, CRC Press, Inc, Boca Raton, FL, 1994.

W. Qiu, C.-C. Chen, L. Xu, L. Cui, D.R. Paul, W.J. Koros, Sub-Tg Cross-Linking of a Polyimide Membrane for Enhanced CO2 Plasticization Resistance for Natural Gas Separation, Macromolecules, 44 (2011) 6046-6056.

L.M. Robeson, M.E. Dose, B.D. Freeman, D.R. Paul, Analysis of the Transport Properties of Thermally Rearranged (TR) Polymers and Polymers of Intrinsic Microporosity (PIM) Relative to Upper Bound Performance, Journal of Membrane Science, 525 (2017) 18-24.

L.M. Robeson, Q. Liu, B.D. Freeman, D.R. Paul, Comparison of Transport Properties of Rubbery and Glassy Polymers and the Relevance to the Upper Bound Relationship, Journal of Membrane Science, 476 (2015) 421-431.

L.M. Robeson, Z.P. Smith, B.D. Freeman, D.R. Paul, Contributions of Diffusion and Solubility Selectivity to the Upper Bound Analysis for Glassy Gas Separation Membranes, Journal of Membrane Science, 453 (2014) 71-83.

M. Rungta, C. Zhang, W.J. Koros, L. Xu, Membrane-Based Ethylene/Ethane Separation: The Upper Bound And Beyond, AIChE Journal, 59 (2013) 3475-3489.

D.F. Sanders, Z.P. Smith, R. Guo, L.M. Robeson, J.E. McGrath, D.R. Paul, B.D. Freeman, Energy-Efficient Polymeric Gas Separation Membranes For A Sustainable Future: A Review, Polymer, 54 (2013) 4729-4761.

Z.P. Smith, D.F. Sanders, C.P. Ribeiro, R. Guo, B.D. Freeman, D.R. Paul, J.E. McGrath, S. Swinnea, Gas Sorption and Characterization of Thermally Rearranged Polyimides Based on 3,3′-Dihydroxy-4,4′-Diamino-Biphenyl (HAB) And 2,2′-Bis-(3,4-Dicarboxyphenyl) Hexafluoropropane Dianhydride (6FDA), Journal of Membrane Science, 415-416 (2012) 558-567.

S.A. Stern, Y. Mii, H. Yamamoto, Structure / Permeability Relationships of Polyimide Membranes. Applications to the Separation of Gas Mixtures, Journal of Polymer Science: Part B: Polymer Physics, 27 (1989) 1887-1909.

S.A. Stern, V. Saxena, Concentration-Dependent Transport of Gases and Vapors in Glassy Polymers, Journal of Membrane Science, 7 (1980) 47-59.

W.R. Vieth, J.M. Howell, J.H. Hsieh, Dual Sorption Theory, Journal of Membrane Science, 1 (1976) 177 - 220.

T. Visser, M. Wessling, Auto and Mutual Plasticization in Single and Mixed Gas C3 Transport Through Matrimid-Based Hollow Fiber Membranes, Journal of Membrane Science, 312 (2008) 84-96.

M. Wessling, S. Schoeman, T. van der Boomgaard, C.A. Smolders, Plasticization of Gas Separation Membranes, Gas Separation & Purification, 5 (1991) 222 - 228.

J.D. Wind, S.M. Sirard, D.R. Paul, P.F. Green, K.P. Johnston, W.J. Koros, Carbon Dioxide-Induced Plasticization of Polyimide Membranes: Pseudo-Equilibrium Relationships of Diffusion, Sorption, and Swelling, Macromolecules, 36 (2003) 6433-6441.

A.G. Wonders, D.R. Paul, Effect of CO2 Exposure History on Sorption and Transport in Polycaronate, Journal of Membrane Science, 5 (1979) 63 - 75.

Y. Yampolskii, Polymeric Gas Separation Membranes, Macromolecules, 45 (2012) 3298-3311.

C. Zhang, P. Li, B. Cao, Decarboxylation Crosslinking of Polyimides with High CO2/CH4 Separation Performance and Plasticization Resistance, Journal of Membrane Science, 528 (2017) 206-216.

Chapter 6

Hydrocarbon Gas Liquids Explained, U.S. Energy Information Administration, https://www.eia.gov/energyexplained/index.php?page=hgls_home, 2018.

U.S. Shale Production, U.S. Energy Information Administration, https://www.eia.gov/dnav/ng/hist/res_epg0_r5302_nus_bcfa.htm, 2018.

J.E. Bachman, Z.P. Smith, T. Li, T. Xu, J.R. Long, Enhanced Ethylene Separation and Plasticization Resistance in Polymer Membranes Incorporating Metal-Organic Framework Nanocrystals, Nat Mater, 15 (2016) 845-849.

R.W. Baker, B.T. Low, Gas Separation Membrane Materials: A Perspective, Macromolecules, 47 (2014) 6999-7013.

A. Bos, I. Punt, H. Strathmann, M. Wessling, Suppression of Gas Separation Membrane Plasticization by Homogeneous Polymer Blending, AIChE Journal, 47 (2001) 1088 - 1093.

M. Brayden, W.J. Koros, L. Xu, M. Martinez, B. Stears, G. Barbay, Carbon Molecular Sieve Hollow Fiber Membranes for Olefin/Paraffin Separations, AIChE National Meeting, San Antonio, TX, 2013, 140C.

M. Calle, H.J. Jo, C.M. Doherty, A.J. Hill, Y.M. Lee, Cross-Linked Thermally Rearranged Poly(benzoxazole-co-imide) Membranes Prepared from ortho-Hydroxycopolyimides Containing Pendant Carboxyl Groups and Gas Separation Properties, Macromolecules, 48 (2015) 2603-2613.

S.S. Chan, T.-S. Chung, Y. Liu, R. Wang, Gas and Hydrocarbon (C2 and C3) Transport Properties of Co-Polyimides Synthesized From 6FDA and 1,5-NDA (Naphthalene)/Durene diamines, Journal of Membrane Science, 218 (2003) 235-245.

M.E. Dose, M. Chwatko, I. Hubacek, N.A. Lynd, D.R. Paul, B.D. Freeman, Thermally Cross-linked Diaminophenylindane (DAPI) Containing Polyimides for Membrane Based Gas Separations, Polymer, Submitted (2018).

M.E. Dose, I. Hubacek, D.R. Paul, B.D. Freeman, CO2, C2H4, and C2H6 Sorption and Mixed Gas Permeability of Thermally Cross-linked Diaminophenylindane (DAPI) Containing Polyimides, Journal of Membrane Science, Submitted (2018).

N. Du, M.M. Dal-Cin, G.P. Robertson, M.D. Guiver, Decarboxylation-Induced Cross-Linking of Polymers of Intrinsic Microporosity (PIMs) for Membrane Gas Separation, Macromolecules, 45 (2012) 5134-5139.

E. Favre, P. Schaetzel, Q.T. Nguygen, R. Clement, J. Neel, Sorption, Diffusion and Vapor Permeation of Various Penetrants Through Dense Poly(dimethylsiloxane) Membranes: A Transport Analysis, Journal of Membrane Science, 92 (1994) 16-184.

G.K. Fleming, W.J. Koros, Dilation of Polymers by Sorption of Carbon Dioxide at Elevated Pressures 1. Silicone Rubber and Unconditioned Polycarbonate, Macromolecules, 19 (1986) 2285-2291.

G.K. Fleming, W.J. Koros, Carbon Dioxide Conditioning Effects on Sorption and Volume Dilation Behavior for Bisphenol A-Polycarbonate, Macromolecules, 23 (1990) 1353-1360.

M. Galizia, C. Daniel, G. Fasano, G. Guerra, G. Mensitieri, Gas Sorption and Diffusion in Amorphous and Semicrystalline Nanoporous Poly(2,6-dimethyl-1,4-phenylene)oxide, Macromolecules, 45 (2012) 3604-3615.

M. Galizia, M.G. De Angelis, E. Finkelshtein, Y.P. Yampolskii, G.C. Sarti, Sorption and Transport of Hydrocarbons and Alcohols in Addition-Type Poly(trimethyl Silyl Norbornene). I: Experimental Data, Journal of Membrane Science, 385-386 (2011) 141-153.

K.L. Gleason, Z.P. Smith, Q. Liu, D.R. Paul, B.D. Freeman, Pure- and Mixed-Gas Permeation of CO2 and CH4 in Thermally Rearranged Polymers Based on 3,3′-Dihydroxy-4,4′-Diamino-Biphenyl (HAB) and 2,2′-Bis-(3,4-Dicarboxyphenyl) Hexafluoropropane Dianhydride (6FDA), Journal of Membrane Science, 475 (2015) 204-214.

[18] S.H. Han, N. Misdan, S. Kim, C.M. Doherty, A.J. Hill, Y.M. Lee, Thermally Rearranged (TR) Polybenzoxazole: Effects of Diverse Imidization Routes on Physical Properties and Gas Transport Behaviors, Macromolecules, 43 (2010) 7657-7667.

Y. Kamiya, T. Hirose, Y. Naito, K. Mizoguchi, Sorptive Dilation of Polysulfone and Poly(ethylene terephthalate) Films by High-pressure Carbon Dioxide, Journal of Polymer Science Part B: Polymer Physics, 26 (1988) 159-177.

Y. Kamiya, K. Mizoguchi, T. Hirose, Y. Naito, Sorption and Dilation in Poly(ethyl methacrylate) -Carbon Dioxide System, Journal of Polymer Science: Part B: Polymer Physics, 27 (1989) 879-892.

Y. Kamiya, Y. Naito, K. Mizoguchi, Sorption and Partial Molar Volume of Gases in Polybutadiene, Journal of Polymer Science Part B: Polymer Physics, 27 (1989) 2243.

R. Kirchheim, Partial Molar Volume of Small Molecules in Glassy Polymers, Journal of Polymer Science: Part B Polymer Physics, 31 (1993) 1373-1382.

A.M. Kratochvil, W.J. Koros, Decarboxylation-Induced Cross-Linking of a Polyimide for Enhanced CO2 Plasticization Resistance, Macromolecules, 41 (2008) 7920-7927.

Y. Liu, R. Wang, T.-S. Chung, Chemical Cross-linking Modification of Polyimide Membranes for Gas Separation, Journal of Membrane Science, 189 (2001) 231–239.

T.C. Merkel, V.I. Bondar, K. Nagai, B. Freeman, Sorption and Transport of Hydrocarbon and Perfluorocarbon Gases in Poly(1-trimthylsilyl-1-propyne), Journal of Polymer Science: Part B Polymer Physics, 38 (2000) 273 - 296.

M. Minelli, M.G. De Angelis, G.C. Sarti, Predictive Calculations of Gas Solubility and Permeability in Glassy Polymeric Membranes: An Overview, Frontiers of Chemical Science and Engineering, 11 (2017) 405-413.

M. Minelli, G.C. Sarti, Permeability and Solubility of Carbon Dioxide in Different Glassy Polymer Systems with and without Plasticization, Journal of Membrane Science, 444 (2013) 429-439.

M. Minelli, G.C. Sarti, Thermodynamic model for the permeability of light gases in glassy polymers, AIChE Journal, 61 (2015) 2776-2788.

J.D. Moon, M. Galizia, H. Borjigin, R. Liu, J.S. Riffle, B. Freeman, D. Paul, Water Vapor Sorption, Diffusion, and Dilation in Polybenzimidazoles, Macromolecules, In Press (2018).

J.Y. Park, D.R. Paul, Correlation and Prediction of Gas Permeability in Glassy Polymer Membrane Materials via a Modified Free Volume Based Group Contribution Method, Journal of Membrane Science, 125 (1997) 23 - 39.

D. Pope, W.J. Koros, Gas Sorption-Induced Dilation of Poly(4-methyl-1-pentene), Journal of Polymer Science Part B: Polymer Physics, 34 (1996) 1861-1868.

D. Punsalan, W.J. Koros, Drifts in penetrant partial molar volumes in glassy polymers due to physical aging, Polymer, 46 (2005) 10214-10220.

W. Qiu, C.-C. Chen, L. Xu, L. Cui, D.R. Paul, W.J. Koros, Sub-Tg Cross-Linking of a Polyimide Membrane for Enhanced CO2 Plasticization Resistance for Natural Gas Separation, Macromolecules, 44 (2011) 6046-6056.

R. Raharjo, B. Freeman, E. Sanders, Pure and Mixed Gas CH4 and n-C4H10 Sorption and Dilation in Poly(dimethylsiloxane), Journal of Membrane Science, 292 (2007) 45-61.

R. Reich, W.T. Ziegler, K.A. Rogers, Adsorption of Methane, Ethane, and Ethylene Gases and Their Binary and Ternary Mixtures and Carbon Dioxide on Activated Carbon at 212-301 K and Pressures to 35 Atmospheres, Industrial & Engineering Chemistry Process Design and Development, 19 (1980) 336-344.

L.M. Robeson, M.E. Dose, B.D. Freeman, D.R. Paul, Analysis of the Transport Properties of Thermally Rearranged (TR) Polymers and Polymers of Intrinsic Microporosity (PIM) Relative to Upper Bound Performance, Journal of Membrane Science, 525 (2017) 18-24.

L.M. Robeson, Q. Liu, B.D. Freeman, D.R. Paul, Comparison of Transport Properties of Rubbery and Glassy Polymers and the Relevance to the Upper Bound Relationship, Journal of Membrane Science, 476 (2015) 421-431.

M. Rungta, L. Xu, W.J. Koros, Carbon Molecular Sieve Dense Film Membranes Derived from Matrimid® for Ethylene/Ethane Separation, Carbon, 50 (2012) 1488-1502.

J.R. Scherer, B. Bolton, Water in Polymer Membranes. 5. On the Existence of Pores and Voids, Journal of Physical Chemistry, 89 (1985) 3535 - 3540.

Z.P. Smith, D.F. Sanders, C.P. Ribeiro, R. Guo, B.D. Freeman, D.R. Paul, J.E. McGrath, S. Swinnea, Gas Sorption and Characterization of Thermally Rearranged Polyimides Based on 3,3′-Dihydroxy-4,4′-Diamino-Biphenyl (HAB) And 2,2′-Bis-(3,4-Dicarboxyphenyl) Hexafluoropropane Dianhydride (6FDA), Journal of Membrane Science, 415-416 (2012) 558-567.

C. Staudt-Bickel, W. J. Koros, Improvement of CO2/CH4 Separation Characteristics of Polyimides by Chemical Crosslinking, Journal of Membrane Science, 155 (1999) 145-154.

C. Staudt-Bickel, W.J. Koros, Olefin/paraffin gas separations with 6FDA-based polyimide membranes, Journal of Membrane Science, 170 (2000) 205-214.

J.S. Vrentas, J.L. Duda, Diffusion in Polymer-Solvent Systems. I. Reexamination of the Free-Volume Theory, Journal of Polymer Science Part B: Polymer Physics, 15 (1977) 403-416.

J.G. Wijmans, R.W. Baker, The Solution-Diffustion Model: A Review, Journal of Membrane Science, 107 (1995) 1-21.

L. Xu, M. Rungta, W.J. Koros, Matrimid® Derived Carbon Molecular Sieve Hollow Fiber Membranes for Ethylene/Ethane Separation, Journal of Membrane Science, 380 (2011) 138-147.

Chapter 7

P. Budd, N. McKeown, B. Ghanem, K. Msayib, D. Fritsch, L. Starannikova, N. Belov, O. Sanfirova, Y. Yampolskii, V. Shantarovich, Gas Permeation Parameters and Other Physicochemical Properties of a Polymer of Intrinsic Microporosity: Polybenzodioxane PIM-1, Journal of Membrane Science, 325 (2008) 851-860.

S.M. Davoodi, M. Sadeghi, M. Naghsh, A. Moheb, Olefin–Paraffin Separation Performance of Polyimide Matrimid®/Silica Nanocomposite Membranes, RSC Advances, 6 (2016) 23746-23759.

M.G. De Angelis, F. Doghieri, G.C. Sarti, B.D. Freeman, Modeling Gas Sorption in Amorphous Teflon Through the Non Equilibrium Thermodynamics for Glassy Polymers (NET-GP) Approach, Desalination, 193 (2006) 82-89.

M.E. Dose, M. Chwatko, I. Hubacek, N.A. Lynd, D.R. Paul, B.D. Freeman, Thermally Cross-linked Diaminophenylindane (DAPI) Containing Polyimides for Membrane Based Gas Separations, Polymer, Submitted (2018).

M.E. Dose, I. Hubacek, D.R. Paul, B.D. Freeman, CO2, C2H4, and C2H6 Sorption and Mixed Gas Permeability of Thermally Cross-linked Diaminophenylindane (DAPI) Containing Polyimides, Journal of Membrane Science, Submitted (2018).

M.E. Dose, J.D. Moon, I. Hubacek, D.R. Paul, B.D. Freeman, Fundamental Gas Transport and Dilation of Studies in Thermally Cross-linked Diaminophenylindane (DAPI) Containing Polyimides, Journal of Polymer Science Part B: Polymer Physics, In Submission (2018).

H. Eguchi, D.J. Kim, W.J. Koros, Chemically Cross-linkable Polyimide Membranes for Improved Transport Plasticization Resistance for Natural Gas Separation, Polymer, 58 (2015) 121-129.

S.H. Han, N. Misdan, S. Kim, C.M. Doherty, A.J. Hill, Y.M. Lee, Thermally Rearranged (TR) Polybenzoxazole: Effects of Diverse Imidization Routes on Physical Properties and Gas Transport Behaviors, Macromolecules, 43 (2010) 7657-7667.

Y. Jiang, F.T. Willmore, D. Sanders, Z.P. Smith, C.P. Ribeiro, C.M. Doherty, A. Thornton, A.J. Hill, B.D. Freeman, I.C. Sanchez, Cavity Size, Sorption and Transport Characteristics of Thermally Rearranged (TR) Polymers, Polymer, 52 (2011) 2244-2254.

S.D. Kelman, S. Matteucci, C.W. Bielawski, B.D. Freeman, Crosslinking Poly(1-Trimethylsilyl-1-Propyne) and Its Effect On Solvent Resistance and Transport Properties, Polymer, 48 (2007) 6881-6892.

B. Kraftschik, W.J. Koros, Cross-Linkable Polyimide Membranes for Improved Plasticization Resistance and Permselectivity in Sour Gas Separations, Macromolecules, 46 (2013) 6908-6921.

A.M. Kratochvil, W.J. Koros, Decarboxylation-Induced Cross-Linking of a Polyimide for Enhanced CO2 Plasticization Resistance, Macromolecules, 41 (2008) 7920-7927.

M.S. McCaig, D.R. Paul, Effect of UV Crosslinking and Physical Aging on the Gas Permeability of Thin Glassy Polyarylate Films, Polymer, 40 (1999) 7209-7225.

M. Minelli, M.G. De Angelis, D. Hofmann, A Novel Multiscale Method for the Prediction of the Volumetric and Gas Solubility Behavior of High-Tg Polyimides, Fluid Phase Equilibria, 333 (2012) 87-96.

M. Minelli, M.G. De Angelis, G.C. Sarti, Predictive Calculations of Gas Solubility and Permeability in Glassy Polymeric Membranes: An Overview, Frontiers of Chemical Science and Engineering, 11 (2017) 405-413.

M. Minelli, F. Doghieri, Predictive Model for Gas and Vapor Solubility and Swelling in Glassy Polymers I: Application to Different Polymer/Penetrant Systems, Fluid Phase Equilibria, 381 (2014) 1-11.

M. Minelli, F. Doghieri, Predictive Model for Gas and Vapor Sorption and Swelling in Glassy Polymers: II. Effect of Sample Previous History, Fluid Phase Equilibria, 444 (2017) 47-55.

M. Minelli, G.C. Sarti, Permeability and Solubility of Carbon Dioxide in Different Glassy Polymer Systems with and without Plasticization, Journal of Membrane Science, 444 (2013) 429-439.

X. Ning, W.J. Koros, Carbon Molecular Sieve Membranes Derived from Matrimid® Polyimide for Nitrogen/Methane Separation, Carbon, 66 (2014) 511-522.

W. Qiu, C.-C. Chen, L. Xu, L. Cui, D.R. Paul, W.J. Koros, Sub-Tg Cross-Linking of a Polyimide Membrane for Enhanced CO2 Plasticization Resistance for Natural Gas Separation, Macromolecules, 44 (2011) 6046-6056.

L.M. Robeson, M.E. Dose, B.D. Freeman, D.R. Paul, Analysis of the Transport Properties of Thermally Rearranged (TR) Polymers and Polymers of Intrinsic Microporosity (PIM) Relative to Upper Bound Performance, Journal of Membrane Science, 525 (2017) 18-24.

M. Rungta, L. Xu, W.J. Koros, Carbon Molecular Sieve Dense Film Membranes Derived from Matrimid® for Ethylene/Ethane Separation, Carbon, 50 (2012) 1488-1502.

D.F. Sanders, Z.P. Smith, C.P. Ribeiro, R. Guo, J.E. McGrath, D.R. Paul, B.D. Freeman, Gas Permeability, Diffusivity, and Free Volume of Thermally Rearranged Polymers Based on 3,3'-Dihydroxy-4,4'-Diamino-Biphenyl (HAB) and 2,2'-Bis-(3,4-Dicarboxyphenyl) Hexafluoropropane Dianhydride (6FDA), Journal of Membrane Science, 409-410 (2012) 232-241.

B.J. Sundell, A.T. Shaver, Q. Liu, A. Nebipasagil, P. Pisipati, S.J. Mecham, J.S. Riffle, B.D. Freeman, J.E. McGrath, Synthesis, Oxidation and Crosslinking of

Tetramethyl Bisphenol F (TMBPF)-Based Polymers for Oxygen/Nitrogen Gas Separations, Polymer, 55 (2014) 5623-5634.

L. Xu, M. Rungta, W.J. Koros, Matrimid® Derived Carbon Molecular Sieve Hollow Fiber Membranes for Ethylene/Ethane Separation, Journal of Membrane Science, 380 (2011) 138-147.

Appendix A

P.R. Bevington, D.K. Robinson, Least-Squares Fit to a Polynomial, in: Data Reduction and Error Analysis for the Physical Sciences, McGraw Hill, Boston, MA, 2003, pp. 116 - 141.

P.R. Bevington, D.K. Robinson, 11.4 F Test, in: Data Reduction and Error Analysis for the Physical Sciences, McGraw Hill, Boston, MA, 2003, pp. 207 - 208.

L.M. Robeson, Z.P. Smith, B.D. Freeman, D.R. Paul, Contributions of Diffusion and Solubility Selectivity to the Upper Bound Analysis for Glassy Gas Separation Membranes, Journal of Membrane Science, 453 (2014) 71-83.

Appendix B

[1] P.C. Hiemenz, T.P. Lodge, Polymer Chemistry, Second ed., CRC Press, New York, 2007.

J.D. Ingle, S.R. Crouch, Spectrochemical Analysis, Printice Hall, Englewood Cliffs, NJ, 1988.

S. Jacobson, Molecular Modeling Studies of Polymeric Gas Separation and Barrier Materials: Structure and Transport Mechanisms, Polymers for Advanced Technologies, 5 (1993) 724-732.

J.H. Kim, W.J. Koros, D.R. Paul, Physical Aging of Thin 6FDA-Based Polyimide Membranes Containing Carboxyl Acid Groups. Part I. Transport Properties, Polymer, 47 (2006) 3094-3103.

A.M. Kratochvil, W.J. Koros, Decarboxylation-Induced Cross-Linking of a Polyimide for Enhanced CO2 Plasticization Resistance, Macromolecules, 41 (2008) 7920-7927.

M. Langsam, W. Burgoyne, Effects of Diamine Monomer Structure on the Gas Permeability of Polyimides. I. Bridged Diamines, Journal of Polymer Science Part A: Polymer Chemistry, 31 (1993) 909-921.

E.W. Lemmon, M.O. McLinden, D.G. Friend, Thermophysical Properties of Fluid Systems, in: P.J. Linstrom, W.G. Mallard (Eds.) NIST Chemistry WebBook,

NIST Standard Reference Database Number 69, National Institute of Standards and Technology, Gaithersburg MD, 2018.

H. Lin, B.D. Freeman, Chapter 7: Permeation and Diffusion, in: Springer Handbook of Materials Measurement Methods, 2006, pp. 371-387.

J.Y. Park, D.R. Paul, Correlation and Prediction of Gas Permeability in Glassy Polymer Membrane Materials via a Modified Free Volume Based Group Contribution Method, Journal of Membrane Science, 125 (1997) 23 - 39.

W. Qiu, L. Xu, C.-C. Chen, D.R. Paul, W.J. Koros, Gas Separation Performance of 6FDA-based Polyimides with Different Chemical Structures, Polymer, 54 (2013) 6226-6235.

L.M. Robeson, B.D. Freeman, D.R. Paul, B.W. Rowe, An Empirical Correlation of Gas Permeability and Permselectivity in Polymers and Its Theoretical Basis, Journal of Membrane Science, 341 (2009) 178-185.

M. Rungta, L. Xu, W.J. Koros, Carbon Molecular Sieve Dense Film Membranes Derived from Matrimid® for Ethylene/Ethane Separation, Carbon, 50 (2012) 1488-1502.

D.F. Sanders, Z.P. Smith, C.P. Ribeiro, R. Guo, J.E. McGrath, D.R. Paul, B.D. Freeman, Gas Permeability, Diffusivity, and Free Volume of Thermally Rearranged Polymers Based on 3,3'-Dihydroxy-4,4'-Diamino-Biphenyl (HAB) and 2,2'-Bis-(3,4-Dicarboxyphenyl) Hexafluoropropane Dianhydride (6FDA), Journal of Membrane Science, 409-410 (2012) 232-241.

A. Shimazu, T. Miyazaki, K. Ikeda, Interpretation of d-Spacing Determined by Wide Angle X-Ray Scattering in 6FDA-Based Polyimide by Molecular Modeling, Journal of Membrane Science, 166 (2000) 113-118.

J.D. Wind, D.R. Paul, W.J. Koros, Natural Gas Permeation in Polyimide Membranes, Journal of Membrane Science, 228 (2004) 227-236.

Y. Zhang, I.H. Musselman, J.P. Ferraris, K.J. Balkus, Gas Permeability Properties of Matrimid® Membranes Containing the Metal-Organic Framework Cu–BPY–HFS, Journal of Membrane Science, 313 (2008) 170-181.

Appendix C

A.F. Ismail, W. Lorna, Penetrant-Induced Plasticization Phenomenon in Glassy Polymers for Gas Separation Membrane, Separation and Purification Technology, 27 (2002) 173 - 194.

E.W. Lemmon, I.H. Bell, M.L. Huber, M.O. McLinden, Standard Reference Data Program, in: NIST Standard Reference Database 23: Reference Fluid Thermodynamic and Transport Properties - REFPROP, Version 10.0, National Institute of Standards and Technology, Gaithersburg, 2018.

E.W. Lemmon, M.O. McLinden, D.G. Friend, Thermophysical Properties of Fluid Systems, in: P.J. Linstrom, W.G. Mallard (Eds.) NIST Chemistry WebBook, NIST Standard Reference Database Number 69, National Institute of Standards and Technology, Gaithersburg MD, 2018.

H. Lin, B.D. Freeman, Chapter 7: Permeation and Diffusion, in: Springer Handbook of Materials Measurement Methods, 2006, pp. 371-387.

L.M. Robeson, B.D. Freeman, D.R. Paul, B.W. Rowe, An Empirical Correlation of Gas Permeability and Permselectivity in Polymers and Its Theoretical Basis, Journal of Membrane Science, 341 (2009) 178-185.

Z.P. Smith, Fundamentals of Gas Sorption and Transport in Thermally Rearranged Polyimides, The University of Texas at Austin, Austin, TX, 2014.

Z.P. Smith, D.F. Sanders, C.P. Ribeiro, R. Guo, B.D. Freeman, D.R. Paul, J.E. McGrath, S. Swinnea, Gas Sorption and Characterization of Thermally Rearranged Polyimides Based on 3,3′-Dihydroxy-4,4′-Diamino-Biphenyl (HAB) And 2,2′-Bis-(3,4-Dicarboxyphenyl) Hexafluoropropane Dianhydride (6FDA), Journal of Membrane Science, 415-416 (2012) 558-567.

Z.P. Smith, R.R. Tiwari, M.E. Dose, K.L. Gleason, T.M. Murphy, D.F. Sanders, G. Gunawan, L.M. Robeson, D.R. Paul, B.D. Freeman, Influence of Diffusivity and Sorption on Helium and Hydrogen Separations in Hydrocarbon, Silicon, and Fluorocarbon-Based Polymers, Macromolecules, 47 (2014) 3170-3184.

Appendix D

R.B. Bird, W.E. Stewart, E.N. Lightfoot, Transport Phenomena, 2nd ed., John Wiley & Sons, 1961.

F. Doghieri, D. Biavati, G.C. Sarti, Solubility and Diffusivity of Ethanol in PTMSP: Effects of Activity and of Polymer Aging, Industrial & Engineering Chemistry Process Design and Development, 35 (1996) 2420-2430.

M.E. Dose, M. Chwatko, I. Hubacek, N.A. Lynd, D.R. Paul, B.D. Freeman, Thermally Cross-linked Diaminophenylindane (DAPI) Containing Polyimides for Membrane Based Gas Separations, Polymer, Submitted (2018).

E. Favre, P. Schaetzel, Q.T. Nguygen, R. Clement, J. Neel, Sorption, Diffusion and Vapor Permeation of Various Penetrants Through Dense Poly(dimethylsiloxane) Membranes: A Transport Analysis, Journal of Membrane Science, 92 (1994) 16-184.

M. Galizia, C. Daniel, G. Fasano, G. Guerra, G. Mensitieri, Gas Sorption and Diffusion in Amorphous and Semicrystalline Nanoporous Poly(2,6-dimethyl-1,4-phenylene)oxide, Macromolecules, 45 (2012) 3604-3615.

M. Galizia, M.G. De Angelis, E. Finkelshtein, Y.P. Yampolskii, G.C. Sarti, Sorption and Transport of Hydrocarbons and Alcohols in Addition-Type Poly(trimethyl Silyl Norbornene). I: Experimental Data, Journal of Membrane Science, 385-386 (2011) 141-153.

M. Galizia, K.A. Stevens, D.R. Paul, B.D. Freeman, Modeling Gas Permeability and Diffusivity in HAB-6FDA Polyimide and Its Thermally Rearranged Analogs, Journal of Membrane Science, 537 (2017) 83-92.

E.W. Lemmon, M.O. McLinden, D.G. Friend, Thermophysical Properties of Fluid Systems, in: P.J. Linstrom, W.G. Mallard (Eds.) NIST Chemistry WebBook, NIST Standard Reference Database Number 69, National Institute of Standards and Technology, Gaithersburg MD, 2018.

J.D. Moon, M. Galizia, H. Borjigin, R. Liu, J.S. Riffle, B. Freeman, D. Paul, Water Vapor Sorption, Diffusion, and Dilation in Polybenzimidazoles, Macromolecules, In Press (2018).

N. Ramesh, P.K. Davis, J.M. Zielinski, R.P. Danner, J.L. Duda, Application of Free-Volume Theory to Self Diffusion of Solvents in Polymers Below the Glass Transition Temperature: A Review, Journal of Polymer Science Part B: Polymer Physics, 49 (2011) 1629-1644.

L.M. Robeson, B.D. Freeman, D.R. Paul, B.W. Rowe, An Empirical Correlation of Gas Permeability and Permselectivity in Polymers and Its Theoretical Basis, Journal of Membrane Science, 341 (2009) 178-185.

J.M. Smith, H.C. Van Ness, M.M. Abbott, Introduction to Chemical Engineering Thermodynamics, 7th ed., McGraw-Hill Education, New York, 2004.

J.S. Vrentas, J.L. Duda, Diffusion in Polymer-Solvent Systems. I. Reexamination of the Free-Volume Theory, Journal of Polymer Science Part B: Polymer Physics, 15 (1977) 403-416.

J.S. Vrentas, J.L. Duda, H.-C. Ling, Free-Volume Theories for Self-Diffusion in Polymer-Solvent Systems. I. Conceptual Differences in Theories, Journal of Polymer Science Part B: Polymer Physics, 23 (1985) 275-288.

J.S. Vrentas, J.L. Duda, H.-C. Ling, C.-C. Hou, Free-Volume Theories for Self-Diffusion in Polymer-Solvent Systems. II. Predictive Capabilities, Journal of Polymer Science Part B: Polymer Physics, 23 (1985) 289-304.

Appendix E

R.B. Bird, W.E. Stewart, E.N. Lightfoot, Transport Phenomena, 2nd ed., John Wiley & Sons, 1961.

J.I. Choi, C.H. Jung, S.H. Han, H.B. Park, Y.M. Lee, Thermally Rearranged (TR) Poly(benzoxazole-co-pyrrolone) Membranes Tuned for High Gas Permeability and Selectivity, Journal of Membrane Science, 349 (2010) 358-368.

K.L. Gleason, Z.P. Smith, Q. Liu, D.R. Paul, B.D. Freeman, Pure- and Mixed-Gas Permeation of CO2 and CH4 in Thermally Rearranged Polymers Based on 3,3′-Dihydroxy-4,4′-Diamino-Biphenyl (HAB) and 2,2′-Bis-(3,4-Dicarboxyphenyl) Hexafluoropropane Dianhydride (6FDA), Journal of Membrane Science, 475 (2015) 204-214.

R. Guo, D.F. Sanders, Z.P. Smith, B.D. Freeman, D.R. Paul, J.E. McGrath, Synthesis and Characterization of Thermally Rearranged (TR) Polymers: Effect of Glass Transition Temperature of Aromatic Poly(hydroxyimide) Precursors on TR Process and Gas Permeation Properties, Journal of Materials Chemistry A, 1 (2013) 6063-6072.

R. Guo, D.F. Sanders, Z.P. Smith, B.D. Freeman, D.R. Paul, J.E. McGrath, Synthesis and Characterization of Thermally Rearranged (TR) polymers: Influence of Ortho-Positioned Functional Groups of Polyimide Precursors on TR process and Gas Transport Properties, J. Mater. Chem. A, 1 (2013) 262-272.

Y. Huang, D. Paul, Experimental Methods for Tracking Physical Aging of Thin Glassy Polymer Films by Gas Permeation, Journal of Membrane Science, 244 (2004) 167-178.

Y. Jiang, F.T. Willmore, D. Sanders, Z.P. Smith, C.P. Ribeiro, C.M. Doherty, A. Thornton, A.J. Hill, B.D. Freeman, I.C. Sanchez, Cavity Size, Sorption and Transport Characteristics of Thermally Rearranged (TR) Polymers, Polymer, 52 (2011) 2244-2254.

J.H. Kim, W.J. Koros, D.R. Paul, Physical Aging of Thin 6FDA-Based Polyimide Membranes Containing Carboxyl Acid Groups. Part I. Transport Properties, Polymer, 47 (2006) 3094-3103.

W.J. Koros, G.K. Fleming, Membrane-Based Gas Separation, Journal of membrane science, 83 (1993) 1-80.

A.V. Lesikar, Effect of Association Complexes on the Glass Transition in Organic Halide Mixtures, The Journal of Physical Chemistry, 80 (1976) 1005 - 1011.

H.B. Park, S.H. Han, C.H. Jung, Y.M. Lee, A.J. Hill, Thermally Rearranged (TR) Polymer Membranes for CO2 Separation, Journal of Membrane Science, 359 (2010) 11-24.

H.B. Park, C.H. Jung, Y.M. Lee, A.J. Hill, S.J. Pas, S.T. Mudie, E. Van Wagner, B.D. Freeman, D.J. Cookson, Polymers with Cavities Tuned for Fast Selective Transport of Small Molecules and Ions, Science, 318 (2007) 254-258.

L.M. Robeson, Correlation of Separation Factor Versus Permeability for Polymeric Membranes, Journal of Membrane Science, 62 (1991) 165-185.

L.M. Robeson, The Upper Bound Revisited, Journal of Membrane Science, 320 (2008) 390-400.

L.M. Robeson, B.D. Freeman, D.R. Paul, B.W. Rowe, An Empirical Correlation of Gas Permeability and Permselectivity in Polymers and Its Theoretical Basis, Journal of Membrane Science, 341 (2009) 178-185.

D. Sanders, The Effect of Synthesis Route and ortho-Position Functional Group on Thermally Rearranged Polymer Thermal and Transport Properties, The University of Texas at Austin, 2013.

D.F. Sanders, R. Guo, Z.P. Smith, K.A. Stevens, Q. Liu, J.E. McGrath, D.R. Paul, B.D. Freeman, Influence of Polyimide Precursor Synthesis Route and Ortho-Position Functional Group on Thermally Rearranged (TR) Polymer Properties: Pure gas Permeability and Selectivity, Journal of Membrane Science, 463 (2014) 73-81.

D.F. Sanders, Z.P. Smith, C.P. Ribeiro, R. Guo, J.E. McGrath, D.R. Paul, B.D. Freeman, Gas Permeability, Diffusivity, and Free Volume of Thermally Rearranged Polymers Based on 3,3'-Dihydroxy-4,4'-Diamino-Biphenyl (HAB) and 2,2'-Bis-(3,4-Dicarboxyphenyl) Hexafluoropropane Dianhydride (6FDA), Journal of Membrane Science, 409-410 (2012) 232-241.

E.J. Sare, C.A. Angell, Glass-Forming Composition Regions and Glass Transition Temperature in Nonaqueous Electrolyte Solutions, Journal of Solution Chemistry, 2 (1973) 53 - 57.

Z.P. Smith, D.F. Sanders, C.P. Ribeiro, R. Guo, B.D. Freeman, D.R. Paul, J.E. McGrath, S. Swinnea, Gas Sorption and Characterization of Thermally Rearranged Polyimides Based on 3,3′-Dihydroxy-4,4′-Diamino-Biphenyl (HAB) And 2,2′-Bis-(3,4-Dicarboxyphenyl) Hexafluoropropane Dianhydride (6FDA), Journal of Membrane Science, 415-416 (2012) 558-567.

A. Weill, E. Dchenaux, The Spin-Coating Process Mechanism Related to Polymer Solution Properties, Polymer Engineering and Science, 28 (1988) 945 - 948.

O. Yamamuro, M. Oguni, T. Matsuo, H. Suga, Calorimetric Study of Pure and KOH-doped Tetrahydrofuran Clathrate Hydrate, Journal of Physics and Chemsitry of Solids, 49 (1988) 425 - 434.

Appendix F

S.K. Christensen, M.C. Chiappelli, R.C. Hayward, Gelation of copolymers with pendent benzophenone photo-cross-linkers, Macromolecules, 45 (2012) 5237-5246.

G. Eisele, J.P. Fouassier, R. Reeb, Kinetics of photocrosslinking reactions of a DCPA/EA matrix in the presence of thiols and acrylates, Journal of Polymer Science, Part A: Polymer Chemistry, 35 (1997) 2333-2345.

A.A. Lin, V.R. Sastri, G. Tesoro, A. Reiser, R. Eachus, On the crosslinking mechanism of benzophenone-containing polyimides, Macromolecules, 21 (1988) 1165-1169.

M.S. McCaig, D.R. Paul, Effect of UV Crosslinking and Physical Aging on the Gas Permeability of Thin Glassy Polyarylate Films, Polymer, 40 (1999) 7209-7225.

G. Porter, F. Wilkinson, Primary photochemical processes in aromatic molecules. Part 5.Flash photolysis of benzophenone in solution, Transactions of the Faraday Society, 57 (1961) 1686-1686.

Vita

Michelle Elizabeth Dose earned her bachelor's degree in chemical and biomolecular engineering, along with a minor in material science, from the Georgia Institute of Technology in 2013. During her doctoral research in chemical engineering at the University of Texas at Austin, Michelle was awarded a National Science Foundation Graduate Student Research Fellowship. Michelle earned her Ph.D. in October of 2018.

Permanent email address: m.dose13@gmail.com

This dissertation was typed by the author.